Temporal and spatial structures of denitrification in crystalline aquifers

Tamara Kolbe

ANNÉE 2017

UNIVERSITÉ DE RENNES 1

UNIVERSITE BRETAGNE LOIRE

THÈSE / UNIVERSITÉ DE RENNES 1
sous le sceau de l'Université Bretagne Loire

pour le grade de

DOCTEUR DE L'UNIVERSITÉ DE RENNES 1

Mention : Science de la Terre

Ecole doctorale Science de la Matière

Tamara Kolbe

Préparée à l'unité de recherche Géoscience Rennes
(UMR CNRS 6118)
OSUR Observatoire des Sciences de l'Univers de Rennes

Temporal and spatial structures of denitrification in crystalline aquifers

Thèse rapportée par :

Christopher GREEN
Professeur, USGS / *rapporteur*

Jérôme MOLENAT
Directeur de recherche, INRA / *rapporteur*

et soutenue à Rennes le 4 juillet 2017

devant le jury composé de :

Christopher GREEN
Professeur, USGS / *rapporteur*

Jérôme MOLENAT
Directeur de recherche, INRA / *rapporteur*

Gunnar LISCHEID
Professeur, ZALF / *examinateur*

Tanguy LE BORGNE
Directeur de recherche, CNAP / *examinateur*

Zahra THOMAS
Maitre de conférence, AGROCAMPUS OUEST / co-directeur de thèse

Jean-Raynald DE DREUZY
Directeur de recherche, CNRS / *directeur de thèse*

Abstract

Unconfined shallow aquifers in agricultural areas are contaminated by nitrates worldwide. Excessive fertilization over the last decades has affected groundwater quality as well as human and ecosystem wellbeing. Nitrate in groundwater can be microbially reduced to dinitrogen gas by heterotrophic (microbes obtaining their energy from surface-derived organic carbon) and autotrophic (microbes obtaining their energy from a lithological source) processes. However, denitrification rates are highly spatially variable, following involved interactions between groundwater flow structures and biogeochemical activity. The location of biogeochemical activity in the aquifer is difficult to access at the catchment scale, but of vast importance to gain predictive capabilities for groundwater management. Even though microbial processes cannot be resolved at the local scale, this dissertation proposes a catchment scale characterization of denitrification rates based on an integrated model- and data-driven approach.

This dissertation proposes an extensive use of conservative and reactive tracers combined with groundwater flow and transport models to identify the geological and biogeochemical controls on aquifer denitrification capacities. The methodology is applied to a crystalline unconfined aquifer of 76 km^2 size in Brittany, France. Based on CFC-12, O_2, NO_3^-, and dissolved N_2 concentrations measured in 16 wells, it is possible to reconstruct historical nitrate inputs to the saturated zone and to define spatiotemporal denitrification activity. It is shown that denitrification is primarily controlled by the location of electron donors. This dissertation proposes a general interpretation framework based on tracer information combined with complementary semi-explicit lumped parameter models to assess regional denitrification capacities and nitrate legacy.

Résumé

Les nitrates constituent la principale source de pollution des eaux souterraines dans les zones agricoles, et affectent aussi bien les humains que les écosystèmes. La dénitrification est un processus naturel de réduction des nitrates en N_2 ou N_2O, pouvant se produire si les conditions nécessaires sont réunies : absence d'oxygène, présence de microorganismes dénitrifiant, disponibilité en donneurs d'électrons. La grande variabilité temporelle de la dénitrification fait de sa caractérisation à l'échelle de l'aquifère un défi. La structure complexe des circulations souterraines et l'activité biogéochimique contrôlent la dégradation des nitrates. Ces deux facteurs sont difficiles à mesurer à l'échelle de l'aquifère, si bien qu'il est délicat d'évaluer l'impact de l'application d'engrais azotés sur la qualité de l'eau souterraine.

L'approche développée ici combine données et modélisations. Elle s'appuie sur des mesures effectuées en puits (O_2, NO_3^-, N_2 et CFC-12) et sur un modèle basé sur les temps de résidence, pour comprendre le processus général de dénitrification dans les aquifères. Les données utilisées dans le modèle ont été collectées au cours de trois campagnes de mesures dans 16 puits localisés dans une zone agricole de 76 km^2.

La méthodologie générale, présentée en chapitre 2, repose sur une approche de modélisation basée sur les temps de résidence. Les concentrations en traceurs dans les puits sont déterminées en convoluant la concentration d'entrée dans la zone de capture du puits à la distribution des temps de résidence correspondante. Les distributions de temps de résidence contiennent des informations sur la structure des circulations, le stockage et l'origine de l'eau. Elles peuvent être déterminées à travers des solutions explicites d'équations de flux souterrains et de transport, ou de modèles

simplifiés (modèles groupés, de type « lumped parameter »). L'objectif principal est de déterminer des temps de réaction caractéristiques de la réduction de l'oxygène et des nitrates, de manière à développer un nouveau cadre conceptuel de la dénitrification dans les aquifères.

Le chapitre 3 présente la structure des circulations souterraines au niveau du site étudié. Un modèle tridimensionnel de circulation souterraine a été élaboré avec le logiciel FEFLOW et utilisé pour déterminer les distributions de temps de résidence dans chacun des puits. Le modèle a été calibré avec le débit de base à l'exutoire du bassin versant et les mesures de CFC-12. Les résultats montrent que les circulations souterraines se font à une échelle très locale, avec une eau souterraine globalement âgée (âge moyen d'environ 40 ans). En outre, les distances parcourues par l'eau souterraine sont corrélées aux distances parcourues par l'eau de surface en un point donné. Le rapport des distances parcourues par l'eau souterraine et par l'eau superficielle semble être un outil prometteur pour obtenir facilement des informations sur les circulations souterraines à partir des gradients topographiques, et mériterait d'être étudié dans d'autres aquifères non confinés pour lesquels des modèles de circulations souterraines existent déjà.

Dans le chapitre 4, les quantités de nitrates introduites au cours des dernières décennies sont estimées en utilisant la méthodologie présentée en chapitre 2 et la structure des circulations souterraines déterminée en chapitre 3. Pour investiguer les processus de dégradation des nitrates, il est nécessaire de connaître ce qui a été apporté au système et d'évaluer l'évolution de la teneur en nitrates des eaux souterraines au cours des dernières décennies. Les informations apportées par les traceurs comme CFC-12, NO_3^- ou N_2 ont été utilisées pour contraindre le modèle et

reconstituer la chronique d'apports de nitrates spécifique au site étudié. En comparaison, une chronique des apports de nitrates à l'échelle de la Bretagne, réalisée dans des études précédentes, montre des tendances similaires, mais des concentrations globalement moins élevées que celles du bassin de Pleine-Fougères. Cette partie de la thèse semble être un point de départ intéressant pour des investigations futures des apports en nitrates à l'échelle du site ou à d'autres échelles.

Le chapitre 5 est dédié aux processus de dénitrification se produisant dans l'aquifère cristallin non confiné. Les temps caractéristiques de dénitrification sont déduits de la modélisation présentée en chapitre 2 et des mesures des traceurs CFC-12, O_2, NO_3^- et N_2. De la même manière que dans d'autres études, la dénitrification présente une grande variabilité temporelle. Les temps de réaction effectifs dépendent fortement de la disponibilité en donneurs d'électrons, qui peuvent soit provenir de la surface, soit être d'origine lithologique. Ceci conduit au développement d'un nouveau cadre conceptuel pour interpréter les temps de réaction observés en termes de temps de réaction effectif et de temps nécessaire pour atteindre ou quitter la zone réactive, où les donneurs d'électrons sont disponibles (Fig. suivante).

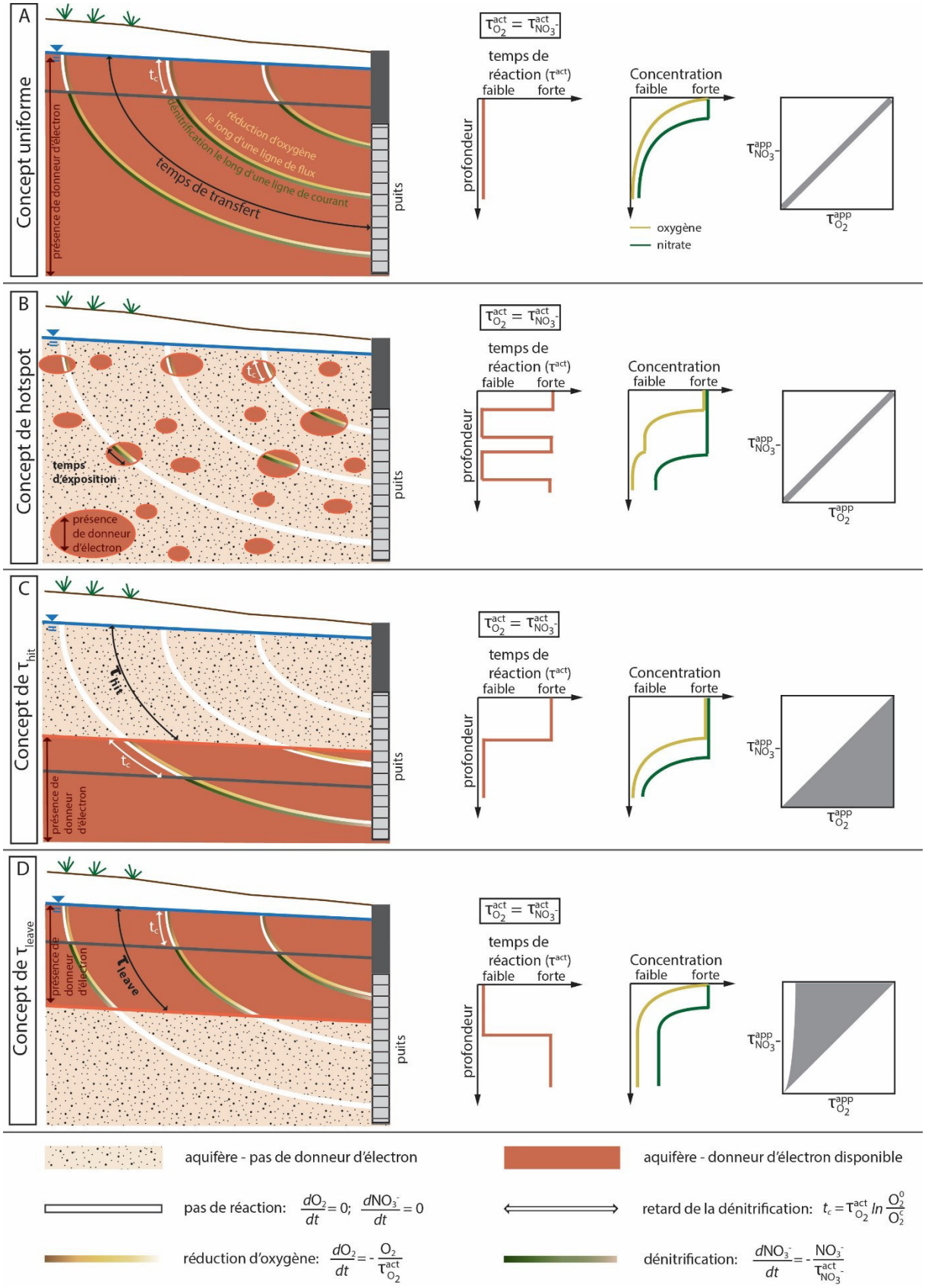

Fig. : Distributions verticales potentielles de dénitrification

Les résultats montrent que les estimations de la résilience de l'eau souterraine dépendent fortement du concept choisi, et qu'appliquer le concept classique de réaction continue le long des lignes de flux peut mener à des sur- ou sous-estimations de la dénitrification effective. Le modèle conceptuel mis en place est applicable aux aquifères peu profonds et peut être utilisé pour étudier la dénitrification effective dans d'autres contextes hydrologiques (Fig. suivante). Cette méthode de calcul, peu coûteuse, permet d'acquérir une compréhension détaillée de la réduction effective des nitrates dans un aquifère donné.

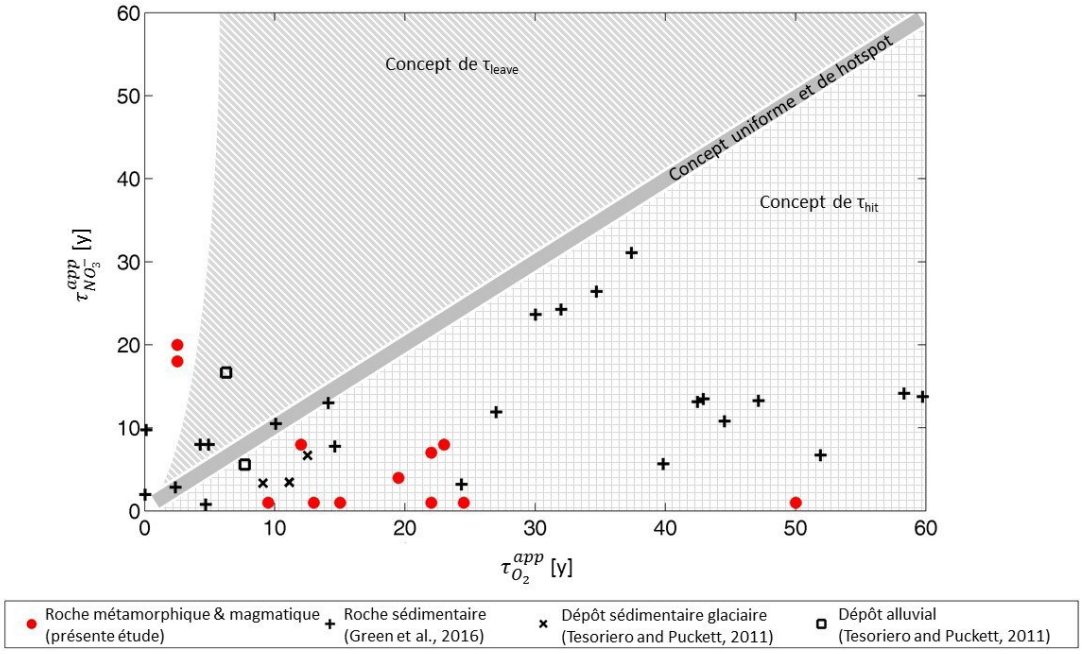

Fig. : Temps de réduction apparent de l'oxygène et des nitrates dans différents types d'aquifères.

Le travail présenté ici utilise des données temporelles et une modélisation des temps de résidence pour aboutir à une compréhension globale des processus de dénitrification dans les aquifères non confinés. Des mesures effectuées au niveau d'un aquifère cristallin sont utilisées pour mettre en œuvre la méthodologie et caractériser intégralement les circulations souterraines et la réactivité, ces deux éléments

définissant conjointement la capacité de dégradation de l'aquifère. Les outils utilisés et le cadre conceptuel mis en place sont applicables à d'autres sites. Il serait intéressant de les vérifier dans d'autres contextes hydrologiques pour obtenir davantage d'informations sur les taux de dénitrification effectifs dans les aquifères. Le cadre général d'interprétation proposé dans cette étude permet d'évaluer la dénitrification à l'échelle régionale ainsi que l'héritage en nitrates.

Acknowledgements

My deep gratitude goes to my Supervisor Jean-Raynald de Dreuzy, who expertly guided me throughout my PhD. I would like to express my sincere appreciation also to my Co-Supervisors Zahra Thomas and Gilles Pinay for their constant guidance and encouragement. It was a pleasure to work with them.

Many special thanks go to my colleagues and friends Ben Abbott and Jean Marçais for their support and advices regarding my research. I very much enjoyed working with them.

I also thank Thierry Labasque, Luc Aquilina, Anniet Laverman and Stefan Peiffer for showing interest in my research and for giving precious advice.

I am very grateful for financial support provided by the European Union's Seventh Framework under grant agreement no. 607150. My dissertation was also supported by the European Union's International Training Network INTERFACES, and I am very thankful for having met all these great INTERFACES scientists.

Many thanks also go to Ben, Jean, Camille Vautier and Camille Minaudo for the positive and familiar atmosphere in our office, and to Daniel Jara Heredia for the best coffee breaks. I am very grateful to my friends Julia Busse, Silvia Poblador, Giorgos Tolias, Flavien Sciortino, Ahmet Iscen, Michele Dominici, and Pantelis Frangoudis for having such a great time during my PhD student life in Rennes.

Many thanks to Daniel Gieseler and my family, especially to my mother, for their moral support.

And Jonatan, thank you for always being there for me.

Table of Contents

This dissertation is focused on nitrate transport and denitrification processes in shallow aquifers. Most aquifers in agricultural areas are contaminated by nitrate with effects on health and wellbeing of humans as well as ecosystems (Balderacchi et al., 2014; Galloway et al., 2003). Data obtained from a crystalline unconfined aquifer in Brittany, France, shows that measured nitrate concentrations exceed the EU Water Framework Directive limit of 50 mg/l in some of the wells used by farmers, whereas other wells show no measureable nitrate concentrations. If nitrate has leached to the aquifer, it is transported with groundwater and potentially degraded in zones favorable for denitrification. Groundwater flow structures are complex due to heterogeneous crystalline geology, and degradation processes that are locally controlled by biogeochemical reactivity are challenging to quantify at the catchment scale. Because management decisions regarding water quality are usually made at the catchment scale, a better understanding of the spatial variability of degradation processes and its controlling factors needs to be further developed to gain predictive capabilities for groundwater resilience.

The objective of this dissertation is to develop an understanding on how groundwater flow structures and biogeochemical activity control the fate of nitrate in aquifers. To investigate transport and degradation processes, a model- and data-driven approach is set-up at a crystalline unconfined aquifer in an area intensive used for agriculture near the town Pleine-Fougères in Brittany, France. A collection of tracers in combination with modeling tools is used to get a better understanding on denitrification activity in the aquifer. New concepts are developed to explain the highly spatial variability of denitrification activity at the study site and also in different hydrogeological settings.

An introduction to groundwater flow dynamics in crystalline aquifers and denitrification processes occurring in groundwater is given in chapter 1. The general modeling approach is presented in chapter 2. Chapter 3 presents investigations on groundwater flow structures performed with a three-dimensional groundwater flow model calibrated with CFC data. Groundwater transit times and travel distances are obtained for any location in the study area and a new indicator to classify local groundwater circulation is presented. To further investigate denitrification activity in the aquifer, historical nitrate inputs to the aquifer are reconstructed in chapter 4. Based on the previous chapters, nitrate transport and degradation in the aquifer is examined in chapter 5. Furthermore, new concepts to interpret denitrification activity in aquifers are proposed. A general discussion is given in chapter 6.

Chapter 1: General Introduction

1.1 Groundwater flow in crystalline aquifers

Nitrate is highly mobile in the liquid phase and if leached to the aquifer, easily transported with the groundwater flow (McClain et al., 2003; Pärn et al., 2012). Because of their proximity to the land surface, crystalline aquifers are especially prone for agricultural pollutants (Taylor and Howard, 2000). Different degrees of weathering and formation of fractures in the geological substrate result in complex groundwater flow patterns within crystalline aquifers. Deep weathering processes, the breakdown of rocks by physical, chemical or biological process, are defining the highly heterogeneous hydrogeological properties of these aquifers (Jaunat et al., 2012; Rempe and Dietrich, 2014; Wyns et al., 2004).

Crystalline aquifers can conceptually be described by three layers (Aquilina et al., 2012; Ayraud et al., 2008; Maréchal et al., 2003; Tarits et al., 2006). The weathered upper zone can be highly permeable with high porosities up to 50 % (Kovács, 2011; Wright and Burgess, 1992). It is followed by the fissured zone that is less permeable and porous. The underlying fresh bedrock is often assumed to be impermeable (*Fig. 1*).

The main volume of the groundwater is located in the upper weathered zone usually showing groundwater ages in the range of some decades (Aquilina et al., 2012; Molénat et al., 2013). The time a nitrate loaded water parcel spent in the aquifer is an important indicator for determining its initial nitrate load at the groundwater table and the potential decay when transported in favorable conditions for denitrification (Böhlke et al., 2002; Green et al., 2016 Tesoriero and Puckett, 2011).

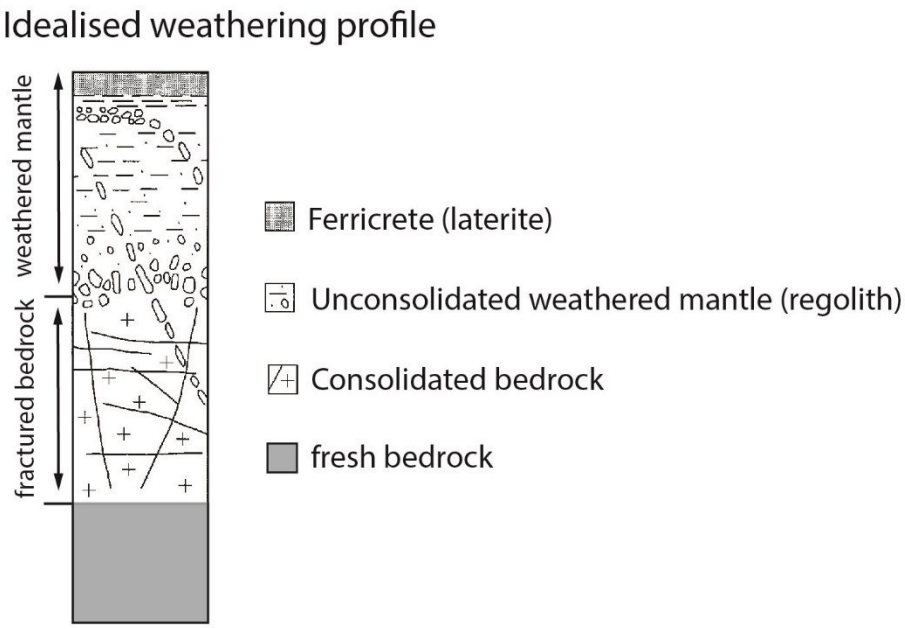

Fig. 1: Idealized weathering profile (modified from Taylor and Howard, 2000)

1.1.1 Dating groundwater flow

Atmospheric tracer data, such as chlorofluorocarbons (CFCs), are a common tool to date young groundwater (< 60 y). CFCs were first produced and released to the atmosphere in the 1940s and have been extensively used as refrigerants and spray can propellants. Since their emission they are taking part in the hydrological cycle and can be used as a tracer to date groundwater. The principles of tracing these anthropogenic gases are based on the assumption that as soon as the tracer enters the saturated zone it moves conservatively along the flow line. The concentrations of CFCs in the atmosphere are recorded regularly at several stations worldwide with only 10% variation between observed concentrations at a station and the average concentrations of all stations. The recorded concentration curves are therefore assumed to be valid all over the world (Kazemi et al., 2006; *Fig. 2*).

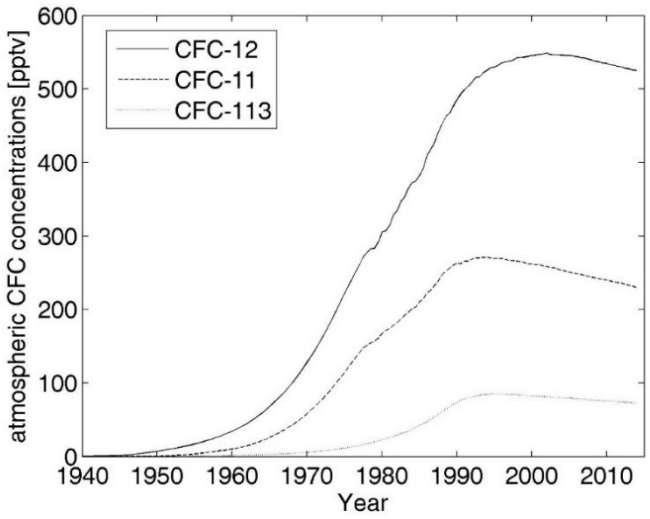

Fig. 2: CFC curves (URL: http://water.usgs.gov/lab/software/air_curve/)

A measured tracer gas concentration in a well represents a mixture of waters with different concentrations (Busenberg and Plummer, 1992). To get information about mixing processes, numerical groundwater flow models (Eberts et al., 2012; Molénat et al., 2013) or simplified lumped parameter models (Jurgens et al., 2012) are used to derive transit time distributions from a single tracer gas concentration. The transit time is here defined as the time water has traveled from the groundwater table to the well. Even in aquifers with heterogeneous flow structures, like crystalline aquifers, the evaluation of transit time distributions with CFC age data is an established method (Kazemi et al., 2006; Leray et al., 2012).

It has been observed that CFCs can be degraded under anoxic conditions (Horneman et al., 2008; Shapiro et al., 1997), adding uncertainty to the use as a tracer. CFC-11 is the most reactive tracer gas, followed by CFC-113 and CFC-12 (Höhener et al., 2003). Other uncertainties could arise from a contamination during sampling, an unsaturated zone of more than five meters, sorption and desorption of CFCs from the

aquifer matrix, as well as diffusion and dispersion, and uncertainty in the estimation of the atmospheric input function (Kazemi et al., 2006).

1.2 Denitrification in groundwater

When nitrate is transported in conditions favorable for denitrification, e.g. under existence of denitrifying microbes, the absence of oxygen and the availability of electron donors, nitrate is reduced to N_2O and N_2 (Korom, 1992; Rivett et al., 2008).

The denitrification process has been reported as highly spatially variable, showing a wide range of reaction rates in the same study site and when comparing several study sites (*Fig. 3)*.

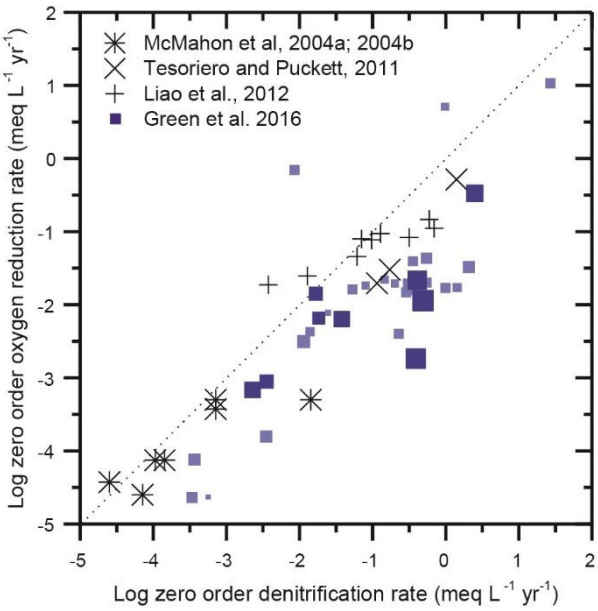

Fig. 3: Comparison of oxygen and nitrate reduction rates (Green et al., 2016)

The distribution of electron donors is the controlling factor on denitrification rates at several sites (Tesoriero and Puckett, 2011). Denitrifying bacteria have been found ubiquitous in groundwater (Beauchamp et al., 1989; Nielsen et al., 2006) and oxygen,

as an electron acceptor that supplies more energy than nitrate, is consumed before nitrate gets reduced (Korom, 1992; McMahon et al., 2011).

Depending on the source of electron donors, denitrifying bacteria can be facultative anaerobic heterotrophs (obtaining their energy and carbon from the oxidation of organic compounds; *Eq. 1*) or autotrophs (obtaining their energy from the oxidation of inorganic species, e.g. reduced Sulphur; *Eq. 2*) (Rivett et al., 2008).

$$5CH_2O + 4NO_3^- \rightarrow 2N_2 + 4HCO_3^- + CO_2 + 3H_2O \quad (1)$$

$$5FeS_2 + 14NO_3^- + 4H^+ \rightarrow 7N_2 + 10SO_4^{2-} + 5Fe^{2-} + 2H_2O \quad (2)$$

The amount of surface-derived dissolved organic carbon in groundwater is usually low (Rivett et al., 2008) and heterotrophic denitrification most likely to occur in the upper five meters (Seitzinger et al., 2006, Tesoriero and Puckett, 2011). An explanation could be that the soil-generated labile dissolved organic carbon which serves as electron donor has been degraded incompletely in the unsaturated zone and transported into the aquifer where it leads to quick oxygen reduction rates and often to subsequent heterotrophic denitrification (Starr and Gillham, 1989; Starr and Gillham, 1993).

In general, heterotrophic denitrification plays a minor role in comparison to solid-phase organic carbon contents in soils or geological deposits or sulfides from lithologic sources (Rivett et al., 2008; Tesoriero and Puckett, 2011). In organic carbon limited aquifers, sulfides are alternative electron donor sources (Rivett et al., 2008; Tesoriero and Puckett, 2011) and several studies suggest that iron sulfide (e.g. pyrite) oxidation is the dominating nitrate removal process, even in the presence of organic carbon (Pauwels et al., 2010; Postma et al., 1991; Tesoriero et al., 2000). Pyrite is the most

abundant sulfide mineral and it is a common accessory mineral in igneous, metamorphic and sedimentary rocks (Craig, 1993).

In Brittany, denitrification in combination with sulfide minerals has been observed in depths from 20 m to 100 m (Pauwels et al., 2000; Pauwels et al., 2010b; Tarits et al., 2006). Reactive zones that depend mainly on the availability of electron donors have been observed in the deeper part of the aquifer (McMahon and Chapelle, 2008; Tesoriero et al., 2000). Böhlke et al. (2002) present a vertical section where active denitrification occurs within a clearly defined zone of the aquifer controlled by a combination of nitrate inputs, flow patterns, and the abundance and distribution of electron donors (*Fig. 4*).

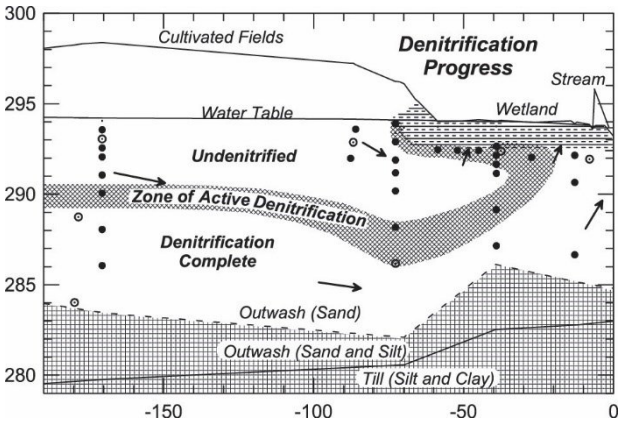

Fig. 4: Vertical section showing the progress of denitrification (Böhlke et al., 2002).

It shows that the high spatial variability of reaction rates arises from the intersection of nitrate loaded water with zones where electron donors, like pyrite, are abundant.

1.2.1 Tracing denitrification in groundwater

Denitrification in groundwater can be observed due to shifts in the isotopic composition of nitrate, carbon and sulfate or quantified by measuring dinitrogen, the denitrification product.

1.2.1.1 Stable isotopes

Due to denitrification a shift in the ratio *R* of the heavy ^{h}C and light isotope ^{l}C concentration (*Eq. 3*; Thullner et al., 2012), reported in the delta (δ) notation, occurs (*Eq.4*; Aelion et al., 2009; Kendall and McDonnell, 1998).

$$R = \frac{h_C}{l_C} \tag{3}$$

$$\delta = 1000\ (\frac{R}{R_{Std}} - 1) \tag{4}$$

With R_{Std} the ratio of the standard material that depends on the investigated chemical element.

Due to denitrification, the $\delta^{15}N$ increases, while the nitrate concentration decreases.

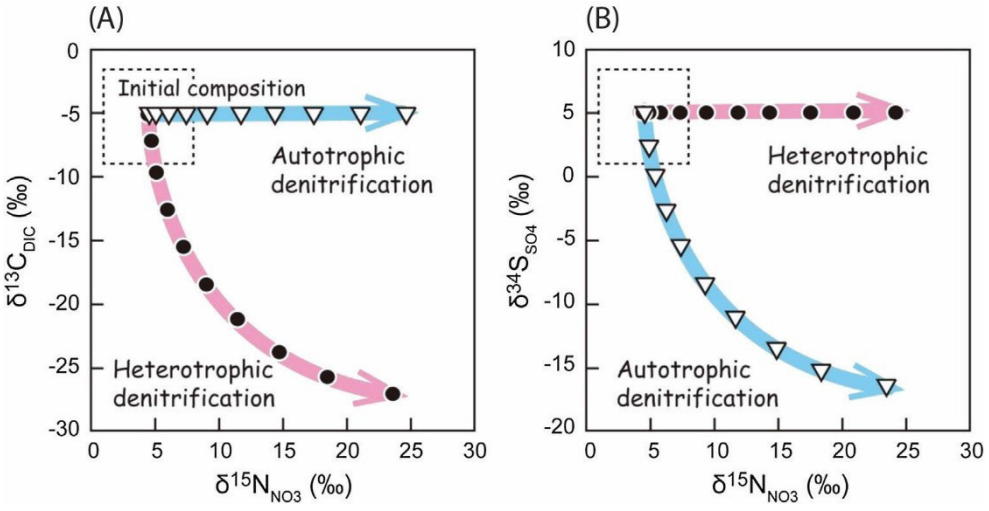

Fig. 5: Conceptual evolution of carbon, nitrate and sulfate stable isotopes for heterotrophic and autotrophic denitrification (Hosono et al., 2014)

In the case of heterotrophic denitrification, where organic carbon is used as an electron donor, the $\delta^{13}C$ value decreases while the $\delta^{15}N$ value increases (*Fig. 5A*). No changes in $\delta^{34}S$ are observed. In the case of autotrophic denitrification, where pyrite (FeS_2) serves as an electron donor, sulfate is produced and a decreased $\delta^{34}S$ value observed

(*Fig. 5B*). SO_4 produced through sulfide oxidation has a $\delta^{34}S$ value close to the $\delta^{34}S$ of FeS_2 (around -15 ‰ in *Fig. 5B*; Aelion et al., 2009; Pauwels et al., 2010) and gets mixed with initial δ34S values in the soil (around 5 ‰ in *Fig. 5B*). Just a slight sulfate isotope fractionation effect of -2.3 ‰ to + 0.5 ‰ is found in laboratory experiments. Therefore, no fractionation effect is taken into account in several field and modeling studies (Aravena and Robertson, 1998; Kendall et al., 2013; Pauwels et al., 2000; Strebel et al., 1990; Schwientek et al., 2008; Van Stempvoort et al., 1994; Toran and Harris, 1989; Zhang et al., 2012; Zhang et al., 2013).

The most commonly used equation to describe isotope fractionation is the Rayleigh equation (*Eq. 5*; Fischer et al., 2007; Green et al., 2010; Höyng et al., 2015).

$$\frac{R}{R_0} = \left(\frac{C}{C_0}\right)^{\alpha-1} \tag{5}$$

With *R* being the ratio of heavy and light isotope concentration, R_0 the standard, *C* the measured and C_0 the initial concentration, and α the isotope fractionation factor. Developed for the distillation of binary mixtures, this approach is also applied to fractionation processes in aquifers. An aquifer, represented as a closed well mixed system where kinetic fractionation occurs, behaves just like an open system equilibrium fractionation as developed by Rayleigh (Kendall and McDonnell, 1998).

However, the Rayleigh equation implies some assumptions that are not necessarily valid for all aquifer investigations. Thullner et al. (2012) give a review about recent developments of the Rayleigh equation approach and discuss applications and their uncertainties. The main assumption of the Rayleigh equation is that a single process (e.g. first-order degradation) affects simultaneously the concentration and the isotope ratio of the contaminant (Van Breukelen and Prommer, 2008), but the fate of the

contaminant in the aquifer is not only determined by degradation. Instead other processes, such as dilution, dispersion or mixing of water in the well during sampling, change the concentration, but have no effect on the isotopic signature.

Changes of isotopic compositions can be used to detect and qualify denitrification. However, quantification remains challenging, because isotopic fractionation factors can vary between denitrification processes and the initial ratios are often not known and difficult to determine (Böhlke, 2002).

1.2.1.2 Dinitrogen

Denitrification is the main nitrate degradation process in groundwater that reduces nitrate to N_2O and N_2 (Galloway 2004; Korom, 1992). A comparison of the measured with the expected atmospheric N_2 concentration allows determining the amount of N_2 produced during denitrification which can be translated to the amount of denitrified nitrate. In combination with other noble gases, like argon and neon that are assumed to be conservative tracers, the excess of N_2 can be precisely determined in the absence of degassing (Aeschbach-Hertig et al., 1999; Aeschbach-Hertig et al., 2001). N_2 excess is a useful indicator for biogeochemical reactivity and tracer to quantify denitrification activity.

Denitrification activity is challenging to predict at the catchment scale due to heterogeneous flow dynamics and the need of favorable conditions for denitrification that depend on several factors. A promising way to resolve these issues is to use a combination of tracers to gain information on hydrogeological as well as reactive processes.

1.3 Combination of tracers to investigate denitrification in aquifers

To investigate the importance of controlling factors on denitrification processes and the source of spatial variable denitrification activity, it is necessary to answer the following fundamental questions that emerge (Abbott et al., 2016; Boyer et al., 2006):

- What are the flow paths of nitrate loaded groundwater and how long has it spent in the aquifer?
- How much nitrate entered the aquifer and how much nitrate is denitrified?
- Where does conditions favorable for denitrification occur in the aquifer and what are the consequences?

In the following presented article a review on multiple tracers and their combined use is given to answer these questions.

1.3.1 Article: "Using multi-tracer inference to move beyond single-catchment ecohydrology", B.W. Abbott, V. Baranov, C. Mendoza-Lera, M. Nikolakopoulou, A. Harjung, T. Kolbe, M. N. Balasubramanian, T. N. Vaessen, F. Ciocca, A. Campeau, M. B. Wallin, P. Romeijn, M. Antonelli, J. Gonçalves, T. Datry, A. M. Laverman, J.-R. de Dreuzy, D. M. Hannah, S. Krause, C. Oldham, G. Pinay, Earth-Science Reviews, 2016

The author's contributions to this article:

The author of this dissertation contributed to the development of concepts and applied the proposed multi-tracer approach at the Pleine-Fougères site to determine where, when and how much nitrate degrades in the aquifer. Together with Astrid Harjung, the author of this dissertation drafted section 3.1 (Water sources and flowpath: where does water go when it rains?). Furthermore, the author of this dissertation prepared the basis for Table 1 (List of tracers and their attributes) that was finalized by Clara Mendoza-Lera.

Earth-Science Reviews 160 (2016) 19–42

Contents lists available at ScienceDirect

Earth-Science Reviews

journal homepage: www.elsevier.com/locate/earscirev

Invited review

Using multi-tracer inference to move beyond single-catchment ecohydrology

Benjamin W. Abbott [a,*], Viktor Baranov [b], Clara Mendoza-Lera [c], Myrto Nikolakopoulou [d], Astrid Harjung [e], Tamara Kolbe [f], Mukundh N. Balasubramanian [g], Timothy N. Vaessen [h], Francesco Ciocca [i], Audrey Campeau [j], Marcus B. Wallin [j], Paul Romeijn [k], Marta Antonelli [l], José Gonçalves [m], Thibault Datry [c], Anniet M. Laverman [a], Jean-Raynald de Dreuzy [f], David M. Hannah [k], Stefan Krause [k], Carolyn Oldham [n], Gilles Pinay [a]

[a] Université de Rennes 1, OSUR, CNRS, UMR 6553 ECOBIO, Rennes, France
[b] Leibniz-Institute of Freshwater Ecology and Inland Fisheries, Germany
[c] Irstea, UR MALY, Centre de Lyon-Villeurbanne, F-69616 Villeurbanne, France
[d] Naturalea, Spain
[e] University of Barcelona, Spain
[f] OSUR-Géosciences Rennes, CNRS, UMR 6118, Université de Rennes 1, France
[g] BioSistemika Ltd., Ljubljana, Slovenia
[h] Centre d'Estudis Avançats de Blanes, Consejo Superior de Investigaciones Científicas (CEAB-CSIC), Girona, Spain
[i] Silixa, UK
[j] Department of Earth Sciences, Uppsala University, Sweden
[k] School of Geography, Earth & Environmental Sciences, University of Birmingham, UK
[l] LIST - Luxembourg Institute of Science and Technology
[m] National Institute of Biology, Slovenia
[n] Civil, Environmental and Mining Engineering, The University of Western Australia, Perth, Australia

ARTICLE INFO

Article history:
Received 1 April 2016
Received in revised form 18 June 2016
Accepted 23 June 2016
Available online 28 June 2016

Keywords:
Hydrological tracer
Water
Environmental hydrology
Flowpath
Residence time
Exposure time
Reactive transport
GW-SW interactions
Hot spots
Hot moments
Damköhler
Péclet
HotDam
Ecohydrology
Crossed proxies
Tracer
Groundwater
Surface water
Aquatic ecology

ABSTRACT

Protecting or restoring aquatic ecosystems in the face of growing anthropogenic pressures requires an understanding of hydrological and biogeochemical functioning across multiple spatial and temporal scales. Recent technological and methodological advances have vastly increased the number and diversity of hydrological, biogeochemical, and ecological tracers available, providing potentially powerful tools to improve understanding of fundamental problems in ecohydrology, notably: 1. Identifying spatially explicit flowpaths, 2. Quantifying water residence time, and 3. Quantifying and localizing biogeochemical transformation. In this review, we synthesize the history of hydrological and biogeochemical theory, summarize modern tracer methods, and discuss how improved understanding of flowpath, residence time, and biogeochemical transformation can help ecohydrology move beyond description of site-specific heterogeneity. We focus on using multiple tracers with contrasting characteristics (crossing proxies) to infer ecosystem functioning across multiple scales. Specifically, we present how crossed proxies could test recent ecohydrological theory, combining the concepts of hotspots and hot moments with the Damköhler number in what we call the HotDam framework.

* Corresponding author.
E-mail address: benabbo@gmail.com (B.W. Abbott).

http://dx.doi.org/10.1016/j.earscirev.2016.06.014

Contents

1. Introduction

> "*The waters of springs taste according to the juice they contain, and they differ greatly in that respect. There are six kinds of these tastes which the worker usually observes and examines: there is the salty, the nitrous, the aluminous, the vitrioline, the sulfurous and the bituminous…Therefore the industrious and diligent man observes and makes use of these things and thus contributes to the common welfare.*"
>
> [Georgius Agricola, *De Re Metallica* (1556)]

The central concerns of ecohydrology can be summarized in three basic questions: where does water go, how long does it stay, and what happens along the way (Fig. 1). Answering these questions at multiple spatial and temporal scales is necessary to quantify human impacts on aquatic ecosystems, evaluate effectiveness of restoration efforts, and detect environmental change (Kasahara et al., 2009; Krause et al., 2011; McDonnell and Beven, 2014; Spencer et al., 2015). Despite a proliferation of catchment-specific studies, numerical models, and theoretical frameworks (many of which are detailed and innovative) predicting biogeochemical and hydrological behavior remains exceedingly difficult, largely limiting ecohydrology to single-catchment science (Krause et al., 2011; McDonnell et al., 2007; Pinay et al., 2015).

A major challenge of characterizing watershed functioning is that many hydrological and biogeochemical processes are not directly observable due to long timescales or inaccessibility (e.g. groundwater

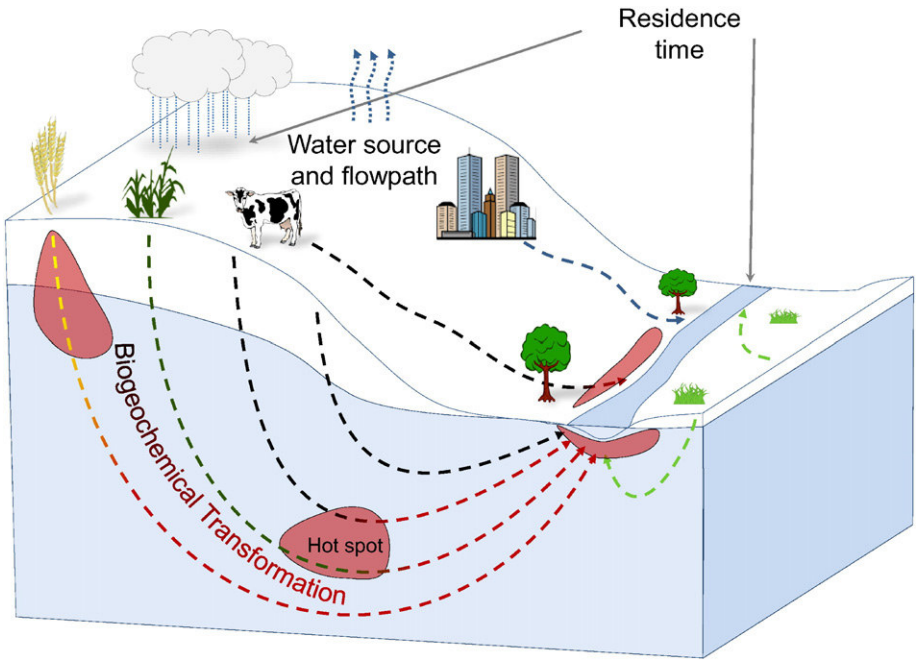

Fig. 1. Conceptual model of a catchment showing the three basic questions of ecohydrology: where does water go, how long does it stay there, and what happens along the way? Dashed lines represent hydrological flowpaths whose color indicates water source and degree of biogeochemical transformation of transported solutes and particulates. The proportion of residence time spent in biogeochemical hot spots where conditions are favorable for a process of interest (McClain et al., 2003) is defined as the exposure time, which determines the retention and removal capacity of the catchment in the HotDam framework (Oldham et al., 2013; Pinay et al., 2015).

circulation or chemical weathering). Consequently, our understanding of many processes depends on how tightly an intermediate, observable parameter (i.e. a tracer or proxy) is associated with the phenomenon of interest. Naturally occurring and injected tracers have been used as proxies of hydrological, ecological, and biogeochemical processes since the founding of those fields (Dole, 1906; Kaufman and Orlob, 1956), and likely since the emergence of thirsty *Homo sapiens* (Agricola, 1556). Methodological advances in ecology, biogeochemistry, hydrology, and other fields including medicine and industry have vastly increased the number of tracers available (Bertrand et al., 2014), and theoretical and computational advances have improved our ability to interpret these chemical and hydrometric proxy data to infer catchment functioning and quantify uncertainty (Beven and Smith, 2015; Davies et al., 2013; Tetzlaff et al., 2015). Multi-tracer approaches have been developed to investigate ecohydrological and biogeochemical functioning unattainable with single proxies (Ettayfi et al., 2012; González-Pinzón et al., 2013; Urresti-Estala et al., 2015). Multi-tracer methods provide tools to address the three fundamental questions in ecohydrology by: 1. Identifying spatially explicit flowpaths, 2. Determining water residence time, and 3. Quantifying and localizing biogeochemical transformation (Fig. 1; Kirchner, 2016a; McDonnell and Beven, 2014; Oldham et al., 2013; Payn et al., 2008; Pinay et al., 2002).

While the diversity and number of tracers applied in different disciplines provide opportunities (Krause et al., 2011), they also represents a logistical and technological challenge for researchers trying to identify optimal methods to test their hypotheses or managers trying to assess ecosystem functioning. Although converging techniques have reduced the methodological distance between hydrological, biogeochemical, and ecological approaches (Frei et al., 2012; Haggerty et al., 2008; McKnight et al., 2015), most work remains discipline specific, particularly in regards to theoretical frameworks (Hrachowitz et al., 2016; Kirchner, 2016a; McDonnell et al., 2007; Rempe and Dietrich, 2014). Furthermore, excitement about what can be measured sometimes eclipses focus on generating general system understanding or testing theoretical frameworks to move beyond description of site-specific heterogeneity (Dooge, 1986; McDonnell et al., 2007).

Several review papers and books have summarized the use of tracers in quantifying hydrological processes, particularly groundwater-surface water exchange (Cook, 2013; Bertrand et al., 2014; Kalbus et al., 2006; Kendall and McDonnell, 2012; Leibundgut et al., 2011; Lu et al., 2014). Here, we expand on this work by exploring how tracers and combinations of tracers (crossed proxies) can reveal ecological, biogeochemical, and hydrological functioning at multiple scales to test general ecohydrological theory and to improve ecosystem management and restoration. Throughout this review we build on an interdisciplinary theoretical framework proposed by Oldham et al. (2013) and Pinay et al. (2015), which combines the ecological concept of hotspots and hot moments (McClain et al., 2003) with the generalized Damköhler number (the ratio of transport and reaction times; Ocampo et al., 2006) in what we call the HotDam framework (Fig. 1). In Section 2, we provide a brief historical perspective on the development of ecohydrological theory. In Section 3, we explore how crossed proxies can be used to better constrain flowpath, residence time, and biogeochemical transformation. Finally, in Section 4, we discuss how ecological and hydrological tracer methods can be applied to generate and test hypotheses of ecohydrological dynamics across scales.

2. A brief history of theories in ecohydrology and watershed hydrology

Over the past 150 years, numerous frameworks and theories have been proposed to conceptualize the transport, transformation, and retention of water and elements in coupled terrestrial-aquatic ecosystems. These frameworks are the basis of our current beliefs about ecohydrological systems and an improved understanding of the historical context of these ideas could illuminate pathways forward (Fisher et al., 2004; McDonnell and Beven, 2014; Pinay et al., 2015). In this section we trace the independent beginnings of catchment hydrology and aquatic ecology in the 19th and 20th centuries followed by a discussion of how increasing overlap and exchange between these fields is contributing to current methodological and conceptual advances.

One of the fundamental goals of catchment hydrology is to quantify catchment water balance, including accounting for inputs from precipitation, internal redistribution and storage, and outputs via flow and evapotranspiration. Early paradigms of catchment hydrology were focused on large river systems or were limited to single components of catchment water balance (e.g. non-saturated flow, in-stream dynamics, overland flow; Darcy, 1856; Horton, 1945; Mulvany, 1851; Sherman, 1932). Computational advances in the mid-20th century allowed more complex mathematical models of watershed hydrology, including the variable source area concept, which replaced the idea of static, distinct flowpaths with the concept of a dynamic terrestrial-aquatic nexus, growing and shrinking based on precipitation inputs and antecedent moisture conditions (Hewlett and Hibbert, 1967). Analysis of catchment hydrographs and water isotopes resolved the apparent paradox between the rapid response of stream discharge to changes in water input (celerity) and the relatively long residence time of stream water, by demonstrating that most of the water mobilized during storms is years or even decades old (Martinec, 1975). Further modeling and experimental work investigating heterogeneity in hydraulic conductivity (preferential flow) and transient storage allowed more realistic simulation of flowpaths at point and catchment scales, providing a scaling framework for predicting temporally-variant flow (Bencala and Walters, 1983; Beven and Germann, 1982; McDonnell, 1990). We note, however, that characterizing preferential flow at multiple scales remains an active subject of research and a major challenge (Beven and Germann, 2013).

Analogous to the hydrological goal of quantifying water balance, a major focus of ecohydrology is closing elemental budgets, including accounting for inputs from primary production, internal redistribution due to uptake and mineralization, and outputs via respiration and lateral export. Early descriptive work gave way to quantitative ecological modelling, using the concept of ecological stoichiometry to link energetic and elemental cycling (Lotka, 1925; Odum, 1957; Redfield, 1958). Work on trophic webs and ecosystem metabolism generated understanding of carbon and nutrient pathways within aquatic ecosystems (Lindeman, 1942) and across terrestrial-aquatic boundaries (Hynes, 1975; Likens and Bormann, 1974). The nutrient retention hypothesis related ecosystem nutrient demand to catchment-scale elemental flux in the context of disturbance and ecological succession (Vitousek and Reiners, 1975), and experimental watershed studies tested causal links between hydrology and biogeochemistry such as evapotranspiration and elemental export (Likens et al., 1970). A major conceptual and technical breakthrough was the concept of nutrient spiraling, which quantitatively linked biogeochemistry with hydrology, incorporating hydrological transport with nutrient turnover in streams (Newbold et al., 1981; Webster and Patten, 1979). In combination with the nutrient retention hypothesis, nutrient spiraling allowed consideration of temporal variability on event, seasonal, and interannual scales for coupled hydrological and biogeochemical dynamics (Mulholland et al., 1985), leading to its application in soil and groundwater systems (Wagener et al., 1998). The telescoping ecosystem model generalized the concept of nutrient spiraling to include any material (e.g. carbon, sediment, organisms), visualizing the stream corridor as a series of cylindrical vectors with varying connectivity depending on hydrological conditions and time since disturbance (Fisher et al., 1998). These hydrological and biogeochemical studies helped re-envision the watershed concept as a temporally dynamic network of vertical, lateral, and longitudinal exchanges, rather than discrete compartments or flowpaths.

The 21st century has seen a continuation of the methodological convergence of catchment hydrology and biogeochemistry (Godsey et al.,

2009; Oldham et al., 2013; Zarnetske et al., 2012). Specifically, two technological advances have strongly influenced the creation and testing of ecological and hydrological theory: 1. Hydrological and biogeochemical models have become vastly more powerful and complex (Davies et al., 2013; McDonnell et al., 2007; McDonnell and Beven, 2014), and 2. High frequency datasets of hydrological and biogeochemical parameters have come online thanks to advances in remote and environmental sensors (Kirchner et al., 2004; Krause et al., 2015; McKnight et al., 2015). Increased computing power has allowed the development of bottom-up, mechanistic models that simulate chemical reactions and water exchange based on realistic physics and biology (Beven and Freer, 2001; Frei et al., 2012; Trauth et al., 2014; Young, 2003). At the same time, more extensive and intensive datasets have allowed the development of top-down, black-box models based on empirical or theoretical relationships between catchment characteristics and biogeochemistry (Godsey et al., 2010; Jasechko et al., 2016; Kirchner, 2016b). While there has been a lively discussion of the merits and drawbacks of these approaches, developing models that are simultaneously physically realistic and capable of prediction remains difficult (Beven and Freer, 2001; Dooge, 1986; Ehret et al., 2014; Kirchner, 2006; Kumar, 2011; McDonnell et al., 2007).

Recently, several frameworks have been proposed to integrate biogeochemical and hydrological dynamics across temporal and spatial scales. Oldham et al. (2013) and Pinay et al. (2015) proposed complementary frameworks that combine the concept of temporally variable connectivity (hot spots and hot moments) with the Damköhler ratio of exposure to reaction times (Fig. 1; Detty and McGuire, 2010; McClain et al., 2003; Ocampo et al., 2006; Zarnetske et al., 2012). The hot spots and hot moments concept is based on the observation that biological activity is not uniformly distributed in natural systems, but that transformation tends to occur where convergent flowpaths bring together reactants or when isolated catchment compartments become reconnected hydrologically (Collins et al., 2014; McClain et al., 2003; Pringle, 2003). This concept has been demonstrated in terrestrial and aquatic ecosystems (Abbott and Jones, 2015; Harms and Grimm, 2008; Vidon et al., 2010) and is appealing because using the predicted or measured frequency of hot spots and hot moments based on landscape characteristics allows for more accurate scaling compared to extrapolation of average rates (Detty and McGuire, 2010; Duncan et al., 2013). The generalized Damköhler number estimates the reaction potential of a catchment or sub-catchment component and is defined as:

$$Da = \frac{\tau_E}{\tau_R}$$

where τ_E is the exposure time defined as the portion of total transport time when conditions are favorable for a specific process, and τ_R is a characteristic reaction time for the process of interest (Oldham et al., 2013). When $Da > 1$ there can be efficient removal or retention of the chemical reactant of interest, whereas when $Da < 1$, the system is transport dominated in regards to that reactant (Fig. 2). *Da* varies systematically with hydrological flow, approaching infinity in isolated components when transport is near zero, and typically decreasing when the ratio of advective transport rate to diffusive transport rate (the Péclet number) increases (Oldham et al., 2013).

The generalized *Da* represents a scalable metric of biogeochemical transformation and has been shown to explain variation in the capacity for catchments or catchment components to remove or retain carbon and nutrients (Fig. 3; Ocampo et al., 2006; Oldham et al., 2013; Zarnetske et al., 2012). Conceptually the hot spots and hot moments concept is concerned with the "where" and "when" of hydrological connectivity and biogeochemical activity while *Da* estimates the "how much" (Fig. 1). The HotDam framework combines these concepts in an effort to provide a realistic and predictive approach to localize and quantify biogeochemical transformation (Oldham et al., 2013; Pinay et al., 2015). While it is straightforward to understand the relevance of exposure time and connectivity, measuring these parameters in natural systems can be extremely challenging, requiring the careful use of multiple tracers. In the following section we outline how tracers can be used to constrain flowpath, residence and exposure times, and biogeochemical transformation at multiple scales to generate process knowledge across multiple catchments.

3. Crossing proxies for flowpath, residence time, and biogeochemical transformation

Almost any attribute of water (e.g. temperature, isotopic signature, hydrometric measures such as hydrograph analysis) or material transported with water (e.g. solutes, particles, organisms) carries information about water source, residence time, or biogeochemical transformation and can be used as a tracer (Table 1; Fig. 4). Tracers vary in their specificity (level of detail for the traced process or pathway), detectability (limit of detection), and reactivity (stability or durability in a given environment). In practice, there are no truly conservative tracers but instead a gradient or spectrum of reactivity. Tracers can be reactive biologically, chemically, or physically, and all these possible interactions need to be accounted for when interpreting results. Compounds that are not used as nutrients or energy sources by biota or which occur at concentrations in excess of biological demand tend to exhibit less biological reactivity, though they may still be chemically or physically reactive. Reactivity is contextual temporally and spatially, particularly in regards to transport through heterogeneous environments typical of the terrestrial-aquatic gradient. Variations in redox conditions and elemental stoichiometry mean that the same substance may be

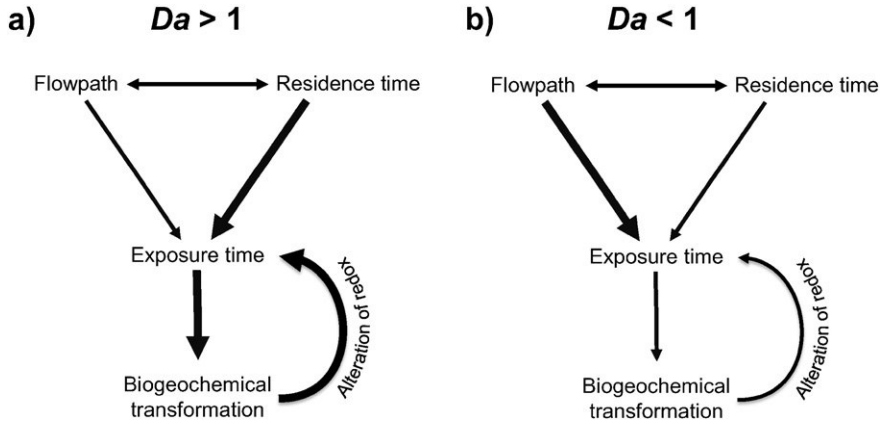

Fig. 2. Schematic relationships between water transport (flowpath and residence time) and biogeochemical processes such as respiration and assimilation when a) $Da > 1$ (diffusion- or reaction-dominated conditions), and b) $Da < 1$ (advection- or transport-dominated conditions). *Da* is the generalized Damköhler number: the ratio of exposure and reaction time scales.

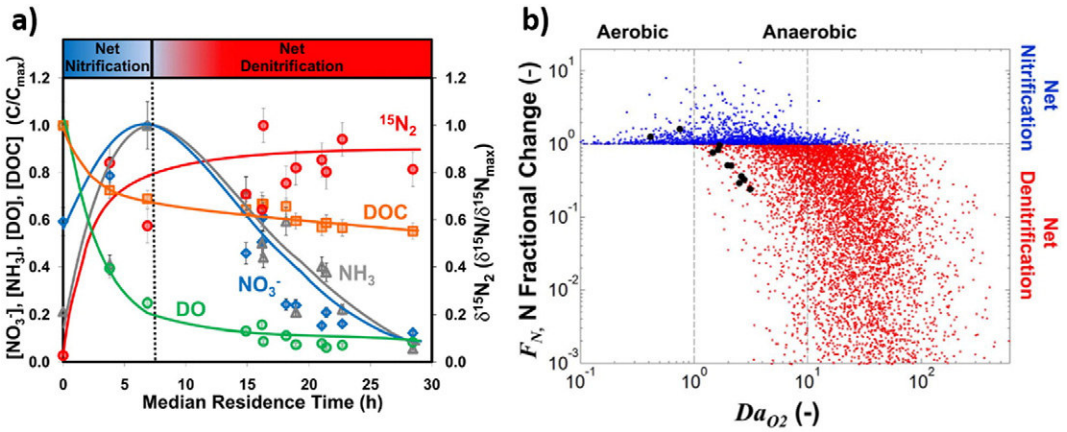

Fig. 3. Examples of the links between residence time, reaction rate, and exposure time. a) Normalized values of dissolved organic carbon (DOC), dissolved oxygen (DO), isotopic signature, and reactant concentration as water passes through a gravel bar. Reproduced from Zarnetske et al. (2011). b) Modeled prevalence of nitrification and denitrification as a function of the ratio of transit to reaction times (i.e. the Damköhler number; *Da*). Reproduced from Zarnetske et al. (2012).

transported conservatively for a portion of its travel time and non-conservatively for another. Often, the very reactivity that renders a tracer unsuitable for conservative duty imparts useful information about interactions and transformations (Haggerty et al., 2008; Lambert et al., 2014). Combining two or more tracers with contrasting properties (crossing proxies) allows partitioning of multiple processes such as dilution and biological uptake (Covino et al., 2010; Bertrand et al., 2014), autotrophic and heterotrophic denitrification (Frey et al., 2014; Hosono et al., 2014; Pu et al., 2014), or aerobic and anaerobic production of dissolved organic matter (DOM; (Lambert et al., 2014). The fact that some tracers are more reactive to certain environmental conditions means that combining a selectively reactive tracer with a generally conservative tracer allows the quantification of exposure time (Haggerty et al., 2008; Oldham et al., 2013; Zarnetske et al., 2012). A final practical distinction in tracer methods is between physicochemical signals that are present within an environment (*environmental tracers*) and substances that are added experimentally (*injected tracers*). Experimentally added tracers have alternatively been referred to as applied or artificial tracers (Leibundgut et al., 2011; Scanlon et al., 2002), but we refer to them as injected tracers since many environmental tracers are anthropogenic (artificial).

3.1. Water source and flowpath: where does water go when it rains?

Besides being one of the existential questions of ecohydrology, asking where water came from and where it has traveled has direct implications for management issues including mitigating human impacts on water quality (Hornberger et al., 2014; Kirkby, 1987) and predicting the movement of nutrients, pollutants, and organisms within and out of the system (Chicharo et al., 2015; Hornberger et al., 2014; Mockler et al., 2015). The course that water takes through a catchment strongly influences residence time and biogeochemical transformation, because where water goes largely determines how long it stays there and what sort of biogeochemical conditions it encounters (Figs. 1, 5; Kirkby, 1987). Flowpaths are influenced by the timing and location of precipitation in combination with catchment characteristics such as vegetation, soil structure, flora and fauna, topography, climate, and geological conditions (Baranov et al., 2016; Beven and Germann, 1982; Blöschl, 2013; Mendoza-Lera and Mutz, 2013). Depending on the purposes of the study, flowpaths can be defined conceptually (e.g. surface, soil, riparian, groundwater) or as spatially-explicitly pathlines describing individual water masses (Fig. 5; Kolbe et al., 2016; Mulholland, 1993). Because flowpaths are temporally dynamic (Blöschl et al., 2007; Hornberger et al., 2014; McDonnell, 1990; Strohmeier et al., 2013), considering seasonal and event-scale variation in whatever tracers are being used is essential (Kirkby, 1987). Evapotranspiration is in some ways a special case, as a dominant flowpath in many environments, and also as a process that influences flowpaths of residual water, influencing soil moisture, groundwater circulation, and water table position (Ellison and Bishop, 2012; Soulsby et al., 2015).

3.1.1. Water isotopes

For a tracer to be an effective proxy of flowpath, it should have high specificity (sufficient degrees of freedom to capture the number of conceptual or explicit flowpaths) and low reactivity over the relevant time period. Perhaps most importantly, it should have similar transport characteristics to water. This is an important consideration because all solute and particulate tracers have different transport dynamics than water, particularly when traveling through complex porous media such as soil, sediment, or bedrock. Even chloride and bromide, the most commonly used "conservative" tracers, can react and be retained by organic and mineral matrices, sometimes resulting in substantial temporal or spatial divergence from the water mass they were meant to trace (Bastviken et al., 2006; Kung, 1990; Mulder et al., 1990; Nyberg et al., 1999; Risacher et al., 2006). Consequently the most effective tracer of water source and flowpath is the isotopic signature of the water itself. Water isotopes have been used to trace storm pulses through catchments (Gat and Gonfiantini, 1981), identify areas of groundwater upwelling (Lewicka-Szczebak and Jędrysek, 2013), and detect environmental change such as thawing permafrost (Abbott et al., 2015; Lacelle et al., 2014). Stable and radioactive isotopes of hydrogen (deuterium and tritium) and oxygen (^{16}O and ^{18}O) are commonly used as environmental tracers but have also been injected (Kendall and McDonnell, 2012; Nyberg et al., 1999; Rodhe et al., 1996). The isotopic signature of water varies based on type and provenance of individual storm systems, climatic context (e.g. distance from ocean, elevation, and latitude), degree of evapotranspiration, and by water source in general (e.g. precipitation or groundwater), allowing the separation of water sources at multiple spatial and temporal scales (Jasechko et al., 2016; Kirchner, 2016a; McDonnell et al., 1990; Rozanski et al., 1993). While water isotopes can behave conservatively at some spatiotemporal scales and in some environments (Abbott et al., 2015; Soulsby et al., 2015), potential alteration of isotopic signature from evaporation, chemical reaction, and plant uptake must be accounted for. If water source and flowpath can be determined with water isotopes, other water chemistry parameters can be used to estimate rates of weathering and biological transformation, or be used as an independent evaluation of model predictions (Barthold et al., 2011; McDonnell and Beven, 2014). Because water isotopes do not have very high specificity (multiple water sources can have the same signature), it is important to characterize site-specific water sources or to cross with another proxy to appropriately solve mixing equations. The recent development of laser

Table 1
List of tracers and their attributes.

Tracer	Type	Specificity	Detectability	Reactivity	Flowpath	Residence time	Biogeochemical transformation	References
Solute								
Dissolved gases								
Propane	I	High	High	volatile	×			Wallin et al. (2011), Soares et al. (2013)
Chlorofluorocarbons (CFCs)	E/I	Intermediate	High	Low (CFC-12, 113) Moderate (CFC-11)		×	×	Lovelock et al. (1973), Thiele and Sarmiento (1990), Thompson et al. (1974)
Sulfur hexafluoride (SF_6)	E/I	Intermediate	High	Very Low		×		Wilson and Mackay (1996)
Radionuclides								
^{3}H, ^{3}He, ^{39}Ar, ^{14}C, ^{234}U, ^{81}Kr, ^{36}Cl	E/I	Intermediate	High	Low		×		Solomon et al. (1998), Lu et al. (2014)
Dissolved organic matter (DOM)	E	High	High	High	×		×	Abbott et al. (2014), Quiers et al. (2013), Baker (2005)
$\delta^{13}C$, $\delta^{14}C$	E/I	Intermediate	High	High	×			Leith et al. (2014), Raymond and Bauer (2001), Schiff et al. (1990)
Chemical properties	E	High	High	High	×		×	Risse-Buhl et al. (2013)
Optical properties	E	High	High	High	×			Fellman et al. (2010)
Fluorescent dyes								
Fluorescein, sodium-fluorescein (uranine)	I	High	High	Low	×	×		Käss et al. (1998), Smart and Laidlaw (1977), Leibundgut et al. (2009)
Rhodamin WT	I	High	High	Low	×	×		Leibundgut et al. (2009), Wilson et al. (1986)
Resazurin	I	High	High	High			×	McNicholl et al. (2007), Haggerty et al. (2008)
Inorganic ions								
Cl^{-}, Br^{-}	I	High	High	Very Low		×		Käss et al. (1998), Bero et al. (2016), Frey et al. (2014)
Other anions and cations								
Rare Earth elements								
e.g. Cerium	E	High	High	Variable	×		×	Davranche et al. (2005), Dia et al. (2000), Gruau et al. (2004), Pourret et al. (2009)
Metabolic products, substrates								
O_2	E		High	High		×	×	Odum (1957), McIntire et al. (1964), Demars et al. (2015)
CO_2, DIC	E/I		High	High			×	Lambert et al. (2014), Wright and Mills (1967)
PO_4^{3-}	E/I		High	High			×	Mulholland et al. (1990), Stream Solute Workshop (1990)
SO_4^{2-}	E/I		High	High			×	Hosono et al. (2014)
DOC (e.g. Acetate)	E/I	Intermediate	Intermediate	High	×		×	Shaw and McIntosh (1990), Baker et al. (1999)
Stable isotopes								
$\delta^{15}N$, $\delta^{18}O$, $\delta^{13}C$, $\delta^{33}P$, $\delta^{34}S$	E/I		High	High		×	×	Newbold et al. (1981), Sigman et al. (2001), Mulholland et al. (2009)
Strontium (^{87}Sr, ^{86}Sr)	E	Intermediate	Intermediate	Very Low	×			Graustein (1989), Wang et al. (1998)
Particulate								
Artificial sweeteners								
Acersulfame-K, sucralose	E	High	High	Very Low	×			Buerge et al. (2009), Lubick (2009), Scheurer et al. (2009)
Pharmaceuticals drugs								
Carbamazepine, sulfamethoxazole, and diclofenac, caffeine, triclosan, and naproxen	E	High	High	High	×			Arvai et al. (2014), Lubick (2009), Riml et al. (2013), Andreozzi et al. (2002), Clara et al. (2004), Kurissery et al. (2012), Durán-Álvarez et al. (2012), Buerge et al. (2003), Liu et al. (2014), Chefetz et al. (2008)
Particles								
Chaff, nano-particles, clay, kaolinite, fluorescent microspheres	I	High	High	variable		×		Davis et al. (1980), Packman et al. (2000a, 2000b), Arnon et al. (2010)
Synthetic DNA (coated or naked)	I	High	High	Low		×		Foppen et al. (2013), Mahler et al. (1998), Sharma et al. (2012)
Particulate organic matter (POM)	E/I	Intermediate	High	variable	×	×	×	Newbold et al. (2005), Trimmer et al. (2012), Drummond et al. (2014)
Macroinvertebrates	E	Intermediate	High		×	×	×	Dole-Olivier and Marmonier (1992), Marmonier et al. (1992), Capderrey et al. (2013), Blinn et al. (2004)
Terrestrial diatoms	E	High	High	Moderate	×			Pfister et al. (2009), Klaus et al. (2015), Tauro et al. (2015), Klaus et al. (2015), Naicheng Wu et al. (2014), Coles et al. (2015)
Bacteria								
Fecal coliforms	E	High	High	Moderate	×			Leclerc et al. (2001), Stapleton et al. (2007), Characklis et al. (2005), Weaver et al. (2013)
Non coliforms	E	High	High	Moderate	×		×	Bakermans et al. (2002), Bakermans and Madsen (2002), Jeon et al. (2003)
Virus								
Pathogens	E	High	High	High	×	×		Harwood et al. (2014), Updyke et al. (2015)
Bacteriophages	E	High	High	High	×	×		Keswick et al. (1982), Rossi et al. (1998), Goldscheider et al. (2007), Shen et al. (2008), Hunt et al. (2014)

Table 1 (*continued*)

Tracer	Type	Specificity	Detectability	Reactivity	Flowpath	Residence time	Biogeochemical transformation	References
Other								
Water temperature	E/I	Intermediate	Low	High	×	×		Carslaw and Jaeger (1986), Stallman (1965), Rau et al. (2014), Hannah and Garner (2015)
Water isotopes (^{3}H, δ^{2}H, δ^{18}O)	E/I	Intermediate	High	Very Low	×	×		Rodhe (1998)

spectrometers has substantially decreased the cost of water isotope analysis, opening up new possibilities for spatially extensive or high frequency measurements (Jasechko et al., 2016; Lis et al., 2008; McDonnell and Beven, 2014).

3.1.2. Solute tracers: pharmaceuticals, ions, dyes, and DOM

While solutes are typically more reactive and have different transport dynamics from the water that carries them, the sheer number of different species that can be measured allows for great specificity in determining water flowpaths. A wide variety of solutes including natural ions, anthropogenic pollutants, fluorescent dyes, and dissolved carbon have been used as environmental tracers to determine water source and flowpath (Hoeg et al., 2000; Kendall and McDonnell, 2012). Solute concentrations and isotopic signatures can convey complementary information, for example strontium (Sr) concentration can distinguish surface and subsurface water, while the $^{87}Sr/^{86}Sr$ ratio which varies between bedrock formations, can reveal regional provenance (Ettayfi et al., 2012; Graustein, 1989; Wang et al., 1998). When many solute concentrations are available, correlated parameters are often combined into principal components before determining water sources via end member mixing analysis (Christophersen and Hooper, 1992). While end member mixing analysis is widely used and provides straightforward estimates of conceptual flowpaths, it is sensitive to the assignment of end members, the selection of tracers, and the assumption of conservancy in solute behavior (Barthold et al., 2011). As always, using multiple tracers of different types (e.g. stable isotopes and solutes) results in more robust and reliable mixing models (Bauer et al., 2001).

Pharmaceuticals and other synthetic compounds have contaminated most aquatic environments and are increasingly being used to trace agricultural and urban wastewater sources and flowpaths (Durán-Álvarez et al., 2012; Liu et al., 2014; Roose-Amsaleg and Laverman, 2015; Stumpf et al., 1999; Ternes, 1998; Tixier et al., 2003). Analyses for many of these compounds have become routine due to emerging concern for human and ecosystem health, bringing down costs and improving detectability (Andreozzi et al., 2002; Clara et al., 2004; Kurissery et al., 2012). Many of these compounds are bioactive or adsorb to

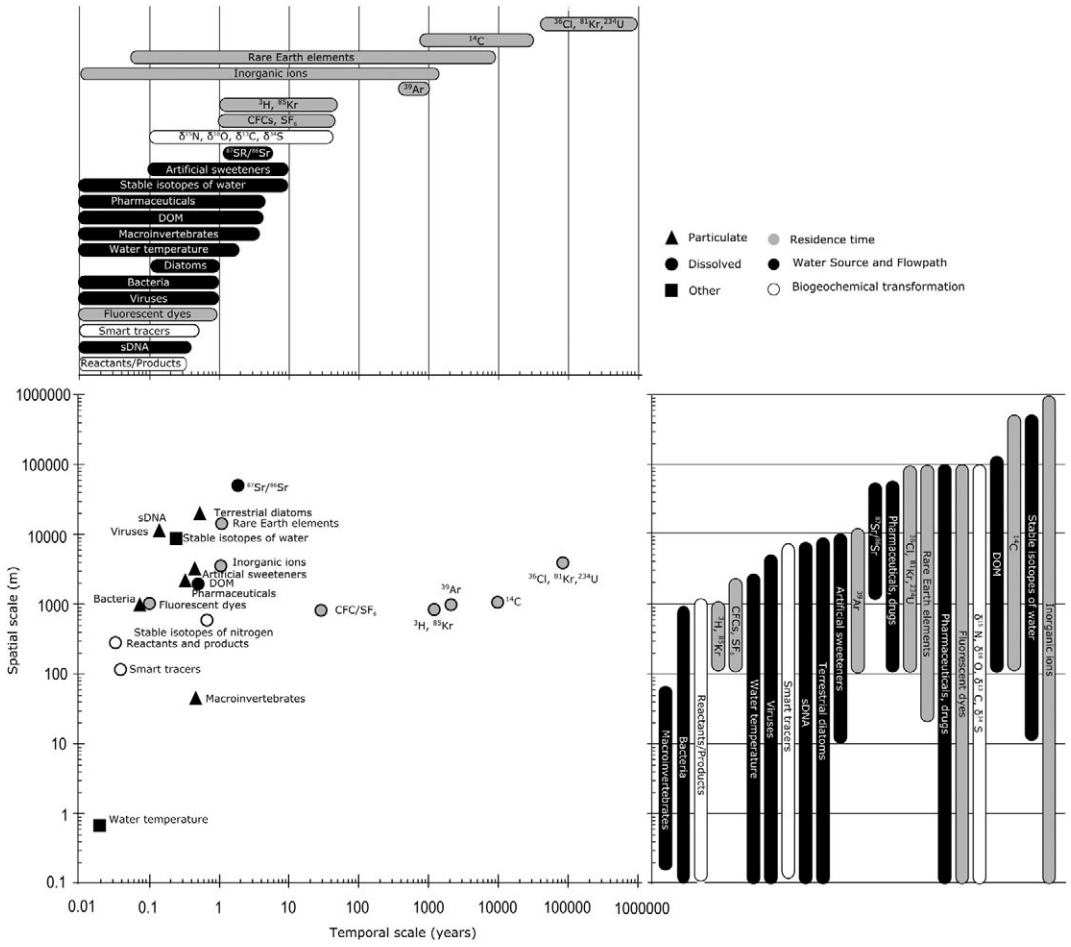

Fig. 4. A variety of ecohydrological tracers organized by temporal and spatial scale. The range of scales reported in the literature for each tracer or group of tracers is indicated by the bars with the points representing the typical or most common scales of use. Shading represents fundamental ecohydrological question (where does water go, how long does it stay, and what happens along the way) and shape represents tracer type.

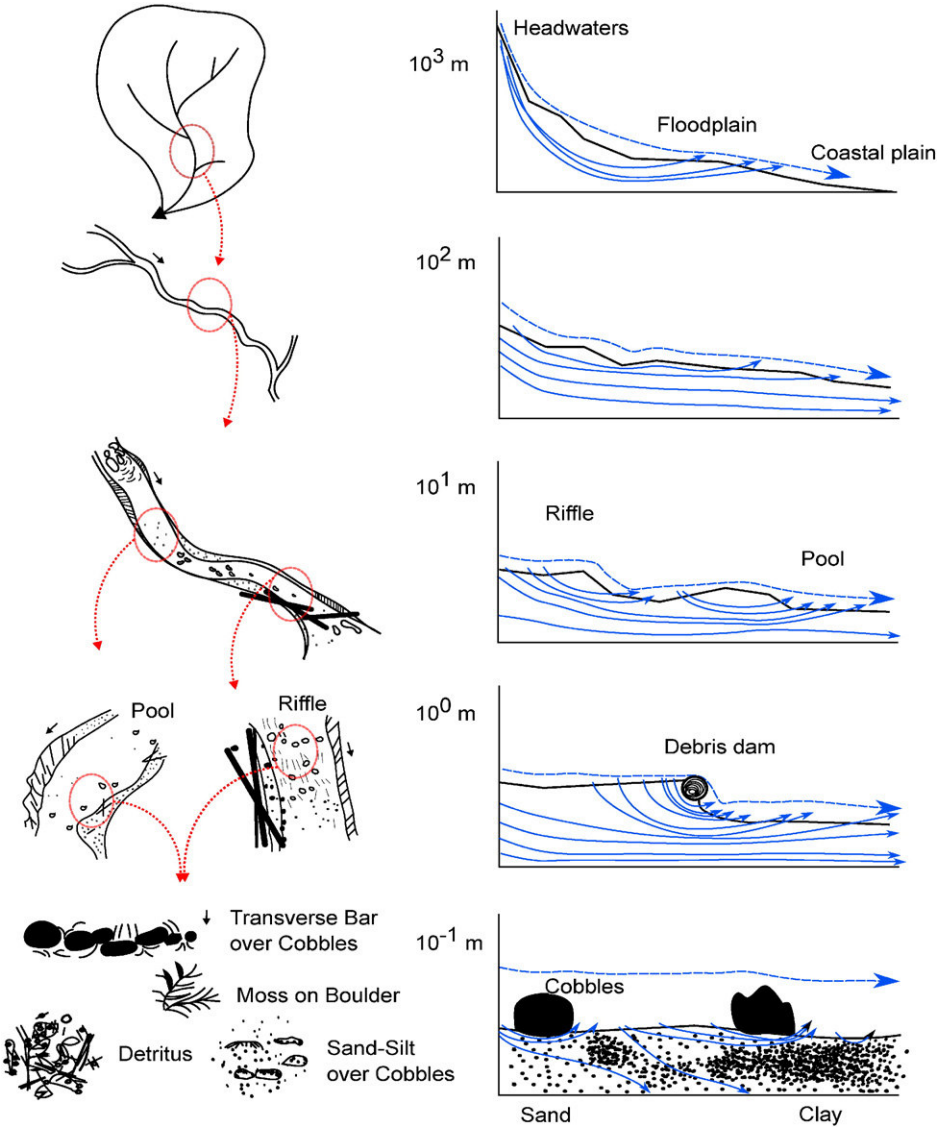

Fig. 5. Hierarchical spatial scales from an ecohydrological perspective for various catchment components. Relevant physical and ecological controls on flowpath, residence time, and biogeochemical reaction often change with scale, requiring the use of tracers with different characteristics. Adapted from Frissell et al. (1986).

sediment (e.g. caffeine, triclosan, and naproxen), limiting most applications to small temporal and spatial scales (Buerge et al., 2003; Chefetz et al., 2008; Durán-Álvarez et al., 2012). However, artificial sweeteners (e.g. acesulfame-K and sucralose) and some drug compounds (e.g. carbamazepine, sulfamethoxazole, and diclofenac) appear to be resistant to degradation for several weeks under a range of conditions and could be used as biomarkers of human activity (Arvai et al., 2014; Buerge et al., 2009; Lubick, 2009; Riml et al., 2013; Scheurer et al., 2009). The biodegradability of some pharmaceuticals (e.g. tetracycline) decreases with redox potential (Cetecioglu et al., 2013), meaning their concentration relative to more resistant compounds could be used to quantify anoxia, though to our knowledge this approach has not yet been used.

In addition to environmental tracers that are already present in a system, experimentally injected solutes have long been used to quantify flowpath and water source. Synthetic fluorescent dyes such as fluorescein have been used since the end of the 19th century and are still widely used today to test connectivity and water transfer (Flury and Wai, 2003; Smart and Laidlaw, 1977). Fluorescent dyes express a range of reactivity and offer outstanding detectability and specificity, with some dyes such as fluorescein and rhodamine WT detectable at concentrations in the parts per trillion range (Turner et al., 1994). Most dyes suitable for duty as flowpath tracers have sulfonic acid groups and are synthesized from sodium salts to increase solubility in water (Cai and Stark, 1997; Leibundgut et al., 2011). Emission wavelengths are characteristic for each dye, making it possible to combine multiple dyes with different properties (Haggerty et al., 2008; Lemke et al., 2014). Drawbacks to fluorescent dyes include a relatively small number of suitable dyes (less than ten families), sensitivity to pH and temperature, adsorption to sediment, and relatively high cost depending on how much dye is needed (Leibundgut et al., 2011).

Dissolved carbon compounds are some of the most versatile solute tracers and also some of the most complex. Unlike the single-compound tracers discussed above, DOM consist of thousands of different compounds with distinct properties (Cole et al., 2007; Zsolnay, 2003) and turnover times that can vary from minutes to millennia (Abbott et al., 2014; Catalá et al., 2015; Hansell and Carlson, 2001). DOM chemical composition, isotopic signature, optical properties, and stoichiometry constitute a highly detailed signature or fingerprint that can be used to determine water source and flowpath (Clark and Fritz, 1997; Schaub and Alewell, 2009). Using multiple DOM characteristics allows DOM to effectively be crossed with itself, e.g. simultaneously determining flowpath, residence time, and biogeochemical transformation (Chasar et al., 2000; Helton et al., 2015; Palmer et al., 2001; Raymond

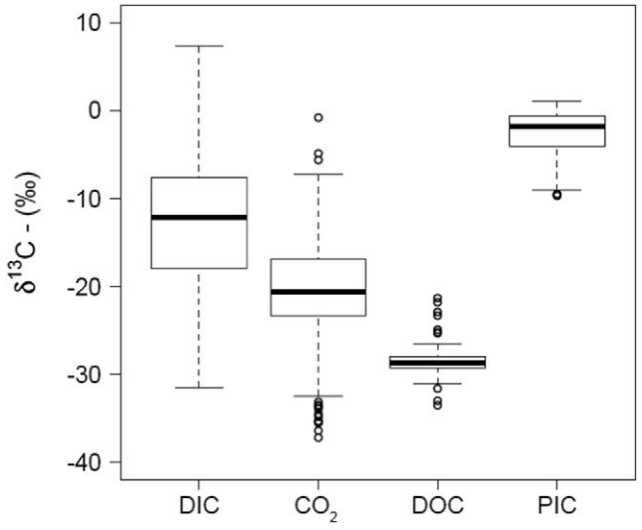

Fig. 6. A meta-analysis including unpublished data of $\delta^{13}C$ values observed in streams and rivers across the globe for dissolved inorganic carbon (DIC), particulate inorganic carbon (PIC), dissolved organic carbon (DOC), and dissolved CO_2. Note that mostly C_3 plant dominated catchments are included.

and Bauer, 2001). While DOM has incredible specificity, it is the primary food and nutrient source for microbial food webs and is therefore highly reactive (Evans and Thomas, 2016; Jansen et al., 2014). Nonetheless, at the catchment scale, DOM concentration is often assumed to be conservative and is regularly included with other solutes to determine water source in end member mixing analysis (Larouche et al., 2015; Morel et al., 2009; Striegl et al., 2005; Voss et al., 2015). Stable and radioactive carbon isotopes of DOM, particulate organic matter (POM), and dissolved inorganic carbon (DIC) have been used to distinguish surface water from groundwater as well as determine connectivity between terrestrial and aquatic environments (Doucett et al., 1996; Farquhar and Richards, 1984; Marwick et al., 2015). Because the $\delta^{13}C$ of dissolved carbon derived from algae and terrestrial plants differs in some environments, $\delta^{13}C$ of dissolved carbon can be used to separate terrestrial and aquatic water and carbon sources (Fig. 6; Mayorga et al., 2005; Myrttinen et al., 2015; Rosenfeld and Roff, 1992; Tamooh et al., 2013; Telmer and Veizer, 1999). The $\Delta^{14}C$ of DOM and POM, an indicator of time since fixation from the atmosphere, has been used to separate depth of flowpaths (e.g. modern surface soil carbon versus deeper, older sources) and also as a general indicator of agricultural and urban disturbance (Adams et al., 2015; Butman et al., 2014; Vonk et al., 2010).

There are many methods to characterize DOM molecular composition (e.g. exclusion chromatography, nuclear magnetic resonance, thermally assisted hydrolysis and methylation-gas chromatography-mass spectrometry, and Fourier transform infrared spectroscopy-mass spectrometry) and optical properties (e.g. ultraviolet-visible absorption spectra and fluorescence spectroscopy; Jaffé et al., 2012; Jeanneau et al., 2014; Spencer et al., 2015). Often the post-processing of these measurements is as technically involved as the measurements themselves (Chen et al., 2003; Jaffé et al., 2008; Stedmon and Bro, 2008), and interpreting the ecological relevance of the outputs of these analyses remains a major challenge and area of active research (Fellman et al., 2009; Huguet et al., 2009; Spencer et al., 2015; Zsolnay, 2003). Consequently, analyses of DOM composition and optical properties are often most useful when paired with field or laboratory assays of DOM reactivity or biodegradability (McDowell et al., 2006; Vonk et al., 2015). The recent development of field-deployable fluorometers and spectrometers has allowed real-time monitoring of DOM characteristics to determine changes in water source and flowpath (Baldwin and Valo, 2015; Downing et al., 2009; Fellman et al., 2010; Khamis et al., 2015; Sandford et al., 2010; Saraceno et al., 2009). For example total fluorescence has been used to trace infiltration of surface water into karst systems and protein-like fluorescence has been used as an indicator of fecal bacteria and DOM biodegradability (Balcarczyk et al., 2009; Baldwin and Valo, 2015; Quiers et al., 2013). Excitation-emission matrices of DOM (Chen et al., 2003) have been used to trace landfill leaching into rivers, with signals detectable at dilutions of 100–1000 fold, suggesting this detection method is fast and cost-effective for river managers and water quality regulators (Baker, 2005; Harun et al., 2015, 2016).

3.1.3. Particulate tracers: synthetic particles, bacteria, viruses, and invertebrates

Particulate tracers such as chaff and sediment have been used for thousands of years to make invisible flowpaths visible (Davis et al., 1980). Bacteria were first used to trace water source before the advent of germ theory when John Snow traced the London Broad Street cholera outbreak to sewage-contaminated water from the Thames and local cesspits (Snow, 1855). More recently, a wide range of particles including biomolecules, viral particles, bacteria, biofilms, diatoms, colloids, and macroinvertebrates have been implemented to trace flow and water source (Capderrey et al., 2013; Foppen et al., 2013; Mendoza-Lera et al., 2016; Rossi et al., 1998). Particles can have extremely high specificity and detectability and have been used in a variety of environments including flowing surface waters, lakes, groundwater, and marine environments (Ben Maamar et al., 2015; Garneau et al., 2009; Harvey and Ryan, 2004; Vega et al., 2003). While particles travel through complex media differently than the water that moves them, this is an advantage when the goal is to trace particulate transport such as sediment or POM. Because POM is an important carbon and nutrient source in aquatic ecosystems (Pace et al., 2004; Vannote et al., 1980), tracing its transport and accumulation provides insight into the development of hot spots and moments (Drummond et al., 2014; Vidon et al., 2010); see Section 3.3).

Bacteria are the most common particulate tracer, with fecal coliforms routinely used to identify human contamination of water sources (Leclerc et al., 2001). The purposeful use of bacteria as tracers began with an antibiotic-resistant strain of the bacterium *Serratia indica* which was readily assayed by its bright red colonies on nutrient agar media (Ormerod, 1964). Subsequent applications combined actively reproducing *Serratia indica* with dormant *Bacillus subtilis* spores that behaved as conservative tracers, to model dispersion and transit times of a field of sewage discharge to a coastal zone (Pike et al., 1969). Starting in the 1970s, improved imaging techniques allowed viruses, particularly bacteriophages, to be used as tracers of groundwater and ocean circulation (Hunt et al., 2014). Because of their small size, high host-specificity, low cost of detection, and resistant physical structure, bacteriophages tend to perform better than bacteria or yeasts, particularly in groundwater applications (Rossi et al., 1998; Wimpenny et al., 1972), suggesting that bacteriophages could fill an important gap in the current hydrogeology toolbox. Improvements in quantitative polymerase chain reaction techniques and biosynthesis technologies have lowered costs of bacterial and viral analyses and opened the way for a new generation of high specificity, high detectability tracers.

Still smaller than bacteriophages, environmental and synthetic DNA (eDNA and sDNA, respectively) have extremely high specificity and detectability and relatively low reactivity (Deiner and Altermatt, 2014; Foppen et al., 2013). While extracellular eDNA has primarily been used for species detection in freshwater environments (Ficetola et al., 2008; Vorkapic et al., 2016), it also has potential as a hydrologic tracer, with eDNA from lacustrine invertebrates used to trace lake water up to 10 km from its source (Deiner and Altermatt, 2014). Tracer sDNA is produced by automatic oligonucleotide synthesis and is normally short (less than 100 nucleotides), which allows approximately limitless unique sequences ($4\ \text{nucleotides}^{100} = 1.61 \times 10^{60}$). Stop codons distinguish the sDNA from eDNA, and injected sDNA is analyzed by quantitative polymerase chain reaction with custom primers. sDNA has been used to trace sediment transport when bound with montmorillonite

clay (Mahler et al., 1998) and in combination with magnetic nano-particles (e.g. polylactic acid microspheres and paramagnetic iron particles) to enhance recoverability and durability in the environment (Sharma et al., 2012). Though high tracer losses (50 to 90%) can occur immediately after injection, the remaining sDNA shows transport dynamics similar to chloride or bromide and is stable for weeks to months (Foppen et al., 2011, 2013; Sharma et al., 2012).

Diatoms (eukaryotic microalgae; 2–500 μm) have long been used as indicators of water quality (Rushforth and Merkley, 1988) and more recently as tracers of flowpath (Pfister et al., 2009). The timing and abundance of the arrival of terrestrial diatoms to the stream channel can indicate the source of stormflow and the extent and duration of hydrologic connectivity across the hillslope-riparian-stream continuum (Pfister et al., 2009). Because some terrestrial diatoms are associated with certain landscape positions or land-use types, this tracer has high specificity, though sample analysis requires substantial expertise (Martínez-Carreras et al., 2015; Naicheng Wu et al., 2014). The possibility of using quantitative polymerase chain reaction techniques to automate diatom identification and quantification could increase the availability and applications of this approach.

Finally, macroinvertebrates (aquatic insects, crustaceans, mollusks, and worms) have been used as indicators of ecosystem health and to delineate surface and groundwater flowpaths (Boulton et al., 1998; Marmonier et al., 1993). The presence or absence of individual macroinvertebrate species can be used to identify zones of hyporheic exchange as well as to distinguish upwelling from down welling zones both at the bedform and reach scales (Blinn et al., 2004; Capderrey et al., 2013; Dole-Olivier and Marmonier, 1992). For example, the presence of stygobiont species (i.e. species living exclusively in groundwater) in the hyporheic zone is indicative of strong upwelling patterns (Boulton and Stanley, 1996).

3.1.4. Heat tracer techniques

Water temperature is an extremely reactive tracer with low specificity and detectability that has nevertheless been widely used to identify water source and flowpath by exploiting thermal differences in groundwater, surface water, and precipitation (Anderson, 2005; Constantz, 2008; Hannah et al., 2008; Krause et al., 2014). Similar to water isotopes, heat is a property of the water itself, rather than a solute or particle. However, unlike isotopes, thermal signature is very rarely conservative over long distances or times. Heat is an effective tracer at ecohydrological interfaces where it has been used to predict the behavior of aquatic organisms in streams (Ebersole et al., 2001, 2003; Torgersen et al., 1999) and to understand the impact of groundwater-surface water exchange flows on catchment-scale biogeochemical budgets (Brunke and Gonser, 1997; Krause et al., 2011; Woessner, 2000). Until recently, the thermal resolution of most temperature sensors has been quite low and temperature data has been limited to point measurements. The development of distributed temperature sensing (DTS) was a watershed moment for heat tracers since DTS allows large-scale, fine resolution temperature measurements. DTS takes advantage of temperature-sensitive properties of standard or specialized fiber optic cable to quantify temperature along the length of the cable (Selker et al., 2006a; Tyler et al., 2009; Westhoff et al., 2007). Because cable can be deployed in any configuration, DTS allows quantification of vertical, lateral, and longitudinal flowpaths and fluxes. Cables in riverbeds have been used to detect spatial variability of groundwater discharge and recharge (Lowry et al., 2007; Mamer and Lowry, 2013; Mwakanyamale et al., 2012; Selker et al., 2006b), identify and model lateral inflows (Boughton et al., 2012; Westhoff et al., 2007), and assess the role of solar radiation and riparian vegetation shading on stream heat exchange (Boughton et al., 2012; Petrides et al., 2011). Cable can be wrapped around poles to increase spatial resolution and installed in streambeds to monitor vertical hyporheic and groundwater flowpaths (Briggs et al., 2012; Lautz, 2012; Vogt et al., 2010). With "active" DTS, heat pulses can be sent along the length of the cable to determine thermal conductivity of the soil and water matrix (Ciocca et al., 2012). In combination with solute or particulate proxies, heat could be a sensitive tracer of changes in water source during storm events and of how much and how fast water moves between different compartments of the catchment.

Another technological breakthrough in heat tracing was the development of thermal imagery techniques that can remotely measure surface and shallow subsurface water temperatures from satellites, airborne platforms, or on the ground (e.g. Cherkauer et al., 2005; Deitchman and Loheide, 2009; Durán-Alarcón et al., 2015; Jensen et al., 2012; Lalot et al., 2015; Lewandowski et al., 2013; Pfister et al., 2010; Schuetz and Weiler, 2011; Stefan Kern et al., 2009; Wawrzyniak et al., 2013). Though quantification of thermal images remains challenging, thermal imaging is a valuable complement to other tracers of flowpath and water source because it makes intersecting water masses visible at ecohydrological interfaces. It has proven effective in characterizing in-stream flowpaths, lateral water exchanges, groundwater inputs, and distribution of thermal refugia (Dugdale et al., 2015; Jensen et al., 2012; Johnson et al., 2008; Lewandowski et al., 2013; Pfister et al., 2010).

3.2. Residence time: how long does it stay there?

Where water goes is closely connected to how long it stays there. Water residence time is a key parameter that influences hydrology, biogeochemistry, and ecology at the catchment scale and within different catchment components (Fig. 5; Kirchner, 2016b). Because residence time is directly proportional to the volume of water, it is also important for management of water resources (Collon et al., 2000; Scanlon et al., 2002). Compared with the infinite variety of potential water sources and flowpaths, residence time is satisfyingly straightforward. It is defined as the amount of time a mass of water stays in a domain of interest (e.g. catchment, reach, bedform; Fig. 4) and can mathematically be described as pool size (amount of water) divided by the rate of inflow (input residence time) or outflow (output residence time), or as the distribution of water ages in the domain of interest (storage residence time; Davies and Beven, 2015). The similarity or divergence of these three parameters of residence time depends on spatiotemporal scale and changes in storage, which can alter interpretation of modeling and tracer estimates of residence time (Botter et al., 2010; Rinaldo et al., 2011). The simplest and most common metric of residence time is the mean residence time, but for many practical problems (e.g. prediction of contaminant propagation or removal) it is desirable to know the residence time distribution or transit time distribution, which can be modelled based on environmental or injected tracer data (Eriksson, 1971; Gilmore et al., 2016; McGuire and McDonnell, 2006; Stream Solute Workshop, 1990). Because residence time is defined by the chosen spatial realm, it is inherently scalable across point, hillslope, catchment, and landscape scales (Fig. 5; Asano et al., 2002; Maloszewski and Zuber, 1993; Michel, 2004; Poulsen et al., 2015; Vaché and McDonnell, 2006), though the relative influence of antecedent storage, celerity, and the ratio of new to old water on residence time varies with scale (Davies and Beven, 2015).

Residence time is central to the HotDam framework because it is necessary to calculate rates of biogeochemical transformation and because the amount of time water, solutes, and particulates spend in different catchment components can determine the location and duration of hot spots (McClain et al., 2003; Oldham et al., 2013; Pinay et al., 2015). Residence time at event and seasonal scales is commonly modeled based on hydrograph analysis. While this method has been very effective at predicting water discharge, it cannot separate young and old outflow due to the celerity problem (see Section 2) and therefore cannot reliably determine residence time on its own (Clark et al., 2011; McDonnell and Beven, 2014). Tracer methods in conjunction with hydrometric analysis can overcome this problem by determining flowpath (Martinec, 1975; Poulsen et al., 2015; Tetzlaff et al., 2015) or

water age directly (Gilmore et al., 2016; Rodhe et al., 1996). Techniques for determining residence time have been reviewed in great detail elsewhere (Darling et al., 2012; Fontes, 1992; Foster, 2007; Hauer and Lamberti, 2011; Kendall and McDonnell, 2012; Kirchner, 2016b; Payn et al., 2008; Plummer and Friedman, 1999; Scanlon et al., 2002), so in this section we will focus on how crossed-proxy methods could be brought to bear to quantify and reduce uncertainty, organized by spatial and temporal scale.

3.2.1. Determining residence time in fast systems

For rapid-transit systems with residence times on the order of minutes to months (e.g. bedforms, river networks, shallow soils, and small lakes), most methods of measuring residence time use injected tracers (Bencala and Walters, 1983; Stream Solute Workshop, 1990). All methods for determining residence time by tracer injection work on the same basic principle. Assuming that a tracer has the same transport dynamics as water, its rate of dilution after injection is proportional to the renewal time of a system. Mean residence time and the distribution of residence times can be calculated from the overall rate of disappearance and the change in removal rate over time, respectively (Payn et al., 2008; Schmadel et al., 2016; Wlostowski et al., 2013). Conservative behavior of the selected proxy is therefore paramount, since removal by any processes other than dilution and advection (e.g. biological, chemical, or physical reactivity) will directly bias the estimate of residence time (Nyberg et al., 1999; Ward et al., 2013). Tracers can be added instantaneously or at a known, constant rate depending on the size of the system and the desired level of detail for the distribution of residence times (Payn et al., 2008; Rodhe et al., 1996; Wlostowski et al., 2013). For surface water systems (e.g. streams), tracer concentration is measured at a downstream sampling point, and for subsurface systems, tracer propagation can be monitored via wells (Zarnetske et al., 2011) or electric resistance tomography for electrically conductive tracers such as salts (González-Pinzón et al., 2015; Kemna et al., 2002; Pinay et al., 1998, 2009). The shape of the breakthrough curve (the change in tracer concentration over time at the sampling point) represents the distribution of residence times. Adequate sampling of the tail of the break through curve is important to capture slower flowpaths and because flowpaths with residence times longer than the arbitrary duration of the monitoring will be missed (González-Pinzón et al., 2015; Schmadel et al., 2016; Ward et al., 2013). Tracers with high detectability that can be monitored continuously (e.g. fluorescent dyes or sodium) are particularly well suited to determine residence time. There is a huge diversity of more or less conservative tracers that have been used to determine short-term residence time including isotopically labelled water (Nyberg et al., 1999; Rodhe et al., 1996), solutes such as chloride, bromide, and fluorescent dyes (González-Pinzón et al., 2013; Payn et al., 2008), dissolved gases such as propane, sulfur hexafluoride (SF6), and chlorofluorocarbons (CFCs; Molénat et al., 2013; Soares et al., 2013; Thompson et al., 1974; Wallin et al., 2011), particulates like sDNA, viral particles, and nanoparticles (Foppen et al., 2011, 2013; Hunt et al., 2014; Ptak et al., 2004; Sharma et al., 2012), and even hot water (Rau et al., 2014).

For systems with residence time greater than a few days but less than a year (e.g. hillslopes, headwater catchments, and the non-saturated zone), hydrometric methods such as mass balance or hydrograph decomposition are often used to estimate residence time (Kirchner, 2016b; McDonnell and Beven, 2014; Poulsen et al., 2015). For systems with available background chemistry data, it is possible to directly trace residence time using variation in system inputs (i.e. precipitation or upstream inflow). Typically the isotopic or chemical signature of precipitation or inflow over time is compared with the signature of system outflow (McGuire et al., 2002; Peralta-Tapia et al., 2015; Rodhe et al., 1996; Stewart and McDonnell, 1991; Stute et al., 1997). The integrated discharge and timing of the arrival of the distinct water mass in different system components allows the calculation of reservoir size and residence time.

3.2.2. Residence time in slow systems

For systems with residence times longer than a year, injected tracer methods are obviously not practical due to time constraints, not to mention the inordinate mass of tracer that would need to be injected into the system. For slow systems, a variety of environmental tracer methods have been used including historical or current anthropogenic pollution, naturally occurring geochemical tracers, and known paleo conditions (Aquilina et al., 2012, 2015; Böhlke and Denver, 1995; Kendall and McDonnell, 2012; Plummer and Friedman, 1999; Schlosser et al., 1988).

For "young" groundwater less than 50 years old, radioactive tritium (^{3}H) from aboveground nuclear testing in the 60s and 70s, radioactive krypton (^{85}Kr) produced during reprocessing of nuclear rods, and CFCs and SF6 from manufacturing have been used to determine the time since a water parcel was last in contact with the atmosphere (Fig. 7; (Ayraud et al., 2008; Leibundgut et al., 2011; Lu et al., 2014). Dating with these tracers relies on comparing the concentration in the groundwater sample with known historical atmospheric concentrations after applying a solubility constant based on recharge temperature and atmospheric partial pressure. ^{3}H and ^{85}Kr have half-lives ($t_{1/2}$) of 12.3 and 10.8 years, respectively, meaning an additional correction must be applied to back calculate initial concentration. The ratio of ^{3}H to ^{3}He (the radioactive decay product of ^{3}H) is often used to achieve greater certainty and precision in this correction (Schlosser et al., 1988). ^{3}H is attractive as a tracer because it recombines with water and therefore has the same transport dynamics, though drawbacks include its short window of production and uneven global distribution (Fig. 7b). As noble gases, ^{85}Kr and ^{3}He are biochemically highly conservative, but dispersion and degassing can complicate interpretation. Until recently, large sampling volumes (>1000 L) were needed for ^{85}Kr and other radionuclide analyses. The development of atom trap trace analysis (ATTA) and advanced gas extraction techniques are bringing these volumes down, though sampling procedures are still non-negligible (Lu et al., 2014). CFCs are synthetic organic compounds that were used in

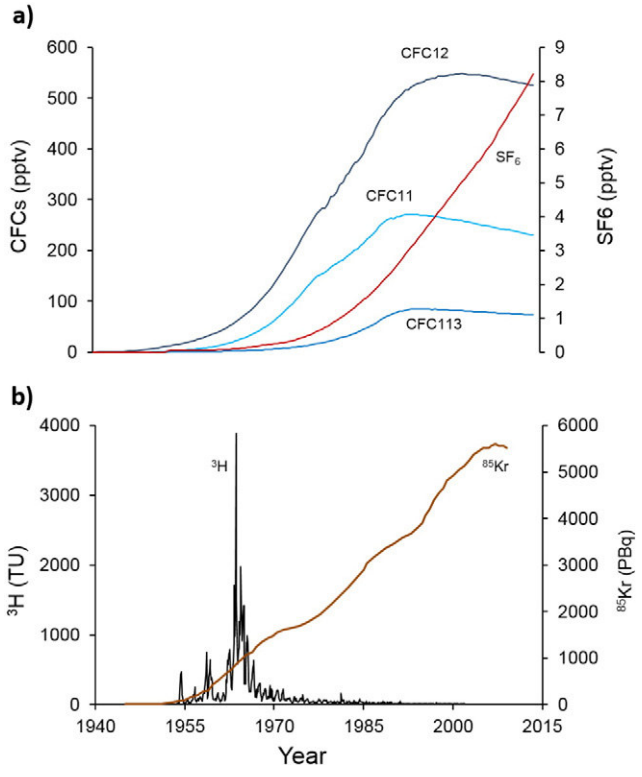

Fig. 7. Atmospheric concentrations of a) chlorofluorocarbons (CFCs) and sulfur hexafluoride (SF_6) produced for refrigeration and insolation, and b) tritium (^{3}H) and ^{85}Kr produced from nuclear testing and rod reprocessing. Data from Ahlswede et al. (2013) and water.usgs.gov/lab/software/air_curve

refrigerants from the 1930s to the 1990s. Trace concentrations of many CFCs, some of which are detectable at extremely low levels, were incorporated into the hydrological cycle, allowing groundwater dating with small sample volumes (<1 L). CFCs have been widely used to date groundwater and ocean residence times (Ayraud et al., 2008; Bullister and Weiss, 1983; Gammon et al., 1982; Hahne et al., 1978; Hammer et al., 1978; Kolbe et al., 2016; Lovelock et al., 1973; Thiele and Sarmiento, 1990). The fact that most CFC concentrations have peaked and are now decreasing means a single concentration can correspond to multiple eligible dates (Fig. 7a). Crossing multiple CFCs with different atmospheric curves is therefore necessary for definitive dating. The success of the Montreal Protocol of 1987 which banned CFC manufacturing means CFC concentrations will soon be too low for effective dating. Fortunately for ecohydrologists, another anthropogenic gas, sulfur hexafluoride (SF_6), is monotonically increasing (Fig. 7a). SF_6 is used primarily as an insulator in electronic components and is very conservative, though it has the limitations of other gas tracers, namely rapid equilibration with the atmosphere in open systems (Glover and Kim, 1993). Current techniques allow SF_6 dating of waters that lost contact with the atmosphere after 1990. Another approach to dating young groundwater is to use the concentration of weathering products as a proxy of residence time (Tesoriero et al., 2005). While dissolution rates are non-linear at very low and very high concentrations, some elements such as silica appear to be suitable for dating groundwater between 2 and 60 years old (Becker, 2013), approximately the same time period previously covered by CFCs.

For "old" groundwater with a residence times longer than 50 years, most dating methods depend on atomic decay of cosmogenic radionuclides such as ^{14}C and ^{39}Ar (Leibundgut et al., 2011; Lu et al., 2014). For example, ^{14}C is created naturally in the upper atmosphere due to the recombination of a nitrogen atom with a free neutron (Geyh et al., 2000). ^{14}C makes its way directly to the water table as dissolved CO_2 in precipitation or indirectly as respired CO_2 in the soil. When groundwater loses contact with the atmosphere its ^{14}C content starts to decrease, acting as an atomic clock (Fontes, 1992). Datable ages and precision depend on sensitivity of the analytical techniques and the half-life of the radionuclide. The most common radionuclides in order of increasing half-life are ^{39}Ar ($t_{1/2}$ = 269 a), ^{14}C ($t_{1/2}$ = 5730 years), ^{234}U ($t_{1/2}$ = 25 ka), 81Kr ($t_{1/2}$ = 230 ka), and ^{36}Cl ($t_{1/2}$ = 300 ka; (Bauer et al., 2001; Collon et al., 2000; Lu et al., 2014). There are several important confounding factors to account for when using any radioactive nuclide, including variation in the background rate of production of the radionuclide, anthropogenic sources, degree of mixing in the atmosphere, geologic sources, and sometimes complex equilibrium dynamics in the non-saturated zone above the water table (Ahlswede et al., 2013; Han and Plummer, 2013; Lu et al., 2014).

One of the major limitations of both young and old groundwater tracers is that none have a unique source and almost none are completely conservative (with the possible exception of ^{3}H). Radionuclides such as ^{39}Ar and gases such as SF_6 can be produced geologically at rates sufficient to obscure the atmospheric signal on decadal timescales (Lehmann et al., 1993) and anthropogenic tracers such as CFCs can be degraded, particularly in anoxic zones typical of soils and wetlands (Oremland et al., 1996), the very environments where determining residence time is the most important for anaerobic metabolisms such as denitrification.

3.2.3. Modeling residence time distributions from tracer data

Each of the measures described above provides a single apparent age (equivalent to the mean residence time) which does not reflect the diversity of flowpaths and residence times characteristic of natural systems (McCallum et al., 2014a). With crossed-proxy estimates of residence time and flowpath, it is possible to model the continuous distribution of residence times (Aquilina et al., 2012; Kolbe et al., 2016; Massoudieh et al., 2014) and consequently the distribution of *Da* (Oldham et al., 2013). The two major approaches for modeling residence time distributions from tracer estimates depend on either multiple independent residence time proxies (the shape-free method) or prior information about the shape of the residence time distribution (lumped-parameter approach; Turnadge and Smerdon, 2014, Marçais et al., 2015).

The shape-free interpretation method represents the residence time distribution as a histogram with a limited number of bins based on multiple environmental tracers of residence time (e.g. ^{85}Kr, SF_6, and CFCs; Fienen et al., 2006; Massoudieh et al., 2014; McCallum et al., 2014b; Visser et al., 2013). Because the atmospheric chronicles for many current tracers are similar (Fig. 7), some of this information is redundant and quantitative Bayesian methods or qualitative screening should be used to extract the salient information and avoid introducing epistemic error (Beven and Smith, 2015; Sambridge et al., 2013).

The second and more common method is the lumped-parameter approach (Jurgens et al., 2012; Maloszewski and Zuber, 1996; Marçais et al., 2015). It can be carried out with fewer tracer estimates of residence time but requires selection of a distribution model a priori. The simplest models are the Dirac and exponential distributions, representing piston-flow advective transport (Begemann and Libby, 1957), and well-mixed advective-diffusive-dispersive transport (Gelhar and Wilson, 1974), respectively. Both have a single degree of freedom and can be calibrated by a single tracer concentration, but they represent widely differing groundwater flow and transport conditions. The Dirac model is appropriate for estimating residence time in areas where flow lines are diverging and where dispersion can be neglected compared to advection (high Péclet numbers; (Koh et al., 2006; Solomon et al., 2010), whereas the exponential model is more relevant for well mixed areas such as deep sampling wells or areas of flow convergence (Haitjema, 1995; Lerner, 1992). Other distributions have been proposed, a comprehensive list of which can be found in Leray et al. (2016), including inverse Gaussian, gamma, and hybrid distributions to bridge the gap between recharge and discharge areas (Engdahl and Maxwell, 2014; Ozyurt and Bayari, 2003; Zheng and Bennett, 2002).

Successfully calibrated models provide a continuous residence time distribution as well as descriptive parameters of the underlying flow structure, allowing prediction of the development of hot spots and hot moments and shedding light on the overall biogeochemical capacity of the catchment (Eberts et al., 2012; Green et al., 2014; Kolbe et al., 2016; Larocque et al., 2009), the key parameters in the HotDam framework (Pinay et al., 2015). The most critical limitation of both shape-free and lumped-parameter approaches is currently the limited variety and temporal coverage of tracers. While repeated measures can partially compensate for this limitation (Cornaton, 2012; Massoudieh et al., 2014), more abundant and diverse residence time tracers are needed to better constrain model assumptions and allow meaningful comparison between catchments (Thomas et al., in press). Identifying or developing more tracers with distinct properties is a priority for hydrologists and ecologist alike, since the systematic bias (epistemic uncertainty) of models is inversely related to the number and quality of independent estimates used in parameterization and testing (Beven and Smith, 2015).

3.3. Biogeochemical transformation: what happens along the way?

Understanding when, where, and how much biogeochemical alteration occurs as materials pass through a catchment is central to many management issues including assessing ecosystem resilience to human disturbance, evaluating effectiveness of restoration and mitigation efforts, and detecting environmental change (Baker and Lamont-Black, 2001; Gaglioti et al., 2014; Kasahara et al., 2009). The huge diversity of biogeochemical reactions can be simplified in terms of respiration and assimilation (Borch et al., 2010; Nicholls and Ferguson, 2013). Respiration is the catabolic transfer of electrons to fuel synthesis of adenosine triphosphate (ATP), the universal energy currency of life. Assimilation is the anabolic uptake of material to build

proteins, enzymes, organelles, and cells. Respiration reactions are typically not easily reversible (e.g. the reduction of NO_3^- to N_2 during denitrification or O_2 to CO_2 and H_2O during heterotrophic respiration) and therefore represent removal pathways. Assimilation uses energy from respiration to incorporate inorganic elements into organic compounds which can be remineralized, representing temporary retention. Assimilation can therefore only "remove" material under non-steady state conditions (i.e. when biomass is increasing), however, because respiration depends in part on community size or biomass, these parameters are functionally linked. The sum of respiration and assimilation determines the rate of removal and retention of biologically reactive material passing through a system. While abiotic reactions do not technically fall within this biological classification, redox and acid-base reactions are analogous to respiration (removal) and sorption reactions are similar to assimilation (retention). The potential types and rates of respiration and assimilation that can occur depend largely on redox potential (Borch et al., 2010). Redox potential is determined by the presence of different electron donors (reducers such as DOM) and electron acceptors (oxidizers including O_2, Fe^{3+}, NO_3^-, SO_4^{2-}, and CO_2 arranged from greatest to least energy yield; (Schlesinger and Bernhardt, 2012). Determining redox conditions in space and time is key to quantifying exposure time and is of particular importance because redox is a major control on and consequence or the removal of contaminants (e.g. NO_3^-; Zarnetske et al., 2011), the mobility of many nutrients and trace elements including heavy metals (Borch et al., 2010), and the likelihood of mercury methylation (Gilmour and Henry, 1991).

Along with characterizing redox conditions, determining connectivity is one of the biggest challenges in predicting biogeochemical transformation (Pringle, 2003; Soulsby et al., 2015). Connectivity (the transfer of material or energy between subsystems) can be defined in regards to any stock or flux of interest (e.g. water, carbon, heat, organisms, sediment) and is a major control on the development and duration of hot spots and hot moments (McClain et al., 2003; Oldham et al., 2013; Pringle, 2003). Connectivity is a concern at all spatial and temporal scales though it generally is less problematic at shorter temporal scales, where connectivity is relatively stable, and larger spatial scales, where small-scale heterogeneities average out (Pringle, 2003; Rastetter et al., 1992).

Tracers of biogeochemical transformation can be classified as *direct tracers*, which are consumed or transformed by the biogeochemical reaction itself, and *indirect tracers*, which are consumed or transformed when exposed to conditions favorable for the reaction of interest. Indirect tracers are effective at quantifying exposure time (the proportion of residence time when physicochemical conditions are favorable for the reaction of interest) and direct tracers can determine reaction rate, the central parameters in the HotDam framework (Oldham et al., 2013; Pinay et al., 2015). The most common direct tracer techniques include monitoring changes in reactants and products (e.g. O_2 consumption or CO_2 production), fractionation of isotopic signature, and application of "smart" tracers that are modified by the reaction in a measurable way (Fontvieille et al., 1992; Frey et al., 2014; Haggerty et al., 2008; Zarnetske et al., 2012). Indirect tracer methods are more numerous and diverse, but typically rely on the divergence of two or more contextually-reactive tracers such as anomalies in rare earth element concentration (Gruau et al., 2004; Hissler et al., 2014), or overall differences in substrate signature, such as enriched $\delta^{13}C$ for DOC produced in oxic versus anoxic environments (Lambert et al., 2014). In the following sections we summarize current techniques used to directly and indirectly trace biogeochemical reactions, and discuss the role of dissolved carbon as both a tracer and control of assimilation and respiration.

3.3.1. Direct tracers of biogeochemical transformation

Measuring the change in concentration of biogeochemical reactants and products is the most fundamental method of directly tracing biogeochemical transformation. Both environmental and injected tracers can be used to determine transformation, though residence time must be constrained if the rate of transformation is of interest. For injected applications a conservative tracer is added with the reactive tracer to correct for hydrologic losses before calculating the rate of respiration or assimilation (Schmadel et al., 2016; Stream Solute Workshop, 1990). Injected reactants may be labeled with radioactive or stable isotopes to allow quantification of turnover as they pass through different system components or trophic levels (Gribsholt et al., 2009; Mulholland et al., 1985; Pace et al., 2004). Recently, a new method has been developed for flowing systems called *tracer additions for spiraling curve characterization* (TASCC), which quantifies nutrient and carbon transformation at multiple concentrations with a single slug injection (Covino et al., 2010). While this method has so far only been used with injected tracers in streams, it could be adapted to take advantage of natural pulses such as storm events.

In addition to or in conjunction with concentration measurements, the isotopic signatures of solutes have been widely used as direct tracers of biogeochemical transformation (Böttcher et al., 1990; Brenot et al., 2015; Hosono et al., 2014; Zarnetske et al., 2012). Assimilation and respiration can cause isotopic fractionation, enriching residual reactants with the heavy isotope and depleting products. When multiple

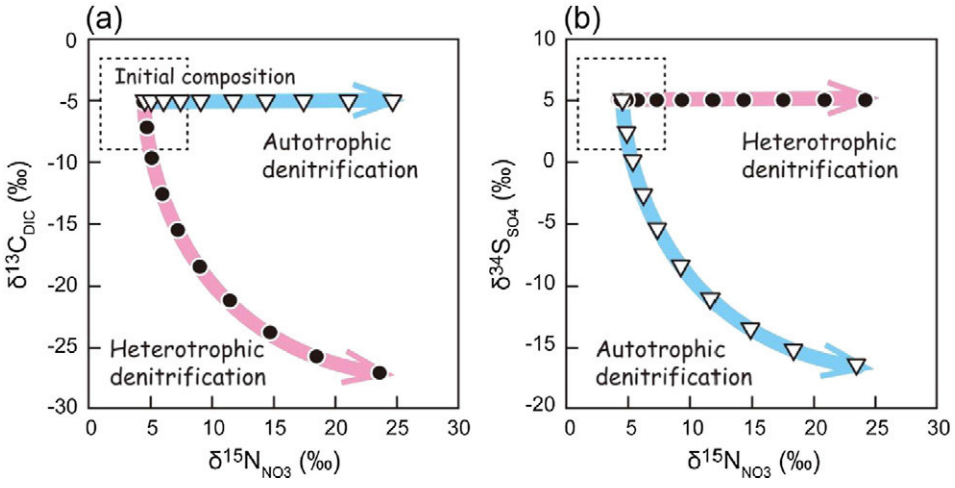

Fig. 8. Theoretical trajectories of carbon, nitrogen, and sulfur stable isotopes for autotrophic and heterotrophic denitrification, demonstrating how crossing isotopic tracers from reactants (NO_3^- and DIC) and products (SO_4^{2-}) allows the partitioning of concurrent biogeochemical reactions. Black circles and pink arrows represent enrichment trajectories of heterotrophic denitrification and white triangles and blue arrows represent autotrophic denitrification. Figure reproduced from Hosono et al. (2014).

concentrations and isotopic ratios are available for reactants and products, simultaneous metabolic pathways can be quantitatively estimated, such as the partitioning of autotrophic and heterotrophic denitrification with stable isotopes of NO_3^-, DIC, and SO_4^{2-} (Fig. 8; Frey et al., 2014; Hosono et al., 2014; Urresti-Estala et al., 2015).

Recent analytical advances have vastly decreased necessary sample volumes and cost for major stable isotope analyses including the development of a bacterial denitrifier method for measuring $\delta^{15}N$ and $\delta^{18}O$ of NO_3^- after bacterial reduction to N_2O (Sigman et al., 2001). Other stable isotope analyses remain somewhat more involved, but straightforward precipitation techniques and availability of elemental analyzers and mass spectrometers have made analysis of $\delta^{13}C$ of DOC and DIC and $\delta^{34}S$ of SO_4^{3-} less costly and time consuming (Hosono et al., 2014; Post, 2002; Zarnetske et al., 2012). The interpretation of isotopic shifts requires a sound understanding of all possible fractionating reactions and usually requires site-specific determination of the initial isotopic signature of reactants. Furthermore, fractionation does not occur all the time for all biogeochemical reactions, notably when reactant concentrations are very low or completely depleted, or when reactants are supplied at or below the biochemical demand (e.g. during diffusive transport; Kritee et al., 2012; Lehmann et al., 2003; Pokrovsky et al., 2006; Sebilo et al., 2003).

Two "smart" dyes have also been used as direct tracers of microbial metabolism. Fluorescein diacetate (FDA) is a non-fluorescent dye which can be metabolized by many microbial enzymes (e.g. proteases, lipases, and esterases; Schnürer and Rosswall, 1982). FDA hydrolysis produces fluorescein, allowing quantification of microbial activity via fluorometry (see Section 3.1.2). Originally developed for soils (Casida et al., 1964), this method has been adapted for aquatic environments including the hyporheic zone and sediment (Battin, 1997; Fontvieille et al., 1992). More recently, resazurin, a mildly fluorescent dye developed for use in medical blood tests (Ahmed et al., 1994), has been used to quantify microbial metabolism (Haggerty et al., 2008; McNicholl et al., 2007). Resazurin irreversibly reduces to resorufin, a highly fluorescent dye, under mildly reducing conditions especially in the presence of microbial activity. The simultaneous quantification of resazurin and resorufin allows the determination of transport dynamics (i.e. transient storage and hydrologic loss) and biogeochemical transformation (Haggerty et al., 2014). Resazurin has been used to quantify microbial capacity in hyporheic sediments, biofilms in flume experiments, and most recently to quantify the effects of bioturbation by chironomids on microbial metabolism in lake sediments (Baranov et al., 2016; Haggerty et al., 2008, 2014).

3.3.2. Indirect tracers of biogeochemical transformation

Tracing biogeochemical transformation with indirect tracers provides information about the physical and biological conditions encountered by a parcel of water and the material it carries. Often the reactivity that is bothersome when using a tracer to quantify flowpath or residence time allows determination of exposure time to certain conditions. Many atoms or compounds are strongly sensitive to changes in redox (e.g. Fe, Mn, Th, and U). However, because many ecohydrological systems are somewhat or mostly inaccessible, to be an effective tracer of redox conditions along a flowpath, the element or combination of elements must somehow record the past conditions until they can be quantified at the sampling point (e.g. catchment outflow, groundwater well, spring). Consequently, irreversible reactions and the combination of tracers with different reactivity portfolios are the most useful tools in determining exposure time.

The abundance of environmental nucleic acids (i.e. eDNA and RNA) from microbial communities capable of different metabolic reactions (e.g. nitrate, iron, or sulfur reduction) can be an effective indirect proxy of substrate and redox conditions (Ben Maamar et al., 2015; Hemme et al., 2010). Analysis of rare earth elements (REEs) has also been used to determine redox conditions and exposure to DOM during transport through near-surface groundwater and riparian zones (Davranche et al., 2005; Gruau et al., 2004). Cerium (Ce; a rare earth in the lanthanide series) readily oxidizes to Ce^{4+} and precipitates as cerianite in the presence of oxygen. Because different bedrocks have characteristic REE ratios, the strength of the departure of Ce from its expected abundance is an indicator of integrated redox conditions along the flowpath. Interpreting a Ce anomaly without other tracers is complicated by the fact that high DOM concentrations can inhibit Ce precipitation, but in combination with other tracers of redox conditions, the Ce anomaly could potentially indicate both redox and exposure to DOM (Davranche et al., 2005; Dia et al., 2000; Gruau et al., 2004; Pourret et al., 2010). Likewise, differences in the anoxic decay rates of various pharmaceuticals (Cetecioglu et al., 2013; Durán-Álvarez et al., 2012) or CFCs could be used to determine exposure time (Horneman et al., 2008; Oremland et al., 1996). Laboratory and field tests indicate that CFC11 decays at least an order of magnitude faster than CFC12 in highly reducing conditions. While this is clearly problematic for the use of CFC11 to date groundwater, the difference in apparent ages of CFC11 and CFC12 could provide a continuous variable of the exposure time to reducing conditions, a major predictor of NO_3^- removal capacity across multiple scales (Ocampo et al., 2006; Pinay et al., 2015; Zarnetske et al., 2012). To our knowledge this proxy has never been used, though it could be widely applied to shallow groundwater systems to characterize exposure times as global CFC concentrations are very well constrained and have been measured in many shallow groundwater systems.

3.3.3. DIC and DOM as tracers and drivers of biogeochemical transformation

In this section we explore applications and limitations of carbon isotopes, both stable ($\delta^{13}C$) and radioactive (^{14}C), as tracers of respiration, assimilation, and abiotic geochemical reactions. Dissolved carbon not only carries information about biogeochemical reactions, it is a major determinant of many of the environmental conditions that modulate biogeochemical reactions including pH, redox, microbial abundance, nutrient supply, and priming (Coleman and Fry, 1991; Guenet et al., 2010; Manzoni et al., 2012; Pinay et al., 2015; Zarnetske et al., 2012). Especially in diffusion dominated systems (Péclet number < 1), where O_2 is not replenished via advective mixing, DOM concentration and biodegradability are the predominant predictors of redox (Fig. 2; Oldham et al., 2013). Despite the fact that carbon is the basis of all organic chemistry, the assumption of conservancy at some time scales can be appropriate such as using the $\delta^{13}C$ or ^{14}C of DOM to link short-term interactions between soil and stream (Leith et al., 2014; Raymond and Bauer, 2001; Schiff et al., 1990). However, in most situations, conservancy should not be assumed, for instance when determining sources of DIC in streams or lakes using $\delta^{13}C$ (Aravena et al., 1992; Finlay, 2003; Waldron et al., 2007). Furthermore, because organic matter originating from different vegetation or soil layers may have systematically different biodegradability, it cannot be assumed that the ratio of ^{12}C, ^{13}C, and ^{14}C in DOM or POM will be preserved once exposed to active mineralization (Marwick et al., 2015). The $\delta^{13}C$ of DIC in a stream, lake, or parcel of groundwater is a composite signal of $\delta^{13}C$ from the products of chemical weathering (HCO_3^- and CO_3^{2-}; carbonate alkalinity) and dissolved CO_2 from soil respiration. DIC $\delta^{13}C$ is therefore a composite tracer of two very different reactions in the carbon cycle, both of which need to be considered for accurate interpretation (Amiotte Suchet et al., 2003). The CO_2 fraction is generally the isotopically lightest component as a result of equilibrium fractionation favoring the accumulation of ^{12}C in CO_2 and ^{13}C in alkalinity (Fig. 6; (Clark and Fritz, 1997; Zhang et al., 1995). Freshwater alkalinity is generated from carbonate and silicate parent material and the $\delta^{13}C$ of alkalinity is a relatively conservative tracer of chemical weathering (Amiotte Suchet et al., 2003). Unlike alkalinity, a series of other fractionation processes govern the $\delta^{13}C$ of dissolved CO_2, including photosynthesis and respiration (Ehleringer et al., 2000; Finlay, 2004), physical fractionation during degassing and dissolution (Doctor et al., 2008), and fermentation and oxidation processes in

anoxic environments (Barker and Fritz, 1981; Whiticar, 1999). The physical fractionation of the $\delta^{13}C$ of CO_2 has been used as a tracer of total CO_2 evasion from streams (Polsenaere and Abril, 2012; Venkiteswaran et al., 2014), though these calculations are sensitive to assumptions about vegetation, geology, and in-stream metabolism, limiting the generality of this approach thus far.

4. Using crossed proxies to move beyond case studies

Agriculture, urbanization, and resource extraction have dramatically increased nutrient loading and altered DOM delivery and production in aquatic inland and estuarine ecosystems. In the past 60 years, human activity has more than doubled global nitrogen fixation (Gruber and Galloway, 2008) and quadrupled phosphorus loading (Elser and Bennett, 2011). At the same time, human land-use has directly disturbed half of global land surface (Vitousek et al., 1997), fundamentally altering the capacity of ecosystems to buffer or process these nutrient inputs (Brooks et al., 2016; Earl et al., 2006; Seitzinger et al., 2006), and climate change is altering multiple dimensions of the water cycle (Haddeland et al., 2014; Taylor et al., 2013). Protecting or restoring aquatic ecosystems in the face of these anthropogenic pressures requires an understanding of hydrological and biogeochemical functioning across multiple spatial and temporal scales.

Experimental watershed studies have generated a huge body of catchment-specific literature that is the foundation of current ecohydrological theory as outlined in Section 2. However, a conceptual chasm still separates descriptions of individual catchment behavior and general understanding of the forces controlling water circulation and biogeochemistry across scales (Dooge, 1986; Hrachowitz et al., 2016; McDonnell et al., 2007), seriously limiting our ability to make meaningful predictions of the response of aquatic ecosystems to human disturbance (Abbott et al., 2016; Taylor et al., 2013). In the final section of this review, we present how crossed proxy methods may contribute to bridging that chasm by reducing epistemic uncertainty and generating process understanding across catchments. Specifically we present a rubric for selecting tracers (Fig. 9), revisit the concept of connectivity, and reiterate the value of multi-tracer tools in moving beyond single-catchment ecohydrology.

The field of ecohydrology is limited on the one hand by technical challenges estimating variables in the water balance equation (Beven and Smith, 2015) and on the other hand by difficulties measuring and conceptualizing carbon and nutrient budgets in intermittent and heterogeneous ecosystems (Pinay et al., 2015). In practice, ecologists tend to use overly simplistic hydrological concepts and hydrologists use overly simplistic ecological concepts, attributing unexplained patterns to unknown phenomena in whichever field is secondary (e.g. "hydrological losses" or "biological uptake"; Hunt and Wilcox, 2003). Because the HotDam framework is relatively process-poor, instead relying on the integration of hotspots into exposure timescales, it may be unsatisfying to mechanistic modelers and process-based experimentalists. However, the dual lens of connectivity and exposure time scales has the advantage of being rooted in parameters that are testable at the spatial and temporal scales of interest (Oldham et al., 2013; Pinay et al., 2015). Using crossed-proxy methods to parameterize the HotDam framework allows determination of decay coefficients at the hillslope and catchment scales directly, integrating spatial heterogeneity and temporal nonstationarity (Fig. 5). These estimates of exposure timescales based on crossed proxies can improve our understanding of coupled ecohydrological functioning in two concrete ways.

First, a major source of epistemic uncertainty in hydrology and ecology is the problem of incomplete tracer recovery during tracer injection experiments (Beven and Smith, 2015; Schmadel et al., 2016). In practice, tracer recovery is usually incomplete, and for some systems and tracers it is common for only a fraction of the "conservative" tracer to be accounted for (Bastviken et al., 2006; Kung, 1990; Mulder et al., 1990; Nyberg et al., 1999; Risacher et al., 2006). Without information on where the tracer went, this can lead to systematic overestimation of hydrological losses or biogeochemical uptake. Using multiple proxies with different transport and reaction portfolios can allow the identification and quantification of unknown loss pathways. As discussed in Section 3.1.1, water isotopes are the ideal tracer for constraining water source and flowpath because they are a part of the water mass itself. Quantifying hydrological losses with water isotopes allows accurate calculation of biogeochemical uptake or respiration. Improvement of laser spectrometers and other water isotope analyzers should continue to be prioritized (Jasechko et al., 2016; Lis et al., 2008; McDonnell and Beven, 2014). Second, testing models with multiple, distinct proxies can quantify uncertainty and evaluate whether models are getting the right answer for the right reasons (Kirchner, 2006). Using proxies with different underlying principles (e.g. hydrometric measures, solute tracers, heat, and dissolved gases) can reduce aleatory and epistemic uncertainty during model parameterization and provide the basis for meaningful model evaluation during model testing (Beven and Smith, 2015; Tetzlaff et al., 2015). The challenge is therefore to increase the number and diversity of usable proxies. Many of the tracers presented in this review were discovered by accident (bacteria as tracers) or were unintended consequences of human activity (CFCs and pharmaceuticals). While the proliferation of proxies will doubtless continue whether or not informed by a conceptual framework, intentional cross pollination between research, commerce, and industry, including medicine, telecommunications, resource extraction, forensics, and robotics, could accelerate this process.

While we mentioned the importance of connectivity in Section 2 and identified several tracers of flowpath that are useful for quantifying

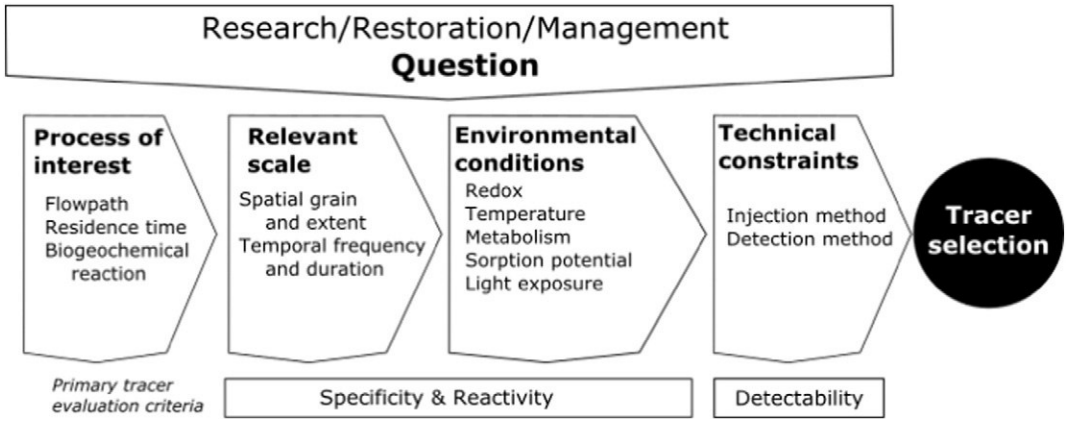

Fig. 9. Rubric for tracer selection based on research question or problem, environmental scale and conditions, and logistical considerations. Using multiple tracers with contrasting characteristics provides greater accuracy and allows quantification of exposure time (Fig. 1).

connectivity in Section 3.1, we wanted to address this key concept in the context of biogeochemical transformation. Identifying the timing and extent of hydrological and material isolation and connectivity between catchment components is key to predicting the frequency and location of hot spots and hot moments and is necessary to calculate the generalized Damköhler number (McClain et al., 2003; Oldham et al., 2013). Combining tracer methods for quantifying flowpath and residence time can allow assessment of connectivity by determining from where and when water or material is coming from (Detty and McGuire, 2010; Martínez-Carreras et al., 2015; Pfister et al., 2010). Detecting connectivity, therefore depends on temporal frequency as much as spatial extent. High frequency measurements of hydrometric parameters, reactant concentrations, optical properties, and isotopic signature can reveal moments of reconnection (Ferrant et al., 2013; Lambert et al., 2014; Saraceno et al., 2009), which if combined with knowledge of flowpath, can be used to localize connectivity. Variability in tracer concentration and characteristics during reconnection events such as storms and isolation events such as low-flow periods can provide an index of connectivity at multiple scales (Kirchner et al., 2004; Krause et al., 2015), allowing quantitative assessment of the ecological relevance of connectivity in regards to the measured parameters (Oldham et al., 2013).

Though the three questions we posed at the outset of this paper are fundamental to ecohydrology, the ultimate goal is not just to understand where, how long, and what happens to water and the materials transported with it. In fact, as important as they are, without comparative measures from multiple catchments, these questions only get us incrementally closer to a conceptual understanding of watershed ecohydrology. The goal is ultimately to explain the "why" of spatial and temporal heterogeneity, that is to say, what factors underlie the co-evolution of hydrological, biogeochemical, and societal behavior (Clark et al., 2011; McDonnell et al., 2007; Thomas et al., 2016a). Generating this type of general understanding of watershed dynamics requires moving between disciplines and across spatial and temporal scales, including ungauged catchments (McDonnell et al., 2007). One of the major advantages of a crossed-proxy approach is the ability to generate process knowledge of flowpath, residence time, and biogeochemical transformation across multiple catchments. Quantifying exposure time with a combination of redox and residence time tracers for a multitude of catchments would improve our ability to predict nutrient retention and pollutant transport and to evaluate between equifinal models (Thomas et al., in press). The application of crossed-proxy methodology across temporal and spatial scales could test the HotDam framework and other general mechanistic theories of watershed function (Dodds et al., 2015; Fisher et al., 2004; McDonnell, 2003; Pinay et al., 2015).

Acknowledgements

This project has been funded by the European Union's Seventh Framework Program for research, technological development and demonstration under grant agreement no. 607150 (FP7-PEOPLE-2013-ITN – INTERFACES - Ecohydrological interfaces as critical hotspots for transformations of ecosystem exchange fluxes and biogeochemical cycling). B. Abbott and G. Pinay were also supported by the French EC2CO grant "Caractérisation hydrologique et biogéochimique de la dénitrification dans les paysages." C. Mendoza-Lera and T. Datry were supported by the French National Agency for Water and Aquatic Environments (ONEMA, Action 13, "Colmatage, échanges nappe-rivière et processus biogéochimiques"). We would like to thank S. Abbott and two anonymous reviewers whose criticisms improved the paper.

References

Abbott, B.W., Jones, J.B., 2015. Permafrost collapse alters soil carbon stocks, respiration, CH4, and N2O in upland tundra. Glob. Chang. Biol. 21, 4570–4587. http://dx.doi.org/10.1111/gcb.13069.

Abbott, B.W., Jones, J.B., Godsey, S.E., Larouche, J.R., Bowden, W.B., 2015. Patterns and persistence of hydrologic carbon and nutrient export from collapsing upland permafrost. Biogeosciences 12, 3725–3740. http://dx.doi.org/10.5194/bg-12-3725-2015.

Abbott, B.W., Jones, J.B., Schuur, E.A.G., III, F.S.C., Bowden, W.B., Bret-Harte, M.S., Epstein, H.E., Flannigan, M.D., Harms, T.K., Hollingsworth, T.N., Mack, M.C., McGuire, A.D., Natali, S.M., Rocha, A.V., Tank, S.E., Turetsky, M.R., Vonk, J.E., Wickland, K.P., Aiken, G.R., Alexander, H.D., Amon, R.M.W., Benscoter, B.W., Bergeron, Y., Bishop, K., Blarquez, O., Bond-Lamberty, B., Breen, A.L., Buffam, I., Cai, Y., Carcaillet, C., Carey, S.K., Chen, J.M., Chen, H.Y.H., Christensen, T.R., Cooper, L.W., Cornelissen, J.H.C., Groot, W.J.d., DeLuca, T.H., Dorrepaal, E., Fetcher, N., Finlay, J.C., Forbes, B.C., French, N.H.F., Gauthier, S., Girardin, M.P., Goetz, S.J., Goldammer, J.G., Gough, L., Grogan, P., Guo, L., Higuera, P.E., Hinzman, L., Hu, F.S., Hugelius, G., Jafarov, E.E., Jandt, R., Johnstone, J.F., Karlsson, J., Kasischke, E.S., Kattner, G., Kelly, R., Keuper, F., Kling, G.W., Kortelainen, P., Kouki, J., Kuhry, P., Laudon, H., Laurion, I., Macdonald, R.W., Mann, P.J., Martikainen, P.J., McClelland, J.W., Molau, U., Oberbauer, S.F., Olefeldt, D., Paré, D., Parisien, M.-A., Payette, S., Peng, C., Pokrovsky, O.S., Rastetter, E.B., Raymond, P.A., Raynolds, M.K., Rein, G., Reynolds, J.F., Robard, M., Rogers, B.M., Schädel, C., Schaefer, K., Schmidt, I.K., Shvidenko, A., Sky, J., Spencer, R.G.M., Starr, G., Striegl, R.G., Teisserenc, R., Tranvik, L.J., Virtanen, T., Welker, J.M., Zimov, S., 2016. Biomass offsets little or none of permafrost carbon release from soils, streams, and wildfire: an expert assessment. Environ. Res. Lett. 11, 34014. http://dx.doi.org/10.1088/1748-9326/11/3/034014.

Abbott, B.W., Larouche, J.R., Jones, J.B., Bowden, W.B., Balser, A.W., 2014. Elevated dissolved organic carbon biodegradability from thawing and collapsing permafrost: permafrost carbon biodegradability. J. Geophys. Res. Biogeosci. 119, 2049–2063. http://dx.doi.org/10.1002/2014JG002678.

Adams, J.L., Tipping, E., Bryant, C.L., Helliwell, R.C., Toberman, H., Quinton, J., 2015. Aged riverine particulate organic carbon in four UK catchments. Sci. Total Environ. 536, 648–654. http://dx.doi.org/10.1016/j.scitotenv.2015.06.141.

Agricola, G., 1556. De Re Metallica. first ed. Salisbury House, London.

Ahlswede, J., Hebel, S., Ross, J.O., Schoetter, R., Kalinowski, M.B., 2013. Update and improvement of the global krypton-85 emission inventory. J. Environ. Radioact. 115, 34–42. http://dx.doi.org/10.1016/j.jenvrad.2012.07.006.

Ahmed, S.A., Gogal, R.M., Walsh, J.E., 1994. A new rapid and simple non-radioactive assay to monitor and determine the proliferation of lymphocytes: an alternative to [3H]thymidine incorporation assay. J. Immunol. Methods 170, 211–224.

Lotka, A.J., 1925. Elements of Physical Biology. Williams and Wilkins Company.

Amiotte Suchet, P., Probst, J.-L., Ludwig, W., 2003. Worldwide distribution of continental rock lithology: Implications for the atmospheric/soil CO2 uptake by continental weathering and alkalinity river transport to the oceans. Glob. Biogeochem. Cycles 17, 1038. http://dx.doi.org/10.1029/2002GB001891.

Anderson, M.P., 2005. Heat as a ground water tracer. Ground Water 43, 951–968. http://dx.doi.org/10.1111/j.1745-6584.2005.00052.x.

Andreozzi, R., Marotta, R., Pinto, G., Pollio, A., 2002. Carbamazepine in water: persistence in the environment, ozonation treatment and preliminary assessment on algal toxicity. Water Res. 36, 2869–2877. http://dx.doi.org/10.1016/S0043-1354(01)00500-0.

Aquilina, L., Vergnaud-Ayraud, V., Labasque, T., Bour, O., Molénat, J., Ruiz, L., de Montety, V., De Ridder, J., Roques, C., Longuevergne, L., 2012. Nitrate dynamics in agricultural catchments deduced from groundwater dating and long-term nitrate monitoring in surface- and groundwaters. Sci. Total Environ. 435–436, 167–178. http://dx.doi.org/10.1016/j.scitotenv.2012.06.028.

Aquilina, L., Vergnaud-Ayraud, V., Les Landes, A.A., Pauwels, H., Davy, P., Pételet-Giraud, E., Labasque, T., Roques, C., Chatton, E., Bour, O., Ben Maamar, S., Dufresne, A., Khaska, M., La Salle, C.L.G., Barbecot, F., 2015. Impact of climate changes during the last 5 million years on groundwater in basement aquifers. Sci. Rep. 5, 14132. http://dx.doi.org/10.1038/srep14132.

Aravena, R., Warner, B.G., MacDonald, G.M., Hanf, K.I., 1992. Carbon isotope composition of lake sediments in relation to lake productivity and radiocarbon dating. Quat. Res. 37, 333–345. http://dx.doi.org/10.1016/0033-5894(92)90071-P.

Arnon, S., Marx, L.P., Searcy, K.E., Packman, A.I., 2010. Effects of overlying velocity, particle size, and biofilm growth on stream–subsurface exchange of particles. Hydrol. Process. 24, 108–114. http://dx.doi.org/10.1002/hyp.7490.

Arvai, A., Klecka, G., Jasim, S., Melcer, H., Laitta, M.T., 2014. Protecting our Great Lakes: assessing the effectiveness of wastewater treatments for the removal of chemicals of emerging concern. Water Qual. Res. J. Can. 49, 23–31. http://dx.doi.org/10.2166/wqrjc.2013.104.

Asano, Y., Uchida, T., Ohte, N., 2002. Residence times and flow paths of water in steep unchannelled catchments, Tanakami, Japan. J. Hydrol. 261, 173–192. http://dx.doi.org/10.1016/S0022-1694(02)00005-7.

Ayraud, V., Aquilina, L., Labasque, T., Pauwels, H., Molenat, J., Pierson-Wickmann, A.-C., Durand, V., Bour, O., Tarits, C., Le Corre, P., Fourre, E., Merot, P., Davy, P., 2008. Compartmentalization of physical and chemical properties in hard-rock aquifers deduced from chemical and groundwater age analyses. Appl. Geochem. 23, 2686–2707. http://dx.doi.org/10.1016/j.apgeochem.2008.06.001.

Baker, M.A., Dahm, C.N., Valett, H.M., 1999. Acetate retention and metabolism in the hyporheic zone of a mountain stream. Limnol. Oceanogr. 44, 1530–1539. http://dx.doi.org/10.4319/lo.1999.44.6.1530.

Baker, A., 2005. Thermal fluorescence quenching properties of dissolved organic matter. Water Res. 39, 4405–4412. http://dx.doi.org/10.1016/j.watres.2005.08.023.

Baker, A., Lamont-Black, J., 2001. Fluorescence of dissolved organic matter as a natural tracer of ground water. Ground Water 39, 745–750. http://dx.doi.org/10.1111/j.1745-6584.2001.tb02365.x.

Bakermans, C., Madsen, E.L., 2002. Diversity of 16S rDNA and Naphthalene Dioxygenase Genes from Coal-Tar-Waste-Contaminated Aquifer Waters. Microb. Ecol. 44, 95–106. http://dx.doi.org/10.1007/s00248-002-0005-8.

Bakermans, C., Hohnstock-Ashe, A.M., Padmanabhan, S., Padmanabhan, P., Madsen, E.L., 2002. Geochemical and Physiological Evidence for Mixed Aerobic and Anaerobic Field Biodegradation of Coal Tar Waste by Subsurface Microbial Communities. Microb. Ecol. 44, 107–117. http://dx.doi.org/10.1007/s00248-002-3011-y.

Balcarczyk, K.L., Jones, J.B., Jaffé, R., Maie, N., 2009. Stream dissolved organic matter bioavailability and composition in watersheds underlain with discontinuous permafrost. Biogeochemistry 94, 255–270. http://dx.doi.org/10.1007/s10533-009-9324-x.

Baldwin, D.S., Valo, W., 2015. Exploring the relationship between the optical properties of water and the quality and quantity of dissolved organic carbon in aquatic ecosystems: strong correlations do not always mean strong predictive power. Environ. Sci. Process. Impacts 17, 619–630. http://dx.doi.org/10.1039/C4EM00473F.

Baranov, V., Lewandowski, J., Romeijn, P., Singer, G., Krause, S., 2016. Effects of bioirrigation of non-biting midges (Diptera: Chironomidae) on lake sediment respiration. Sci. Rep. 6, 27329. http://dx.doi.org/10.1038/srep27329.

Barker, J.F., Fritz, P., 1981. Carbon isotope fractionation during microbial methane oxidation. Nature 293, 289–291. http://dx.doi.org/10.1038/293289a0.

Barthold, F.K., Tyralla, C., Schneider, K., Vaché, K.B., Frede, H.-G., Breuer, L., 2011. How many tracers do we need for end member mixing analysis (EMMA)? A sensitivity analysis. Water Resour. Res. 47, W08519. http://dx.doi.org/10.1029/2011WR010604.

Bastviken, D., Sandén, P., Svensson, T., Ståhlberg, C., Magounakis, M., Öberg, G., 2006. Chloride retention and release in a boreal forest soil: effects of soil water residence time and nitrogen and chloride loads. Environ. Sci. Technol. 40, 2977–2982. http://dx.doi.org/10.1021/es0523237.

Battin, T.J., 1997. Assessment of fluorescein diacetate hydrolysis as a measure of total esterase activity in natural stream sediment biofilms. Sci. Total Environ. 198, 51–60. http://dx.doi.org/10.1016/S0048-9697(97)05441-7.

Bauer, S., Fulda, C., Schäfer, W., 2001. A multi-tracer study in a shallow aquifer using age dating tracers 3H, 85Kr, CFC-113 and SF6 — indication for retarded transport of CFC-113. J. Hydrol. 248, 14–34. http://dx.doi.org/10.1016/S0022-1694(01)00381-X.

Becker, S.K., 2013. Assessing the Use of Dissolved Silicon as a Proxy for Groundwater Age: A Critical Analysis of Published Data and New Data from the North Carolina Coastal Plain. (M.S.). North Carolina State University, Raleigh, North Carolina.

Begemann, F., Libby, W.F., 1957. Continental water balance, ground water inventory and storage times, surface ocean mixing rates and world-wide water circulation patterns from cosmic-ray and bomb tritium. Geochim. Cosmochim. Acta 12, 277–296. http://dx.doi.org/10.1016/0016-7037(57)90040-6.

Ben Maamar, S., Aquilina, L., Quaiser, A., Pauwels, H., Michon-Coudouel, S., Vergnaud-Ayraud, V., Labasque, T., Roques, C., Abbott, B.W., Dufresne, A., 2015. Groundwater isolation governs chemistry and microbial community structure along hydrologic flowpaths. Front. Microbiol. Microbiol. Chem. Geomicrobiol. 6, 1457. http://dx.doi.org/10.3389/fmicb.2015.01457.

Bencala, K.E., Walters, R.A., 1983. Simulation of solute transport in a mountain pool-and-riffle stream: a transient storage model. Water Resour. Res. 19, 718–724. http://dx.doi.org/10.1029/WR019i003p00718.

Bero, N.J., Ruark, M.D., Lowery, B., 2016. Bromide and chloride tracer application to determine sufficiency of plot size and well depth placement to capture preferential flow and solute leaching. Geoderma 262, 94–100. http://dx.doi.org/10.1016/j.geoderma.2015.08.001.

Beven, K., Freer, J., 2001. Equifinality, data assimilation, and uncertainty estimation in mechanistic modelling of complex environmental systems using the GLUE methodology. J. Hydrol. 249, 11–29.

Beven, K., Germann, P., 2013. Macropores and water flow in soils revisited. Water Resour. Res. 49, 3071–3092. http://dx.doi.org/10.1002/wrcr.20156.

Beven, K., Germann, P., 1982. Macropores and water flow in soils. Water Resour. Res. 18, 1311–1325. http://dx.doi.org/10.1029/WR018i005p01311.

Beven, K., Smith, P., 2015. Concepts of information content and likelihood in parameter calibration for hydrological simulation models. J. Hydrol. Eng. 20, A4014010. http://dx.doi.org/10.1061/(ASCE)HE.1943-5584.0000991.

Blinn, D., Halse, S., Pinder, A., Shiel, R., 2004. Diatom and micro-invertebrate communities and environmental determinants in the western Australian wheatbelt: a response to salinization. Hydrobiologia 528, 229–248. http://dx.doi.org/10.1007/s10750-004-2350-8.

Blöschl, G., 2013. Runoff Prediction in Ungauged Basins: Synthesis Across Processes, Places and Scales. Cambridge University Press.

Blöschl, G., Ardoin-Bardin, S., Bonell, M., Dorninger, M., Goodrich, D., Gutknecht, D., Matamoros, D., Merz, B., Shand, P., Szolgay, J., 2007. At what scales do climate variability and land cover change impact on flooding and low flows? Hydrol. Process. 21, 1241–1247. http://dx.doi.org/10.1002/hyp.6669.

Böhlke, J.K., Denver, J.M., 1995. Combined use of groundwater dating, chemical, and isotopic analyses to resolve the history and fate of nitrate contamination in two agricultural watersheds, Atlantic Coastal Plain, Maryland. Water Resour. Res. 31, 2319–2339. http://dx.doi.org/10.1029/95WR01584.

Borch, T., Kretzschmar, R., Kappler, A., Cappellen, P.V., Ginder-Vogel, M., Voegelin, A., Campbell, K., 2010. Biogeochemical redox processes and their impact on contaminant dynamics. Environ. Sci. Technol. 44, 15–23. http://dx.doi.org/10.1021/es9026248.

Böttcher, J., Strebel, O., Voerkelius, S., Schmidt, H.-L., 1990. Using isotope fractionation of nitrate-nitrogen and nitrate-oxygen for evaluation of microbial denitrification in a sandy aquifer. J. Hydrol. 114, 413–424. http://dx.doi.org/10.1016/0022-1694(90)90068-9.

Botter, G., Bertuzzo, E., Rinaldo, A., 2010. Transport in the hydrologic response: travel time distributions, soil moisture dynamics, and the old water paradox. Water Resour. Res. 46, W03514. http://dx.doi.org/10.1029/2009WR008371.

Boughton, D.A., Hatch, C., Mora, E., 2012. Identifying distinct thermal components of a creek. Water Resour. Res. 48, W09506. http://dx.doi.org/10.1029/2011WR011713.

Boulton, A.J., Findlay, S., Marmonier, P., Stanley, E.H., Valett, H.M., 1998. The functional significance of the hyporheic zone in streams and rivers. Annu. Rev. Ecol. Syst. 59–81.

Boulton, A.J., Stanley, E.H., 1996. But the story gets better: subsurface invertebrates in stream ecosystems. Trends Ecol. Evol. 11, 430.

Brenot, A., Négrel, P., Petelet-Giraud, E., Millot, R., Malcuit, E., 2015. Insights from the salinity origins and interconnections of aquifers in a regional scale sedimentary aquifer system (Adour-Garonne district, SW France): contributions of $\delta^{34}S$ and $\delta^{18}O$ from dissolved sulfates and the $^{87}Sr/^{86}Sr$ ratio. Appl. Geochem. 53, 27–41. http://dx.doi.org/10.1016/j.apgeochem.2014.12.002.

Briggs, M.A., Lautz, L.K., McKenzie, J.M., Gordon, R.P., Hare, D.K., 2012. Using high-resolution distributed temperature sensing to quantify spatial and temporal variability in vertical hyporheic flux. Water Resour. Res. 48, W02527. http://dx.doi.org/10.1029/2011WR011227.

Brooks, B.W., Lazorchak, J.M., Howard, M.D.A., Johnson, M.-V.V., Morton, S.L., Perkins, D.A.K., Reavie, E.D., Scott, G.I., Smith, S.A., Steevens, J.A., 2016. Are harmful algal blooms becoming the greatest inland water quality threat to public health and aquatic ecosystems? Environ. Toxicol. Chem. 35, 6–13. http://dx.doi.org/10.1002/etc.3220.

Brunke, M., Gonser, T., 1997. The ecological significance of exchange processes between rivers and groundwater. Freshw. Biol. 37, 1–33. http://dx.doi.org/10.1046/j.1365-2427.1997.00143.x.

Buerge, I.J., Poiger, T., Muller, M.D., Buser, H.-R., 2003. Caffeine, an anthropogenic marker for wastewater comtamination of surface waters. Environ. Sci. Technol. 37, 691–700. http://dx.doi.org/10.1021/es020125z.

Buerge, I.J., Buser, H.-R., Kahle, M., Mueller, M.D., Poiger, T., 2009. Ubiquitous occurrence of the artificial sweetener acesulfame in the aquatic environment: an ideal chemical marker of domestic wastewater in groundwater. Environ. Sci. Technol. 43, 4381–4385. http://dx.doi.org/10.1021/es900126x.

Bullister, J.L., Weiss, R.F., 1983. Anthropogenic chlorofluoromethanes in the Greenland and Norwegian Seas. Science 221, 265–268. http://dx.doi.org/10.1126/science.221.4607.265.

Butman, D.E., Wilson, H.F., Barnes, R.T., Xenopoulos, M.A., Raymond, P.A., 2014. Increased mobilization of aged carbon to rivers by human disturbance. Nat. Geosci. 8, 112–116. http://dx.doi.org/10.1038/ngeo2322.

Cai, S.-S., Stark, J.D., 1997. Evaluation of five fluorescent dyes and triethyl phosphate as atmospheric tracers of agricultural sprays. J. Environ. Sci. Health B 32, 969–983. http://dx.doi.org/10.1080/03601239709373123.

Capderrey, C., Datry, T., Foulquier, A., Claret, C., Malard, F., 2013. Invertebrate distribution across nested geomorphic features in braided-river landscapes. Freshw. Sci. 32, 1188–1204. http://dx.doi.org/10.1899/12-188.1.

Carslaw, H.S., Jaeger, J.C., 1986. Conduction of Heat in Solids. second ed. Oxford University Press, Oxford Oxfordshire: New York.

Casida, L.E., Klein, D.A., Santoro, T., 1964. Soil dehydrogenase activity. Soil Sci. 98, 371–376.

Catalá, T.S., Reche, I., Fuentes-Lema, A., Romera-Castillo, C., Nieto-Cid, M., Ortega-Retuerta, E., Calvo, E., Álvarez, M., Marrasé, C., Stedmon, C.A., Álvarez-Salgado, X.A., 2015. Turnover time of fluorescent dissolved organic matter in the dark global ocean. Nat. Commun. 6, 5986. http://dx.doi.org/10.1038/ncomms6986.

Cetecioglu, Z., Ince, B., Azman, S., Ince, O., 2013. Biodegradation of tetracycline under various conditions and effects on microbial community. Appl. Biochem. Biotechnol. 172, 631–640. http://dx.doi.org/10.1007/s12010-013-0559-6.

Characklis, G.W., Dilts, M.J., Simmons, O.D., Likirdopulos, C.A., Krometis, L.A., Sobsey, M.D., 2005. Microbial partitioning to settleable particles in stormwater. Water Res. 39, 1773–1782. http://dx.doi.org/10.1016/j.watres.2005.03.004.

Chasar, L.S., Chanton, J.P., Glaser, P.H., Siegel, D.I., Rivers, J.S., 2000. Radiocarbon and stable carbon isotopic evidence for transport and transformation of dissolved organic carbon, dissolved inorganic carbon, and CH4 in a northern Minnesota peatland. Glob. Biogeochem. Cycles 14, 1095–1108. http://dx.doi.org/10.1029/1999GB001221.

Chefetz, B., Mualem, T., Ben-Ari, J., 2008. Sorption and mobility of pharmaceutical compounds in soil irrigated with reclaimed wastewater. Chemosphere 73, 1335–1343. http://dx.doi.org/10.1016/j.chemosphere.2008.06.070.

Chen, W., Westerhoff, P., Leenheer, J.A., Booksh, K., 2003. Fluorescence excitation — emission matrix regional integration to quantify spectra for dissolved organic matter. Environ. Sci. Technol. 37, 5701–5710. http://dx.doi.org/10.1021/es034354c.

Cherkauer, K.A., Burges, S.J., Handcock, R.N., Kay, J.E., Kampf, S.K., Gillespie, A.R., 2005. Assessing satellite-based and aircraft-based thermal infrared remote sensing for monitoring Pacific Northwest river temperature1. JAWRA J. Am. Water Resour. Assoc. 41, 1149–1159. http://dx.doi.org/10.1111/j.1752-1688.2005.tb03790.x.

Chicharo, L., Müller, F., Fohrer, N., 2015. Ecosystem Services and River Basin Ecohydrology. Springer.

Christophersen, N., Hooper, R.P., 1992. Multivariate analysis of stream water chemical data: The use of principal components analysis for the end-member mixing problem. Water Resour. Res. 28, 99–107.

Ciocca, F., Lunati, I., Van de Giesen, N., Parlange, M.B., 2012. Heated optical fiber for distributed soil-moisture measurements: a lysimeter experiment. Vadose Zone J. 11 (0). http://dx.doi.org/10.2136/vzj2011.0199.

Clara, M., Strenn, B., Kreuzinger, N., 2004. Carbamazepine as a possible anthropogenic marker in the aquatic environment: investigations on the behaviour of Carbamazepine in wastewater treatment and during groundwater infiltration. Water Res. 38, 947–954. http://dx.doi.org/10.1016/j.watres.2003.10.058.

Clark, I.D., Fritz, P., 1997. Environmental Isotopes in Hydrogeology. CRC Press.

Clark, M.P., Kavetski, D., Fenicia, F., 2011. Pursuing the method of multiple working hypotheses for hydrological modeling. Water Resour. Res. 47, W09301. http://dx.doi.org/10.1029/2010WR009827.

Cole, J.J., Prairie, Y.T., Caraco, N.F., McDowell, W.H., Tranvik, L.J., Striegl, R.G., Duarte, C.M., Kortelainen, P., Downing, J.A., Middelburg, J.J., Melack, J., 2007. Plumbing the global carbon cycle: integrating inland waters into the terrestrial carbon budget. Ecosystems 10, 172–185. http://dx.doi.org/10.1007/s10021-006-9013-8.

Coles, A.E., Wetzel, C.E., Martínez-Carreras, N., Ector, L., McDonnell, J.J., Frentress, J., Klaus, J., Hoffmann, L., Pfister, L., 2015. Diatoms as a tracer of hydrological connectivity: are they supply limited? Ecohydrology http://dx.doi.org/10.1002/eco.1662 (n/a-n/a).
Coleman, D.C., Fry, B., 1991. Carbon Isotope Techniques (Isotopic Techniques in Plant, Soil and Aquatic Biology series). Academic Press, London, UK.
Collins, S.L., Belnap, J., Grimm, N.B., Rudgers, J.A., Dahm, C.N., D'Odorico, P., Litvak, M., Natvig, D.O., Peters, D.C., Pockman, W.T., Sinsabaugh, R.L., Wolf, B.O., 2014. A multiscale, hierarchical model of pulse dynamics in arid-land ecosystems. Annu. Rev. Ecol. Evol. Syst. 45, 397–419. http://dx.doi.org/10.1146/annurev-ecolsys-120213-091650.
Collon, P., Kutschera, W., Loosli, H.H., Lehmann, B.E., Purtschert, R., Love, A., Sampson, L., Anthony, D., Cole, D., Davids, B., Morrissey, D.J., Sherrill, B.M., Steiner, M., Pardo, R.C., Paul, M., 2000. ^{81}Kr in the Great Artesian Basin, Australia: a new method for dating very old groundwater. Earth Planet. Sci. Lett. 182, 103–113. http://dx.doi.org/10.1016/S0012-821X(00)00234-X.
Constantz, J., 2008. Heat as a tracer to determine streambed water exchanges. Water Resour. Res. 44, W00D10. http://dx.doi.org/10.1029/2008WR006996.
Cook, P.G., 2013. Estimating groundwater discharge to rivers from river chemistry surveys. Hydrol. Process. 27, 3694–3707. http://dx.doi.org/10.1002/hyp.9493.
Cornaton, F.J., 2012. Transient water age distributions in environmental flow systems: the time-marching Laplace transform solution technique. Water Resour. Res. 48. http://dx.doi.org/10.1029/2011wr010606.
Covino, T.P., McGlynn, B.L., McNamara, R.A., 2010. Tracer Additions for Spiraling Curve Characterization (TASCC): quantifying stream nutrient uptake kinetics from ambient to saturation. Limnol. Oceanogr. Methods 8, 484–498. http://dx.doi.org/10.4319/lom.2010.8.484.
Darcy, H., 1856. Les fontaines publiques de la ville de Dijon: Exposition et application des principes a suivre et des formules à employer dans les questions de distribution d'eau; ouvrage terminé par un appendice relatif aux fournitures d'eau de plusieurs villes au filtrage des eaux et à la fabrication des tuyaux de fonte, de plomb, de tole et de bitume. Victor Dalmont, Libraire des Corps imperiaux des ponts et chaussées et des mines.
Darling, W.G., Gooddy, D.C., MacDonald, A.M., Morris, B.L., 2012. The practicalities of using CFCs and SF 6 for groundwater dating and tracing. Appl. Geochem. 27, 1688–1697.
Davies, J., Beven, K., Rodhe, A., Nyberg, L., Bishop, K., 2013. Integrated modeling of flow and residence times at the catchment scale with multiple interacting pathways. Water Resour. Res. 49, 4738–4750. http://dx.doi.org/10.1002/wrcr.20377.
Davies, J.A.C., Beven, K., 2015. Hysteresis and scale in catchment storage, flow and transport. Hydrol. Process. 29, 3604–3615. http://dx.doi.org/10.1002/hyp.10511.
Davis, S.N., Thompson, G.M., Bentley, H.W., Stiles, G., 1980. Ground-water tracers — a short review. Ground Water 18, 14–23. http://dx.doi.org/10.1111/j.1745-6584.1980.tb03366.x.
Davranche, M., Pourret, O., Gruau, G., Dia, A., Le Coz-Bouhnik, M., 2005. Adsorption of REE(III)-humate complexes onto MnO2: experimental evidence for cerium anomaly and lanthanide tetrad effect suppression. Geochim. Cosmochim. Acta 69, 4825–4835. http://dx.doi.org/10.1016/j.gca.2005.06.005.
Deiner, K., Altermatt, F., 2014. Transport distance of invertebrate environmental DNA in a natural river. PLoS ONE 9, e88786. http://dx.doi.org/10.1371/journal.pone.0088786.
Deitchman, R.S., Loheide, S.P., 2009. Ground-based thermal imaging of groundwater flow processes at the seepage face. Geophys. Res. Lett. 36, L14401. http://dx.doi.org/10.1029/2009GL038103.
Demars, B.O.L., Thompson, J., Manson, J.R., 2015. Stream metabolism and the open diel oxygen method: Principles, practice, and perspectives. Limnol. Oceanogr. Methods 13, 356–374. http://dx.doi.org/10.1002/lom3.10030.
Detty, J.M., McGuire, K.J., 2010. Topographic controls on shallow groundwater dynamics: implications of hydrologic connectivity between hillslopes and riparian zones in a till mantled catchment. Hydrol. Process. 24, 2222–2236. http://dx.doi.org/10.1002/hyp.7656.
Dia, A., Gruau, G., Olivié-Lauquet, G., Riou, C., Molénat, J., Curmi, P., 2000. The distribution of rare earth elements in groundwaters: assessing the role of source-rock composition, redox changes and colloidal particles. Geochim. Cosmochim. Acta 64, 4131–4151. http://dx.doi.org/10.1016/S0016-7037(00)00494-4.
Doctor, D.H., Kendall, C., Sebestyen, S.D., Shanley, J.B., Ohte, N., Boyer, E.W., 2008. Carbon isotope fractionation of dissolved inorganic carbon (DIC) due to outgassing of carbon dioxide from a headwater stream. Hydrol. Process. 22, 2410–2423. http://dx.doi.org/10.1002/hyp.6833.
Dodds, W.K., Gido, K., Whiles, M.R., Daniels, M.D., Grudzinski, B.P., 2015. The Stream Biome Gradient Concept: factors controlling lotic systems across broad biogeographic scales. Freshw. Sci. 34, 1–19. http://dx.doi.org/10.1086/679756.
Dole, R.B., 1906. Use of fluorescein in the study of underground waters. In: Fuller, M.C. (Ed.), Underground-Water Papers. Government Printing Office, Washington.
Dole-Olivier, M.j., Marmonier, P., 1992. Patch distribution of interstitial communities: prevailing factors. Freshw. Biol. 27, 177–191. http://dx.doi.org/10.1111/j.1365-2427.1992.tb00532.x.
Dooge, J.C.I., 1986. Looking for hydrologic laws. Water Resour. Res. 22, 46S–58S. http://dx.doi.org/10.1029/WR022i09Sp0046S.
Doucett, R.R., Barton, D.R., Guiguer, K., Power, G., Drimmie, R.J., 1996. Comment: critical examination of stable isotope analysis as a means for tracing carbon pathways in stream ecosystems. Can. J. Fish. Aquat. Sci. 53, 1913–1915. http://dx.doi.org/10.1139/f96-114.
Downing, B.D., Boss, E., Bergamaschi, B.A., Fleck, J.A., Lionberger, M.A., Ganju, N.K., Schoellhamer, D.H., Fujii, R., 2009. Quantifying fluxes and characterizing compositional changes of dissolved organic matter in aquatic systems in situ using combined acoustic and optical measurements. Limnol. Oceanogr. Methods 7, 119–131. http://dx.doi.org/10.4319/lom.2009.7.119.
Drummond, J.D., Aubeneau, A.F., Packman, A.I., 2014. Stochastic modeling of fine particulate organic carbon dynamics in rivers. Water Resour. Res. 50, 4341–4356. http://dx.doi.org/10.1002/2013WR014665.
Dugdale, S.J., Bergeron, N.E., St-Hilaire, A., 2015. Spatial distribution of thermal refuges analysed in relation to riverscape hydromorphology using airborne thermal infrared imagery. Remote Sens. Environ. 160, 43–55. http://dx.doi.org/10.1016/j.rse.2014.12.021.
Duncan, J.M., Groffman, P.M., Band, L.E., 2013. Towards closing the watershed nitrogen budget: spatial and temporal scaling of denitrification. J. Geophys. Res. Biogeosci. 118, 1105–1119. http://dx.doi.org/10.1002/jgrg.20090.
Durán-Alarcón, C., Gevaert, C.M., Mattar, C., Jiménez-Muñoz, J.C., Pasapera-Gonzales, J.J., Sobrino, J.A., Silvia-Vidal, Y., Fashé-Raymundo, O., Chavez-Espiritu, T.W., Santillan-Portilla, N., 2015. Recent trends on glacier area retreat over the group of Nevados Caullaraju-Pastoruri (Cordillera Blanca, Peru) using Landsat imagery. J. S. Am. Earth Sci. 59, 19–26. http://dx.doi.org/10.1016/j.jsames.2015.01.006.
Durán-Álvarez, J.C., Prado-Pano, B., Jiménez-Cisneros, B., 2012. Sorption and desorption of carbamazepine, naproxen and triclosan in a soil irrigated with raw wastewater: estimation of the sorption parameters by considering the initial mass of the compounds in the soil. Chemosphere 88, 84–90. http://dx.doi.org/10.1016/j.chemosphere.2012.02.067.
Earl, S.R., Valett, H.M., Webster, J.R., 2006. Nitrogen saturation in stream ecosystems. Ecology 87, 3140–3151. http://dx.doi.org/10.1890/0012-9658(2006)87[3140:NSISE]2.0.CO;2.
Ebersole, J.L., Liss, W.J., Frissell, C.A., 2003. Thermal heterogeneity, stream channel morphology, and salmonid abundance in northeastern Oregon streams. Can. J. Fish. Aquat. Sci. 60, 1266–1280. http://dx.doi.org/10.1139/f03-107.
Ebersole, J.L., Liss, W.J., Frissell, C.A., 2001. Relationship between stream temperature, thermal refugia and rainbow trout *Oncorhynchus mykiss* abundance in arid-land streams in the northwestern United States. Ecol. Freshw. Fish 10, 1–10. http://dx.doi.org/10.1034/j.1600-0633.2001.100101.x.
Eberts, S.M., Bohlke, J.K., Kauffman, L.J., Jurgens, B.C., 2012. Comparison of particle-tracking and lumped-parameter age-distribution models for evaluating vulnerability of production wells to contamination. Hydrogeol. J. 20, 263–282. http://dx.doi.org/10.1007/s10040-011-0810-6.
Ehleringer, J.R., Buchmann, N., Flanagan, L.B., 2000. Carbon isotope ratios in belowground carbon cycle processes. Ecol. Appl. 10, 412–422. http://dx.doi.org/10.1890/1051-0761(2000)010[0412:CIRIBC]2.0.CO;2.
Ehret, U., Gupta, H.V., Sivapalan, M., Weijs, S.V., Schymanski, S.J., Blöschl, G., Gelfan, A.N., Harman, C., Kleidon, A., Bogaard, T.A., Wang, D., Wagener, T., Scherer, U., Zehe, E., Bierkens, M.F.P., Di Baldassarre, G., Parajka, J., van Beek, L.P.H., van Griensven, A., Westhoff, M.C., Winsemius, H.C., 2014. Advancing catchment hydrology to deal with predictions under change. Hydrol. Earth Syst. Sci. 18, 649–671. http://dx.doi.org/10.5194/hess-18-649-2014.
Ellison, D., Futter, M.N., Bishop, K., 2012. On the forest cover-water yield debate: from demand- to supply-side thinking. Glob. Chang. Biol. 18, 806–820. http://dx.doi.org/10.1111/j.1365-2486.2011.02589.x.
Elser, J., Bennett, E., 2011. Phosphorus cycle: a broken biogeochemical cycle. Nature 478, 29–31. http://dx.doi.org/10.1038/478029a.
Engdahl, N.B., Maxwell, R.M., 2014. Approximating groundwater age distributions using simple streamtube models and multiple tracers. Adv. Water Resour. 66, 19–31. http://dx.doi.org/10.1016/j.advwatres.2014.02.001.
Eriksson, E., 1971. Compartment models and reservoir theory. Annu. Rev. Ecol. Syst. 2, 67–84. http://dx.doi.org/10.1146/annurev.es.02.110171.000435.
Ettayfi, N., Bouchaou, L., Michelot, J.L., Tagma, T., Warner, N., Boutaleb, S., Massault, M., Lgourna, Z., Vengosh, A., 2012. Geochemical and isotopic (oxygen, hydrogen, carbon, strontium) constraints for the origin, salinity, and residence time of groundwater from a carbonate aquifer in the Western Anti-Atlas Mountains, Morocco. J. Hydrol. 438–439, 97–111. http://dx.doi.org/10.1016/j.jhydrol.2012.03.003.
Evans, C.D., Thomas, D.N., 2016. Controls on the processing and fate of terrestrially-derived organic carbon in aquatic ecosystems: synthesis of special issue. Aquat. Sci. http://dx.doi.org/10.1007/s00027-016-0470-7.
Farquhar, G., Richards, R., 1984. Isotopic composition of plant carbon correlates with water-use efficiency of wheat genotypes. Funct. Plant Biol. 11, 539–552.
Fellman, J.B., Hood, E., Edwards, R.T., D'Amore, D.V., 2009. Changes in the concentration, biodegradability, and fluorescent properties of dissolved organic matter during stormflows in coastal temperate watersheds. J. Geophys. Res. 114, G01021. http://dx.doi.org/10.1029/2008JG000790.
Fellman, J.B., Hood, E., Spencer, R.G.M., 2010. Fluorescence spectroscopy opens new windows into dissolved organic matter dynamics in freshwater ecosystems: a review. Limnol. Oceanogr. 55, 2452–2462. http://dx.doi.org/10.4319/lo.2010.55.6.2452.
Ferrant, S., Laplanche, C., Durbe, G., Probst, A., Dugast, P., Durand, P., Sanchez-Perez, J.M., Probst, J.L., 2013. Continuous measurement of nitrate concentration in a highly event-responsive agricultural catchment in south-west of France: is the gain of information useful? Hydrol. Process. 27, 1751–1763. http://dx.doi.org/10.1002/hyp.9324.
Ficetola, G.F., Miaud, C., Pompanon, F., Taberlet, P., 2008. Species detection using environmental DNA from water samples. Biol. Lett. 4, 423–425. http://dx.doi.org/10.1098/rsbl.2008.0118.
Fienen, M.N., Luo, J., Kitanidis, P.K., 2006. A Bayesian geostatistical transfer function approach to tracer test analysis. Water Resour. Res. 42. http://dx.doi.org/10.1029/2005WR004576.
Finlay, J.C., 2004. Patterns and controls of lotic algal stable carbon isotope ratios. Limnol. Oceanogr. 49, 850–861. http://dx.doi.org/10.4319/lo.2004.49.3.0850.
Finlay, J.C., 2003. Controls of streamwater dissolved inorganic carbon dynamics in a forested watershed. Biogeochemistry 62, 231–252. http://dx.doi.org/10.1023/A:1021183023963.

Fisher, S.G., Grimm, N.B., Martí, E., Holmes, R.M., Jones Jr., J.B., 1998. Material spiraling in stream corridors: a telescoping ecosystem model. Ecosystems 1, 19–34.

Fisher, S.G., Sponseller, R.A., Heffernan, J.B., 2004. Horizons in stream biogeochemistry: flowpaths to progress. Ecology 85, 2369–2379.

Flury, M., Wai, N.N., 2003. Dyes as tracers for vadose zone hydrology. Rev. Geophys. 41, 1002. http://dx.doi.org/10.1029/2001RG000109.

Fontes, J.-C., 1992. Chemical and Isotopic Constraints on 14C Dating of Groundwater. In: Taylor, R.E., Long, A., Kra, R.S. (Eds.), Radiocarbon After Four Decades. Springer, New York, pp. 242–261.

Fontvieille, D.A., Outaguerouine, A., Thevenot, D.R., 1992. Fluorescein diacetate hydrolysis as a measure of microbial activity in aquatic systems: application to activated sludges. Environ. Technol. 13, 531–540. http://dx.doi.org/10.1080/09593339209385181.

Foppen, J.W., Orup, C., Adell, R., Poulalion, V., Uhlenbrook, S., 2011. Using multiple artificial DNA tracers in hydrology. Hydrol. Process. 25, 3101–3106. http://dx.doi.org/10.1002/hyp.8159.

Foppen, J.W., Seopa, J., Bakobie, N., Bogaaard, T., 2013. Development of a methodology for the application of synthetic DNA in stream tracer injection experiments. Water Resour. Res. 49, 5369–5380. http://dx.doi.org/10.1002/wrcr.20438.

Foster, G.N., 2007. In: Hauer, F.R., Lamberti, G.A. (Eds.), Methods in stream ecology. J. Insect Conserv. 12, pp. 583–584. http://dx.doi.org/10.1007/s10841-007-9120-7.

Frei, S., Knorr, K.H., Peiffer, S., Fleckenstein, J.H., 2012. Surface micro-topography causes hot spots of biogeochemical activity in wetland systems: a virtual modeling experiment. J. Geophys. Res. Biogeosci. 117, G00N12. http://dx.doi.org/10.1029/2012JG002012.

Frissell, C.A., Liss, W.J., Warren, C.E., Hurley, M.D., 1986. A hierarchical framework for stream habitat classification: viewing streams in a watershed context. Environ. Manage 10, 199–214.

Frey, C., Hietanen, S., Jürgens, K., Labrenz, M., Voss, M., 2014. N and O isotope fractionation in nitrate during chemolithoautotrophic denitrification by *Sulfurimonas gotlandica*. Environ. Sci. Technol. 48, 13229–13237. http://dx.doi.org/10.1021/es503456g.

Bertrand, G., D.S., Ala-Aho, P., P.M.R., 2014. Environmental tracers and indicators bringing together groundwater, surface water and groundwater-dependent ecosystems: importance of scale in choosing relevant tools. Environ. Earth Sci.

Gaglioti, B.V., Mann, D.H., Jones, B.M., Pohlman, J.W., Kunz, M.L., Wooller, M.J., 2014. Radiocarbon age-offsets in an arctic lake reveal the long-term response of permafrost carbon to climate change: radiocarbon age-offsets. J. Geophys. Res. Biogeosci. 119, 1630–1651. http://dx.doi.org/10.1002/2014JG002688.

Gammon, R.H., Cline, J., Wisegarver, D., 1982. Chlorofluoromethanes in the northeast Pacific Ocean: measured vertical distributions and application as transient tracers of upper ocean mixing. J. Geophys. Res. Oceans 87, 9441–9454. http://dx.doi.org/10.1029/JC087iC12p09441.

Garneau, M.-È., Vincent, W.F., Terrado, R., Lovejoy, C., 2009. Importance of particle-associated bacterial heterotrophy in a coastal Arctic ecosystem. J. Mar. Syst. 75, 185–197. http://dx.doi.org/10.1016/j.jmarsys.2008.09.002.

Gat, J.R., Gonfiantini, R., 1981. Stable isotope hydrology. Deuterium and Oxygen-18 in the Water Cycle.

Gelhar, L.W., Wilson, J.L., 1974. Ground-water quality modeling. Ground Water 12, 399–408. http://dx.doi.org/10.1111/j.1745-6584.1974.tb03050.x.

Geyh, M.A., et al., 2000. An overview of ^{14}C analysis in the study of groundwater. Radiocarbon 42, 99–114.

Gilmore, T.E., Genereux, D.P., Solomon, D.K., Solder, J.E., 2016. Groundwater transit time distribution and mean from streambed sampling in an agricultural coastal plain watershed, North Carolina, USA. Water Resour. Res.

Gilmour, C.C., Henry, E.A., 1991. Mercury methylation in aquatic systems affected by acid deposition. Environ. Pollut. 71, 131–169.

Glover, R.B., Kim, J.P., 1993. SF6-a new nonradioactive geothermal tracer. Fifteenth New Zealand Geothermal Workshop, pp. 121–132.

Godsey, S.E., Aas, W., Clair, T.A., de Wit, H.A., Fernandez, I.J., Kahl, J.S., Malcolm, I.A., Neal, C., Neal, M., Nelson, S.J., Norton, S.A., Palucis, M.C., Skjelkvåle, B.L., Soulsby, C., Tetzlaff, D., Kirchner, J.W., 2010. Generality of fractal 1/f scaling in catchment tracer time series, and its implications for catchment travel time distributions. Hydrol. Process. 24, 1660–1671. http://dx.doi.org/10.1002/hyp.7677.

Godsey, S.E., Kirchner, J.W., Clow, D.W., 2009. Concentration–discharge relationships reflect chemostatic characteristics of US catchments. Hydrol. Process. 23, 1844–1864. http://dx.doi.org/10.1002/hyp.7315.

Goldscheider, N., Haller, L., Pote, J., Wildi, W., Zopfi, J., 2007. Characterizing water circulation and contaminant transport in Lake Geneva using bacteriophage tracer experiments and limnological methods. Environ. Sci. Technol. 41, 5252–5258. http://dx.doi.org/10.1021/es070369p.

González-Pinzón, R., Haggerty, R., Dentz, M., 2013. Scaling and predicting solute transport processes in streams. Water Resour. Res. 49, 4071–4088. http://dx.doi.org/10.1002/wrcr.20280.

González-Pinzón, R., Ward, A.S., Hatch, C.E., Wlostowski, A.N., Singha, K., Gooseff, M.N., Haggerty, R., Harvey, J.W., Cirpka, O.A., Brock, J.T., 2015. A field comparison of multiple techniques to quantify groundwater–surface-water interactions. Freshw. Sci. 34, 139–160. http://dx.doi.org/10.1086/679738.

Graustein, W.C., 1989. $^{87}Sr/^{86}Sr$ ratios measure the sources and flow of strontium in terrestrial ecosystems. In: Rundel, P.W., Ehleringer, J.R., Nagy, K.A. (Eds.), Stable Isotopes in Ecological Research, Ecological Studies. Springer, New York, pp. 491–512.

Green, C.T., Zhang, Y., Jurgens, B.C., Starn, J.J., Landon, M.K., 2014. Accuracy of travel time distribution (TTD) models as affected by TTD complexity, observation errors, and model and tracer selection. Water Resour. Res. 6191–6213 http://dx.doi.org/10.1002/2014WR015625.

Gribsholt, B., Veuger, B., Tramper, A., Middelburg, J.J., Boschker, H.T.S., 2009. Long-term 15N-nitrogen retention in tidal freshwater marsh sediment: elucidating the microbial contribution. Limnol. Oceanogr. 54, 13–22. http://dx.doi.org/10.4319/lo.2009.54.1.0013.

Gruau, G., Dia, A., Olivie-Lauquet, G., Davranche, M., Pinay, G., 2004. Controls on the distribution of rare earth elements in shallow groundwaters. Water Res. 38, 3576–3586.

Gruber, N., Galloway, J.N., 2008. An Earth-system perspective of the global nitrogen cycle. Nature 451, 293–296. http://dx.doi.org/10.1038/nature06592.

Guenet, B., Danger, M., Abbadie, L., Lacroix, G., 2010. Priming effect: bridging the gap between terrestrial and aquatic ecology. Ecology 91, 2850–2861. http://dx.doi.org/10.1890/09-1968.1.

Haddeland, I., Heinke, J., Biemans, H., Eisner, S., Flörke, M., Hanasaki, N., Konzmann, M., Ludwig, F., Masaki, Y., Schewe, J., et al., 2014. Global water resources affected by human interventions and climate change. Proc. Natl. Acad. Sci. 111, 3251–3256.

Haggerty, R., Argerich, A., Martí, E., 2008. Development of a "smart" tracer for the assessment of microbiological activity and sediment-water interaction in natural waters: the resazurin-resorufin system. Water Resour. Res. 44, W00D01. http://dx.doi.org/10.1029/2007WR006670.

Haggerty, R., Ribot, M., Singer, G.A., Martí, E., Argerich, A., Agell, G., Battin, T.J., 2014. Ecosystem respiration increases with biofilm growth and bed forms: flume measurements with resazurin. J. Geophys. Res. Biogeosci. 119. http://dx.doi.org/10.1002/2013JG002498 (2013JG002498).

Hahne, A., Volz, A., Ehhalt, D.H., Cosatto, H., Roether, W., Weiss, W., Kromer, B., 1978. Depth profiles of chlorofluoromethanes in the Norwegian sea. Pure Appl. Geophys. 116, 575–582. http://dx.doi.org/10.1007/BF01636910.

Haitjema, H.M., 1995. On the residence time distribution in idealized groundwatersheds. J. Hydrol. 172, 127–146. http://dx.doi.org/10.1016/0022-1694(95)02732-5.

Hammer, P.M., Hayes, J.M., Jenkins, W.J., Gagosian, R.B., 1978. Exploratory analyses of trichlorofluoromethane (F-11) in North Atlantic water columns. Geophys. Res. Lett. 5, 645–648. http://dx.doi.org/10.1029/GL005i008p00645.

Han, L.-F., Plummer, L.N., 2013. Revision of Fontes & Garnier's model for the initial ^{14}C content of dissolved inorganic carbon used in groundwater dating. Chem. Geol. 351, 105–114.

Hannah, D.M., Malcolm, I.A., Soulsby, C., Youngson, A.F., 2008. A comparison of forest and moorland stream microclimate, heat exchanges and thermal dynamics. Hydrol. Process. 22, 919–940. http://dx.doi.org/10.1002/hyp.7003.

Hannah, D.M., Garner, G., 2015. River water temperature in the United Kingdom Changes over the 20th century and possible changes over the 21st century. Prog. Phys. Geogr. 39, 68–92. http://dx.doi.org/10.1177/0309133314550669.

Hansell, D.A., Carlson, C.A., 2001. Marine dissolved organic matter and the carbon cycle. Oceanography 14, 41–49.

Harms, T.K., Grimm, N.B., 2008. Hot spots and hot moments of carbon and nitrogen dynamics in a semiarid riparian zone. J. Geophys. Res. Biogeosci. 113, G01020. http://dx.doi.org/10.1029/2007JG000588.

Harun, S., Baker, A., Bradley, C., Pinay, G., 2016. Spatial and seasonal variations in the composition of dissolved organic matter in a tropical catchment: the Lower Kinabatangan River, Sabah, Malaysia. Environ. Sci. Process. Impacts 18, 137–150. http://dx.doi.org/10.1039/C5EM00462D.

Harun, S., Baker, A., Bradley, C., Pinay, G., Boomer, I., Liz Hamilton, R., 2015. Characterisation of dissolved organic matter in the Lower Kinabatangan River, Sabah, Malaysia. Hydrol. Res. 46, 411. http://dx.doi.org/10.2166/nh.2014.196.

Harvey, R.W., Ryan, J.N., 2004. Use of PRD1 bacteriophage in groundwater viral transport, inactivation, and attachment studies. FEMS Microbiol. Ecol. 49, 3–16. http://dx.doi.org/10.1016/j.femsec.2003.09.015.

Harwood, V.J., Staley, C., Badgley, B.D., Borges, K., Korajkic, A., 2014. Microbial source tracking markers for detection of fecal contamination in environmental waters: relationships between pathogens and human health outcomes. FEMS Microbiol. Rev. 38, 1–40. http://dx.doi.org/10.1111/1574-6976.12031.

Hauer, F.R., Lamberti, G.A., 2011. Methods in Stream Ecology. Academic Press.

Helton, A.M., Ardón, M., Bernhardt, E.S., 2015. Thermodynamic constraints on the utility of ecological stoichiometry for explaining global biogeochemical patterns. Ecol. Lett. 18, 1049–1056. http://dx.doi.org/10.1111/ele.12487.

Hemme, C.L., Deng, Y., Gentry, T.J., Fields, M.W., Wu, L., Barua, S., Barry, K., Tringe, S.G., Watson, D.B., He, Z., Hazen, T.C., Tiedje, J.M., Rubin, E.M., Zhou, J., 2010. Metagenomic insights into evolution of a heavy metal-contaminated groundwater microbial community. ISME J. 4, 660–672. http://dx.doi.org/10.1038/ismej.2009.154.

Hewlett, J.D., Hibbert, A.R., 1967. Factors affecting the response of small watersheds to precipitation in humid areas. For. Hydrol. 275–290.

Hissler, C., Stille, P., Guignard, C., Iffly, J.F., Pfister, L., 2014. Rare earth elements as hydrological tracers of anthropogenic and critical zone contributions: a case study at the Alzette River Basin Scale. Geochemistry of the Earth's surface GES-10 Paris France, 18–23 August, 2014. Procedia Earth Planet. Sci. 10, pp. 349–352. http://dx.doi.org/10.1016/j.proeps.2014.08.036.

Hoeg, S., Uhlenbrook, S., Leibundgut, C., 2000. Hydrograph separation in a mountainous catchment — combining hydrochemical and isotopic tracers. Hydrol. Process. 14, 1199–1216. http://dx.doi.org/10.1002/(SICI)1099-1085(200005)14:7<1199::AID-HYP35>3.0.CO;2-K.

Hornberger, G.M., Wiberg, P.L., D'Odorico, P., Raffensperger, J.P., 2014. Elements of Physical Hydrology. JHU Press.

Horneman, A., Stute, M., Schlosser, P., Smethie, W., Santella, N., Ho, D.T., Mailloux, B., Gorman, E., Zheng, Y., van Geen, A., 2008. Degradation rates of CFC-11, CFC-12 and CFC-113 in anoxic shallow aquifers of Araihazar, Bangladesh. J. Contam. Hydrol. 97, 27–41. http://dx.doi.org/10.1016/j.jconhyd.2007.12.001.

Horton, R.E., 1945. Erosional development of streams and their drainage basins; hydrophysical approach quantitative morphology. Geol. Soc. Am. Bull. 56, 275. http://dx.doi.org/10.1130/0016-7606(1945)56[275:EDOSAT]2.0.CO;2.

Hosono, T., Tokunaga, T., Tsushima, A., Shimada, J., 2014. Combined use of $\delta^{13}C$, $\delta^{15}N$, and $\delta^{34}S$ tracers to study anaerobic bacterial processes in groundwater flow systems. Water Res. 54, 284–296. http://dx.doi.org/10.1016/j.watres.2014.02.005.

Hrachowitz, M., Benettin, P., van Breukelen, B.M., Fovet, O., Howden, N.J.K., Ruiz, L., van der Velde, Y., Wade, A.J., 2016. Transit times—the link between hydrology and water quality at the catchment scale. Wiley Interdiscip. Rev. Water 1–29 http://dx.doi.org/10.1002/wat2.1155.

Huguet, A., Vacher, L., Relexans, S., Saubusse, S., Froidefond, J.M., Parlanti, E., 2009. Properties of fluorescent dissolved organic matter in the Gironde Estuary. Org. Geochem. 40, 706–719. http://dx.doi.org/10.1016/j.orggeochem.2009.03.002.

Hunt, R.J., Borchardt, M.A., Bradbury, K.R., 2014. Viruses as groundwater tracers: using ecohydrology to characterize short travel times in aquifers. Ground Water 52, 187–193. http://dx.doi.org/10.1111/gwat.12158.

Hunt, R.J., Wilcox, D.A., 2003. Ecohydrology-why hydrologists should care. Ground Water 41, 289. http://dx.doi.org/10.1111/j.1745-6584.2003.tb02592.x.

Hynes, H., 1975. The stream and its valley. Verh. Intern. Ver. Limnol. 19, 1–15.

Jaffé, R., McKnight, D., Maie, N., Cory, R., McDowell, W.H., Campbell, J.L., 2008. Spatial and temporal variations in DOM composition in ecosystems: the importance of long-term monitoring of optical properties. J. Geophys. Res. Biogeosci. 113, G04032. http://dx.doi.org/10.1029/2008JG000683.

Jaffé, R., Yamashita, Y., Maie, N., Cooper, W.T., Dittmar, T., Dodds, W.K., Jones, J.B., Myoshi, T., Ortiz-Zayas, J.R., Podgorski, D.C., Watanabe, A., 2012. Dissolved organic matter in headwater streams: compositional variability across climatic regions of North America. Geochim. Cosmochim. Acta 94, 95–108. http://dx.doi.org/10.1016/j.gca.2012.06.031.

Jansen, B., Kalbitz, K., McDowell, W.H., 2014. Dissolved organic matter: linking soils and aquatic systems. Vadose Zone J. 13, 1–4. http://dx.doi.org/10.2136/vzj2014.05.0051.

Jasechko, S., Kirchner, J.W., Welker, J.M., McDonnell, J.J., 2016. Substantial proportion of global streamflow less than three months old. Nat. Geosci. 9, 126–129. http://dx.doi.org/10.1038/ngeo2636.

Jeanneau, L., Jaffrezic, A., Pierson-Wickmann, A.-C., Gruau, G., Lambert, T., Petitjean, P., 2014. Constraints on the sources and production mechanisms of dissolved organic matter in soils from molecular biomarkers. Vadose Zone J. 13 (0). http://dx.doi.org/10.2136/vzj2014.02.0015.

Jensen, A.M., Neilson, B.T., McKee, M., Chen, Y., 2012. Thermal remote sensing with an autonomous unmanned aerial remote sensing platform for surface stream temperatures. Geoscience and Remote Sensing Symposium (IGARSS), 2012 IEEE International. Presented at the Geoscience and Remote Sensing Symposium (IGARSS), 2012 IEEE International, pp. 5049–5052 http://dx.doi.org/10.1109/IGARSS.2012.6352476.

Jeon, C.O., Park, W., Padmanabhan, P., DeRito, C., Snape, J.R., Madsen, E.L., 2003. Discovery of a bacterium, with distinctive dioxygenase, that is responsible for in situ biodegradation in contaminated sediment. Proc. Natl. Acad. Sci. 100, 13591–13596. http://dx.doi.org/10.1073/pnas.1735529100.

Johnson, A.G., Glenn, C.R., Burnett, W.C., Peterson, R.N., Lucey, P.G., 2008. Aerial infrared imaging reveals large nutrient-rich groundwater inputs to the ocean. Geophys. Res. Lett. 35, L15606. http://dx.doi.org/10.1029/2008GL034574.

Jurgens, B.C., Böhlke, J.K., Eberts, S.M., 2012. An Excel® workbook for interpreting groundwater age distributions from environmental tracer data. U.S. Geological Survey Techniques and Methods.

Kalbus, E., Reinstorf, F., Schirmer, M., 2006. Measuring methods for groundwater, surface water and their interactions: a review. Hydrol. Earth Syst. Sci. Discuss. 3, 1809–1850. http://dx.doi.org/10.5194/hessd-3-1809-2006.

Kasahara, T., Datry, T., Mutz, M., Boulton, A.J., 2009. Treating causes not symptoms: restoration of surface–groundwater interactions in rivers. Mar. Freshw. Res. 60, 976. http://dx.doi.org/10.1071/MF09047.

Käss, W., Behrens, H.(.H.)., Käss, W., 1998. Tracing technique in geohydrology. Balkema.

Kaufman, W.J., Orlob, G.T., 1956. An evaluation of ground-water tracers. EOS Trans. Am. Geophys. Union 37, 297–306. http://dx.doi.org/10.1029/TR037i003p00297.

Kemna, A., Kulessa, B., Vereecken, H., 2002. Imaging and characterisation of subsurface solute transport using electrical resistivity tomography (ERT) and equivalent transport models. J. Hydrol. 267, 125–146.

Kendall, C., McDonnell, J.J., 2012. Isotope Tracers in Catchment Hydrology. Elsevier.

Keswick, B.H., Wang, D.-S., Gerba, C.P., 1982. The Use of Microorganisms as Ground-Water Tracers: A Review. Ground Water 20, 142–149. http://dx.doi.org/10.1111/j.1745-6584.1982.tb02741.x.

Khamis, K., Sorensen, J.P.R., Bradley, C., Hannah, D.M., Lapworth, D.J., Stevens, R., 2015. In situ tryptophan-like fluorometers: assessing turbidity and temperature effects for freshwater applications. Environ. Sci. Process. Impacts 17, 740–752. http://dx.doi.org/10.1039/C5EM00030K.

Kirchner, J.W., 2016a. Aggregation in environmental systems – part 1: seasonal tracer cycles quantify young water fractions, but not mean transit times, in spatially heterogeneous catchments. Hydrol. Earth Syst. Sci. 20, 279–297. http://dx.doi.org/10.5194/hess-20-279-2016.

Kirchner, J.W., 2016b. Aggregation in environmental systems – part 2: catchment mean transit times and young water fractions under hydrologic nonstationarity. Hydrol. Earth Syst. Sci. 20, 299–328. http://dx.doi.org/10.5194/hess-20-299-2016.

Kirchner, J.W., 2006. Getting the right answers for the right reasons: linking measurements, analyses, and models to advance the science of hydrology: getting the right answers for the right reasons. Water Resour. Res. 42, W03S04. http://dx.doi.org/10.1029/2005WR004362.

Kirchner, J.W., Feng, X., Neal, C., Robson, A.J., 2004. The fine structure of water-quality dynamics: the (high-frequency) wave of the future. Hydrol. Process. 18, 1353–1359. http://dx.doi.org/10.1002/hyp.5537.

Kirkby, M.J., 1987. The hurst effect and its implications for extrapolating process rates. Earth Surf. Process. Landf. 12, 57–67. http://dx.doi.org/10.1002/esp.3290120108.

Klaus, J., Wetzel, C.E., Martínez-Carreras, N., Ector, L., Pfister, L., 2015. A tracer to bridge the scales: on the value of diatoms for tracing fast flow path connectivity from headwaters to meso-scale catchments. Hydrol. Process. 29, 5275–5289. http://dx.doi.org/10.1002/hyp.10628.

Koh, D.-C., Niel Plummer, L., Kip Solomon, D., Busenberg, E., Kim, Y.-J., Chang, H.-W., 2006. Application of environmental tracers to mixing, evolution, and nitrate contamination of ground water in Jeju Island, Korea. J. Hydrol. 327, 258–275. http://dx.doi.org/10.1016/j.jhydrol.2005.11.021.

Kolbe, T., Marçais, J., Thomas, Z., Abbott, B.W., de Dreuzy, J.-R., Rousseau-Gueutin, P., Aquilina, L., Labasque, T., Pinay, G., 2016. Coupling 3D groundwater modeling with CFC-based age dating to classify local groundwater circulation in an unconfined crystalline aquifer. J. Hydrol. http://dx.doi.org/10.1016/j.jhydrol.2016.05.020.

Krause, S., Boano, F., Cuthbert, M.O., Fleckenstein, J.H., Lewandowski, J., 2014. Understanding process dynamics at aquifer-surface water interfaces: an introduction to the special section on new modeling approaches and novel experimental technologies: introduction. Water Resour. Res. 50, 1847–1855. http://dx.doi.org/10.1002/2013WR014755.

Krause, S., Hannah, D.M., Fleckenstein, J.H., Heppell, C.M., Kaeser, D., Pickup, R., Pinay, G., Robertson, A.L., Wood, P.J., 2011. Inter-disciplinary perspectives on processes in the hyporheic zone. Ecohydrology 4, 481–499. http://dx.doi.org/10.1002/eco.176.

Krause, S., Lewandowski, J., Dahm, C.N., Tockner, K., 2015. Frontiers in real-time ecohydrology - a paradigm shift in understanding complex environmental systems: frontiers in real-time ecohydrology. Ecohydrology 8, 529–537. http://dx.doi.org/10.1002/eco.1646.

Kritee, K., Sigman, D.M., Granger, J., Ward, B.B., Jayakumar, A., Deutsch, C., 2012. Reduced isotope fractionation by denitrification under conditions relevant to the ocean. Geochim. Cosmochim. Acta 92, 243–259. http://dx.doi.org/10.1016/j.gca.2012.05.020.

Kumar, P., 2011. Typology of hydrologic predictability. Water Resour. Res. 47, W00H05. http://dx.doi.org/10.1029/2010WR009769.

Kung, K.-J.S., 1990. Influence of plant uptake on the performance of bromide tracer. Soil Sci. Soc. Am. J. 54, 975. http://dx.doi.org/10.2136/sssaj1990.03615995005400040006x.

Kurissery, S., Kanavillil, N., Verenitch, S., Mazumder, A., 2012. Caffeine as an anthropogenic marker of domestic waste: A study from Lake Simcoe watershed. Ecol. Indic. 23, 501–508. http://dx.doi.org/10.1016/j.ecolind.2012.05.001.

Lacelle, D., Fontaine, M., Forest, A.P., Kokelj, S., 2014. High-resolution stable water isotopes as tracers of thaw unconformities in permafrost: A case study from western Arctic Canada. Chem. Geol. 368, 85–96. http://dx.doi.org/10.1016/j.chemgeo.2014.01.005.

Lalot, E., Curie, F., Wawrzyniak, V., Baratelli, F., Schomburgk, S., Flipo, N., Piegay, H., Moatar, F., 2015. Quantification of the contribution of the Beauce groundwater aquifer to the discharge of the Loire River using thermal infrared satellite imaging. Hydrol. Earth Syst. Sci. 19, 4479–4492. http://dx.doi.org/10.5194/hess-19-4479-2015.

Lambert, T., Pierson-Wickmann, A.-C., Gruau, G., Jaffrezic, A., Petitjean, P., Thibault, J.N., Jeanneau, L., 2014. DOC sources and DOC transport pathways in a small headwater catchment as revealed by carbon isotope fluctuation during storm events. Biogeosciences 11, 3043–3056. http://dx.doi.org/10.5194/bg-11-3043-2014.

Larocque, M., Cook, P.G., Haaken, K., Simmons, C.T., 2009. Estimating flow using tracers and hydraulics in synthetic heterogeneous aquifers. Ground Water 47, 786–796. http://dx.doi.org/10.1111/j.1745-6584.2009.00595.x.

Larouche, J.R., Abbott, B.W., Bowden, W.B., Jones, J.B., 2015. The role of watershed characteristics, permafrost thaw, and wildfire on dissolved organic carbon biodegradability and water chemistry in Arctic headwater streams. Biogeosciences 12, 4221–4233. http://dx.doi.org/10.5194/bg-12-4221-2015.

Lautz, L.K., 2012. Observing temporal patterns of vertical flux through streambed sediments using time-series analysis of temperature records. J. Hydrol. 464–465, 199–215. http://dx.doi.org/10.1016/j.jhydrol.2012.07.006.

Leclerc, H., Mossel, D.A.A., Edberg, S.C., Struijk, C.B., 2001. Advances in the bacteriology of the coliform group: their suitability as markers of microbial water safety. Annu. Rev. Microbiol. 55, 201–234. http://dx.doi.org/10.1146/annurev.micro.55.1.201.

Lehmann, B.E., Davis, S.N., Fabryka-Martin, J.T., 1993. Atmospheric and subsurface sources of stable and radioactive nuclides used for groundwater dating. Water Resour. Res. 29, 2027–2040. http://dx.doi.org/10.1029/93WR00543.

Lehmann, M.F., Reichert, P., Bernasconi, S.M., Barbieri, A., McKenzie, J.A., 2003. Modelling nitrogen and oxygen isotope fractionation during denitrification in a lacustrine redox-transition zone. Geochim. Cosmochim. Acta 67, 2529–2542. http://dx.doi.org/10.1016/S0016-7037(03)00085-1.

Leibundgut, C., Maloszewski, P., Külls, C., 2009. Tracers in Hydrology, Tracers in Hydrology. John Wiley & Sons, Ltd.

Leibundgut, C., Maloszewski, P., Külls, C., 2011. Tracers in Hydrology. John Wiley & Sons.

Leith, F.I., Garnett, M.H., Dinsmore, K.J., Billett, M.F., Heal, K.V., 2014. Source and age of dissolved and gaseous carbon in a peatland–riparian–stream continuum: a dual isotope (^{14}C and $\delta^{13}C$) analysis. Biogeochemistry 119, 415–433. http://dx.doi.org/10.1007/s10533-014-9977-y.

Lemke, D., González-Pinzón, R., Liao, Z., Wöhling, T., Osenbrück, K., Haggerty, R., Cirpka, O.A., 2014. Sorption and transformation of the reactive tracers resazurin and resorufin in natural river sediments. Hydrol. Earth Syst. Sci. 18, 3151–3163. http://dx.doi.org/10.5194/hess-18-3151-2014.

Leray, S., Engdahl, N.B., Massoudieh, A., Bresciani, E., McCallum, J., 2016. Residence time distributions for hydrologic systems: mechanistic foundations and steady-state analytical solutions. J. Hydrol. http://dx.doi.org/10.1016/j.jhydrol.2016.01.068.

Lerner, D.N., 1992. Well catchments and time-of-travel zones in aquifers with recharge. Water Resour. Res. 28, 2621–2628. http://dx.doi.org/10.1029/92wr01170.

Lewandowski, J., Meinikmann, K., Ruhtz, T., Pöschke, F., Kirillin, G., 2013. Localization of lacustrine groundwater discharge (LGD) by airborne measurement of thermal infrared radiation. Remote Sens. Environ. 138, 119–125. http://dx.doi.org/10.1016/j.rse.2013.07.005.

Lewicka-Szczebak, D., Jędrysek, M.-O., 2013. Tracing and quantifying lake water and groundwater fluxes in the area under mining dewatering pressure using coupled O and H stable isotope approach. Isot. Environ. Health Stud. 49, 9–28. http://dx.doi.org/10.1080/10256016.2012.700641.

Likens, G.E., Bormann, F.H., 1974. Linkages between terrestrial and aquatic ecosystems. Bioscience 24, 447–456. http://dx.doi.org/10.2307/1296852.

Likens, G.E., Bormann, F.H., Johnson, N.M., Fisher, D.W., Pierce, R.S., 1970. Effects of forest cutting and herbicide treatment on nutrient budgets in the Hubbard Brook watershed-ecosystem. Ecol. Monogr. 40, 23. http://dx.doi.org/10.2307/1942440.

Lindeman, R.L., 1942. The trophic-dynamic aspect of ecology. Ecology 23, 399–417. http://dx.doi.org/10.2307/1930126.

Lis, G., Wassenaar, L.I., Hendry, M.J., 2008. High-precision laser spectroscopy D/H and $^{18}O/^{16}O$ measurements of microliter natural water samples. Anal. Chem. 80, 287–293. http://dx.doi.org/10.1021/ac701716q.

Liu, Y., Blowes, D.W., Groza, L., Sabourin, M.J., Ptacek, C.J., 2014. Acesulfame-K and pharmaceuticals as co-tracers of municipal wastewater in a receiving river. Environ. Sci. Process. Impacts 16, 2789–2795. http://dx.doi.org/10.1039/C4EM00237G.

Lovelock, J.E., Maggs, R.J., Wade, R.J., 1973. Halogenated hydrocarbons in and over the Atlantic. Nature 241, 194–196. http://dx.doi.org/10.1038/241194a0.

Lowry, C.S., Walker, J.F., Hunt, R.J., Anderson, M.P., 2007. Identifying spatial variability of groundwater discharge in a wetland stream using a distributed temperature sensor. Water Resour. Res. 43, W10408. http://dx.doi.org/10.1029/2007WR006145.

Lu, Z.-T., Schlosser, P., Smethie Jr., W.M., Sturchio, N.C., Fischer, T.P., Kennedy, B.M., Purtschert, R., Severinghaus, J.P., Solomon, D.K., Tanhua, T., Yokochi, R., 2014. Tracer applications of noble gas radionuclides in the geosciences. Earth-Sci. Rev. 138, 196–214. http://dx.doi.org/10.1016/j.earscirev.2013.09.002.

Lubick, N., 2009. Artificial sweetener makes ideal tracer. Environ. Sci. Technol. 43, 4220. http://dx.doi.org/10.1021/es901127x.

Mahler, B.J., Winkler, M., Bennett, P., Hillis, D.M., 1998. DNA-labeled clay: a sensitive new method for tracing particle transport. Geology 26, 831–834. http://dx.doi.org/10.1130/0091-7613(1998)026<0831:DLCASN>2.3.CO;2.

Maloszewski, P., Zuber, A., 1996. Lumped parameter models for the interpretation of environmentaltracer data. Manual On Mathematical Models in Isotope Hydrology. Vienna Austria IAEA-TECDOC 910, pp. 9–58.

Maloszewski, P., Zuber, A., 1993. Tracer experiments in fractured rocks: matrix diffusion and the validity of models. Water Resour. Res. 29, 2723–2735. http://dx.doi.org/10.1029/93WR00608.

Mamer, E.A., Lowry, C.S., 2013. Locating and quantifying spatially distributed groundwater/surface water interactions using temperature signals with paired fiber-optic cables. Water Resour. Res. 49, 7670–7680. http://dx.doi.org/10.1002/2013WR014235.

Manzoni, S., Piñeiro, G., Jackson, R.B., Jobbágy, E.G., Kim, J.H., Porporato, A., 2012. Analytical models of soil and litter decomposition: solutions for mass loss and time-dependent decay rates. Soil Biol. Biochem. 50, 66–76. http://dx.doi.org/10.1016/j.soilbio.2012.02.029.

Marçais, J., de Dreuzy, J.R., Ginn, T.R., Rousseau-Gueutin, P., Leray, S., 2015. 6. Inferring transit time distributions from atmospheric tracer data: assessment of the predictive capacities of lumped parameter models on a 3D crystalline aquifer model. J. Hydrol. 525, 619–631. http://dx.doi.org/10.1016/j.jhydrol.2015.03.055.

Marmonier, P., Dole-Olivier, M.J., Creuz Chătelliers, M.É.D., 1992. Spatial distribution of interstitial assemblages in the floodplain of the rhŏne river. Regul. Rivers Res. Manag. 7, 75–82. http://dx.doi.org/10.1002/rrr.3450070110.

Marmonier, P., Vervier, P., Giber, J., Dole-Olivier, M.-J., 1993. Biodiversity in ground waters. Trends Ecol. Evol. 8, 392–395. http://dx.doi.org/10.1016/0169-5347(93)90039-R.

Martinec, J., 1975. Subsurface flow from snowmelt traced by tritium. Water Resour. Res. 11, 496–498. http://dx.doi.org/10.1029/WR011i003p00496.

Martínez-Carreras, C.E.W.N., Frentress, J., L.E., McDonnell, J.J., L.H., Pfister, L., 2015. Hydrological connectivity as indicated by transport of diatoms through the riparian–stream system. Hydrol. Earth Syst. Sci. Discuss. 12, 2391–2434. http://dx.doi.org/10.5194/hessd-12-2391-2015.

Marwick, T.R., Tamooh, F., Teodoru, C.R., Borges, A.V., Darchambeau, F., Bouillon, S., 2015. The age of river-transported carbon: a global perspective. Glob. Biogeochem. Cycles 29. http://dx.doi.org/10.1002/2014GB004911 (2014GB004911).

Massoudieh, A., Visser, A., Sharifi, S., Broers, H.P., 2014. A Bayesian modeling approach for estimation of a shape-free groundwater age distribution using multiple tracers. Appl. Geochem. 50, 252–264. http://dx.doi.org/10.1016/j.apgeochem.2013.10.004.

Mayorga, E., Aufdenkampe, A.K., Masiello, C.A., Krusche, A.V., Hedges, J.I., Quay, P.D., Richey, J.E., Brown, T.A., 2005. Young organic matter as a source of carbon dioxide outgassing from Amazonian rivers. Nature 436, 538–541. http://dx.doi.org/10.1038/nature03880.

McCallum, J.L., Cook, P.G., Simmons, C.T., Werner, A.D., 2014a. Bias of apparent tracer ages in heterogeneous environments. Groundwater 52, 239–250.

McCallum, J.L., Engdahl, N.B., Ginn, T.R., Cook, P.G., 2014b. Nonparametric estimation of groundwater residence time distributions: what can environmental tracer data tell us about groundwater residence time? Water Resour. Res. 50, 2022–2038. http://dx.doi.org/10.1002/2013wr014974.

McClain, M.E., Boyer, E.W., Dent, C.L., Gergel, S.E., Grimm, N.B., Groffman, P.M., Hart, S.C., Harvey, J.W., Johnston, C.A., Mayorga, E., et al., 2003. Biogeochemical hot spots and hot moments at the interface of terrestrial and aquatic ecosystems. Ecosystems 6, 301–312.

McDonnell, J.J., 2003. Where does water go when it rains? Moving beyond the variable source area concept of rainfall-runoff response. Hydrol. Process. 17, 1869–1875. http://dx.doi.org/10.1002/hyp.5132.

McDonnell, J.J., 1990. A rationale for old water discharge through macropores in a steep, humid catchment. Water Resour. Res. 26, 2821–2832. http://dx.doi.org/10.1029/WR026i011p02821.

McDonnell, J.J., Beven, K., 2014. Debates—the future of hydrological sciences: a (common) path forward? A call to action aimed at understanding velocities, celerities and residence time distributions of the headwater hydrograph. Water Resour. Res. 50, 5342–5350. http://dx.doi.org/10.1002/2013WR015141.

McDonnell, J.J., Bonell, M., Stewart, M.K., Pearce, A.J., 1990. Deuterium variations in storm rainfall: Implications for stream hydrograph separation. Water Resour. Res. 26, 455–458. http://dx.doi.org/10.1029/WR026i003p00455.

McDonnell, J.J., Sivapalan, M., Vaché, K., Dunn, S., Grant, G., Haggerty, R., Hinz, C., Hooper, R., Kirchner, J., Roderick, M.L., Selker, J., Weiler, M., 2007. Moving beyond heterogeneity and process complexity: a new vision for watershed hydrology. Water Resour. Res. 43, W07301. http://dx.doi.org/10.1029/2006WR005467.

McDowell, W.H., Zsolnay, A., Aitkenhead-Peterson, J.A., Gregorich, E.G., Jones, D.L., Jödemann, D., Kalbitz, K., Marschner, B., Schwesig, D., 2006. A comparison of methods to determine the biodegradable dissolved organic carbon from different terrestrial sources. Soil Biol. Biochem. 38, 1933–1942. http://dx.doi.org/10.1016/j.soilbio.2005.12.018.

McGuire, K.J., DeWalle, D.R., Gburek, W.J., 2002. Evaluation of mean residence time in subsurface waters using oxygen-18 fluctuations during drought conditions in the mid-Appalachians. J. Hydrol. 261, 132–149. http://dx.doi.org/10.1016/S0022-1694(02)00006-9.

McGuire, K.J., McDonnell, J.J., 2006. A review and evaluation of catchment transit time modeling. J. Hydrol. 330, 543–563. http://dx.doi.org/10.1016/j.jhydrol.2006.04.020.

Mclntire, C.D., Garrison, R.L., Phinney, H.K., Warren, C.E., 1964. Primary Production in Laboratory Streams 1,2. Limnol. Oceanogr. 9, 92–102. http://dx.doi.org/10.4319/lo.1964.9.1.0092.

McKnight, D.M., Cozzetto, K., Cullis, J.D.S., Gooseff, M.N., Jaros, C., Koch, J.C., Lyons, W.B., Neupauer, R., Wlostowski, A., 2015. Potential for real-time understanding of coupled hydrologic and biogeochemical processes in stream ecosystems: future integration of telemetered data with process models for glacial meltwater streams. Water Resour. Res. 51, 6725–6738. http://dx.doi.org/10.1002/2015WR017618.

McNicholl, B.P., McGrath, J.W., Quinn, J.P., 2007. Development and application of a resazurin-based biomass activity test for activated sludge plant management. Water Res. 41, 127–133. http://dx.doi.org/10.1016/j.watres.2006.10.002.

Mendoza-Lera, C., Federlein, L.L., Knie, M., Mutz, M., 2016. The algal lift: buoyancy-mediated sediment transport. Water Resour. Res. 52, 108–118. http://dx.doi.org/10.1002/2015WR017315.

Mendoza-Lera, C., Mutz, M., 2013. Microbial activity and sediment disturbance modulate the vertical water flux in sandy sediments. Freshw. Sci. 32, 26–38. http://dx.doi.org/10.1899/11-165.1.

Michel, R.L., 2004. Tritium hydrology of the Mississippi River basin. Hydrol. Process. 18, 1255–1269. http://dx.doi.org/10.1002/hyp.1403.

Mockler, E.M., O'Loughlin, F.E., Bruen, M., 2015. Understanding hydrological flow paths in conceptual catchment models using uncertainty and sensitivity analysis. Comput. Geosci. http://dx.doi.org/10.1016/j.cageo.2015.08.015.

Molénat, J., Gascuel-Odoux, C., Aquilina, L., Ruiz, L., 2013. Use of gaseous tracers (CFCs and SF6) and transit-time distribution spectrum to validate a shallow groundwater transport model. J. Hydrol. 480, 1–9. http://dx.doi.org/10.1016/j.jhydrol.2012.11.043.

Morel, B., Durand, P., Jaffrezic, A., Gruau, G., Molenat, J., 2009. Sources of dissolved organic carbon during stormflow in a headwater agricultural catchment. Hydrol. Process. 23, 2888–2901. http://dx.doi.org/10.1002/hyp.7379.

Mulder, J., Christophersen, N., Hauhs, M., Vogt, R.D., Andersen, S., Andersen, D.O., 1990. Water flow paths and hydrochemical controls in the Birkenes Catchment as inferred from a rainstorm high in seasalts. Water Resour. Res. 26, 611–622. http://dx.doi.org/10.1029/WR026i004p00611.

Mulholland, P.J., Steinman, A.D., Elwood, J.W., 1990. Measurement of Phosphorus Uptake Length in Streams: Comparison of Radiotracer and Stable PO4 Releases. Can. J. Fish. Aquat. Sci. 47, 2351–2357. http://dx.doi.org/10.1139/f90-261.

Mulholland, P.J., 1993. Hydrometric and stream chemistry evidence of three storm flowpaths in Walker Branch Watershed. J. Hydrol. 151, 291–316. http://dx.doi.org/10.1016/0022-1694(93)90240-A.

Mulholland, P.J., Newbold, J.D., Elwood, J.W., Ferren, L.A., Webster, J.R., 1985. Phosphorus spiralling in a woodland stream: seasonal variations. Ecology 66, 1012. http://dx.doi.org/10.2307/1940562.

Mulholland, P.J., Hall, R.O., Sobota, D.J., Dodds, W.K., Findlay, S.E.G., Grimm, N.B., Hamilton, S.K., McDowell, W.H., O'Brien, J.M., Tank, J.L., Ashkenas, L.R., Cooper, L.W., Dahm, C.N., Gregory, S.V., Johnson, S.L., Meyer, J.L., Peterson, B.J., Poole, G.C., Valett, H.M., Webster, J.R., Arango, C.P., Beaulieu, J.J., Bernot, M.J., Burgin, A.J., Crenshaw, C.L., Helton, A.M., Johnson, L.T., Niederlehner, B.R., Potter, J.D., Sheibley, R.W., Thomasn, S.M., 2009. Nitrate removal in stream ecosystems measured by 15N addition experiments: Denitrification. Limnol. Oceanogr. 54, 666–680. http://dx.doi.org/10.4319/lo.2009.54.3.0666.

Mulvany, T.J., 1851. On the use of self-registering rain and flood gauges in making observations of the relations of rain fall and flood discharges in a given catchment. IV, 18–33.

Mwakanyamale, K., Slater, L., Day-Lewis, F.D., Elwaseif, M., Johnson, C.D., 2012. Spatially variable stage-driven groundwater-surface water interaction inferred from time-frequency analysis of distributed temperature sensing data. Geophys. Res. Lett. 39, 6. http://dx.doi.org/10.1029/2011GL050824.

Myrttinen, A., Becker, V., Mayer, B., van Geldern, R., Barth, J.A.C., 2015. Determining in situ pH values of pressurised fluids using stable carbon isotope techniques. Chem. Geol. 391, 1–6. http://dx.doi.org/10.1016/j.chemgeo.2014.10.015.

Naicheng Wu, C.F., Uta Ulrich, B.S., Fohrer, N., 2014. Diatoms as an indicator for tile drainage flow in a German lowland catchment. Geophys. Res. Abstr. 16.

Newbold, J.D., Elwood, J.W., O'Neill, R.V., Winkle, W.V., 1981. Measuring nutrient spiralling in streams. Can. J. Fish. Aquat. Sci. 38, 860–863.

Newbold, J.D., Thomas, S.A., Minshall, G.W., Cushing, C.E., Georgian, T., 2005. Deposition, benthic residence, and resuspension of fine organic particles in a mountain stream. Limnol. Oceanogr. 50, 1571–1580. http://dx.doi.org/10.4319/lo.2005.50.5.1571.

Nicholls, D.G., Ferguson, S., 2013. Bioenergetics. Academic Press.

Nyberg, L., Rodhe, A., Bishop, K., 1999. Water transit times and flow paths from two line injections of ^{3}H and ^{36}Cl in a microcatchment at Gårdsjön, Sweden. Hydrol. Process. 13, 1557–1575. http://dx.doi.org/10.1002/(SICI)1099-1085(19990815)13:11<1557::AID-HYP835>3.0.CO;2-S.

Ocampo, C.J., Oldham, C.E., Sivapalan, M., 2006. Nitrate attenuation in agricultural catchments: shifting balances between transport and reaction. Water Resour. Res. 42, W01408. http://dx.doi.org/10.1029/2004WR003773.

Odum, H.T., 1957. Trophic structure and productivity of Silver Springs, Florida. Ecol. Monogr. 27, 55–112. http://dx.doi.org/10.2307/1948571.

Oldham, C.E., Farrow, D.E., Peiffer, S., 2013. A generalized Damköhler number for classifying material processing in hydrological systems. Hydrol. Earth Syst. Sci. 17, 1133–1148. http://dx.doi.org/10.5194/hess-17-1133-2013.

Oremland, R.S., Lonergan, D.J., Culbertson, C.W., Lovley, D.R., 1996. Microbial degradation of hydrochlorofluorocarbons (CHCl2F and CHCl2CF3) in soils and sediments. Appl. Environ. Microbiol. 62, 1818–1821.

Ormerod, J.G., 1964. *Serratia indica* as a bacterial tracer for water movements. J. Appl. Bacteriol. 27, 342–349. http://dx.doi.org/10.1111/j.1365-2672.1964.tb04920.x.

Ozyurt, N.N., Bayari, C.S., 2003. LUMPED: a visual basic code of lumped-parameter models for mean residence time analyses of groundwater systems. Comput. Geosci. 29, 79–90. http://dx.doi.org/10.1016/s0098-3004(02)00075-4.

Pace, M.L., Cole, J.J., Carpenter, S.R., Kitchell, J.F., Hodgson, J.R., Van de Bogert, M.C., Bade, D.L., Kritzberg, E.S., Bastviken, D., 2004. Whole-lake carbon-13 additions reveal terrestrial support of aquatic food webs. Nature 427, 240–243. http://dx.doi.org/10.1038/nature02227.

Packman, A.I., Brooks, N.H., Morgan, J.J., 2000a. Kaolinite exchange between a stream and streambed: Laboratory experiments and validation of a colloid transport model. Water Resour. Res. 36, 2363–2372. http://dx.doi.org/10.1029/2000WR900058.

Packman, A.I., Brooks, N.H., Morgan, J.J., 2000b. A physicochemical model for colloid exchange between a stream and a sand streambed with bed forms. Water Resour. Res. 36, 2351–2361. http://dx.doi.org/10.1029/2000WR900059.

Palmer, S.M., Hope, D., Billett, M.F., Dawson, J.J.C., Bryant, C.L., 2001. Sources of organic and inorganic carbon in a headwater stream: evidence from carbon isotope studies. Biogeochemistry 52, 321–338. http://dx.doi.org/10.1023/A:1006447706565.

Payn, R.A., Gooseff, M.N., Benson, D.A., Cirpka, O.A., Zarnetske, J.P., Bowden, W.B., McNamara, J.P., Bradford, J.H., 2008. Comparison of instantaneous and constant-rate stream tracer experiments through non-parametric analysis of residence time distributions: residence time distributions from stream tracer experiments. Water Resour. Res. 44, 1–10. http://dx.doi.org/10.1029/2007WR006274.

Peralta-Tapia, A., Sponseller, R.A., Tetzlaff, D., Soulsby, C., Laudon, H., 2015. Connecting precipitation inputs and soil flow pathways to stream water in contrasting boreal catchments. Hydrol. Process. 29, 3546–3555. http://dx.doi.org/10.1002/hyp.10300.

Petrides, A.C., Huff, J., Arik, A., van de Giesen, N., Kennedy, A.M., Thomas, C.K., Selker, J.S., 2011. Shade estimation over streams using distributed temperature sensing. Water Resour. Res. 47, W07601. http://dx.doi.org/10.1029/2010WR009482.

Pfister, L., McDonnell, J.J., Hissler, C., Hoffmann, L., 2010. Ground-based thermal imagery as a simple, practical tool for mapping saturated area connectivity and dynamics. Hydrol. Process. 24, 3123–3132. http://dx.doi.org/10.1002/hyp.7840.

Pfister, L., McDonnell, J.J., Sebastian Wrede, D.H., Patrick Matgen, F.F., Luc Ector, L.H., 2009. The rivers are alive: on the potential for diatoms as a tracer of water source and hydrological connectivity. Hydrol. Process. 23, 2841–2845. http://dx.doi.org/10.1002/hyp.7426.

Pike, E.B., Bufton, A.W.J., Gould, D.J., 1969. The use of *Serratia indica* and *Bacillus subtilis* var. *niger* spores for tracing sewage dispersion in the sea. J. Appl. Bacteriol. 32, 206–216. http://dx.doi.org/10.1111/j.1365-2672.1969.tb00968.x.

Pinay, G., Clément, J.C., Naiman, R.J., 2002. Basic principles and ecological consequences of changing water regimes on nitrogen cycling in fluvial systems. Environ. Manag. 30, 481–491.

Pinay, G., O'Keefe, T.C., Edwards, R.T., Naiman, R.J., 2009. Nitrate removal in the hyporheic zone of a salmon river in Alaska. River Res. Appl. 25, 367–375.

Pinay, G., Peiffer, S., De Dreuzy, J.-R., Krause, S., Hannah, D.M., Fleckenstein, J.H., Sebilo, M., Bishop, K., Hubert-Moy, L., 2015. Upscaling nitrogen removal capacity from local hotspots to low stream orders' drainage basins. Ecosystems 18, 1101–1120. http://dx.doi.org/10.1007/s10021-015-9878-5.

Pinay, G., Ruffinoni, C., Wondzell, S., Gazelle, F., 1998. Change in groundwater nitrate concentration in a large river floodplain: denitrification, uptake, or mixing? J. N. Am. Benthol. Soc. 17, 179–189. http://dx.doi.org/10.2307/1467961.

Plummer, L.N., Friedman, L.C., 1999. Tracing and Dating Young Ground Water (No. FS-134-99). US Geological Survey.

Pokrovsky, O.S., Schott, J., Dupré, B., 2006. Trace element fractionation and transport in boreal rivers and soil porewaters of permafrost-dominated basaltic terrain in Central Siberia. Geochim. Cosmochim. Acta 70, 3239–3260. http://dx.doi.org/10.1016/j.gca.2006.04.008.

Polsenaere, P., Abril, G., 2012. Modelling CO_2 degassing from small acidic rivers using water pCO_2, DIC and $\delta^{13}C$-DIC data. Geochim. Cosmochim. Acta 91, 220–239. http://dx.doi.org/10.1016/j.gca.2012.05.030.

Post, D.M., 2002. Using stable isotopes to estimate trophic position: models, methods, and assumptions. Ecology 83, 703. http://dx.doi.org/10.2307/3071875.

Poulsen, J.R., Sebok, E., Duque, C., Tetzlaff, D., Engesgaard, P.K., 2015. Detecting groundwater discharge dynamics from point-to-catchment scale in a lowland stream: combining hydraulic and tracer methods. Hydrol. Earth Syst. Sci. 19, 1871–1886. http://dx.doi.org/10.5194/hess-19-1871-2015.

Pourret, O., Gruau, G., Dia, A., Davranche, M., Molénat, J., 2009. Colloidal Control on the Distribution of Rare Earth Elements in Shallow Groundwaters. Aquat. Geochem. 16, 31–59. http://dx.doi.org/10.1007/s10498-009-9069-0.

Pourret, O., Gruau, G., Dia, A., Davranche, M., Molénat, J., 2010. Colloidal control on the distribution of rare earth elements in shallow groundwaters. Aquat. Geochem. 16, 31–59. http://dx.doi.org/10.1007/s10498-009-9069-0.

Pringle, C., 2003. The need for a more predictive understanding of hydrologic connectivity. Aquat. Conserv. Mar. Freshwat. Ecosyst. 13, 467–471. http://dx.doi.org/10.1002/aqc.603.

Ptak, T., Piepenbrink, M., Martac, E., 2004. Tracer tests for the investigation of heterogeneous porous media and stochastic modelling of flow and transport—a review of some recent developments. J. Hydrol. 294, 122–163. http://dx.doi.org/10.1016/j.jhydrol.2004.01.020.

Pu, J., Feng, C., Liu, Y., Li, R., Kong, Z., Chen, N., Tong, S., Hao, C., Liu, Y., 2014. Pyrite-based autotrophic denitrification for remediation of nitrate contaminated groundwater. Bioresour. Technol. 173, 117–123. http://dx.doi.org/10.1016/j.biortech.2014.09.092.

Quiers, M., Batiot-Guilhe, C., Bicalho, C.C., Perrette, Y., Seidel, J.-L., Exter, S.V., 2013. Characterisation of rapid infiltration flows and vulnerability in a karst aquifer using a decomposed fluorescence signal of dissolved organic matter. Environ. Earth Sci. 71, 553–561. http://dx.doi.org/10.1007/s12665-013-2731-2.

Rastetter, E.B., King, A.W., Cosby, B.J., Hornberger, G.M., O'Neill, R.V., Hobbie, J.E., 1992. Aggregating fine-scale ecological knowledge to model coarser-scale attributes of ecosystems. Ecol. Appl. 2, 55–70. http://dx.doi.org/10.2307/1941889.

Rau, G.C., Andersen, M.S., McCallum, A.M., Roshan, H., Acworth, R.I., 2014. Heat as a tracer to quantify water flow in near-surface sediments. Earth-Sci. Rev. 129, 40–58. http://dx.doi.org/10.1016/j.earscirev.2013.10.015.

Raymond, P.A., Bauer, J.E., 2001. Use of ^{14}C and ^{13}C natural abundances for evaluating riverine, estuarine, and coastal DOC and POC sources and cycling: a review and synthesis. Org. Geochem. 32, 469–485. http://dx.doi.org/10.1016/S0146-6380(00)00190-X.

Redfield, A.C., 1958. The biological control of chemical factors in the environment. Am. Sci. 46, 230A–2221.

Rempe, D.M., Dietrich, W.E., 2014. A bottom-up control on fresh-bedrock topography under landscapes. Proc. Natl. Acad. Sci. 111, 6576–6581. http://dx.doi.org/10.1073/pnas.1404763111.

Riml, J., Worman, A., Kunkel, U., Radke, M., 2013. Evaluating the fate of six common pharmaceuticals using a reactive transport model: insights from a stream tracer test. Sci. Total Environ. 458, 344–354. http://dx.doi.org/10.1016/j.scitotenv.2013.03.077.

Rinaldo, A., Beven, K.J., Bertuzzo, E., Nicotina, L., Davies, J., Fiori, A., Russo, D., Botter, G., 2011. Catchment travel time distributions and water flow in soils. Water Resour. Res. 47, W07537. http://dx.doi.org/10.1029/2011WR010478.

Risacher, F., Fritz, B., Alonso, H., 2006. Non-conservative behavior of bromide in surface waters and brines of Central Andes: a release into the atmosphere? Geochim. Cosmochim. Acta 70, 2143–2152. http://dx.doi.org/10.1016/j.gca.2006.01.019.

Risse-Buhl, U., Hagedorn, F., Dümig, A., Gessner, M.O., Schaaf, W., Nii-Annang, S., Gerull, L., Mutz, M., 2013. Dynamics, chemical properties and bioavailability of DOC in an early successional catchment. Biogeosciences 10, 4751–4765. http://dx.doi.org/10.5194/bg-10-4751-2013.

Rodhe, A., Nyberg, L., Bishop, K., 1996. Transit times for water in a small till catchment from a step shift in the oxygen 18 content of the water input. Water Resour. Res. 32, 3497–3511. http://dx.doi.org/10.1029/95WR01806.

Roose-Amsaleg, C., Laverman, A.M., 2015. Do antibiotics have environmental side-effects? Impact of synthetic antibiotics on biogeochemical processes. Environ. Sci. Pollut. Res. http://dx.doi.org/10.1007/s11356-015-4943-3.

Rosenfeld, J.S., Roff, J.C., 1992. Examination of the carbon base in southern Ontario streams using stable isotopes. J. N. Am. Benthol. Soc. 1–10.

Rossi, P., Dörfliger, N., Kennedy, K., Müller, I., Aragno, M., 1998. Bacteriophages as surface and ground water tracers. Hydrol. Earth Syst. Sci. 2, 101–110. http://dx.doi.org/10.5194/hess-2-101-1998.

Rozanski, K., Araguás-Araguás, L., Gonfiantini, R., 1993. Isotopic patterns in modern global precipitation. In: Swart, P.K., Lohmann, K.C., Mckenzie, J., Savin, S. (Eds.), Climate Change in Continental Isotopic Records. American Geophysical Union, pp. 1–36.

Rushforth, S.R., Merkley, G.S., 1988. Comprehensive list by habitat of the algae of Utah, USA. Great Basin Nat. 48, 154–179.

Sambridge, M., Bodin, T., Gallagher, K., Tkalcic, H., 2013. Transdimensional inference in the geosciences. Philos. Trans. R. Soc. Math. Phys. Eng. Sci. 371. http://dx.doi.org/10.1098/rsta.2011.0547.

Sandford, R.C., Bol, R., Worsfold, P.J., 2010. In situ determination of dissolved organic carbon in freshwaters using a reagentless UV sensor. J. Environ. Monit. 12, 1678–1683. http://dx.doi.org/10.1039/C0EM00060D.

Saraceno, J.F., Pellerin, B.A., Downing, B.D., Boss, E., Bachand, P.A.M., Bergamaschi, B.A., 2009. High-frequency in situ optical measurements during a storm event: assessing relationships between dissolved organic matter, sediment concentrations, and hydrologic processes. J. Geophys. Res. Biogeosci. 114. http://dx.doi.org/10.1029/2009JG000989.

Scanlon, B.R., Healy, R.W., Cook, P.G., 2002. Choosing appropriate techniques for quantifying groundwater recharge. Hydrogeol. J. 10, 18–39. http://dx.doi.org/10.1007/s10040-001-0176-2.

Schaub, M., Alewell, C., 2009. Stable carbon isotopes as an indicator for soil degradation in an alpine environment (Urseren Valley, Switzerland). Rapid Commun. Mass Spectrom. 23, 1499–1507. http://dx.doi.org/10.1002/rcm.4030.

Scheurer, M., Brauch, H.-J., Lange, F., 2009. Analysis and occurrence of seven artificial sweeteners in German waste water and surface water and in soil aquifer treatment (SAT). Anal. Bioanal. Chem. 394, 1585–1594. http://dx.doi.org/10.1007/s00216-009-2881-y.

Schiff, S.L., Aravena, R., Trumbore, S.E., Dillon, P.J., 1990. Dissolved organic carbon cycling in forested watersheds: a carbon isotope approach. Water Resour. Res. 26, 2949–2957. http://dx.doi.org/10.1029/WR026i012p02949.

Schlesinger, W.H., Bernhardt, E.S., 2012. Biogeochemistry: An Analysis of Global Change. Academic Press.

Schlosser, P., Stute, M., Dörr, H., Sonntag, C., Münnich, K.O., 1988. Tritium/^{3}He dating of shallow groundwater. Earth Planet. Sci. Lett. 89, 353–362. http://dx.doi.org/10.1016/0012-821X(88)90122-7.

Schmadel, N.M., Ward, A.S., Kurz, M.J., Fleckenstein, J.H., Zarnetske, J.P., Hannah, D.M., Blume, T., Vieweg, M., Blaen, P.J., Schmidt, C., Knapp, J.L.A., Klaar, M.J., Romeijn, P., Datry, T., Keller, T., Folegot, S., Arricibita, A.I.M., Krause, S., 2016. Stream solute tracer timescales changing with discharge and reach length confound process interpretation. Water Resour. Res. 52, 3227–3245. http://dx.doi.org/10.1002/2015WR018062.

Schnürer, J., Rosswall, T., 1982. Fluorescein diacetate hydrolysis as a measure of total microbial activity in soil and litter. Appl. Environ. Microbiol. 43, 1256–1261.

Schuetz, T., Weiler, M., 2011. Quantification of localized groundwater inflow into streams using ground-based infrared thermography. Geophys. Res. Lett. 38, L03401. http://dx.doi.org/10.1029/2010GL046198.

Sebilo, M., Billen, G., Grably, M., Mariotti, A., 2003. Isotopic composition of nitrate-nitrogen as a marker of riparian and benthic denitrification at the scale of the whole Seine River system. Biogeochemistry 63, 35–51.

Seitzinger, S., Harrison, J.A., Böhlke, J.K., Bouwman, A.F., Lowrance, R., Peterson, B., Tobias, C., Drecht, G.V., 2006. Denitrification across landscapes and waterscapes: a synthesis. Ecol. Appl. 16, 2064–2090. http://dx.doi.org/10.1890/1051-0761(2006)016[2064:DALAWA]2.0.CO;2.

Selker, J., van de Giesen, N., Westhoff, M., Luxemburg, W., Parlange, M.B., 2006a. Fiber optics opens window on stream dynamics. Geophys. Res. Lett. 33, L24401. http://dx.doi.org/10.1029/2006GL027979.

Selker, J.S., Thévenaz, L., Huwald, H., Mallet, A., Luxemburg, W., van de Giesen, N., Stejskal, M., Zeman, J., Westhoff, M., Parlange, M.B., 2006b. Distributed fiber-optic temperature sensing for hydrologic systems. Water Resour. Res. 42, W12202. http://dx.doi.org/10.1029/2006WR005326.

Sharma, A.N., Luo, D., Walter, T.M., 2012. Hydrological tracers using nanobiotechnology: proof of concept. Environ. Sci. Technol. 46, 8928–8936. http://dx.doi.org/10.1021/es301561q.

Shaw, D.G., McIntosh, D.J., 1990. Acetate in recent anoxic sediments: Direct and indirect measurements of concentration and turnover rates. Estuar. Coast. Shelf Sci. 31, 775–788. http://dx.doi.org/10.1016/0272-7714(90)90082-3.

Shen, C., Phanikumar, M.S., Fong, T.T., Aslam, I., McElmurry, S.P., Molloy, S.L., Rose, J.B., 2008. Evaluating bacteriophage P22 as a tracer in a complex surface water system: the Grand River, Michigan. Environ. Sci. Technol. 42, 2426–2431. http://dx.doi.org/10.1021/acs.est.5b05747.

Sherman, 1932. Streamflow from rainfall by the unit-graph method. Eng. News Rec. 108, 501–505.

Sigman, D.M., Casciotti, K.L., Andreani, M., Barford, C., Galanter, M., Böhlke, J.K., 2001. A bacterial method for the nitrogen isotopic analysis of nitrate in seawater and freshwater. Anal. Chem. 73, 4145–4153. http://dx.doi.org/10.1021/ac010088e.

Smart, P.L., Laidlaw, I.M.S., 1977. An evaluation of some fluorescent dyes for water tracing. Water Resour. Res. 13, 15–33. http://dx.doi.org/10.1029/WR013i001p00015.

Snow, J., 1855. On the Mode of Communication of Cholera. John Churchill.

Soares, P.A., Faht, G., Pinheiro, A., da Silva, M.R., Zucco, E., 2013. Determination of reaeration-rate coefficient by modified tracer gas technique. Hydrol. Process. 27, 2710–2720. http://dx.doi.org/10.1002/hyp.9371.

Solomon, D.K., Cook, P.G., Sanford, W.E., 1998. Chapter 9 - Dissolved Gases in Subsurface Hydrology A2. In: McDonnell, J.J., Kendall, C. (Eds.), Isotope Tracers in Catchment Hydrology. Elsevier, Amsterdam, pp. 291–318.

Solomon, D.K., Genereux, D.P., Plummer, L.N., Busenberg, E., 2010. Testing mixing models of old and young groundwater in a tropical lowland rain forest with environmental tracers. Water Resour. Res. 46. http://dx.doi.org/10.1029/2009wr008341.

Soulsby, C., Birkel, C., Geris, J., Dick, J., Tunaley, C., Tetzlaff, D., 2015. Stream water age distributions controlled by storage dynamics and nonlinear hydrologic connectivity: modeling with high-resolution isotope data. Water Resour. Res. 51, 7759–7776. http://dx.doi.org/10.1002/2015WR017888.

Spencer, R.G.M., Mann, P.J., Dittmar, T., Eglinton, T.I., McIntyre, C., Holmes, R.M., Zimov, N., Stubbins, A., 2015. Detecting the signature of permafrost thaw in Arctic rivers. Geophys. Res. Lett. 42, 2830–2835. http://dx.doi.org/10.1002/2015GL063498.

Stedmon, C.A., Bro, R., 2008. Characterizing dissolved organic matter fluorescence with parallel factor analysis: a tutorial. Limnol. Oceanogr. Methods 6, 572–579. http://dx.doi.org/10.4319/lom.2008.6.572.

Kern, S., Brath, M., Fontes, R., Gade, M., Gurgel, K.-W., Kaleschke, L., Spreen, G., Schulz, S., Winderlich, A., Stammer, D., 2009. Multi Scat—a helicopter-based scatterometer for snow-cover and sea-ice investigations. IEEE Geosci. Remote Sens. Lett. 6, 703–707. http://dx.doi.org/10.1109/LGRS.2009.2023823.

Stallman, R.W., 1965. Steady one-dimensional fluid flow in a semi-infinite porous medium with sinusoidal surface temperature. J. Geophys. Res. 70, 2821–2827. http://dx.doi.org/10.1029/JZ070i012p02821.

Stapleton, C.M., Wyer, M.D., Kay, D., Crowther, J., McDonald, A.T., Walters, M., Gawler, A., Hindle, T., 2007. Microbial source tracking: a forensic technique for microbial source identification? J. Environ. Monit. 9, 427–439. http://dx.doi.org/10.1039/b617059e.

Stewart, M.K., McDonnell, J.J., 1991. Modeling base flow soil water residence times from deuterium concentrations. Water Resour. Res. 27, 2681–2693. http://dx.doi.org/10.1029/91WR01569.

Stream Solute Workshop, 1990. Concepts and methods for assessing solute dynamics in stream ecosystems. J. N. Am. Benthol. Soc. 9, 95–119. http://dx.doi.org/10.2307/1467445.

Striegl, R.G., Aiken, G.R., Dornblaser, M.M., Raymond, P.A., Wickland, K.P., 2005. A decrease in discharge-normalized DOC export by the Yukon River during summer through autumn. Geophys. Res. Lett. 32. http://dx.doi.org/10.1029/2005GL024413.

Strohmeier, S., Knorr, K.-H., Reichert, M., Frei, S., Fleckenstein, J.H., Peiffer, S., Matzner, E., 2013. Concentrations and fluxes of dissolved organic carbon in runoff from a forested catchment: insights from high frequency measurements. Biogeosciences 10, 905–916. http://dx.doi.org/10.5194/bg-10-905-2013.

Stumpf, M., Ternes, T.A., Wilken, R.-D., Rodrigues, S.V., Baumann, W., 1999. Polar drug residues in sewage and natural waters in the state of Rio de Janeiro, Brazil. Sci. Total Environ. 225, 135–141. http://dx.doi.org/10.1016/S0048-9697(98)00339-8.

Stute, M., Deák, J., Révész, K., Böhlke, J.K., Deseö, E., Weppernig, R., Schlosser, P., 1997. Tritium/^{3}He dating of river infiltration: an example from the Danube in the Szigetköz Area, Hungary. Ground Water 35, 905–911. http://dx.doi.org/10.1111/j.1745-6584.1997.tb00160.x.

Tamooh, F., Borges, A.V., Meysman, F.J.R., Van Den Meersche, K., Dehairs, F., Merckx, R., Bouillon, S., 2013. Dynamics of dissolved inorganic carbon and aquatic metabolism in the Tana River basin, Kenya. Biogeosciences 10, 6911–6928. http://dx.doi.org/10.5194/bg-10-6911-2013.

Tauro, F., Martínez-Carreras, N., Barnich, F., Juilleret, J., Wetzel, C.E., Ector, L., Hissler, C., Pfister, L., 2015. Diatom percolation through soils: a proof of concept laboratory experiment. Ecohydrology http://dx.doi.org/10.1002/eco.1671 (n/a-n/a).

Taylor, R.G., Scanlon, B., Döll, P., Rodell, M., Van Beek, R., Wada, Y., Longuevergne, L., Leblanc, M., Famiglietti, J.S., Edmunds, M., et al., 2013. Ground water and climate change. Nat. Clim. Chang. 3, 322–329.

Telmer, K., Veizer, J., 1999. Carbon fluxes, pCO_2 and substrate weathering in a large northern river basin, Canada: carbon isotope perspectives. Chem. Geol. 159, 61–86. http://dx.doi.org/10.1016/S0009-2541(99)00034-0.

Ternes, T.A., 1998. Occurrence of drugs in German sewage treatment plants and rivers. Water Res. 32, 3245–3260. http://dx.doi.org/10.1016/S0043-1354(98)00099-2.

Tesoriero, A.J., Spruill, T.B., Mew, H.E., Farrell, K.M., Harden, S.L., 2005. Nitrogen transport and transformations in a coastal plain watershed: Influence of geomorphology on flow paths and residence times. Water Resour. Res. 41, W02008. http://dx.doi.org/10.1029/2003WR002953.

Tetzlaff, D., Buttle, J., Carey, S.K., McGuire, K., Laudon, H., Soulsby, C., 2015. Tracer-based assessment of flow paths, storage and runoff generation in northern catchments: a review. Hydrol. Process. 29, 3475–3490. http://dx.doi.org/10.1002/hyp.10412.

Thiele, G., Sarmiento, J.L., 1990. Tracer dating and ocean ventilation. J. Geophys. Res. Oceans 95, 9377–9391. http://dx.doi.org/10.1029/JC095iC06p09377.

Thomas, Z., Abbott, B.W., Troccaz, O., Baudry, J., Pinay, G., 2016a. Proximate and ultimate controls on carbon and nutrient dynamics of small agricultural catchments. Biogeosciences 13, 1863–1875. http://dx.doi.org/10.5194/bg-13-1863-2016.

Thomas, Z., Rousseau-Gueutin, P., Kolbe, T., Abbott, B.W., Marçais, J., Peiffer, S., Frei, S., Bishop, K., Pichelin, P., Pinay, G., de Dreuzy, J.-R., 2016b. Residence time distribution in small catchments: constitution of a virtual observatory to assess generic flow and transport models. J. Hydrol. http://dx.doi.org/10.1016/j.jhydrol.2016.04.067 (in press).

Thompson, G.M., Hayes, J.M., Davis, S.N., 1974. Fluorocarbon tracers in hydrology. Geophys. Res. Lett. 1, 177–180. http://dx.doi.org/10.1029/GL001i004p00177.

Tixier, C., Singer, H.P., Oellers, S., Müller, S.R., 2003. Occurrence and fate of carbamazepine, clofibric acid, diclofenac, ibuprofen, ketoprofen, and naproxen in surface waters. Environ. Sci. Technol. 37, 1061–1068. http://dx.doi.org/10.1021/es025834r.

Torgersen, C.E., Price, D.M., Li, H.W., McIntosh, B.A., 1999. Multiscale thermal refugia and stream habitat associations of chinook salmon in northeastern Oregon. Ecol. Appl. 9, 301–319.

Trauth, N., Schmidt, C., Vieweg, M., Maier, U., Fleckenstein, J.H., 2014. Hyporheic transport and biogeochemical reactions in pool-riffle systems under varying ambient groundwater flow conditions. J. Geophys. Res. Biogeosci. 119, 910–928. http://dx.doi.org/10.1002/2013JG002586.

Trimmer, M., Grey, J., Heppell, C.M., Hildrew, A.G., Lansdown, K., Stahl, H., Yvon-Durocher, G., 2012. River bed carbon and nitrogen cycling: state of play and some new directions. Sci. Total Environ. 434, 143–158. http://dx.doi.org/10.1016/j.scitotenv.2011.10.074.

Turnadge, C., Smerdon, B.D., 2014. A review of methods for modelling environmental tracers in groundwater: advantages of tracer concentration simulation. J. Hydrol. 519, 3674–3689. http://dx.doi.org/10.1016/j.jhydrol.2014.10.056.

Turner, E.G., Getsinger, K.D., Netherland, M.D., 1994. Correlation of triclopyr and rhodamine WT dye dissipation in the Pend Oreille River. J. Aquat. Plant Manag. 32, 39–41.

Tyler, S.W., Selker, J.S., Hausner, M.B., Hatch, C.E., Torgersen, T., Thodal, C.E., Schladow, S.G., 2009. Environmental temperature sensing using Raman spectra DTS fiber-optic methods. Water Resour. Res. 45, W00D23. http://dx.doi.org/10.1029/2008WR007052.

Updyke, E.A., Wang, Z., Sun, S., Connell, C., Kirs, M., Wong, M., Lu, Y., 2015. Human enteric viruses–potential indicators for enhanced monitoring of recreational water quality. Virol. Sin. 30, 344–353. http://dx.doi.org/10.1007/s12250-015-3644-x.

Urresti-Estala, B., Vadillo-Pérez, I., Jiménez-Gavilán, P., Soler, A., Sánchez-García, D., Carrasco-Cantos, F., 2015. Application of stable isotopes (δ^{34}S-SO_4, δ^{18}O-SO_4, δ^{15}N-NO_3, δ^{18}O-NO_3) to determine natural background and contamination sources in the Guadalhorce River Basin (southern Spain). Sci. Total Environ. 506–507, 46–57. http://dx.doi.org/10.1016/j.scitotenv.2014.10.090.

Vaché, K.B., McDonnell, J.J., 2006. A process-based rejectionist framework for evaluating catchment runoff model structure: process-based model rejection. Water Resour. Res. 42. http://dx.doi.org/10.1029/2005WR004247 (n/a-n/a).

Vannote, R.L., Minshall, G.W., Cummins, K.W., Sedell, J.R., Cushing, C.E., 1980. The river continuum concept. Can. J. Fish. Aquat. Sci. 37, 130–137.
Vega, E., Lesikar, B., Pillai, S.D., 2003. Transport and survival of bacterial and viral tracers through submerged-flow constructed wetland and sand-filter system. Bioresour. Technol. 89, 49–56. http://dx.doi.org/10.1016/S0960-8524(03)00029-4.
Venkiteswaran, J.J., Schiff, S.L., Wallin, M.B., 2014. Large carbon dioxide fluxes from head-water boreal and sub-boreal streams. PLoS One 9, e101756.
Vidon, P., Allan, C., Burns, D., Duval, T.P., Gurwick, N., Inamdar, S., Lowrance, R., Okay, J., Scott, D., Sebestyen, S., 2010. Hot spots and hot moments in riparian zones: potential for improved water quality management1. JAWRA J. Am. Water Resour. Assoc. 46, 278–298. http://dx.doi.org/10.1111/j.1752-1688.2010.00420.x.
Visser, A., Broers, H.P., Purtschert, R., Sültenfuß, J., de Jonge, M., 2013. Groundwater age distributions at a public drinking water supply well field derived from multiple age tracers (^{85}Kr, ^{3}H/^{3}He, and ^{39}Ar). Water Resour. Res. 49, 7778–7796. http://dx.doi.org/10.1002/2013WR014012.
Vitousek, P.M., Mooney, H.A., Lubchenco, J., Melillo, J.M., 1997. Human domination of Earth's ecosystems. Science 277, 494–499. http://dx.doi.org/10.1126/science.277.5325.494.
Vitousek, P.M., Reiners, W.A., 1975. Ecosystem succession and nutrient retention: a hypothesis. Bioscience 25, 376–381. http://dx.doi.org/10.2307/1297148.
Vogt, T., Schneider, P., Hahn-Woernle, L., Cirpka, O.A., 2010. Estimation of seepage rates in a losing stream by means of fiber-optic high-resolution vertical temperature profiling. J. Hydrol. 380, 154–164. http://dx.doi.org/10.1016/j.jhydrol.2009.10.033.
Vonk, J.E., Sánchez-García, L., Semiletov, I., Dudarev, O., Eglinton, T., Andersson, A., Gustafsson, Ö., 2010. Molecular and radiocarbon constraints on sources and degradation of terrestrial organic carbon along the Kolyma paleoriver transect, East Siberian Sea. Biogeosciences 7, 3153–3166. http://dx.doi.org/10.5194/bg-7-3153-2010.
Vonk, J.E., Tank, S.E., Mann, P.J., Spencer, R.G.M., Treat, C.C., Striegl, R.G., Abbott, B.W., Wickland, K.P., 2015. Biodegradability of dissolved organic carbon in permafrost soils and aquatic systems: a meta-analysis. Biogeosciences 12, 6915–6930. http://dx.doi.org/10.5194/bg-12-6915-2015.
Vorkapic, D., Pressler, K., Schild, S., 2016. Multifaceted roles of extracellular DNA in bacterial physiology. Curr. Genet. 62, 71–79. http://dx.doi.org/10.1007/s00294-015-0514-x.
Voss, B.M., Peucker-Ehrenbrink, B., Eglinton, T.I., Spencer, R.G.M., Bulygina, E., Galy, V., Lamborg, C.H., Ganguli, P.M., Montluçon, D.B., Marsh, S., Gillies, S.L., Fanslau, J., Epp, A., Luymes, R., 2015. Seasonal hydrology drives rapid shifts in the flux and composition of dissolved and particulate organic carbon and major and trace ions in the Fraser River, Canada. Biogeosciences 12, 5597–5618. http://dx.doi.org/10.5194/bg-12-5597-2015.
Wagener, S.M., Oswood, M.W., Schimel, J.P., 1998. Rivers and soils: parallels in carbon and nutrient processing. Bioscience 48, 104–108. http://dx.doi.org/10.2307/1313135.
Waldron, S., Scott, E.M., Soulsby, C., 2007. Stable isotope analysis reveals lower-order river dissolved inorganic carbon pools are highly dynamic. Environ. Sci. Technol. 41, 6156–6162. http://dx.doi.org/10.1021/es0706089.
Wallin, M.B., Öquist, M.G., Buffam, I., Billett, M.F., Nisell, J., Bishop, K.H., 2011. Spatiotemporal variability of the gas transfer coefficient (KCO_2) in boreal streams: Implications for large scale estimates of CO_2 evasion. Glob. Biogeochem. Cycles 25, GB3025. http://dx.doi.org/10.1029/2010GB003975.
Wang, Y., Huntington, T.G., Osher, L.J., Wassenaar, L.I., Trumbore, S.E., Amundson, R.G., Harden, J.W., McKnight, D.M., Schiff, S.L., Aiken, G.R., Lyons, W.B., Aravena, R.O., Baron, J.S., 1998. Chapter 17 - carbon cycling in terrestrial environments. Isotope Tracers in Catchment Hydrology. Elsevier, Amsterdam, pp. 577–610.
Ward, A.S., Gooseff, M.N., Voltz, T.J., Fitzgerald, M., Singha, K., Zarnetske, J.P., 2013. How does rapidly changing discharge during storm events affect transient storage and channel water balance in a headwater mountain stream? Water Resour. Res. 49, 5473–5486. http://dx.doi.org/10.1002/wrcr.20434.
Wawrzyniak, V., Piégay, H., Allemand, P., Vaudor, L., Grandjean, P., 2013. Prediction of water temperature heterogeneity of braided rivers using very high resolution thermal infrared (TIR) images. Int. J. Remote Sens. 34, 4812–4831. http://dx.doi.org/10.1080/01431161.2013.782113.
Weaver, L., Sinton, L.W., Pang, L., Dann, R., Close, M., 2013. Transport of microbial tracers in clean and organically contaminated silica sand in laboratory columns compared with their transport in the field. Sci. Total Environ. 443, 55–64. http://dx.doi.org/10.1016/j.scitotenv.2012.09.049.
Webster, J.R., Patten, B.C., 1979. Effects of watershed perturbation on stream potassium and calcium dynamics. Ecol. Monogr. 49, 51–72. http://dx.doi.org/10.2307/1942572.
Westhoff, M.C., Savenije, H.H.G., Luxemburg, W.M.J., Stelling, G.S., van de Giesen, N.C., Selker, J.S., Pfister, L., Uhlenbrook, S., 2007. A distributed stream temperature model using high resolution temperature observations. Hydrol. Earth Syst. Sci. Discuss. 4, 125–149.
Whiticar, M.J., 1999. Carbon and hydrogen isotope systematics of bacterial formation and oxidation of methane. Chem. Geol. 161, 291–314. http://dx.doi.org/10.1016/S0009-2541(99)00092-3.
Wilson, J.F., Cobb, E.D., Kilpatrick, F.A., 1986. Fluorometric procedures for dye tracing. Department of the Interior, US Geological Survey.
Wilson, R.D., Mackay, D.M., 1996. SF6 as a Conservative Tracer in Saturated Media with High Intragranular Porosity or High Organic Carbon Content. Ground Water 34, 241–249. http://dx.doi.org/10.1111/j.1745-6584.1996.tb01884.x.
Wimpenny, J.W.T., Cotton, N., Statham, M., 1972. Microbes as tracers of water movement. Water Res. 6, 731–739. http://dx.doi.org/10.1016/0043-1354(72)90188-1.
Wlostowski, A.N., Gooseff, M.N., Wagener, T., 2013. Influence of constant rate versus slug injection experiment type on parameter identifiability in a 1-D transient storage model for stream solute transport. Water Resour. Res. 49, 1184–1188. http://dx.doi.org/10.1002/wrcr.20103.
Woessner, W.W., 2000. Stream and fluvial plain ground water interactions: rescaling hydrogeologic thought. Ground Water 38, 423–429. http://dx.doi.org/10.1111/j.1745-6584.2000.tb00228.x.
Wright, J.C., Mills, I.K., 1967. Productivity Studies on the Madison River, Yellowstone National Park1. Limnol. Oceanogr. 12, 568–577. http://dx.doi.org/10.4319/lo.1967.12.4.0568.
Wu, N., Faber, C., Ulrich, U., Schmalz, B., Fohrer, N., 2014. Diatoms as an indicator for tile drainage flow in a German lowland catchment. Presented at the EGU General Assembly Conference Abstracts, p. 4955.
Young, P., 2003. Top-down and data-based mechanistic modelling of rainfall–flow dynamics at the catchment scale. Hydrol. Process. 17, 2195–2217.
Zarnetske, J.P., Haggerty, R., Wondzell, S.M., Baker, M.A., 2011. Dynamics of nitrate production and removal as a function of residence time in the hyporheic zone. J. Geophys. Res. Biogeosci. 116, G01025. http://dx.doi.org/10.1029/2010JG001356.
Zarnetske, J.P., Haggerty, R., Wondzell, S.M., Bokil, V.A., González-Pinzón, R., 2012. Coupled transport and reaction kinetics control the nitrate source-sink function of hyporheic zones. Water Resour. Res. 48, W11508. http://dx.doi.org/10.1029/2012WR011894.
Zhang, J., Quay, P.D., Wilbur, D.O., 1995. Carbon isotope fractionation during gas-water exchange and dissolution of CO_2. Geochim. Cosmochim. Acta 59, 107–114.
Zheng, C., Bennett, G.D., 2002. Applied Contaminant Transport Modeling. second ed. Wiley Interscience.
Zsolnay, Á., 2003. Dissolved Organic Matter: Artefacts, Definitions, and Functions. Geoderma, Ecological Aspects of Dissolved Organic Matter in Soils 113 pp. 187–209. http://dx.doi.org/10.1016/S0016-7061(02)00361-0.

Chapter 2: Methodology

2.1 Introduction

In this chapter the modeling approach that is used throughout the next chapters (chapter 3-5) is presented. The data- and modeling driven approach is used to interpret tracer concentrations measured in 16 wells (Appendix B) and to gain information on conservative and reactive transport parameter. Tracer concentrations in the wells are simulated with a time-based modeling approach that describes the tracer transport from an input zone (capture zone of the well) to an outlet (well) through a closed system. The aquifer is assumed to be a close system in which mass fluxes are conserved for conservative tracer. The approach is applicable to all kind of tracers whose transport depend on the time in a closed system with a defined input and output zone.

2.2 Modeling approach

A measured nitrate concentration in a well represents a mixture of waters with different nitrate loads arriving at the well at the time of the sampling date. The arriving waters might have different sources with varying distances of the recharge location to the well. This is why transit times, the time the waters have traveled from the groundwater table to the well, vary. With a magnitude of possible pathways, some of the nitrate loaded water might have also passed zones favorable for denitrification and been degraded which can lead to the same concentration shift as a mixing of a nitrate rich with a nitrate free water. The challenge for the interpretation of concentrations measured in the well is to distinguish between mixing and reactivity effects occurring in the aquifer simultaneously.

A commonly used modeling tool to account for mixing and reaction processes is a time-based modeling approach based on the convolution integral (*Eq. 6-9*) introduced by Maloszewski and Zuber (1982).

$$C^w(t) = \int_0^\infty p(u)\ [C^0(t-u) + b(u)]\ du \tag{6}$$

$$b(u) = C^0(t-u)\ \left[e^{\left(-\frac{1}{\tau}\theta(u)\right)} - 1\right] \tag{7}$$

$$b(u) = -k\theta(u) \tag{8}$$

$$\theta(u) = \int_0^u y(\eta)\ d\eta \text{ and } \begin{cases} y = 1 \text{ (degradation)} \\ y = 0 \text{ (no degradation)} \end{cases} \tag{9}$$

The resulting concentration in the well $C^w(t)$ is a mix of concentrations arriving at the well weighted by the transit time distribution $p(t)$. With $C^0(t)$ the tracer inputs and $b(u)$ a degradation term that can be either first- (*Eq. 7*) or zero-order (*Eq.8*), τ the first-order reaction time, k the zero-order reaction rate coefficient, $\theta(u)$ the time in which the solute is degraded or not, and η the time counted along the flowline.

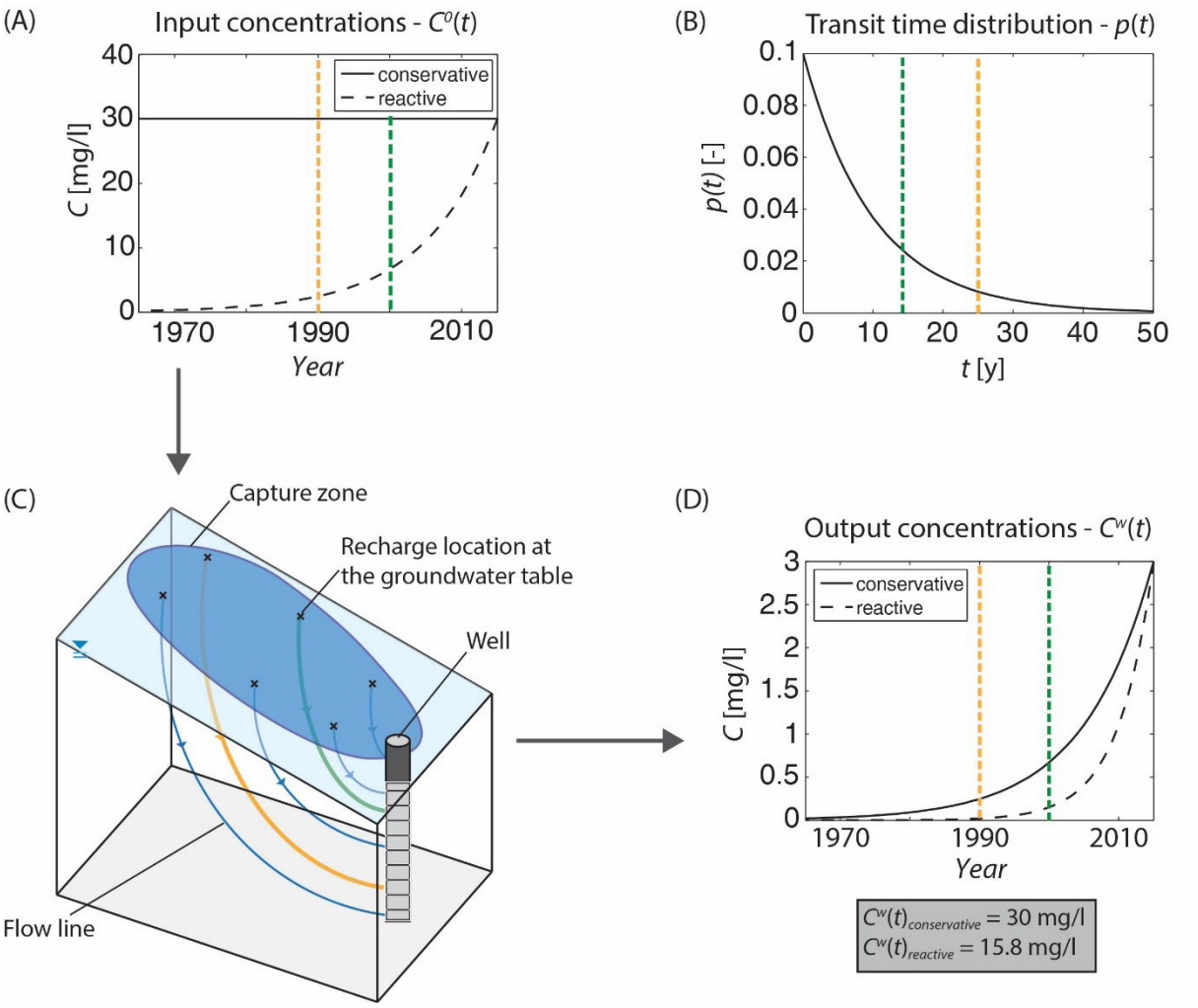

Fig. 6: Illustration of the time-based modeling approach

Fig. 6 illustrates the transfer function modeling approach for conservative and reactive nitrate. The initial constant nitrate concentration is 30 mg/l and applied uniformly at the groundwater table (*Fig. 6A*, solid line). Two flowlines with different transit times are marked in orange and green (*Fig. 6A* and *C*). Identical tracer concentrations spent different times in the aquifer to reach the well. Water spent 25 y (orange flowline) or 12.5 y (green flowline) in the aquifer, if the sampling date 2015 is assumed. The probability that the tracer arrives at the well can be obtained by the transit time distribution (*Fig. 6B*). The shape of the transit time distribution is exponential with a mean transit time of 10 y. A convolution of input concentrations with the transit time

distribution lead to the output concentration distribution (*Fig. 6D*). The sum of all arriving concentrations weighted by the transit time distribution is a mix of concentrations that can be compared to measured concentrations in the field. The calculated concentration considering just conservative transport would be 30 mg/l.

Considering reactive transport, constant nitrate input concentrations of 30 mg/l get reduced by a first-order reaction (*Fig. 6A,* dashed line). The arriving concentration in the well depends on the time nitrate has spent in the aquifer. The first order decay is here determined by a characteristic reaction time of 10 y. Concentrations decrease exponentially, depending on the applied reaction time and the time the solute spent in the aquifer (*Fig. 6A*, dashed line). These concentrations are weighted by the transit time distribution to obtain the output concentration distribution (*Fig. 6D*, dashed line). The sum of all these output concentrations give a concentration of 15.8 mg/l, which means that 14.2 mg/l of the nitrate has been degraded.

2.2.1 Tracer Inputs

Tracer inputs at the recharge location (groundwater table) can be variable or constant in time. Input concentrations are uniformly applied within the capture zone. This condition is especially valid for atmospheric tracers, like CFCs. If a tracer is not uniformly applied, this could be the case for nitrate, when distinct land use practices are observed within the capture zone, the usage of a mean value for the area of interest is a common practice (Osenbrück et al., 2006).

Investigations on nitrate inputs to the aquifer over the last decades are performed in chapter 4.

2.2.2 Transit Time Distribution

The transit time distribution is a probability density function of water transit times and provides a stochastic description of how solutes are retained in a well. The transit time is defined as the time a water molecule spent in the aquifer from recharging at the groundwater table until the arrival at the well. The transit time distribution serves as a weighting function for tracer inputs and incorporates internal flow dynamics of the aquifer, e.g. information about flow structures, storage, and water origin. Transit time distributions are directly related to internal and external catchment characteristics.

Generally, transit time distributions are time variant, but depending on the research question and if the simplification of steady-state conditions can be made, a steady-state transit time distribution is used. Steady-state conditions are assumed if the temporal variation of the volume are small compared to the total aquifer volume.

Transit time distributions can be derived by lumped parameter models or full groundwater flow and transport simulations and be evaluated by comparing modeled and measured CFC data (see chapter 3) or other tracers that inform groundwater age (e.g. SF6, ^{3}H). Lumped parameter models are chosen depending on aquifer characteristics and well properties (Jurgens et al., 2012; Maloszewski and Zuber, 1982; Leray et al., 2016). For example, an exponential distribution is valid for hydrogeological settings where the hydraulic conductivity decreases with depth or in settings with uniform permeability and porosity (Haitjema, 1995; Maloszewski and Zuber, 1982).

2.2.3 Reactivity

Reactivity can be included via a reaction term that assumes simplified reaction kinetics, either a zero-order (reaction rate is independent of the reactant concentration) or a

first-order kinetics (reaction rate depends linearly on the reactant concentration). The underlying assumption of reactive transport is that the solute concentration stored in a volume at a given time depends only on the injection time and the time the particle spent inside this volume (Botter et al., 2010). Botter et al. (2010) state that this linearity assumption is valid for nonpoint sources and refers to Botter et al. (2005), Botter et al. (2009), Rinaldo et al. (2006a) and Rinaldo et al. (2006b). The decay reaction is applied to each flowline and no mixing between them is assumed, before the concentrations mix in the well.

The assumption of continuous reactions in the aquifer might not be valid everywhere and might lead to errors in determining the denitrification capacity of the aquifer. To the best of the author's knowledge, no studies have been found that include other concepts of reactivity in this kind of modeling approach. Investigations on reactivity are performed in chapter 5 and new concepts to implement denitrification activity presented.

2.3 Calibration procedure

The calibration is based on a multi-objective function and performed successively for conservative and reactive parameter to find the best fit between modeled and observed tracer concentrations and to optimize reaction times (Flavelle, 1992; Marler and Arora, 2004). First, conservative transport parameter (nitrate inputs over time, porosity, and depth of water arrivals at the location of a well) are calibrated against CFC-12 and NO_3^-,total (NO_3^-,total is the sum of the measured nitrate concentration in the well and the amount that has been degraded NO_3^-,deg determined by N_2 excess). In a second step, reactive transport parameter (reaction times for oxygen reduction and denitrification) are calibrated against O_2, NO_3^-, and NO_3^-,deg.

The calibration procedure is based on the following objective function. For each kind of data D (CFC-12, O_2, NO_3^-, $NO_{3,total}^-$, and $NO_{3,deg}^-$) the following objective function is computed (*Eq. 10*).

$$\Phi_D(\mathrm{P}) = \mathrm{w}_D \left(\frac{1}{n} \sum_{i=1}^{n} \left(D^m - D_i^d \right)^2 \right) \tag{10}$$

With D^m the simulated values, D_i^d the measured value for each of the three sampling dates (n=1,2,3) and w the weighting term that equals 1. Due to distinct units of the different kind of data, the functions had to be normalized as follows (*Eq. 11*).

$$\Phi_D(\mathrm{P})^{trans} = \frac{\Phi_D(\mathrm{P}) - \Phi_D(\mathrm{P})^0}{\Phi_D(\mathrm{P})^{max} - \Phi_D(\mathrm{P})^0} \tag{11}$$

For each calibration step, the global objective function is calculated (*Eq. 12*).

$$\Phi_{gloabl}(\mathrm{P}) = \sum_{s=1}^{n_w} \sum_{j=1}^{n_d} \Phi_D(\mathrm{P})_{n_d,n_w}^{trans} \tag{12}$$

The global objective function is a sum of all objective functions of each data n_d and each of the wells n_w.

Chapter 3: Groundwater flow dynamics at the Pleine-Fougères site

3.1 Introduction

Around 80-90 % of Brittany's groundwater is situated in hard-rock aquifers (Wyns et al., 2004) which are close to the land surface and extremely vulnerable to non-point source contaminations coming from agricultural activity, like nitrate. Hydrogeological and biogeochemical process are key controls in determining the fate of nitrate through the aquifer.

In this chapter the groundwater flow circulations of the Pleine-Fougères aquifer in Brittany are analyzed and classified in relation to surface water travel distances. With groundwater dating (CFC groundwater age data) and the development of a three-dimensional mechanistic groundwater flow model, groundwater flow can be visualized and travel distances compared to surface water travel distance. Depending on the groundwater table configuration, an index ($r_{GW\text{-}LOCAL}$) is proposed that describes the relation between surface and groundwater flow distances. Modeling results also reveal water arrivals and their corresponding transit times to the wells, the basis for further investigations on the denitrification capacity of the aquifer.

3.2 Article: "Coupling 3D groundwater modeling with CFC-based age dating to classify local groundwater circulation in an unconfined crystalline aquifer", T. Kolbe, J. Marçais, Z. Thomas, B. W. Abbott, J.-R. de Dreuzy, P. Rousseau-Gueutin, L. Aquilina, T. Labasque, G. Pinay, Journal of Hydrology, 2016

Journal of Hydrology 543 (2016) 31–46

Contents lists available at ScienceDirect

Journal of Hydrology

journal homepage: www.elsevier.com/locate/jhydrol

Coupling 3D groundwater modeling with CFC-based age dating to classify local groundwater circulation in an unconfined crystalline aquifer

Tamara Kolbe [a,*], Jean Marçais [b,a], Zahra Thomas [c], Benjamin W. Abbott [d], Jean-Raynald de Dreuzy [a], Pauline Rousseau-Gueutin [e], Luc Aquilina [a], Thierry Labasque [a], Gilles Pinay [d]

[a] Géoscience Rennes, UMRCNRS 6118, Université de Rennes 1, 35042 Rennes Cedex, France
[b] Agroparistech, 16 rue Claude Bernard, 75005 Paris, France
[c] Agrocampus Ouest, Sol Agro et Hydrosystème Spatialisation, 35000 Rennes, France
[d] OSUR, Ecobio, CNRS, Université de Rennes 1, 35042 Rennes Cedex, France
[e] EHESP Rennes, Sorbonne Paris Cité, Paris, France

ARTICLE INFO

Article history:
Available online 14 May 2016

Keywords:
Transit time distribution
Groundwater travel distance
Groundwater table controls
Groundwater circulation
Small catchment
Crystalline aquifer

SUMMARY

Nitrogen pollution of freshwater and estuarine environments is one of the most urgent environmental crises. Shallow aquifers with predominantly local flow circulation are particularly vulnerable to agricultural contaminants. Water transit time and flow path are key controls on catchment nitrogen retention and removal capacity, but the relative importance of hydrogeological and topographical factors in determining these parameters is still uncertain. We used groundwater dating and numerical modeling techniques to assess transit time and flow path in an unconfined aquifer in Brittany, France. The 35.5 km^2 study catchment has a crystalline basement underneath a ~60 m thick weathered and fractured layer, and is separated into a distinct upland and lowland area by an 80 m-high butte. We used groundwater discharge and groundwater ages derived from chlorofluorocarbon (CFC) concentration to calibrate a free-surface flow model simulating groundwater flow circulation. We found that groundwater flow was highly local (mean travel distance = 350 m), substantially smaller than the typical distance between neighboring streams (~1 km), while CFC-based ages were quite old (mean = 40 years). Sensitivity analysis revealed that groundwater travel distances were not sensitive to geological parameters (i.e. arrangement of geological layers and permeability profile) within the constraints of the CFC age data. However, circulation was sensitive to topography in the lowland area where the water table was near the land surface, and to recharge rate in the upland area where water input modulated the free surface of the aquifer. We quantified these differences with a local groundwater ratio ($r_{GW\text{-}LOCAL}$), defined as the mean groundwater travel distance divided by the mean of the reference surface distances (the distance water would have to travel across the surface of the digital elevation model). Lowland, $r_{GW\text{-}LOCAL}$ was near 1, indicating primarily topographical controls. Upland, $r_{GW\text{-}LOCAL}$ was 1.6, meaning the groundwater recharge area is almost twice as large as the topographically-defined catchment for any given point. The ratio $r_{GW\text{-}LOCAL}$ is sensitive to recharge conditions as well as topography and it could be used to compare controls on groundwater circulation within or between catchments.

1. Introduction

Groundwater flow is a key factor in determining the fate of non-point source agricultural pollution such as nitrate (Böhlke, 2002; Dunn et al., 2012; Weyer et al., 2014). In contrast with surface flow paths, which can rapidly transport contaminants to streams and rivers, contaminant transport in aquifers is thought to be much slower and to span larger distances, depending on geological structure and hydraulic conductivity (Forster and Smith, 1988; Grathwohl et al., 2013; McDonnell et al., 2007). These long transit times can enhance biogeochemical alteration of solutes if reactants encounter each other (McClain et al., 2003; Pinay et al., 2015; Vogel et al., 2015). Moreover, the high surface area to volume ratio of the geological substratum in aquifers enhances interactions between water and rock, leading to weathering and chemotrophic

* Corresponding author. Tel.: +33 2 23 23 37 52.
E-mail address: Tamara.Kolbe@univ-rennes1.fr (T. Kolbe).

http://dx.doi.org/10.1016/j.jhydrol.2016.05.020
0022-1694/

metabolism such as autotrophic denitrification of nitrate by pyrite oxidation (Appelo and Postma, 2005; Engesgaard and Kipp, 1992). Along with stimulating removal of pollutants, the mixing of multiple water sources can reduce contaminant concentrations by dilution (Chapelle et al., 2009; Green et al., 2010). The overall impact of groundwater on the fate of nonpoint source contaminants depends on transit time, location and timing of recharge inputs, and internal flow structure either promoting or limiting lateral and vertical exchange in the aquifer. While internal flow structures in the saturated zone are difficult to measure, they can be approximated by mechanistic numerical models, a robust tool to follow water molecules and pollutants through the aquifer, even if they simplify prevailing flow dynamics (Anderson et al., 2015; Bear and Verruijt, 2012).

Groundwater circulation in aquifers has typically been conceptualized in terms of local, intermediate, and regional flow paths (Tóth, 1963, 2009). These flow paths contribute differentially to the overall groundwater flow, resulting in a multi-modal distribution of transit times (Cardenas, 2007; Goderniaux et al., 2013). For hard-rock aquifers the majority of groundwater flow occurs in the weathered zone, typically varying from a depth of a few meters to tens of meters, and is characterized by a highly heterogeneous physical structure and variable hydraulic conductivity (Jaunat et al., 2012; Lebedeva et al., 2007; Rempe and Dietrich, 2014). The fact that the weathered zone overlays the fractured bedrock (Wyns et al., 2004), means that the most active groundwater compartment (and the most vulnerable to pollution) may be conceptualized with only local or local and intermediate flow paths. Topography also has a strong influence on shallow aquifers because the water table is close to the land surface. Consequently, groundwater circulation is controlled by a combination of geologic structure, topographical gradients, and recharge conditions (Freer et al., 1997; Gleeson and Manning, 2008; Haitjema and Mitchell-Bruker, 2005; McGuire et al., 2005; Tetzlaff et al., 2009). Haitjema and Mitchell-Bruker (2005) developed a criterion for large aquifers to quantify the relative importance of topography and recharge rate in determining water table height (Eq. (1)):

$$\begin{aligned} \frac{RL^2}{mkHd} &> 1 \rightarrow \text{water table is topography controlled} \\ \frac{RL^2}{mkHd} &< 1 \rightarrow \text{water table is recharge controlled} \end{aligned} \quad (1)$$

where R is the effective recharge (m d^{-1}), L is the distance between hydrological boundaries (m), m is a coefficient equal to 8 for rectangular areas or 16 for circular shapes, k is the hydraulic conductivity (m d^{-1}), H is the saturated thickness (m) and d is the maximum terrain raise (m). For a topography controlled groundwater table, local circulation dominates total flow, whereas intermediate and regional circulation is predominant in aquifers with a recharge controlled groundwater table (Gleeson and Manning, 2008).

Despite the limited depth of shallow aquifers, groundwater age stratification has been observed based on atmospheric tracers such as chlorofluorocarbons (CFCs) and SF_6, providing some important constraints on the flow structure (Ayraud et al., 2008; Busenberg and Plummer, 1992; Cook and Herczeg, 2000). Groundwater age information can be integrated into groundwater models to generate new understanding about the relationship between flow structure and transit time distribution (Cook and Herczeg, 2000; Eberts et al., 2012; Leray et al., 2012; Molénat and Gascuel-Odoux, 2002; Molson and Frind, 2012).

To determine the extent of groundwater flow circulations and to quantify topographical and hydrogeological controls on groundwater flow, we modeled groundwater flow dynamics of a shallow hard-rock aquifer in Brittany France. Given the relatively old observed groundwater ages (~40 years based on CFC concentrations), we hypothesized that groundwater would have traveled long distances from the recharge location to the sampling zone, integrating water recharge from a large area and increasing the likelihood of agricultural contamination. Furthermore, we hypothesized that these travel distances would increase moving from uplands towards lowlands due to the increasing contributing area (catchment size) and the relatively large topographical relief in this catchment. To test these hypotheses, we constructed and calibrated groundwater flow models using geological, topographical, hydrological, and groundwater age data to constrain groundwater transit time distributions, flow line organization, and the distance that groundwater traveled from recharge locations to sampling zones. To test the influence of topography on groundwater circulation, we compared modeled groundwater travel distances with corresponding flow lengths across the digital elevation model (DEM), further called reference distances. Similar reference and groundwater travel distances would suggest strong topographical control on the groundwater table, while relatively longer groundwater travel distances would indicate less connection with the land surface and more of a recharge control on the groundwater table with hydrogeological properties dominating the flow circulation.

2. Material and methods

We performed our study in a 35 km^2 agricultural catchment near the town of Pleine–Fougères in Brittany, France (Fig. 1 and 48°36′N, 1°32′W), which is part of the European Long-Term Ecosystem Research network LTER (www.lter-europe.net). Extensive background data from previous studies (Jaunat et al., 2012; Lachassagne et al., 2011; Thomas et al., 2016a) provided physical and chemical constraints allowing the construction of realistic groundwater flow models to test our hypotheses about flow dynamics and transit time distributions. The transit time was defined as the time a water molecule spends between the recharge location and the sampling zone. All transit times of water molecules arriving at the sampling zone were used to calculate the mean transit time of the sample.

2.1. Pleine–Fougères aquifer

The Pleine–Fougères aquifer is located in the northern part of the east–west shear zone of the North Armorican Massif (Fig. 1a). This zone is underlain by a crystalline basement (Bernard-Griffiths et al., 1985). The aquifer straddles a geologic transition between granite in the south and schist in the north (Fig. 1b). The unconfined groundwater flow mainly occurs in the weathered zone which overlies a less pervious fractured zone (Jaunat et al., 2012; Lachassagne et al., 2011; Wyns et al., 2004). The mean thickness of the weathered and fractured zone is respectively 9 m and 48 m, though the thickness of both layers is variable (Fig. 2a and b). Elevation ranges from 9 to 118 m, with most of the relief occurring at a steep slope at the boundary between schist and granite with a mean gradient of 7.5%, creating three distinct landscape components: upland, lowland and the transition area (Fig. 3). Most rivers in the catchment flow from the south to the north. Secondary topographical gradients from the differential incision of rivers are oriented in an east–west direction. Mean groundwater recharge R is estimated at 167 mm y^{-1} using meteorological data and the one dimensional Interaction Soil–Biosphere–Atmosphere-Model (Boone et al., 1999; Noilhan and Mahfouf, 1996; Noilhan and Planton, 1989). We estimated mean annual groundwater discharge, constituting the baseflow at the outlet of the catchment (Fig. 4), at 4.5×10^6 m^3 y^{-1}, based on hydrograph separation of predicted long term stream discharge (mean of

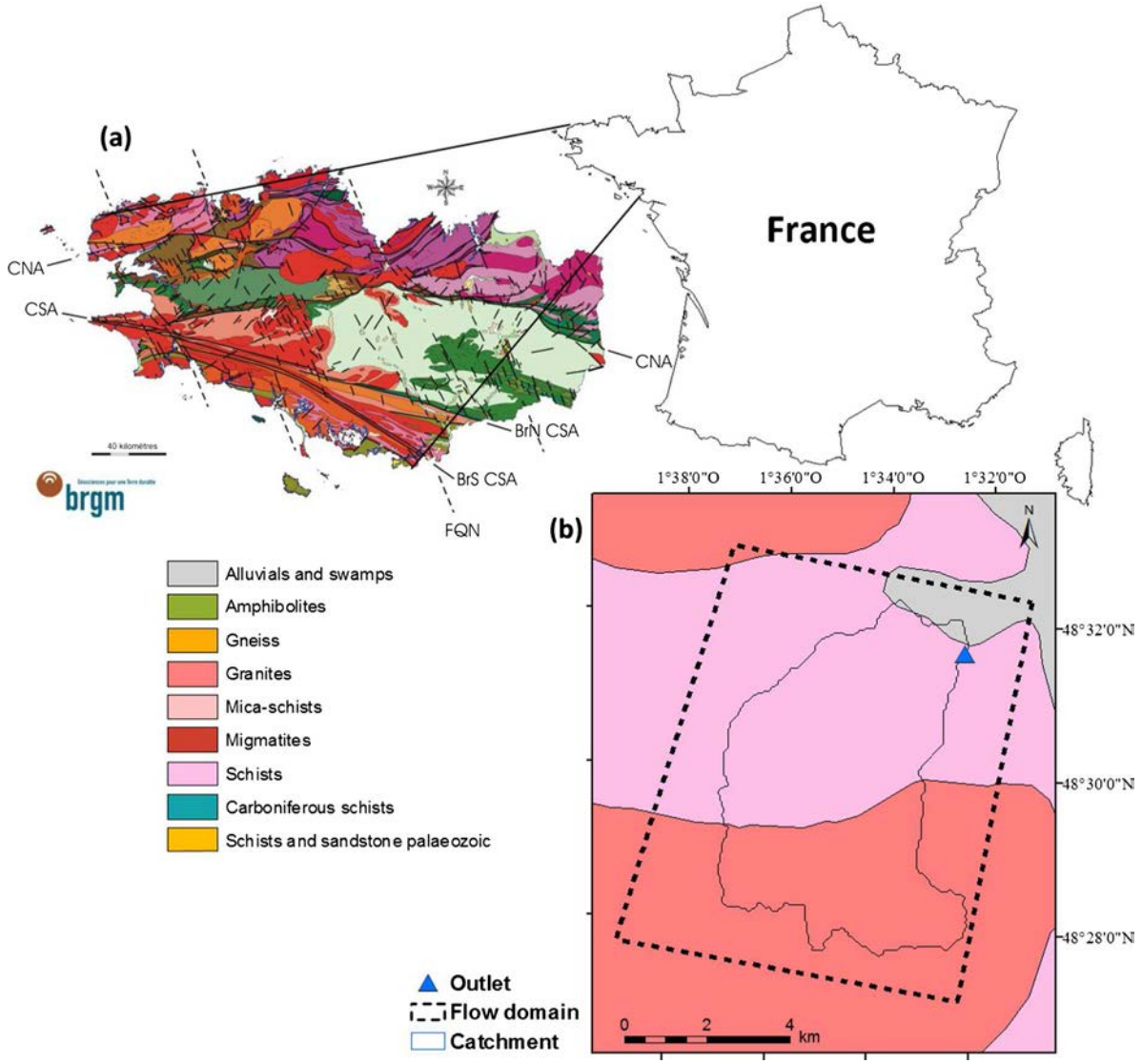

Fig. 1. Location of the Pleine–Fougères site, (a) on the geological map of the Armorican Massif (west of France), (b) geological map of the studied zone. The black dashed rectangle indicates the flow domain. The black polygon and blue triangle delineate the monitored catchment boundary and its outlet, respectively. Map layers were provided by the French Geological Survey (BRGM). (For interpretation of the references to color in this figure legend, the reader is referred to the web version of this article.)

9.1 $m^3\ y^{-1}$) using a power equation. The hydrograph separation was performed with a one-parameter algorithm described in Chapman (1999, Eq. 8), where the baseflow was determined as a simple weighted average of the direct runoff and the baseflow at the previous time interval. In the absence of direct runoff, the baseflow was constant.

2.2. Groundwater models

The effective modeled zone (76 km^2) was substantially larger than the drainage basin (35 km^2) to limit boundary effects. The modeled zone extended beyond the watershed divide in the south (upland) and downslope from the outlet in the north, and was delimited by two rivers in the east and west (Fig. 4). We selected hydraulic conductivities based on average values in the literature (Ayraud et al., 2008; Batu, 1998; Grimaldi et al., 2009; Kovács, 2011), assigning a single conductivity value to each of the four compartments, i.e. weathered schist (K_{WS}), fractured schist (K_{FS}), weathered granite (K_{WG}), and fractured granite (K_{FG}). In the reference groundwater model (REF), the hydraulic conductivity of granite was double that of schist ($K_{WG} = 2K_{WS}$ and $K_{FG} = 2K_{FS}$) and the thickness of the weathered and fractured zones was derived from near-surface geologic maps of the area (Fig. 2). We assigned a greater hydraulic conductivity to the weathered granite compared to the hydraulic conductivity in the weathered schist, because of its higher susceptibility to weathering (Bala et al., 2011; Dewandel et al., 2006; Edet and Okereke, 2004). In the calibration procedure, hydraulic conductivities were optimized within a range of 8.64×10^{-2}–1.7 m d^{-1} predetermined by previous studies performed in similar weathered zone aquifers in Brittany (Ayraud et al., 2008; Clement et al., 2003; Le Borgne et al., 2004; Martin et al., 2006; Roques et al., 2014). Due to weathering processes in the weathered zone, porosities up to 50% are reported in the literature (Kovács, 2011; Wright and Burgess, 1992). Below the weathered zone, bedrock metamorphic and igneous rocks like schist and granite have a very low primary porosity (0.1–1%; Singhal and Gupta, 2013). However, depending on the fracture and fissure density, the porosity in the fractured zone can be up to 10% (Earle, 2015; Hiscock, 2009). For our models, the effective porosity, i.e. the pore volume that contributes to fluid flow, was set higher in the weathered zone (θ_W) than in the fractured zone (θ_F) and was assumed to be uniform across both geologies. Values were derived

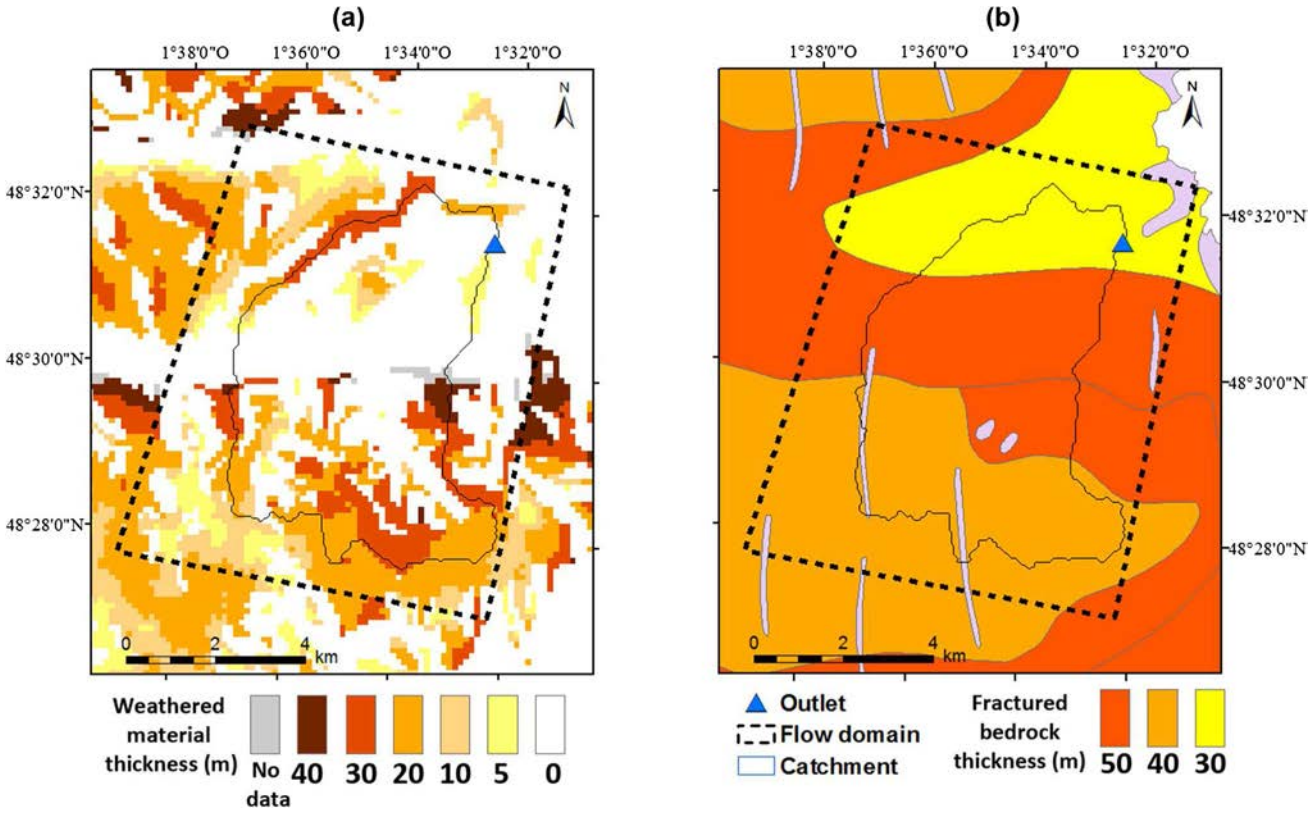

Fig. 2. Map of (a) weathered zone thickness and (b) fractured bedrock zone thickness. Permeable weathered zone lies over the less fractured bedrock zone. Map data were provided by the French Geological Survey (BRGM).

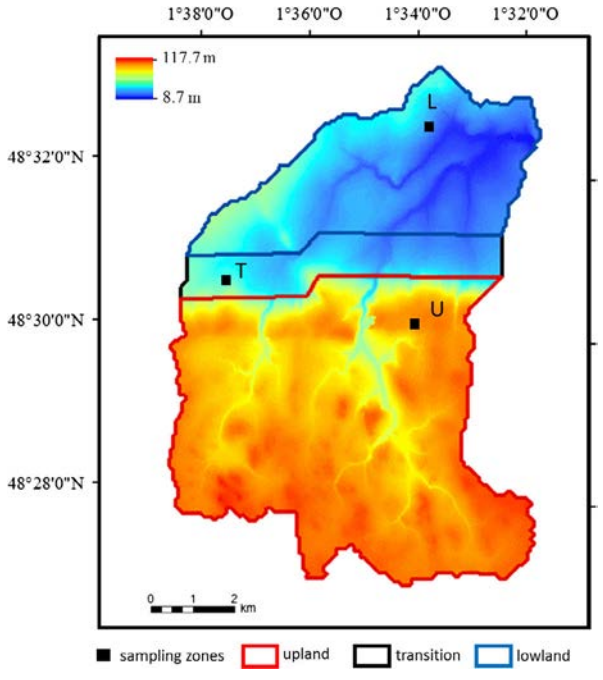

Fig. 3. Digital elevation model with a 5 m resolution. Colored polygons represent the three distinct areas of the Pleine–Fougères site, i.e. upland in red, transition in black and lowland in blue. Three representative sampling zones (black squares) identified by letters (U, T and L) are shown in each area. (For interpretation of the references to color in this figure legend, the reader is referred to the web version of this article.)

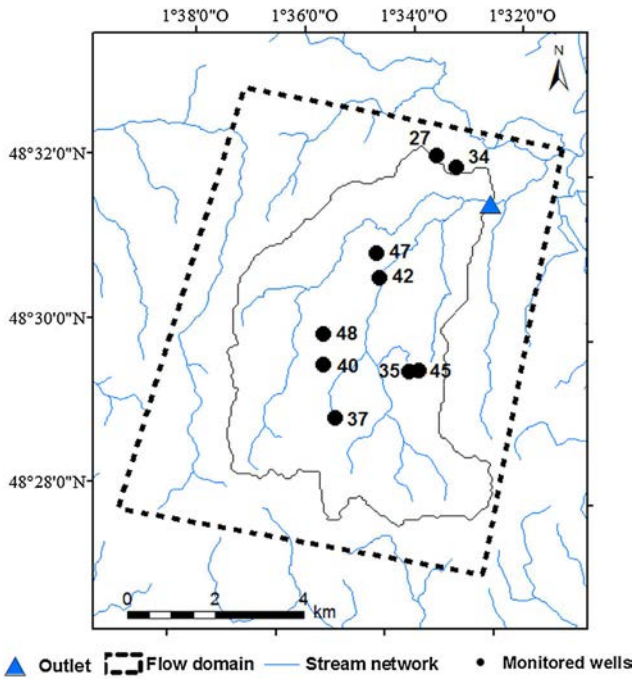

Fig. 4. Stream network (blue lines) of the Pleine–Fougères site (black polygon). Monitored well positions (black points) indicating mean CFC groundwater ages from sampling performed in December 2014 and March 2015. (For interpretation of the references to color in this figure legend, the reader is referred to the web version of this article.)

through the calibration against the measured groundwater ages (see Section 2.5.). Altogether, the groundwater model was parameterized by K_{WG}, K_{FG}, θ_W, and θ_F. All four parameters were calibrated against baseflow at the catchment outlet, and groundwater age data estimated using CFC measurements from 9 wells (Fig. 4; see Section 2.4 for detailed description of calibration).

In total, five groundwater flow models were developed (Table 1). To investigate the influence of weathered zone thickness on groundwater flow, we tested three models with different ratios of weathered to fractured zone thickness. We compared the model with a thin weathered zone, half the thickness of the reference model (THIN), to a model with twice the thickness of the reference model (THICK). For the reference groundwater model (REF), the ratio of the weathered to fractured zone thickness was 0.19, for the THICK model the ratio was 0.58, and for the THIN model it was 0.05. To test our assumptions about differences in hydraulic conductivity between the two geologies, we developed a fourth groundwater model (AHC) with an alternative hydraulic conductivity ratio ($K_{WG} = 10K_{WS}$), but the same thickness ratio as the reference model. To test the impact of these modifications, we developed a homogeneous model (HOM) that had a uniform hydraulic conductivity and effective porosity. All five models were calibrated using the same procedure, described in detail in Section 2.4. The comparison of the reference model with the alternative models is developed in Section 3.3.

2.3. Groundwater flow simulations

Groundwater flow of the unconfined aquifer was simulated in the 76 km^2 flow domain (black dashed rectangle in Fig. 4) under free surface conditions (Bear, 1973). Flow was simulated in steady state, because the groundwater ages measured at high and low groundwater conditions at the site did not show any significant variations (data not shown). Also seasonal recharge variations over 42 years derived from the ISBA model (Boone et al., 1999; Noilhan and Mahfouf, 1996; Noilhan and Planton, 1989) did not show any trend, indicating that transient flow simulations were unnecessary. We applied a uniform recharge of 167 mm y^{-1} on the top layer of the model. The effective recharge of 5.8×10^6 m^3 y^{-1} over the 35.5 km^2 catchment is 25% larger than the discharge of 4.5×10^6 m^3 y^{-1}. This is explained by seepage areas that are not integrated in the discharge computation, which cover 8% of the land surface. Lateral and bottom boundary conditions were set as no flow.

Groundwater flow equations with the previously described recharge and boundary conditions were solved with the finite element modeling package FEFLOW (Diersch, 2013). The movable free surface was iteratively determined with the best-adaptation-to-stratigraphic-data technique (BASD), an algorithm that adapts the mesh structure to the free surface height, while respecting as far as possible the layering of the hydraulic conductivity. Because the underlying bedrock at our site had a uniform and very low hydraulic conductivity of 1×10^9 m d^{-1}, it acted effectively as an impervious layer. Its variable thickness gave an overall uniform aquifer domain thickness appropriate for FEFLOW modeling purposes. The mesh generated by FEFLOW contained 6188 triangle prisms per slice, with 2 slices per layer. The vertical discretization was adapted to the weathered zone thickness for each of the different models. The mesh contained 12,218 mesh elements per layer, with a total of 122,180 mesh elements over 10 layers. The mesh followed surface structures and was automatically refined close to surface waters, where convergence induces larger flows (Fig. 5). The DEM (Fig. 3) shows a marked difference in elevation near channel banks where mesh refinement was implemented.

Table 1
Characteristic parameters (K: hydraulic conductivity, H_{mean}: mean thickness of the zone, θ: effective porosity; subscript W: weathered zone, subscript F: fractured zone) of the five models (REF: reference model, THICK: model with thicker weathered zone, THIN: model with thinner weathered zone, AHC: model with higher hydraulic conductivity in granite, HOM: homogeneous model).

		REF	THICK	THIN	AHC	HOM
K_W (m d^{-1})	G	0.68	0.3	0.68	2	0.15
	S	0.34	0.6	0.34	0.2	0.15
K_F (m d^{-1})	G	0.34	0.15	0.34	1	0.15
	S	0.17	0.3	0.17	0.1	0.15
$H_{W,mean}$ (m)	G	11.3	19.5	3.7	22.3	
	S	6.6	22	1.9	4.3	
$H_{F,mean}$ (m)	G	49.3	37.1	56.3	42.8	90
	S	47.4	34.8	51.7	43.4	
$H_{B,mean}$ (m)	G	30.6	35.4	31.3	23.8	
	S	34.5	30.4	34.9	41.5	
θ_W (–)	G, S	0.45	0.45	0.55	0.45	0.35
θ_F (–)	G, S	0.15	0.15	0.25	0.15	0.35

2.4. Groundwater flow lines and sampling

Flow lines were determined using the particle tracking algorithm of FEFLOW (Diersch, 2013), with particles seeded at a density proportional to the imposed recharge at the water table. In order to provide a sufficient representation of the flow field, at least 4×10^5 flow lines were required. Groundwater flow lines in the modeled area are presented in Fig. 6. The red lines mark the seepage zones, which were defined as zones where the groundwater table (extracted from the groundwater flow model) reaches the land surface.

In a post-processing step, we used MATLAB to analyze the flow lines. We created a regular grid of 100×100 m sampling zones over the whole flow domain and sampled flow lines where they intersected the rectangular columns of the grid at any depth. The selected grid size ensured sufficient flow lines in each sampling zone while avoiding spurious mixing effects. Ultimately model results, e.g. mean transit times, were quite robust to sampling zone size with sensitivity tests revealing little difference between 50×50 m and 200×200 m sampling zones sizes (Fig. A.1). The 100×100 m grid over the whole catchment area resulted in sampling zones every 340 m, for a total of 278 sampling zones in the catchment area without considering sampling zones that were located in streams.

2.5. Calibration

We used groundwater flow simulations to determine the overall groundwater discharge at the catchment outlet. Hydraulic conductivities (K_{WG} and K_{FG}) were manually calibrated to fit the observed discharge value of 1.2×10^4 m^3 day^{-1} derived from hydrograph separation.

We estimated the mean groundwater age at the 9 sampling wells with CFC concentrations. CFCs are anthropogenic gases whose atmospheric concentrations increased linearly from 1960 to 1990 (when they were banned) and have been gradually decreasing, allowing the calculation of the average time since a groundwater parcel was in equilibrium with the atmosphere (Ayraud et al., 2008). Groundwater samples were collected in December 2014 and March 2015 and were analyzed at the Geoscience Laboratory (Rennes, France; for detailed methodology see Ayraud et al., 2008; Busenberg and Plummer, 1992; Cook and Herczeg, 2000). No systematic spatial trends were apparent in the measured groundwater age data from the sampled wells (Fig. 4), so we calibrated the model parameters K_{WG}, K_{FG}, θ_W and θ_F (Table 1) based on the mean and standard deviation of the groundwater age and the discharge (Table 2). The model

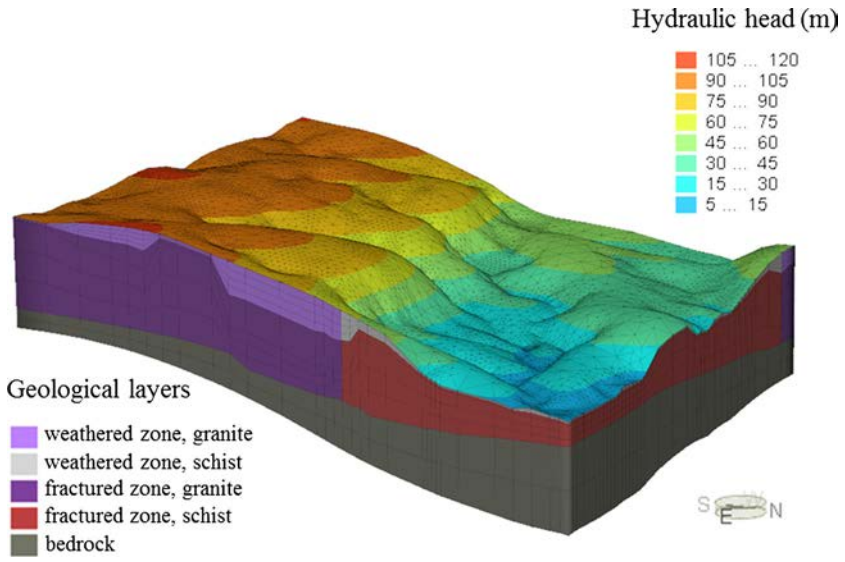

Fig. 5. Three-dimensional representation of the geological layers. Each color on the lateral boundaries correspond to a particular geological layer. Hydraulic heads are shown by colors projected on the free surface. The model is vertically exaggerated by a factor of 20. (For interpretation of the references to color in this figure legend, the reader is referred to the web version of this article.)

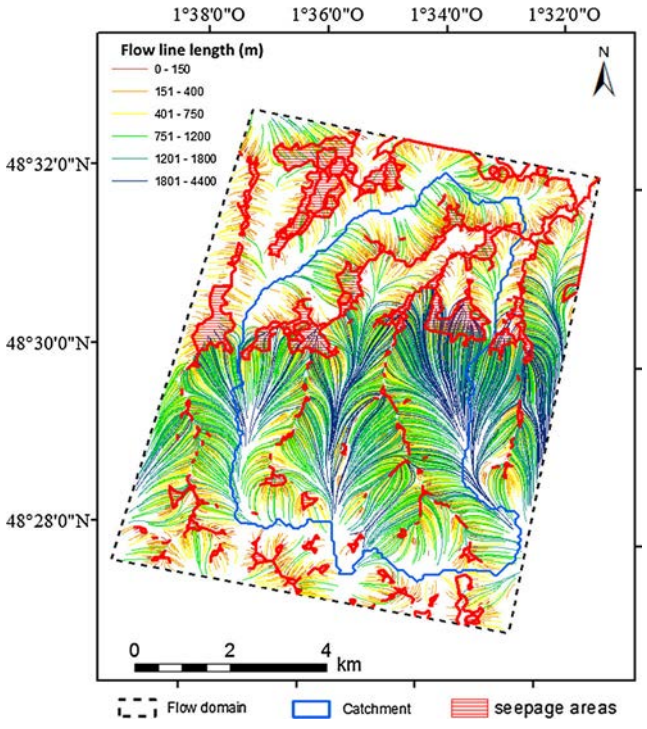

Fig. 6. Flow lines of the reference model projected in 2D. Colored lines identify the groundwater flow lines according to their overall length (from recharge point to discharge location). Seepage areas are identified by red lines. The catchment boundary is represented by the blue polygon. The model domain is delineated by the black dashed rectangle. (For interpretation of the references to color in this figure legend, the reader is referred to the web version of this article.)

calibration against the measured mean groundwater age was also done manually. We used the same sampling zone size (100×100 m) for the 9 wells when calculating modeled groundwater ages. Modeled groundwater ages are the convolution product of the recorded tracer input chronicle and the transit time distribution (Maloszewski and Zuber, 1996; Marçais et al., 2015).

For model calibration this meant reducing hydraulic conductivity decreases the overall discharge and increases the groundwater age or vice versa. As expected, effective porosity did not have any influence on the catchment discharge at steady state conditions, but was positively correlated with the groundwater age. Ratios of effective porosities and hydraulic conductivities were constrained by the dispersion of the groundwater age. All five models were considered to be satisfactory calibrated (Table 2).

2.6. Transit time and groundwater travel distance distributions

For each of the 100×100 m sampling zones, we derived transit time distributions as well as groundwater travel distance distributions and computed spatial statistics for intersecting flow lines. We computed the transit time for each particle and the mean transit time of all particles reaching the sampling zone. We also calculated the lateral distance traveled by particles intersecting the water column defined by the sampling zone. The groundwater travel distance was defined as the distance from the flow line origin to the center of the sampling zone projected on the ground surface (Fig. 7). These groundwater travel distances were used to build groundwater travel distance distributions and mean groundwater travel distances for each of the 278 sampling zones. We calculated summary statistics for the three catchment areas: upland, transition, and lowland. Because the influence of the topographical transition on transit time and groundwater travel distance distributions extended beyond the steep section of the slope, we defined the transition area as the area extending from the head of the slope to 650 m to the north of the slope (Fig. 3). Upland and lowland areas were then defined to the south and north of the transition area.

We also compared the groundwater travel distance with the mean distance between two streams, which represented the average Euclidean distance between surface channels calculated with the ArcToolbox of ArcMap (ESRI® ArcMapTM, 2010).

2.7. Analysis of groundwater circulation

To determine the local nature of the groundwater circulation which is related to the groundwater table configuration, we compared groundwater travel distances with reference surface

Table 2
Groundwater discharge, mean and standard deviation of groundwater ages of the five models (REF: reference model, THICK: model with thicker weathered zone, THIN: model with thinner weathered zone, AHC: model with higher hydraulic conductivity in granite, HOM: homogeneous model). ε is the relative error between the modeled and measured values. Measured baseflow = 1.24×10^4 m^3 d^{-1}, mean of the sampled groundwater ages = 38.9 y, standard deviation of the sampled groundwater ages = 7.2 y.

	REF	THICK	THIN	AHC	HOM
Groundwater discharge (m^3 d^{-1})	1.25×10^4	1.27×10^4	1.23×10^4	1.23×10^4	1.28×10^4
ε (%)	1.8	3.2	0.2	0.2	3.8
Groundwater age, mean (y)	37.5	37.7	38.1	37.8	38.5
ε (%)	3.6	3.1	2.0	2.8	1.0
Groundwater age, SD (y)	6.2	6.8	7.6	6.6	5.8
ε (%)	13.9	5.5	5.5	8.3	19.4

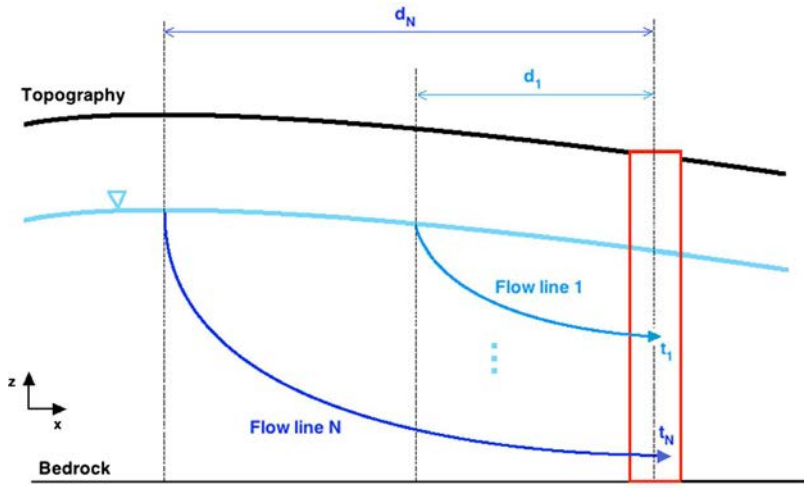

Fig. 7. Cross-section illustrating the sampling in a sampling zone (red) over the whole water column. For each flow line N, the groundwater distances (d_{1-N}) and times (t_{1-N}) are calculated. (For interpretation of the references to color in this figure legend, the reader is referred to the web version of this article.)

distances. We determined the length of those reference distances as the travel distance water would have traveled along the impermeable ground surface from a topographical height to the sampling zone. We used a 5 m LiDAR DEM with the D8 algorithm implemented in the TopoToolbox Matlab software (Schwanghart and Kuhn, 2010; Schwanghart and Scherler, 2014). Using a D8 algorithm, the flow passes from each cell to its lowest neighboring cell. Reference distances were generated for the whole model domain to calculate mean values for each of the 287 sampling zones (100 × 100 m) and summary statistics for the upland, transition and lowland area. The comparison of mean groundwater travel distances with mean reference distances was performed for sampling zones with mean distances greater than 100 m because the mesh size and flow processes that the numerical model accounted for were insufficient for an analysis at a smaller groundwater flow scale (less than 100 m).

We used the ratio of mean groundwater travel distance to mean reference distance ($r_{\text{GW-LOCAL}}$) as a metric of the relative influence of topography and recharge on the groundwater table (Fig. 8). Conceptually, when the mean groundwater travel distance is similar to the mean reference distance ($r_{\text{GW-LOCAL}}$ approaches 1), the saturated fraction of the subsurface volume (defined as the volume between the land surface and the impermeable bedrock) is higher than 95%. The groundwater table is therefore limited by the land surface and groundwater flow is strongly influenced by topographical gradients (Fig. 8a). When $r_{\text{GW-LOCAL}}$ is greater than 1, the saturated fraction fills less than 95% of the subsurface volume, meaning the groundwater table elevation depends mainly on the recharge rate and groundwater flow circulation is dominated by the hydrogeological conditions (Fig. 8c). Fig. 8b demonstrates that locally topography and recharge controls can occur at the same time in an aquifer. We calculated $r_{\text{GW-LOCAL}}$ based on the average of the mean groundwater travel distances (see Section 2.4) and the mean of the reference distances in the upland and lowland area of the aquifer. We did not calculate this ratio for the transition area due to less well-constrained distances and compound uncertainties, meaning that flow lines crossed that zone could not be associated exclusively with the transition area. We also determined the subsurface fraction of subsurface volume for the upland and lowland areas separately. We used this metric at the small catchment scale to quantify groundwater travel distances of local circulation, but it would equally applicable at larger scales where it could be used to classify groundwater circulations in relation to the reference distances.

3. Results

In Sections 3.1 we present the results of the reference model. In Section 3.2 we compare the modeled groundwater travel distances with reference distances and explore their ratio $r_{\text{GW-LOCAL}}$ in relation to the saturated fraction of the subsurface volume. In Section 3.3 we present how modifications in the alternative models alter model behavior. Specifically we report the relationship between the groundwater travel distances, transit times, and their spatial arrangement in the catchment.

3.1. Transit times and groundwater travel distances

All of the metrics of groundwater travel distance and transit time followed the same pattern, with greatest mean transit times and distances in the transition area, followed by the upland, and

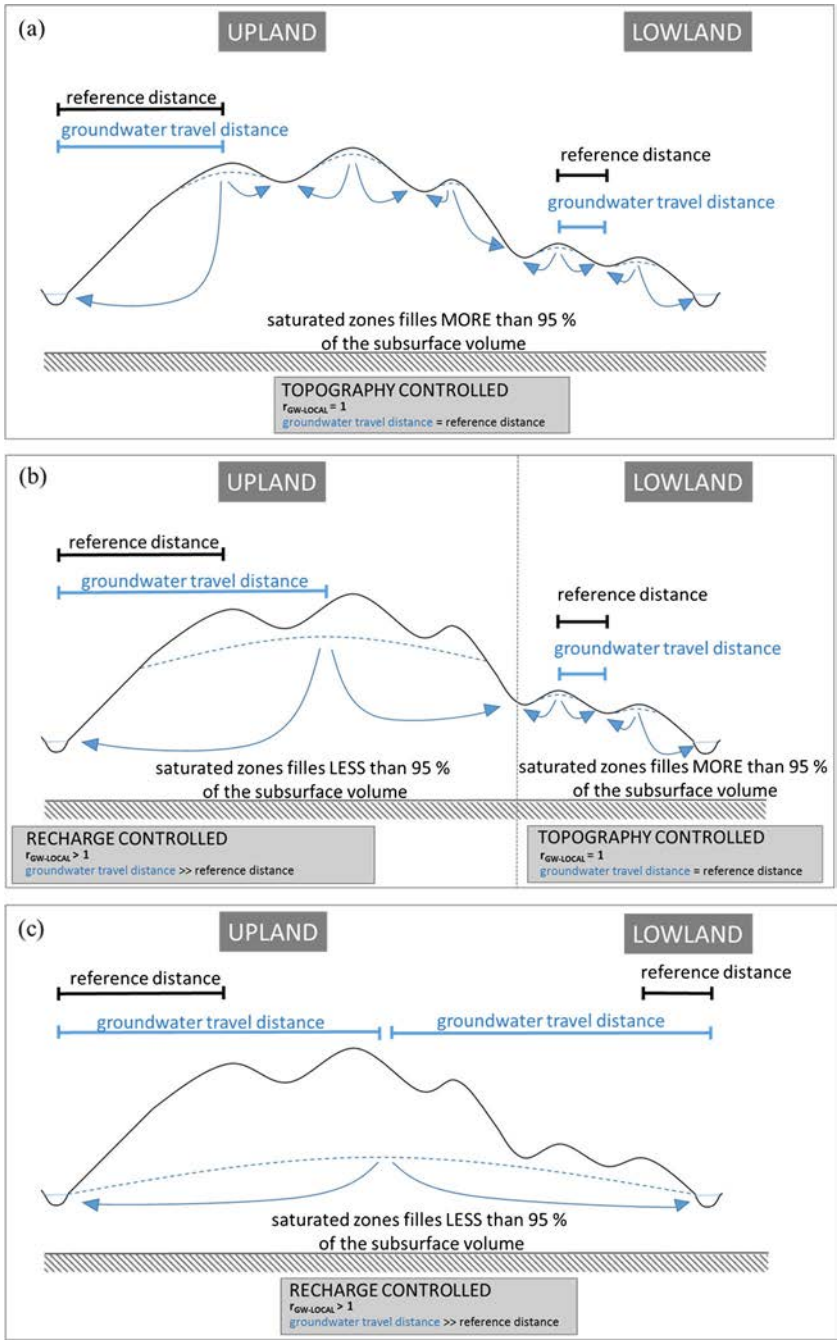

Fig. 8. Conceptual representation of recharge and topography controlled groundwater table conditions in a shallow aquifer. High groundwater table conditions result in topography controls in the upland and lowland area (a). For lower groundwater table conditions, a recharge controlled system in the upland and a topography control system in the lowland can occur (b). Very low groundwater table conditions (c) can result in recharge control in both areas. The authors were inspired by Haitjema and Mitchell-Bruker (2005, Fig. 4).

then lowland area (Table 3). Mean transit times were on the order of decades, while groundwater travel distances remained on the order of hundreds of meters.

Considering transit time and groundwater travel distance distributions for individual sampling zones of the reference model, Fig. 9 shows distributions for three representative sampling zones in the upland, transition, and lowland area (Fig. 3). The three sampling zones are representative for their area as they show a common shape with an appropriate mean value of all investigated distributions in the related area. In the upland and lowland area, the transit time distributions had an exponential-like shape while the transition zone had a more bimodal shape with maxima around zero and 65 years (Fig. 9a). The mean transit time was 42 years (SD = 43) in the upland sampling zone and 35 years (SD = 29) in the lowland sampling zone. These results were consistent with an exponential distribution, where the mean transit time is equal to the standard deviation, and also with the mean transit time τ_A given by Haitjema (1995):

$$\tau_A = \frac{\theta \cdot H}{R} \tag{2}$$

where τ_A is the mean transit time, H is the mean hydraulic thickness of the aquifer, θ is the effective porosity and R is the recharge. The mean transit time according to this equation averaged 30 years

Table 3
Groundwater mean distances and mean transit times and their coefficient of variation for each of the five groundwater flow models (REF: reference model, THICK: model with thicker weathered zone, THIN: model with thinner weathered zone, AHC: model with higher hydraulic conductivity in granite, HOM: homogeneous model).

		REF	HOM	THIN	THICK	AHC
Catchment	Mean distance (m)	334	358	323	307	438
	CV distance (%)	59	62	60	65	57
	Mean time (y)	51	148	65	55	53
	CV time (%)	29	26	31	26	30
Lowland	Mean distance (m)	219	285	214	300	202
	CV distance (%)	59	52	62	48	0.72
	Mean time (y)	47	141	62	52	53
	CV time (%)	34	26	35	23	48
Transition	Mean distance (m)	576	713	572	639	398
	CV distance (%)	49	35	49	34	44
	Mean time (y)	57	171	75	51	53
	CV time (%)	44	28	43	27	32
Upland	Mean distance (m)	326	296	313	223	566
	CV distance (%)	40	47	41	48	38
	Mean time (y)	51	146	64	58	53
	CV time (%)	18	24	21	26	14

for the upland area and 16 years for the lowland area when the aquifer thickness was constrained to the weathered zone (11.3 m and 6 m for the two areas respectively). The mean transit time increased to 74 years upland and 58 years lowland when the aquifer thickness was allowed to include both, the weathered and fractured zones (60.3 m and 54 m, respectively). The groundwater travel distance distribution in Fig. 9b resembled an exponential distribution in the upland and transition sampling zone. The distance distribution in the lowland sampling zone peaked around 50 m and only included distances less than 750 m.

The differences of mean transit times and groundwater travel distances for the whole aquifer were visible on the map derived from interpolation of the pointwise values obtained in each sampling zone (Fig. 10a and b). Mean values and the coefficient of variation (CV) of all sampling zones in an area revealed mean transit times of 51 (CV = 18%), 57 (CV = 44%), and 47 (CV = 34%) years, and mean groundwater travel distances of 326 m (CV = 40%), 576 m (CV = 49%), and 219 m (CV = 59%) in the upland, transition, and lowland area, respectively. Variability was higher for distances than for times. The transition area had the highest mean groundwater travel distance, though even in this area circulation remained local according to Tóth's flow structure definitions (Tóth, 1963, 2009), because flow lines did not extend under any streams. Even the maximum of the mean groundwater travel distances in the three areas were small compared to the size of the catchment (9 km from south to north and 5 km from east to west) at 751, 1741, and 648 m in the upland, transition, and lowland area, respectively. The mean distance between two streams was *ca.* 1000 m upland and 600 m lowland indicating a denser stream network in the lowland area. Only 0.1% of the flow lines connected

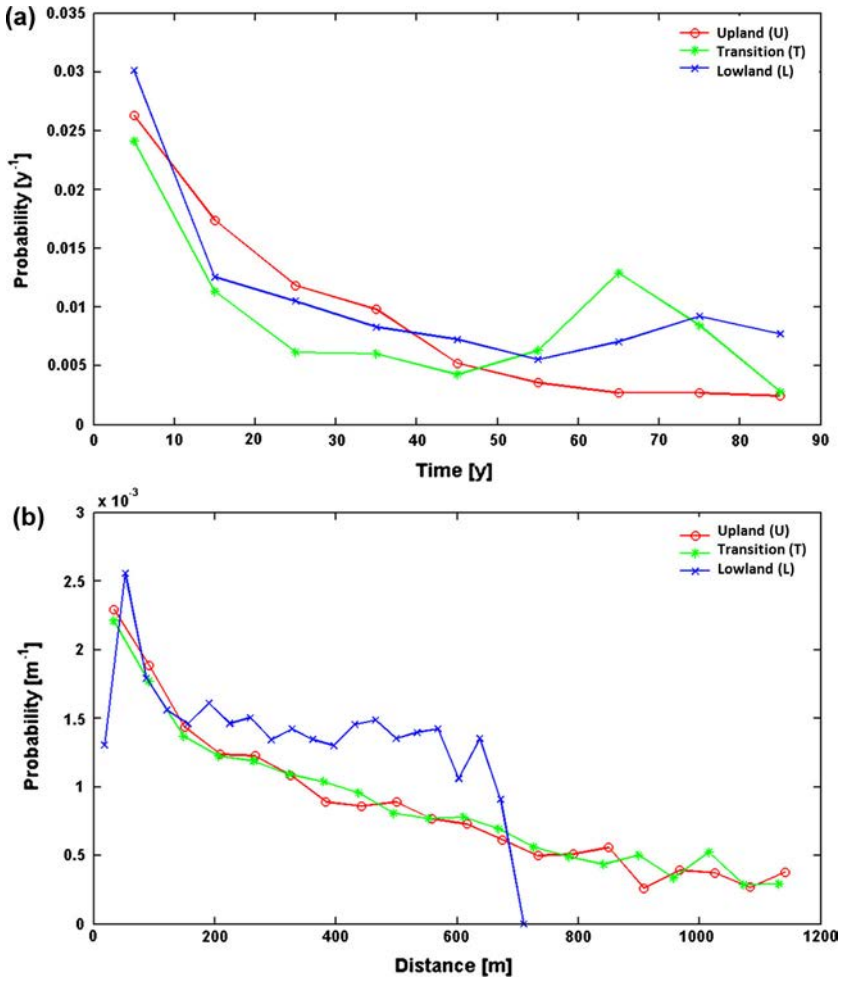

Fig. 9. Representative plots of (a) transit time distributions and (b) groundwater travel distance distributions taken from three sampling zones each belonging to a different catchment area (upland, transition, lowland). The transit time is defined as the time a water molecule spends between the recharge location and the sampling zone. Transit times show an exponential-like distribution. The groundwater travel distance distribution was shorter in the lowland area than in the upland and transition area.

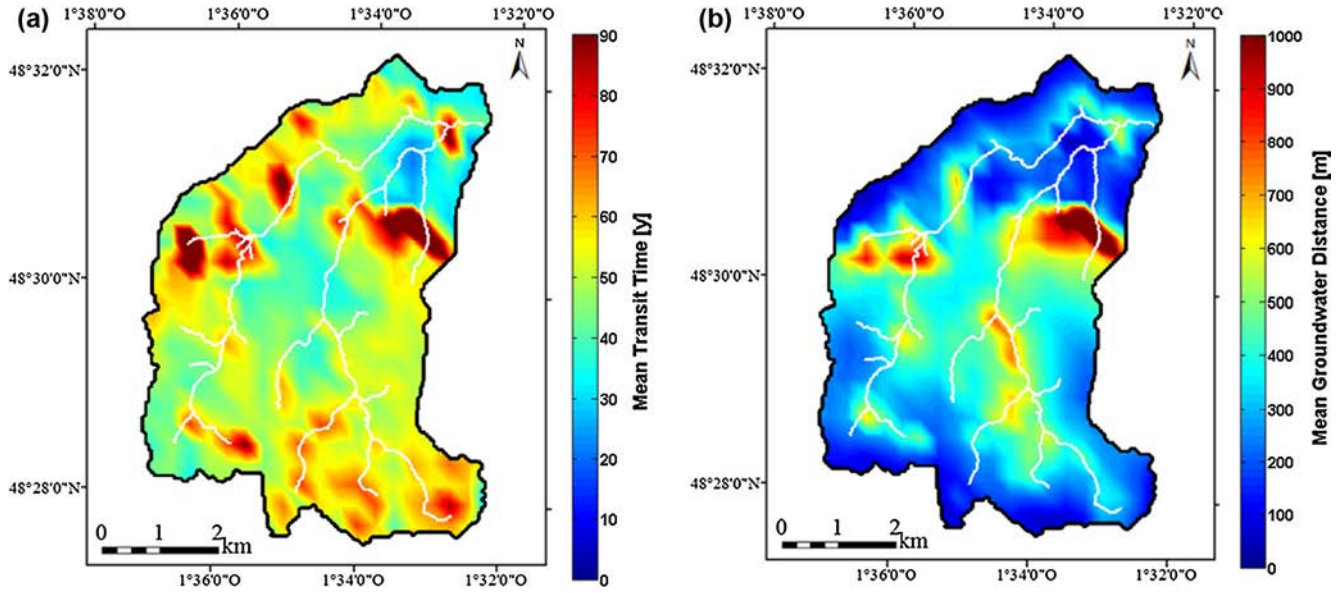

Fig. 10. Spatial analysis of the Pleine–Fougères aquifer in regards to (a) mean transit times, and (b) mean groundwater travel distances, obtained by interpolating the results of 278 sampling zones. The transit time is defined as the time a water molecule spends between the recharge location and the sampling zone. Contours of the maps correspond to the catchment boundaries (black polygons).

the upland and lowland area without going under a stream, indicating a dominance of local, rather than intermediate or regional flow. Groundwater flow lines were generally oriented along the east–west direction, except in the transition zone where flow moved primarily from south to north (Fig. 6). Some flow lines intersected the surface along the stream network or just downslope of the steep transition, consistent with observations of springs and surface water in the catchment. The groundwater table was close to the surface, showing groundwater outcropping at 80% of the total length of the stream channel throughout the catchment, though the groundwater table was more connected with the land surface in the lowland than upland area (Table 4). Some long groundwater flow lines crossed the boundary of the hydrological catchment, but they did not approach the boundary of the modeled domain (Fig. 6).

3.2. Groundwater circulation and $r_{GW\text{-}LOCAL}$

For the whole aquifer, groundwater circulation remained local with larger groundwater travel distances than the reference distances. Fig. 11 shows the three representative sampling zones for the upland, transition and lowland area of the reference model with the origin of the groundwater and reference flow lines. For the lowland and transition sampling zone, both recharge areas partially overlapped with a larger groundwater recharge area. For the upland sampling zone with higher topographical gradients, recharge areas only overlapped at the sampling zone showing groundwater flow lines and reference flow lines coming from an opposite direction. This is possible because this sampling zone was not in the seepage area and all cases of overlapping and non-overlapping may occur.

The relationship between the ratio $r_{GW\text{-}LOCAL}$ (mean groundwater travel distance divided by the mean of the reference distance) and the proportion of saturated fraction related to the subsurface volume of the reference model revealed different controls for the upland and lowland area (Fig. 12). In the upland area, the saturated fraction filled less than 95% of the subsurface volume with a ratio $r_{GW\text{-}LOCAL}$ of 1.6. The groundwater table was recharge controlled showing larger distances with deeper circulations than in the lowland area. The groundwater flow in the upland area was more influenced by the hydrogeological conditions than the topographical gradients. Groundwater flow was limited by the fresh bedrock which prevented larger circulation. In the lowland area the groundwater table was limited by the topography with the saturated fraction filling more than 95% of the subsurface volume and a ratio $r_{GW\text{-}LOCAL}$ of 1.3. Due to the high groundwater table elevation, the groundwater flow was mainly affected by the topography. Flow lines were shallow and they followed the topographical gradients from the closest topographical height (the recharge location) to the discharge location (sampling zone). For the whole aquifer, $r_{GW\text{-}LOCAL}$ was 1.7, meaning that the mean groundwater travel distances were nearly twice as long as the mean of the local reference distances.

Table 4
Intersection rate of the groundwater table with the surface at stream channels for the five models (REF: reference model, THICK: model with thicker weathered zone, THIN: model with thinner weathered zone, AHC: model with higher hydraulic conductivity in granite, HOM: homogeneous model). Rate is expressed as the percentage of the connected length to the full stream length.

	REF	THICK	THIN	AHC	HOM
Catchment (%)	77	85	85	68	82
Upland (%)	97	94	98	100	96
Lowland (%)	70	82	79	56	76

3.3. Alternative models

To test how our model assumptions influenced the results of the reference model, which indicated that groundwater circulations were local (<1 km) and mean transit times were quite long (51 years), we ran simulations of the four alternative models presented in Section 2.2. Our comparison was based on the characteristic mean transit times and mean groundwater travel distances for the full aquifer and the individual upland, transition, and lowland area (Table 3). Despite structural differences, the five models gave similar groundwater table heights, with a maximum mean difference of 2.2 m between the most different models (REF and AHC), meaning that all five models had a similar aquifer volume.

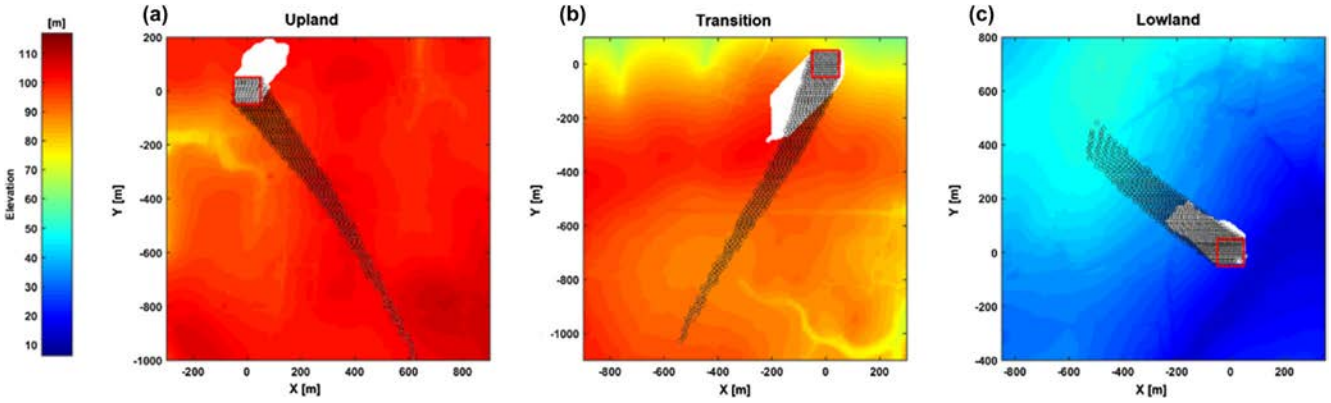

Fig. 11. Groundwater contributing areas (black circles) to the sampling zones (red squares): (a) upslope, (b) transition, and (c) downslope. White recharge areas are derived from the local reference distances. For each of the three plots, the corresponding elevation of the land surface is presented in colors. (For interpretation of the references to color in this figure legend, the reader is referred to the web version of this article.)

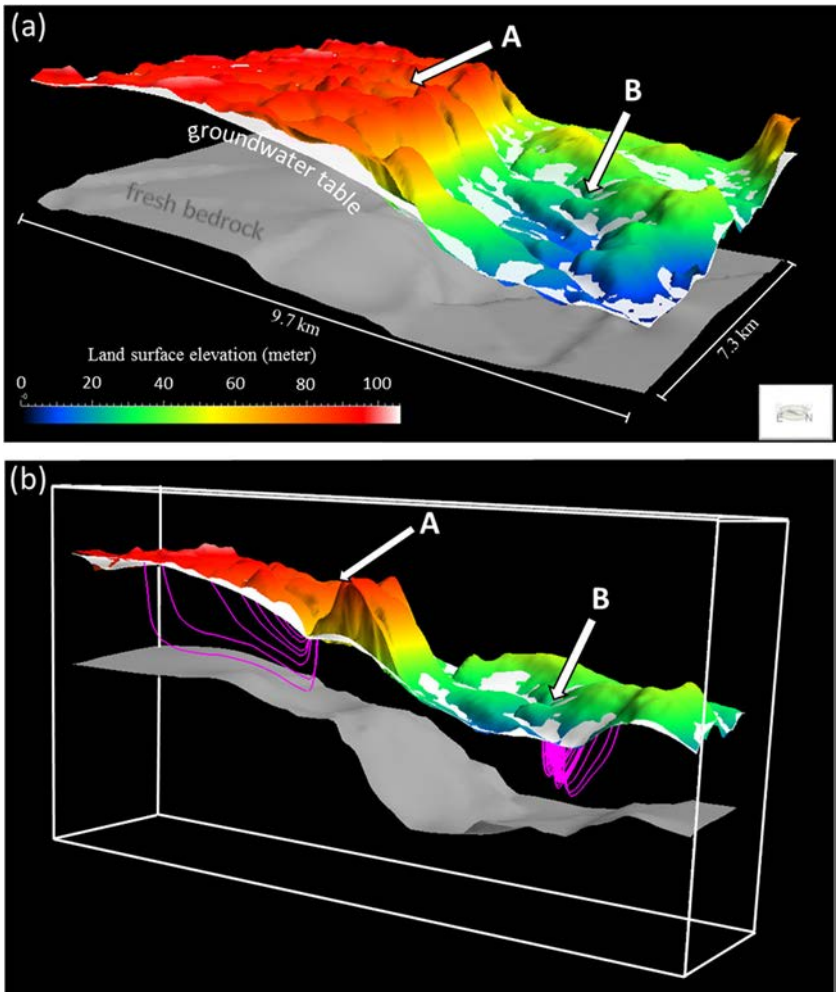

Fig. 12. Land surface (in color), groundwater (white) and fresh bedrock elevation (grey) of the model domain. Flow lines are presented for the lowland area, which had a topography controlled groundwater table, and the upland area, which had a recharge controlled groundwater table. (For interpretation of the references to color in this figure legend, the reader is referred to the web version of this article.)

Mean transit times of the aquifer, like aquifer volumes, given by the five models were less variable than mean groundwater travel distances influenced by permeability and topography structures. Except for the homogeneous model (HOM), mean transit times were similar between models both for the whole aquifer and the individual upland, transition, and lowland areas, though this result is not surprising since all models were calibrated using the same groundwater age data. HOM was different because sampling was performed over the full depth of the model (90 m), whereas the other models were limited by the impervious bedrock, resulting

in a shallower aquifer thickness (around 60 m; Table 3), and in mean transit times that were substantially larger for HOM. While mean transit times were highly sensitive to the overall aquifer volume, mean groundwater travel distances were consistent between models, showing greater sensitivity to topography and geological structure. The alternative hydraulic conductivity model (AHC), which had highly pervious granite upland and less pervious schist lowland showed much larger mean groundwater travel distances upland than the reference model (566 m for AHC and 326 m for REF; Table 3). Higher permeability in the upland area decreased hydraulic head gradients, resulting in a lower water table for AHC. Consequently, topography played a smaller role and groundwater distances were larger upland. The abrupt reduction of permeability by a factor of 10 from upland to lowland shortened the mean groundwater travel distance in the transition area from 576 m to 398 m. In the THICK model, with a thicker weathered zone, there was marginally more circulation through the transition area relative to the reference model (639 m versus 576 m) and the opposite effect was observed for the THIN model. However, mean groundwater travel distances were the same or smaller relative to REF in the upland area for both the THICK and THIN model (REF = 326 m, THICK = 296 m, THIN = 313 m).

4. Discussion

In this study we used groundwater flow models of a crystalline unconfined aquifer in Brittany, France to investigate the importance of local flow paths and to identify groundwater table controls at the small catchment scale. We hypothesized that relatively old groundwater would have traveled long distances from the recharge location to the sampling zone with increasing distances towards the catchment outlet. Contrary to our hypothesis we found highly local groundwater flow, with groundwater traveling less than 500 m on average (Table 3), and groundwater travel distances decreasing moving lowland (Table 3). To localize the flow circulation we used the ratio of groundwater travel distances derived by the numerical model to reference distances from the DEM. Topographical gradients were the major controls on groundwater flow in the lowland area whereas recharge dynamics governed the groundwater table in the upland area with a strong influence of the hydrogeological conditions on groundwater circulation. These results represent a departure from the historical conceptualization of the small-catchment hydrology (Tóth, 1963, 2009) with potentially important water source and water quality implications.

4.1. Patterns of groundwater circulation in shallow aquifers

Circulation was highly local for all models across a range of weathered and fractured zone thicknesses, not extending below stream beds, indicating a general lack of intermediate and regional flow paths (Gburek and Folmar, 1999). We were particularly interested in identifying mechanisms underlying this behavior, because local groundwater flow is sensitive to local permeability and topography structure, which can be very diverse at the sub-kilometer scale. Several dynamics could explain the contrasting circulation pattern we observed in the upland and lowland area of all models, including the limited aquifer thickness, topographical gradients and groundwater table configuration. The ratio $r_{GW\text{-}LOCAL}$ clearly showed a stronger influence of the topography on the flow circulation in the lowland area than in the upland area. Whether linked groundwater travel distances and topographical gradients promote short groundwater flow lines is readily testable and should be confirmed with a more systematic study on synthetic topographical structures (Crave and Davy, 2001; Lague et al., 2000) and by comparing trends in multiple catchments (Thomas et al., 2016b).

Based on the reference model (REF) we wanted to demonstrate how the ratio $r_{GW\text{-}LOCAL}$ and the proportion of the saturated fraction in relation to the subsurface volume evolve under varying recharge and constant hydraulic conductivity conditions (Fig. 13). To analyze the change between recharge and topographical control, we performed simulations with several recharge rates ranging from 1/10 average recharge (16.7 mm a^{-1}) to 4 times average recharge (668 mm a^{-1}). Fig. 13 shows how groundwater flow circulation change depending on the groundwater table configuration which is in general related to hydraulic conductivity and the recharge rate. For a four-fold higher recharge rate (Fig. 13a) the groundwater table moved closer to the land surface and flow lines got shorter over the whole domain than for the initial recharge rate R (Fig. 13b), especially in the upland area. Also the flow lines followed more topographical gradients. Under a lesser recharge rate (Fig. 13c) the groundwater table is deeper and less connected to the land surface inducing longer groundwater travel distances. Most of the flow lines that started in the upland area traveled longer distances towards the lowland area. For the three example recharge rates we presented, not only the length of the groundwater travel distances, but also flow directions changed. Under topography controlled conditions (4R, Fig. 13a) flow lines are more east–west oriented due to local topographical roughness, whereas under recharge controlled conditions (R/10, Fig. 13c) flow lines follow the steep slope in south-north direction, again demonstrating the link between hydrogeological and topographical controls. The extent of the hydrogeological active zone varied proportionally to the induced recharge rate and the limiting depth coming from the unaltered bedrock. Particularly in the upland area, the groundwater table elevation was more susceptible to changes in recharge and deeper flow lines were limited by the fresh bedrock.

We propose the ratio of groundwater travel distance to reference distance ($r_{GW\text{-}LOCAL}$) as a useful tool to quantify the spatial extent of the groundwater circulation. The evolution of $r_{GW\text{-}LOCAL}$ with the proportion of the saturated fraction in relation to the subsurface volume at differing recharge levels give an indication of the recharge versus topography controls on the groundwater table and therefore on flow dynamics (Fig. 14). The ratio $r_{GW\text{-}LOCAL}$ decreased as the saturated fraction increased, reaching 1 when the saturated fraction exceeded 95% of the subsurface volume. This meant that when the aquifer filled the whole subsurface volume (groundwater table at the land surface), groundwater distances became similar to reference distances derived by the DEM, and topography mainly influenced the groundwater circulation. By contrast, a recharge controlled regime developed as the saturated fraction decreased and $r_{GW\text{-}LOCAL}$ became larger than 1. $r_{GW\text{-}LOCAL}$ decreased linearly with an increase of the saturated fraction despite increasing dispersion, i.e. longer flow lines due to greater distances between the land surface and the water table. The ratio $r_{GW\text{-}LOCAL}$ showed a distinct asymptotic behavior for the upland and lowland area. While the overall pattern was similar, the ratio $r_{GW\text{-}LOCAL}$ responded more strongly to changes in the extent of the saturated fraction in the upland area. This suggest two distinct regimes, one for the upland and the other for the lowland area (Fig. 14). The ratio $r_{GW\text{-}LOCAL}$ varied strongly ranging from 0.03 to 7.47 (lower quartile = 1.0 and upper quartile 2.2) dependent on the applied recharge rate, though the groundwater travel distance with their respective transit times remained larger than the reference distances in most areas. These results underline the need for a local analysis of groundwater table controls in small catchments and provide the ratio $r_{GW\text{-}LOCAL}$ to perform this analysis. While the criterion of Haitjema and Mitchell-Bruker (2005) is relevant to quantify topography and recharge controls at larger scales, our criterion is appropriate at smaller scales and for shallow aquifers.

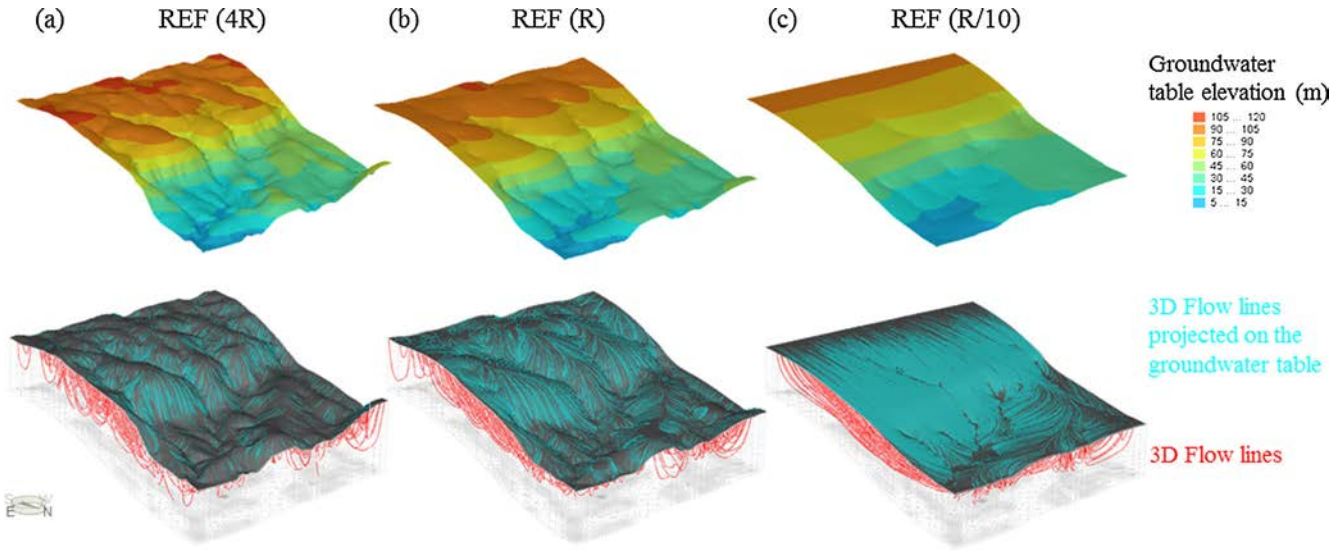

Fig. 13. Groundwater table elevations (colored plane) and 3D flowlines for the reference model (REF) with different recharge rates: (a) 668 mm y^{-1}, (b) 167 mm y^{-1}, and (c) 16.7 mm y^{-1}. 3D flowlines are represented in red in the flow domain and in blue projected on the top of the model i.e. the free surface. (For interpretation of the references to color in this figure legend, the reader is referred to the web version of this article.)

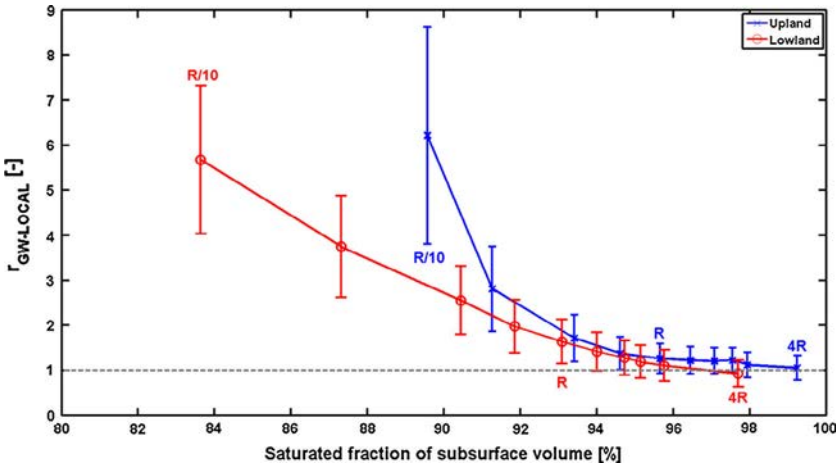

Fig. 14. Ratio $r_{GW\text{-}LOCAL}$ [−] of groundwater distance over local reference distance as a function of the proportion of the saturated fraction in relation to the whole subsurface volume [%] for the upland (red circled line) and lowland areas (blue crossed line). Mean values with their standard deviation are given for recharge rates from *R*/10 to 4*R*. The grey line indicates a ratio $r_{GW\text{-}LOCAL}$ equal to 1 corresponding to topography controlled conditions. As the Recharge increases from *R*/10 to 4*R* both zones become topography controlled with a saturated zone filling more than 95% of the subsurface volume. Below 95% the groundwater table is recharge controlled. (For interpretation of the references to color in this figure legend, the reader is referred to the web version of this article.)

4.2. What does old and local flow mean for water quality?

Our results revealed that groundwater mean transit times and groundwater travel distances in this aquifer do not fit within the concept of local, intermediate and regional groundwater flow (Tóth, 1963, 2009) but that the majority of groundwater occurred within the shallow, weathered zone. While flow remained local, mean transit times were surprisingly long with mean transit times greater than 50 years. These mean transit times are much larger than values typically used in models forecasting water quality in shallow aquifers (Ayraud et al., 2008; Molénat et al., 2013). One of the implications of this finding is that any changes in land use or agricultural practice may take decades to influence groundwater quality. This time-lag between changes in management and potential improvements of water quality, complicates the evaluation of the efficacy of efforts to protect water quality such as fertilizer reduction or land cover change because cause and effect are so temporally separated. Current water quality should therefore be related to past land-use and the duration of monitoring programs should be scaled depending on the distribution of transit times. Another implication of the long mean transit times observed here is that trends in groundwater quality could be influenced by long-term changes in water balance. Because the rate of recovery of a polluted aquifer depends largely on water turnover time, changes in groundwater recharge resulting from shifts in precipitation and evapotranspiration could strongly influence groundwater chemistry independent of any changes in land management. Marked latitudinal differences in climate projections of water balance in Europe (Forzieri et al., 2014) suggest a shortening of transit times (and associated recovery times) in northern Europe and a lengthening of transit times in southern Europe.

The second finding, that most groundwater stays highly local, traveling an average of less than 500 m from where it entered the aquifer, reinforces the importance of addressing groundwater

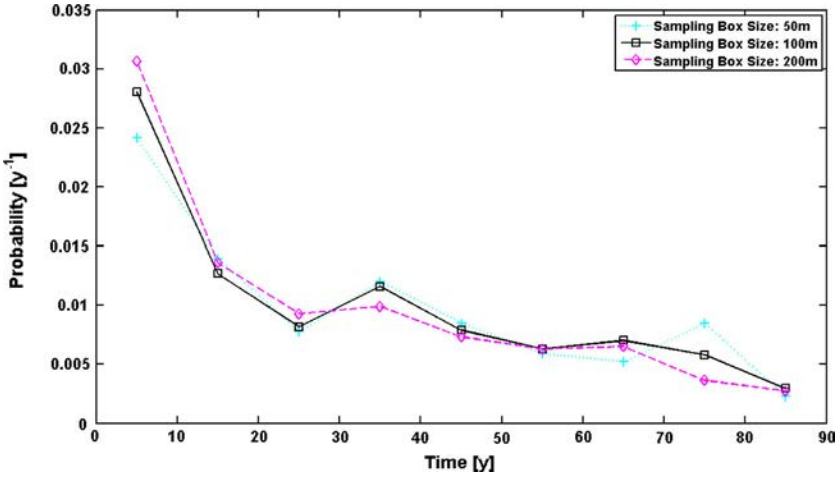

Fig. A.1. Transit time distributions for 50 × 50 m, 100 × 100 m, and 200 × 200 m sampling zone sizes showed no significant variations. Three sampling zones, centered at the same location, are designed to sample the entire groundwater column.

quality at highly local scales including plot-level scales of individual fields. The topography and recharge control on the groundwater table and therefore on groundwater travel distances during high and low flows, suggests that a reconsideration is warranted of the role of landscape features such as riparian zones, hedgerows, and groundwater surface water exchange zones in mitigating diffuse nitrogen pollution originating from groundwater via a temporally dynamic modeling approach. On a general note, it is worthwhile to notice that the transit time and travel distance distributions could not have been derived from each other because of their different shapes (i.e. independent modeling of these parameters were necessary). Only both distributions together reveal detailed information about the water source and the time spent in the aquifer.

Our results highlight several interesting phenomena regarding groundwater dynamics in shallow aquifers. In surface waters such as rivers and streams, water comes from large catchments very quickly, while groundwater systems in small catchments have old water coming from very local sources. The surface water contributing area increases moving downstream as catchment size increases. Conversely, from our study and other recent work (Gburek and Folmar, 1999), groundwater "catchments" seem to stay the same size or even decrease moving downslope, due to shifts in topographical controls and recharge dynamics. These distinct hydrological and landscape-level patterns mean that surface waters are more likely to be impacted by acute or diffuse pollution since they drain a larger region, but that quick transit time and small water volume mean contaminants can quickly be transported away or diluted. Groundwater systems are much more modular and are therefore potentially less likely to experience pollution. However, if there is a local contaminant source, long transit times and limited long-distance water exchange means that the impact may be extreme and long-lasting.

5. Conclusion

The comprehensive analysis of several numerical groundwater flow models developed for a shallow hard-rock aquifer in Brittany, France gave insights in internal flow structures that are impossible to measure in the field. The unconfined aquifer was dominated by local flow circulation that was more vulnerable to contamination than deeper flows. The mean length of groundwater flow paths was limited to a few hundred meters (334 m), while the mean transit times were on the order of decades (51 y). A clear distinction could be drawn between the upland, transition, and lowland area for flow circulation and mean transit times, with greatest mean transit times and mean groundwater travel distances in the transition area followed by the upland and then the lowland area. Transit time distributions had an exponential-like distribution in the upland and lowland area, whereas the transition area showed a bimodal distribution. An examination of circulation in the upland and lowland area revealed distinct controls on the groundwater table and therefore on the flow behavior despite identical recharge conditions. We proposed the ratio $r_{GW\text{-}LOCAL}$ as an index of whether the groundwater table is limited by the topography or determined by the recharge rate at the small catchment scale, complementing the regional criterion of Haitjema and Mitchell-Bruker (2005; see Eq. (1)). At this site, the ratio $r_{GW\text{-}LOCAL}$ has proved a robust tool to describe the extent of groundwater circulation, and its generality should be tested between catchments (Thomas et al., 2016b).

Acknowledgements

Financial support for this research was provided by the European Union's Seventh Framework for research, technological development and demonstration under grant agreement no. 607150. The authors are grateful to the Marie Curie Actions for funding this research. This paper was supported by the European Union International Training Network "INTERFACES: Ecohydrological interfaces as critical hotspots for transformations of ecosystem exchange fluxes and biogeochemical cycling". The authors acknowledge MIKE Powered by DHI for sponsoring the license file for the MIKE Powered by DHI Software – FEFLOW. We further acknowledge the French Geological Survey (BRGM) for providing geological maps of the study site and the AquiFR project for developing and gathering Aquifer models in France. This work was also supported by the French National Program EC2CO Continental and Coastal Ecosphere. We also acknowledge the LTER Zone Atelier Armorique. The authors would like to thank the anonymous reviewers for their valuable comments and suggestions to improve the quality of the paper.

Appendix A

See Fig. A.1.

References

Anderson, M.P., Woessner, W.W., Hunt, R.J., 2015. Applied Groundwater Modeling: Simulation of Flow and Advective Transport. Elsevier Science.

Appelo, C., Postma, D., 2005. Geochemistry Groundwater and Pollution, second ed. A.A. Balkema Publishers, Leiden, The Netherlands a member of the Taylor & Francis Group plc.

Ayraud, V., Aquilina, L., Labasque, T., Pauwels, H., Molenat, J., Pierson-Wickmann, A. C., Durand, V., Bour, O., Tarits, C., Le Corre, P., Fourre, E., Merot, P., Davy, P., 2008. Compartmentalization of physical and chemical properties in hard-rock aquifers deduced from chemical and groundwater age analyses. Appl. Geochem. 23, 2686–2707. http://dx.doi.org/10.1016/j.apgeochem.2008.06.001.

Bala, A., Eduvie, O., Byami, J., 2011. Borehole depth and regolith aquifer hydraulic characteristics of bedrock types in Kano area, Northern Nigeria. Afr. J. Environ. Sci. Technol. http://dx.doi.org/10.4314/ajest.v5i3.71936.

Batu, V., 1998. Aquifer Hydraulics: A Comprehensive Guide to Hydrogeologic Data Analysis, first ed. Wiley Interscience.

Bear, J., 1973. Dynamics of Fluids in Porous Media. American Elsevier Publishing Company Inc.

Bear, J., Verruijt, A., 2012. Modeling Groundwater Flow and Pollution. Springer Science & Business Media.

Bernard-Griffiths, J., Peucat, J.J., Sheppard, S., Vidal, P., 1985. Petrogenesis of Hercynian leucogranite from the southern Armorican Massif: contribution of REE and isotopic (Sr, Nd, Pb and O) geochemical data to the study of source rock characteristics and ages. Earth Planet. Sci. Lett. 74, 235–250. http://dx.doi.org/10.1016/0012-821X(85)90024-X.

Böhlke, J.-K., 2002. Groundwater recharge and agricultural contamination. Hydrogeol. J. 10, 153–179. http://dx.doi.org/10.1007/s10040-001-0183-3.

Boone, A., Calvet, J.-C., Noilhan, J., 1999. Inclusion of a third soil layer in a land surface scheme using the force-restore method. J. Appl. Meteorol. 38, 1611–1630. http://dx.doi.org/10.1175/1520-0450(1999)038<1611:IOATSL>2.0.CO;2.

Busenberg, E., Plummer, L.N., 1992. Use of chlorofluorocarbons (CCl_3F and CCl_2F_2) as hydrologic tracers and age-dating tools: the alluvium and terrace system of central Oklahoma. Water Resour. Res. 28, 2257–2283. http://dx.doi.org/10.1029/92WR01263.

Cardenas, M.B., 2007. Potential contribution of topography-driven regional groundwater flow to fractal stream chemistry: residence time distribution analysis of Tóth flow. Geophys. Res. Lett. 34, L05403. http://dx.doi.org/10.1029/2006GL029126.

Chapelle, F.H., Bradley, P.M., Goode, D.J., Tiedeman, C., Lacombe, P.J., Kaiser, K., Benner, R., 2009. Biochemical indicators for the bioavailability of organic carbon in ground water. Ground Water 47, 108–121. http://dx.doi.org/10.1111/j.1745-6584.2008.00493.x.

Chapman, T., 1999. A comparison of algorithms for streamflow recession and baseflow separation. Hydrol. Process. 13, 701–714. http://dx.doi.org/10.1002/(SICI)1099-1085(19990415)13:5<701::AID-HYP774>3.0.CO;2-2.

Clement, J.C., Aquilina, L., Bour, O., Plaine, K., Burt, T.P., Pinay, G., 2003. Hydrological flowpaths and nitrate removal rates within a riparian floodplain along a fourth-order stream in Brittany (France). Hydrol. Process. 17, 1177–1195. http://dx.doi.org/10.1002/hyp.1192.

Cook, P.G., Herczeg, A.L., 2000. Environmental Tracers in Subsurface Hydrology. Springer, US.

Crave, A., Davy, P., 2001. A stochastic "precipiton" model for simulating erosion/sedimentation dynamics. Comput. Geosci. 27, 815–827. http://dx.doi.org/10.1016/S0098-3004(00)00167-9.

Dewandel, B., Lachassagne, P., Wyns, R., Marechal, J.C., Krishnamurthy, N.S., 2006. A generalized 3-D geological and hydrogeological conceptual model of granite aquifers controlled by single or multiphase weathering. J. Hydrol. 330, 260–284. http://dx.doi.org/10.1016/j.jhydrol.2006.03.026.

Diersch, H.-J., 2013. FEFLOW: Finite Element Modeling of Flow, Mass and Heat Transport in Porous and Fractured Media. Springer Science & Business Media.

Dunn, S.M., Darling, W.G., Birkel, C., Bacon, J.R., 2012. The role of groundwater characteristics in catchment recovery from nitrate pollution. Hydrol. Res. 43, 560. http://dx.doi.org/10.2166/nh.2012.020.

Earle, S., 2015. Physical Geology. BC Open Textbooks.

Eberts, S.M., Böhlke, J.K., Kauffman, L.J., Jurgens, B.C., 2012. Comparison of particle-tracking and lumped-parameter age-distribution models for evaluating vulnerability of production wells to contamination. Hydrogeol. J. 20, 263–282. http://dx.doi.org/10.1007/s10040-011-0810-6.

Edet, A., Okereke, C., 2004. Hydrogeological and hydrochemical character of the regolith aquifer, northern Obudu Plateau, southern Nigeria. Hydrogeol. J. 13, 391–415. http://dx.doi.org/10.1007/s10040-004-0358-9.

Engesgaard, P., Kipp, K., 1992. A geochemical transport model for redox-controlled movement of mineral fronts in groundwater flow systems: a case of nitrate removal by oxidation of pyrite. Water Resour. Res. 28, 2829–2843. http://dx.doi.org/10.1029/92wr01264.

ESRI, 2011. ArcGIS Desktop: Release 10. Environmental Systems Research Institute, Redlands, CA, n.d.

Forster, C., Smith, L., 1988. Groundwater flow systems in mountainous terrain: 2. Controlling factors. Water Resour. Res. 24, 1011–1023. http://dx.doi.org/10.1029/WR024i007p01011.

Forzieri, G., Feyen, L., Rojas, R., Flörke, M., Wimmer, F., Bianchi, A., 2014. Ensemble projections of future streamflow droughts in Europe. Hydrol. Earth Syst. Sci. 18, 85–108. http://dx.doi.org/10.5194/hess-18-85-2014.

Freer, J., McDonnell, J., Beven, K.J., Brammer, D., Burns, D., Hooper, R.P., Kendal, C., 1997. Topographic controls on subsurface storm flow at the hillslope scale for two hydrologically distinct small catchments. Hydrol. Process. 11, 1347–1352. http://dx.doi.org/10.1002/(SICI)1099-1085(199707)11:9<1347::AID-HYP592>3.3.CO;2-I.

Gburek, W.J., Folmar, G.J., 1999. Patterns of contaminant transport in a layered fractured aquifer. J. Contam. Hydrol. 37, 87–109. http://dx.doi.org/10.1016/S0169-7722(98)00158-2.

Gleeson, T., Manning, A.H., 2008. Regional groundwater flow in mountainous terrain: three-dimensional simulations of topographic and hydrogeologic controls. Water Resour. Res. 44, W10403. http://dx.doi.org/10.1029/2008WR006848.

Goderniaux, P., Davy, P., Bresciani, E., de Dreuzy, J.-R., Le Borgne, T., 2013. Partitioning a regional groundwater flow system into shallow local and deep regional flow compartments. Water Resour. Res. 49, 2274–2286. http://dx.doi.org/10.1002/wrcr.20186.

Grathwohl, P., Rügner, H., Wöhling, T., Osenbrück, K., Schwientek, M., Gayler, S., Wollschläger, U., Selle, B., Pause, M., Delfs, J.-O., Grzeschik, M., Weller, U., Ivanov, M., Cirpka, O.A., Maier, U., Kuch, B., Nowak, W., Wulfmeyer, V., Warrach-Sagi, K., Streck, T., Attinger, S., Bilke, L., Dietrich, P., Fleckenstein, J.H., Kalbacher, T., Kolditz, O., Rink, K., Samaniego, L., Vogel, H.-J., Werban, U., Teutsch, G., 2013. Catchments as reactors: a comprehensive approach for water fluxes and solute turnover. Environ. Earth Sci. 69, 317–333. http://dx.doi.org/10.1007/s12665-013-2281-7.

Green, C.T., Böhlke, J.K., Bekins, B.A., Phillips, S.P., 2010. Mixing effects on apparent reaction rates and isotope fractionation during denitrification in a heterogeneous aquifer. Water Resour. Res. 46, 1–19. http://dx.doi.org/10.1029/2009WR008903.

Grimaldi, C., Thomas, Z., Fossey, M., Fauvel, Y., Merot, P., 2009. High chloride concentrations in the soil and groundwater under an oak hedge in the West of France: an indicator of evapotranspiration and water movement. Hydrol. Process. 23, 1865–1873. http://dx.doi.org/10.1002/hyp.7316.

Haitjema, H.M., 1995. On the residence time distribution in idealized groundwatersheds. J. Hydrol. 172, 127–146. http://dx.doi.org/10.1016/0022-1694(95)02732-5.

Haitjema, H.M., Mitchell-Bruker, S., 2005. Are water tables a subdued replica of the topography? Ground Water 43, 781–786. http://dx.doi.org/10.1111/j.1745-6584.2005.00090.x.

Hiscock, K.M., 2009. Hydrogeology: Principles and Practice. John Wiley & Sons.

Jaunat, J., Huneau, F., Dupuy, a., Celle-Jeanton, H., Vergnaud-Ayraud, V., Aquilina, L., Labasque, T., Le Coustumer, P., 2012. Hydrochemical data and groundwater dating to infer differential flowpaths through weathered profiles of a fractured aquifer. Appl. Geochem. 27, 2053–2067. http://dx.doi.org/10.1016/j.apgeochem.2012.06.009.

Kovács, G., 2011. Seepage Hydraulics. Elsevier.

Lachassagne, P., Wyns, R., Dewandel, B., 2011. The fracture permeability of Hard Rock Aquifers is due neither to tectonics, nor to unloading, but to weathering processes. Terra Nov. 23, 145–161. http://dx.doi.org/10.1111/j.1365-3121.2011.00998.x.

Lague, D., Davy, P., Crave, A., 2000. Estimating uplift rate and erodibility from the area-slope relationship: examples from Brittany (France) and numerical modelling. Phys. Chem. Earth, Part A Solid Earth Geod. 25, 543–548. http://dx.doi.org/10.1016/S1464-1895(00)00083-1.

Le Borgne, T., Bour, O., de Dreuzy, J.R., Davy, P., Touchard, F., 2004. Equivalent mean flow models for fractured aquifers: insights from a pumping tests scaling interpretation. Water Resour. Res. 40, W03512. http://dx.doi.org/10.1029/2003WR002436.

Lebedeva, M.I., Fletcher, R.C., Balashov, V.N., Brantley, S.L., 2007. A reactive diffusion model describing transformation of bedrock to saprolite. Chem. Geol. 244, 624–645. http://dx.doi.org/10.1016/j.chemgeo.2007.07.008.

Leray, S., de Dreuzy, J.-R., Bour, O., Labasque, T., Aquilina, L., 2012. Contribution of age data to the characterization of complex aquifers. J. Hydrol. 464–465, 54–68. http://dx.doi.org/10.1016/j.jhydrol.2012.06.052.

Maloszewski, P., Zuber, A., 1996. Lumped parameter models for the interpretation of environmental tracer data.

Marçais, J., de Dreuzy, J.-R., Ginn, T.R., Rousseau-Gueutin, P., Leray, S., 2015. Inferring transit time distributions from atmospheric tracer data: assessment of the predictive capacities of Lumped Parameter Models on a 3D crystalline aquifer model. J. Hydrol. 525, 619–631. http://dx.doi.org/10.1016/j.jhydrol.2015.03.055.

Martin, C., Molenat, J., Gascuel Odoux, C., Vouillamoz, J.-M., Robain, H., Ruiz, L., Faucheux, M., Aquilina, L., 2006. Modelling the effect of physical and chemical characteristics of shallow aquifers on water and nitrate transport in small agricultural catchments. J. Hydrol. 326, 25–42. http://dx.doi.org/10.1016/j.jhydrol.2005.10.040.

McClain, M.E., Boyer, E.W., Dent, C.L., Gergel, S.E., Grimm, N.B., Groffman, P.M., Hart, S.C., Harvey, J.W., Johnston, C.a., Mayorga, E., McDowell, W.H., Pinay, G., 2003. Biogeochemical hot spots and hot moments at the interface of terrestrial and aquatic ecosystems. Ecosystems 6, 301–312. http://dx.doi.org/10.1007/s10021-003-0161-9.

McDonnell, J.J., Sivapalan, M., Vaché, K., Dunn, S., Grant, G., Haggerty, R., Hinz, C., Hooper, R., Kirchner, J., Roderick, M.L., Selker, J., Weiler, M., 2007. Moving beyond heterogeneity and process complexity: a new vision for watershed hydrology. Water Resour. Res. 43, W07301. http://dx.doi.org/10.1029/2006WR005467.

McGuire, K.J., McDonnell, J.J., Weiler, M., Kendall, C., McGlynn, B.L., Welker, J.M., Seibert, J., 2005. The role of topography on catchment-scale water residence time. Water Resour. Res. 41, 1–14. http://dx.doi.org/10.1029/2004WR003657.

Molénat, J., Gascuel-Odoux, C., 2002. Modelling flow and nitrate transport in groundwater for the prediction of water travel times and of consequences of land use evolution on water quality. Hydrol. Process. 16, 479–492. http://dx.doi.org/10.1002/hyp.328.

Molénat, J., Gascuel-Odoux, C., Aquilina, L., Ruiz, L., 2013. Use of gaseous tracers (CFCs and SF6) and transit-time distribution spectrum to validate a shallow groundwater transport model. J. Hydrol. 480, 1–9. http://dx.doi.org/10.1016/j.jhydrol.2012.11.043.

Molson, J.W., Frind, E.O., 2012. On the use of mean groundwater age, life expectancy and capture probability for defining aquifer vulnerability and time-of-travel zones for source water protection. J. Contam. Hydrol. 127, 76–87. http://dx.doi.org/10.1016/j.jconhyd.2011.06.001.

Noilhan, J., Mahfouf, J.F., 1996. The ISBA land surface parameterisation scheme. Glob. Planet. Change 13, 145–159. http://dx.doi.org/10.1016/0921-8181(95)00043-7.

Noilhan, J., Planton, S., 1989. A simple parameterization of land surface processes for meteorological models. Mon. Weather Rev. 117, 536–549. http://dx.doi.org/10.1175/1520-0493(1989)117<0536:ASPOLS>2.0.CO;2.

Pinay, G., Peiffer, S., De Dreuzy, J.-R., Krause, S., Hannah, D.M., Fleckenstein, J.H., Sebilo, M., Bishop, K., Hubert-Moy, L., 2015. Upscaling nitrogen removal capacity from local hotspots to low stream orders' drainage basins. Ecosystems 18, 1101–1120. http://dx.doi.org/10.1007/s10021-015-9878-5.

Rempe, D.M., Dietrich, W.E., 2014. A bottom-up control on fresh-bedrock topography under landscapes. Proc. Natl. Acad. Sci. USA 111, 6576–6581. http://dx.doi.org/10.1073/pnas.1404763111.

Roques, C., Aquilina, L., Bour, O., Maréchal, J.-C., Dewandel, B., Pauwels, H., Labasque, T., Vergnaud-Ayraud, V., Hochreutener, R., 2014. Groundwater sources and geochemical processes in a crystalline fault aquifer. J. Hydrol. 519, 3110–3128. http://dx.doi.org/10.1016/j.jhydrol.2014.10.052.

Schwanghart, W., Kuhn, N.J., 2010. TopoToolbox a set of Matlab functions for topographic analysis. Environ. Model. Softw., 770–781

Schwanghart, W., Scherler, D., 2014. Short Communication: TopoToolbox 2 – MATLAB-based software for topographic analysis and modeling in Earth surface sciences. Earth Surf. Dyn. 2, 1–7. http://dx.doi.org/10.5194/esurf-2-1-2014.

Singhal, B.B.S., Gupta, R.P., 2013. Applied Hydrogeology of Fractured Rocks. Springer Science & Business Media.

Tetzlaff, D., Seibert, J., Soulsby, C., 2009. Inter-catchment comparison to assess the influence of topography and soils on catchment transit times in a geomorphic province; the Cairngorm mountains, Scotland. Hydrol. Process. 23, 1874–1886. http://dx.doi.org/10.1002/hyp.7318.

Thomas, Z., Abbott, B.W., Troccaz, O., Baudry, J., Pinay, G., 2016a. Proximate and ultimate controls on carbon and nutrient dynamics of small agricultural catchments across scales. Biogeosciences 13, 1–13. http://dx.doi.org/10.5194/bg-13-1863-2016.

Thomas, Z., Rousseau-Gueutin, P., Kolbe, T., Abbott, B.W., Marçais, J., Peiffer, S., Frei, S., Bishop, K., Pinay, G., Pichelin, P., de Dreuzy, J.-R., 2016b. Constitution of a catchment virtual observatory for sharing flow and transport model outputs. J. Hydrol. 543 (PA), 59–66.

Tóth, J., 2009. Gravitational Systems of Groundwater Flow. Cambridge University Press. http://dx.doi.org/10.1017/CBO9780511576546.

Tóth, J., 1963. A theoretical analysis of groundwater flow in small drainage basins. J. Geophys. Res. 68, 4795–4812. http://dx.doi.org/10.1029/JZ068i016p04795.

Vogel, L.E., Makowski, D., Garnier, P., Vieublé-Gonod, L., Coquet, Y., Raynaud, X., Nunan, N., Chenu, C., Falconer, R., Pot, V., 2015. Modeling the effect of soil meso- and macropores topology on the biodegradation of a soluble carbon substrate. Adv. Water Resour. 83, 123–136. http://dx.doi.org/10.1016/j.advwatres.2015.05.020.

Weyer, C., Peiffer, S., Schulze, K., Borken, W., Lischeid, G., 2014. Catchments as heterogeneous and multi-species reactors: an integral approach for identifying biogeochemical hot-spots at the catchment scale. J. Hydrol. 519, 1560–1571. http://dx.doi.org/10.1016/j.jhydrol.2014.09.005.

Wright, E.P., Burgess, W.G., 1992. The hydrogeology of crystalline basement aquifers in Africa. Geol. Soc. Spec. Publ., 1–27

Wyns, R., Baltassat, J.M., Lachassagne, P., Legchenko, A., Vairon, J., Mathieu, F., 2004. Application of proton magnetic resonance soundings to groundwater reserve mapping in weathered basement rocks (Brittany, France). Bull. La Soc. Geol. Fr. 175, 21–34. http://dx.doi.org/10.2113/175.1.21.

3.3 Conclusion

The analysis of groundwater flow circulations revealed that groundwater travel distances are short (mean travel distance of 350 m) compared to the times water has spent in the aquifer (mean groundwater age of 40 y).

Even without investigating denitrification processes explicitly, these results have several implications for water quality management.

For groundwater that stays highly local with long transit times, changes in fertilization or land use may take a long time to affect groundwater quality and if zones are locally intensively used the impacts on the groundwater quality may be extreme.

To get further insights in the fate of nitrate at the catchment scale, the groundwater flow study constitute as the basis for further investigations of past nitrate inputs to the aquifer (chapter 4) and denitrification processes (chapter 5). The different means and distributions of transit times derived for each well in combination with tracers (e.g. dissolved N_2 and NO_3^-) that reveal the amount of nitrate that has been degraded along the flow paths allow to reconstruct nitrate inputs to the aquifer representative for the catchment area.

Chapter 4: Reconstruction of nitrate inputs to the aquifer

4.1 Introduction

Around 70 years ago, nitrogen inputs into agricultural catchments increased tremendous due to an increase of livestock and food production. The discovery of the Haber-Bosch process in the first half of the 20th century allowed to produce ammonia easily by converting nonreactive N_2 to reactive NH_3 (Galloway et al., 2003) which led fertilizer applications to increase sharply. The discovery of this process is of huge importance for sustaining food production, but also entails serious consequences, because exceeding nitrogen applications on fields that cannot be taken up by plants leach as nitrate to the aquifer and pollute groundwater (Strebel et al., 1989). Nitrate is then transported with the groundwater and can stay there for several decades depending on flow structures and degradation processes. As nitrate inputs to an aquifer cannot be directly monitored, solutions have to be found to quantify inputs from the past to today, to determine the nitrate removal capacity and the nitrate legacy within the aquifer.

Mineral and organic fertilizer applications for several departments in western France are reported for a period from 1940 to 2010 (*Fig. 7* and *Fig. 8*). A strong increase of mineral fertilizer is recorded until 1990. After this time, fertilizer applications decrease again (*Fig. 7*).

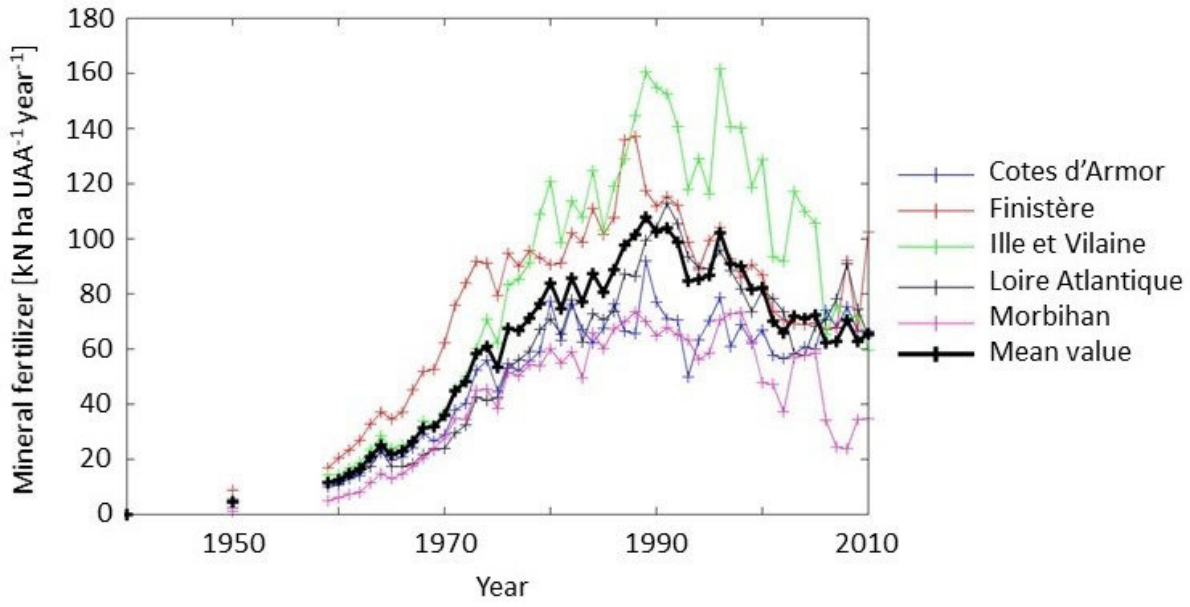

Fig. 7: Mineral fertilizer applications in Brittany from 1940 to 2010 (data from Poisvert et al., 2016)

Organic fertilizer applications follow a similar trend as seen for mineral fertilizer, but in a more moderate way (*Fig. 8*).

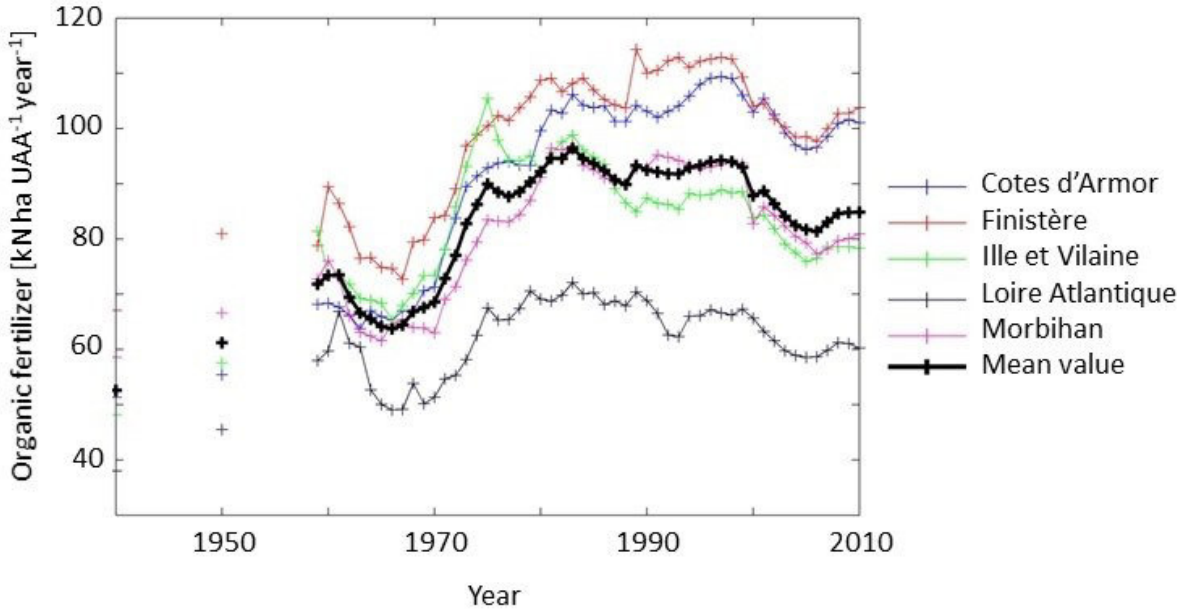

Fig. 8: Organic fertilizer applications in Brittany from 1940 to 2010 (data from Poisvert et al. 2016).

The amount of nitrate leaching to the aquifer cannot be directly deduced from fertilization, because it is not known how much nitrogen was uptaken by plants in the past. Also nitrification as well as denitrification processes occurring in the soil make a direct calculation difficult. In the literature mainly two approaches are presented to estimate nitrate inputs to the aquifer. One modeling approach is to follow nitrogen through the soil and to consider transformation processes to finally determine nitrate concentrations entering the aquifer (Almasri and Kaluarachchi, 2007; Refsgaard et al., 1999). Another way is a back calculation from monitored wells. Knowing the amount of nitrate in the well and the amount that has been degraded in combination with the time water spent in the aquifer, nitrate inputs can be reconstructed.

Several studies exist in which nitrate inputs to the aquifer are reconstructed by using NO_3^- and N_2 excess tracers combined with groundwater age dating (Aquilina et al., 2012; Böhlke, 2002; Green et al., 2010; McMahon et al., 2008; Tesoriero et al., 2007). Attention has to be given to the fact that the groundwater age represents a mixture of waters with different transit times arriving at a well. Either a single flow line has to be sampled to estimate the nitrate concentration for the corresponding recharge date or a full distribution of transit times has to be derived from the groundwater age by using for example a lumped parameter model (Jurgens et al., 2012) or a full groundwater flow and transport model (chapter 3).

Estimations of nitrate inputs into the groundwater in France has already been performed at the scale of the region of Brittany (34 023 km^2). A reason for the large-scale investigation is that a variety of different groundwater ages has to be available to relate nitrate concentrations to different dates in the past. Land use and practices can

be quite variable between catchments, also reflected in fertilizer applications. Nitrate inputs to the aquifer, therefore, can vary highly between the departments.

For the investigation of the nitrate removal capacity of the Pleine-Fougères aquifer, specific estimations for nitrate inputs to the aquifer were made. Transit time distributions derived from 16 wells (chapter 3) show a variety of distributions giving sufficient information to determine past nitrate inputs over time. Therefore, several questions can be answered by applying the following methodology.

- Has the peak of nitrate inputs already reached the aquifer?
- Does nitrate concentration further increase or decrease over time due to changes in agricultural practice?
- And how fast does concentration increase or decrease?

4.2 Methodology

4.2.1 Sampling & Analysis

Noble gases (argon, neon, and N_2), nitrate and CFC-12 concentrations were measured in 16 wells of the agriculturally used Pleine-Fougères catchment at three different sampling dates (chapter 3 and 5, Appendix B).

Argon, neon and N_2 were measured to determine the N_2 excess. N_2 is the final product of denitrification and contains inherent information on how much nitrate has been degraded. The N_2 excess is determined by comparing N_2 measurements with argon and neon that do not change during denitrification. The measured nitrate concentration in a well plus the amount that has been degraded is then equal the total nitrate concentration. The method used is presented in Aeschbach-Hertig et al., (1999) and Aeschbach-Hertig et al., (2001).

4.2.2 Transit Time Distributions

Transit time distributions are derived from the developed groundwater flow and transport model (chapter 3). While in the former work transmissivity and porosity were well constrained by the overall flux and CFC-12 concentrations, here transit time distributions are adapted to local sampling conditions, meaning the depth of water arrivals (Jurgens et al., 2016).

4.2.3 Determination of NO_3^- inputs to the aquifer

Land use information of the whole study area from 1993 to 2013 show no significant evolution of land use types. Furthermore, a uniformity of practices has been observed that lead to the assumption of spatially uniform nitrate inputs at the catchment scale. Land use parcels are small and alternating, meaning that well information cannot be associated to a specific land use type or a combination of land use types occurring in the capture zone (Appendix A and B).

A variation of nitrate input chronicles are predefined to find the best fit of modeled to observed data (CFC-12 and NO_3^-,total). CFC-12 and NO_3^-,total simulations are based on conservative transport conditions. Concentration calculations and the calibration of water arrivals as well as the nitrate input chronicle are performed at the same time and based on the general methodology presented in chapter 3.

In total 2736 input chronicles were generated with the following equations (*Eq. 13-16*, *Fig. 9*).

$$f_0(\mathrm{t}) = C_0 \tag{13}$$

$$f_1(\mathrm{t}) = C_{max}\frac{(t - t_{start})^2}{(t_{change} - t_{start})(t_{Cmax} - t_{start})} \tag{14}$$

$$f_2(\mathrm{t}) = C_{max}\left(1 - \frac{(t - t_{Cmax})^2}{(t_{Cmax} - t_{change})(t_{Cmax} - t_{start})}\right) \quad (15)$$

$$f_3(\mathrm{t}) = C_{max} - (C_{max} - C_{2015})\frac{(t - t_{Cmax})^2}{(date - t_{Cmax})} \quad (16)$$

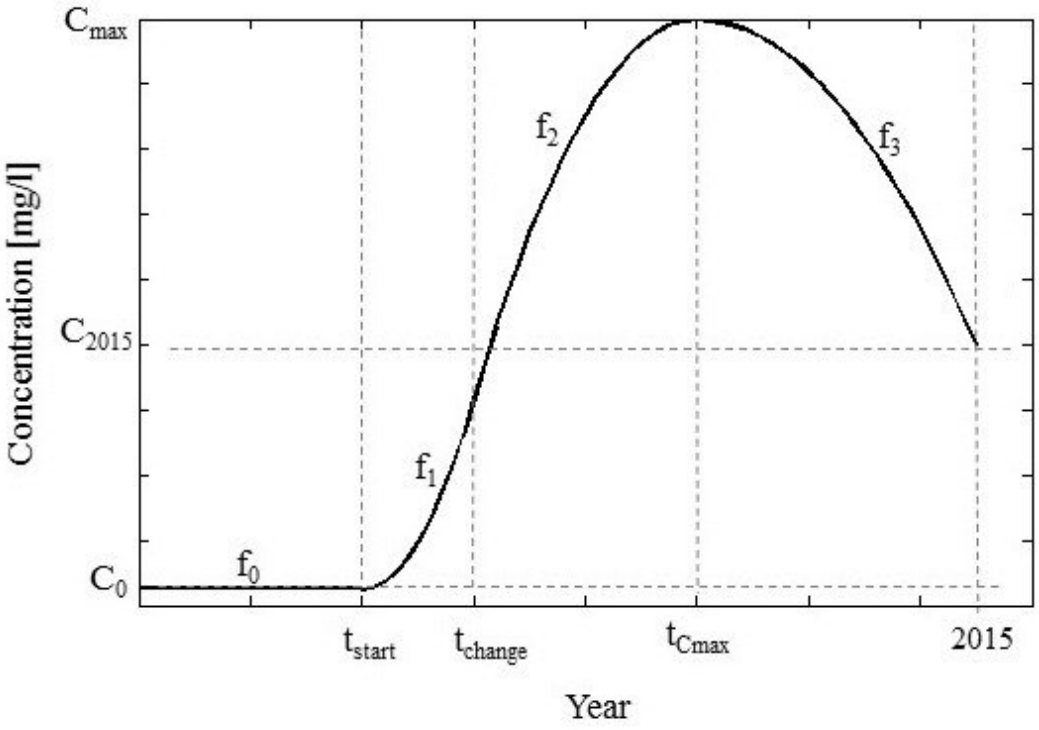

Fig. 9: Shape of nitrate input chronicle described by f_0, f_1, f_2 and f_3.

The initial nitrate concentration C_0 was set in the range of 0 to 12.5 mg/l with an interval of 2.5 mg/l. Input concentrations were assumed to start increasing at t_{start} equal to 1950, 1960 or 1970. The change of concentration increase was set at t_{change} equal to 1955, 1975, or 1995. The max concentrations C_{max} were applied between 60 mg/l and 100 mg/l (10 mg/l interval) at t_{Cmax} equal to 1975, 1990, or 2005. The concentration in 2015 C_{2015} was applied between 50 mg/l and 90 mg/l (10 mg/l interval).

4.3 Results

The best fit of measured and observed concentration is obtained for the following nitrate input chronicle (*Fig. 10*). Before fertilizer applications started to increase, nitrate inputs to the aquifer were about 12.5 mg/l. In 1960 the concentration started to increase with a change in increase in 1970. The maximum concentration of 100 mg/l was reached in 1990. After 1990, nitrate input concentration decreased again to a value of 50 mg/l in 2015.

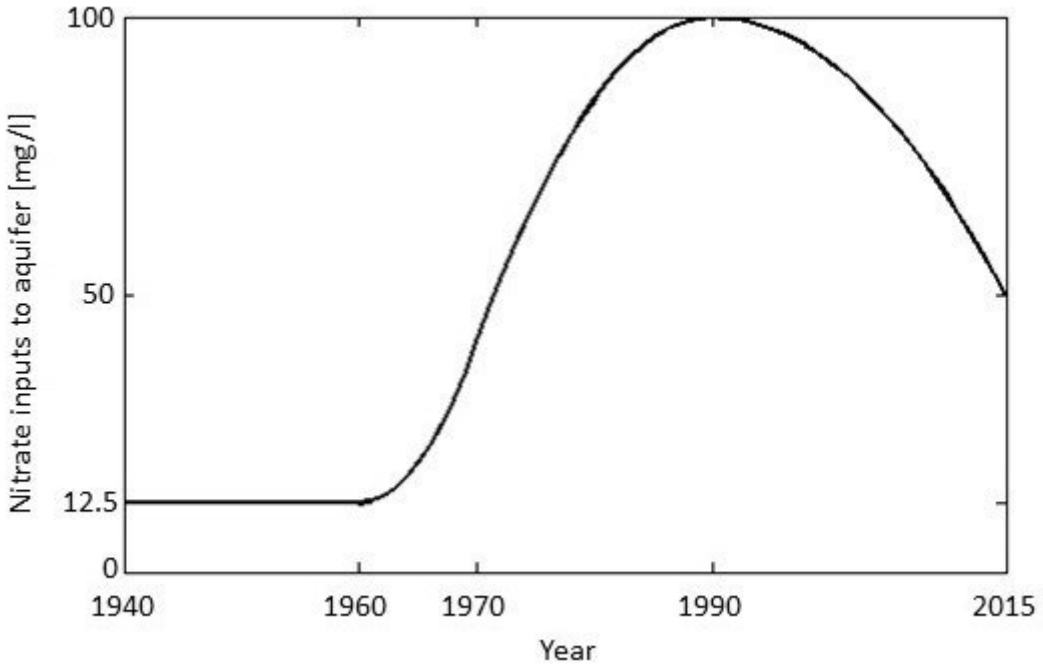

Fig. 10: Nitrate input chronicle with best fit.

The range of global misfits of all simulations is in between 1.95 and 6.08 (Fig. 11). A small range compared to the minimum and maximum value that could be reached during the optimization (min global misfit = 0, max global misfit = 32). *Fig. 12* shows the parameter that describe the nitrate input chronicle in relation to the global misfit of the best models (the best 10 % are presented).

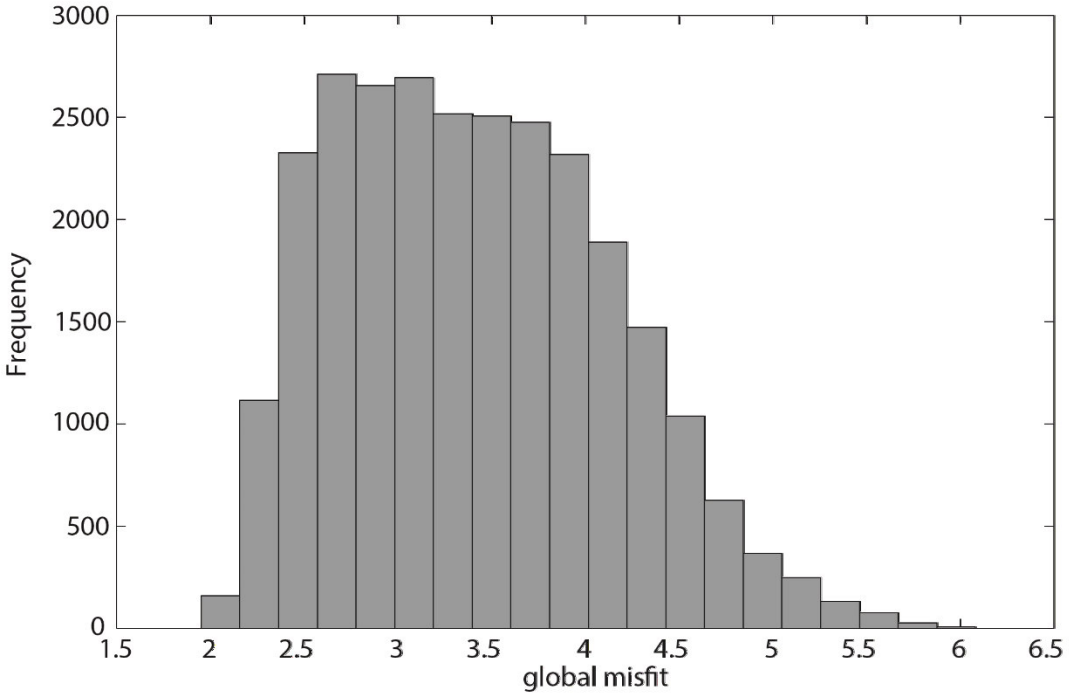

Fig. 11: Frequency of global misfit. Conservative transport simulations of CFC-12 and NO_3^- to reconstruct NO_3^- inputs to the aquifer.

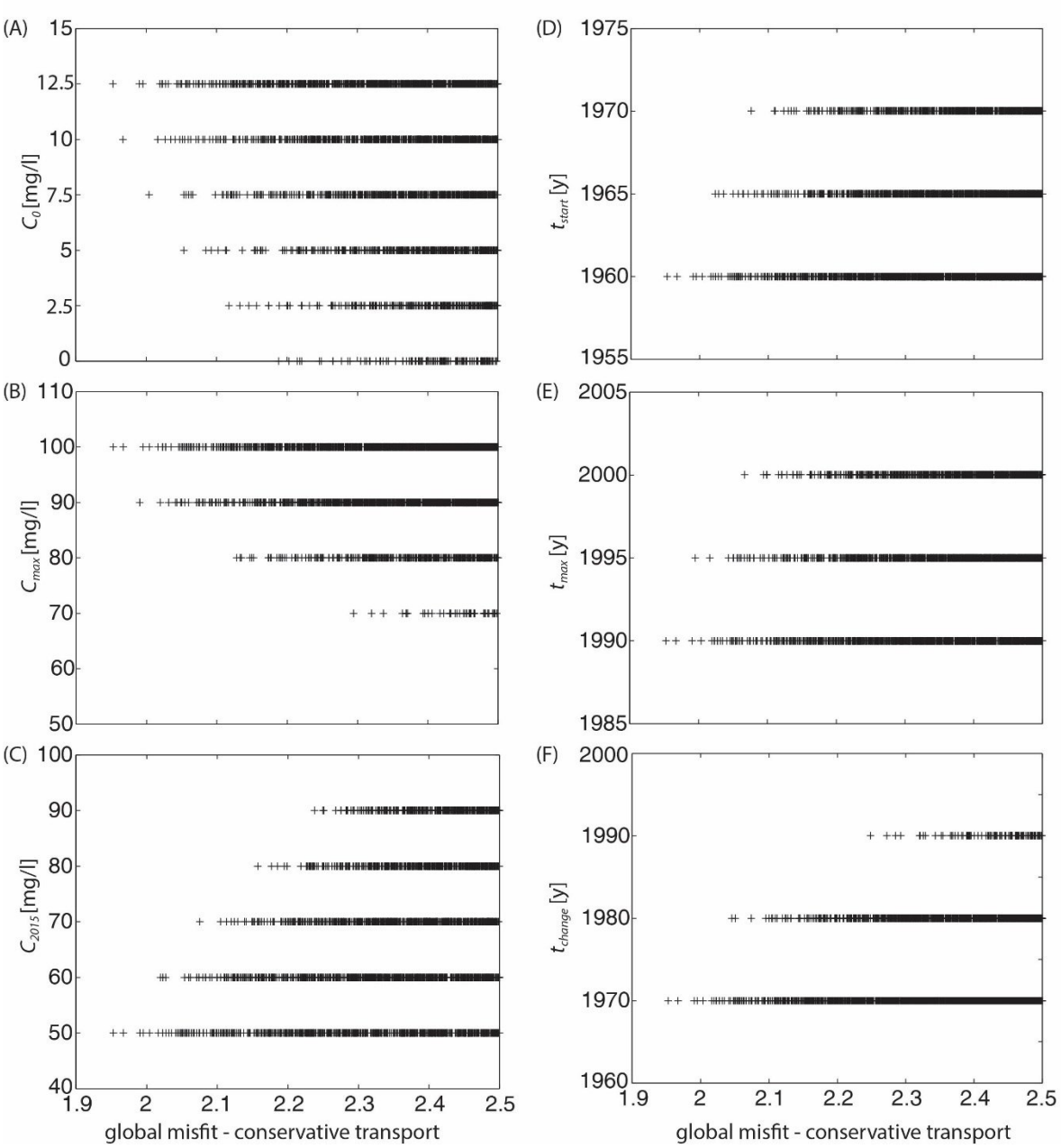

Fig. 12: Parameter that describe NO_3^- inputs to the aquifer in relation to the global misfit.

4.4 Discussion & Conclusion

An interesting phenomenon of the calibrated nitrate input chronicle is its similarity to the CFC-12 curve (*Fig. 13*). Both curves show a strong increase starting around 1965 that is related to the tremendous growths of both, technology and population in the 20th century. The peak of nitrate inputs is reached almost 10 years earlier than the peak of

the CFC-12 curve and nitrate inputs increase stronger than CFC concentrations afterwards. CFC-12 concentrations start to decrease slightly from the year 2000, which makes groundwater dating especially for measured concentrations between 520 - 545 pptv ($C_{normalized}$ = 0.95..1) difficult, because there is no unique groundwater age corresponding to these concentrations. Complementary information, like silica concentration, would be necessary to resolve groundwater ages younger than 17 y.

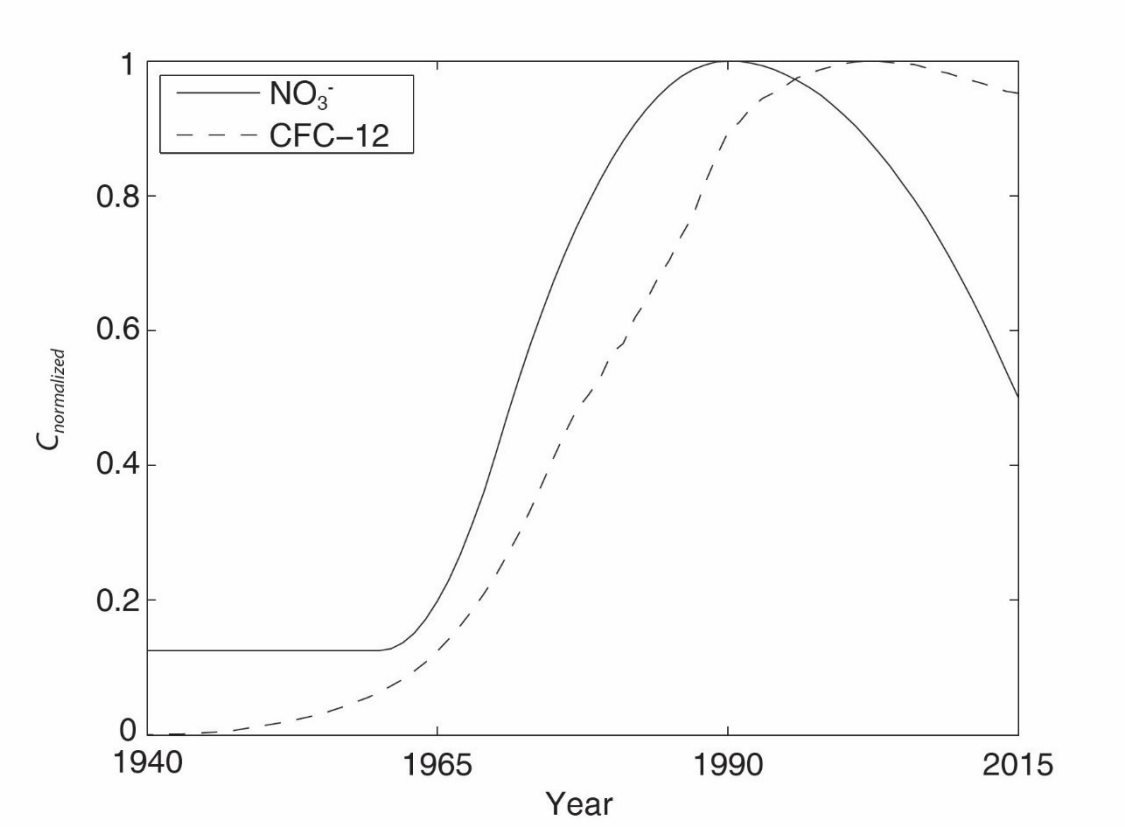

Fig. 13: Comparison of calibrated nitrate inputs to the aquifer with CFC-12 input chronicle

The curve of the calibrated nitrate inputs has a similar shape as the inputs estimated at the scale of Brittany with constant higher concentrations of about 10 to 20 mg/l (*Fig. 14*). Nitrate inputs at the Brittany-scale were estimated from 1950 to 2009 using the groundwater dating studies presented in Ayraud et al. (2008). In Aquilina et al. (2012), nitrate concentrations are assumed to evolve due to dilution of nitrate inputs in

an unpolluted aquifer. It is found for the Pleine-Fougères aquifer that this assumption is not valid. The assumption of the background concentration (C_0) has a big impact on the estimated chronicle and represent here the main difference of the two chronicles (regardless the methodology).

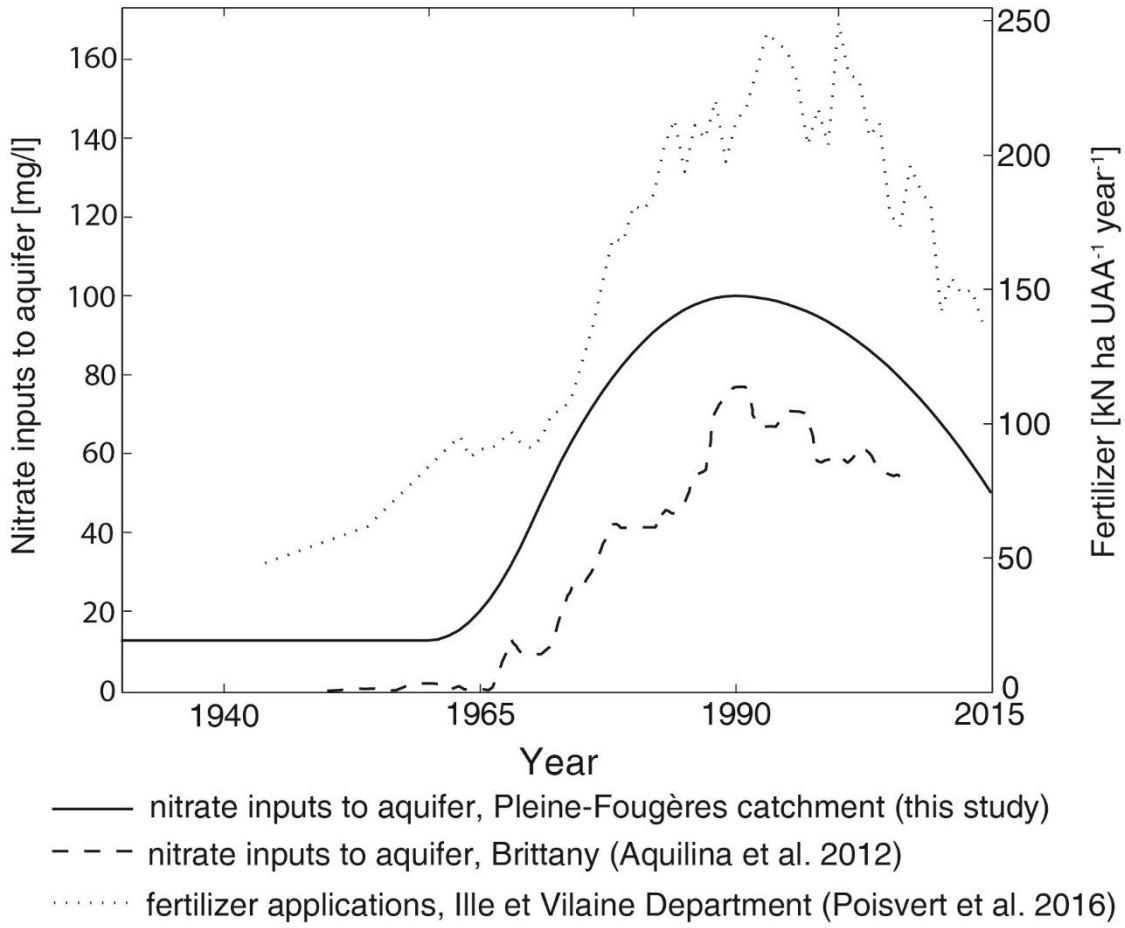

Fig. 14: Comparison of calibrated nitrate inputs with inputs at the scale of Brittany and fertilizer application in the Ille et Vilaine department.

A comparison of the calibrated nitrate input chronicle with fertilizer applications in the Ille et Vilaine department shows that nitrate inputs to the aquifer follow the trend of fertilizer applications in the Ille et Vilaine department, with some derivations. Nitrate inputs to the aquifer increase faster from 1965 than fertilization. The peak of the maximum nitrate input concentration is reached in 1990, around 5 y to 10 y earlier than

the maximum fertilizer input. Comparing the Ille et Vilaine fertilizer inputs with the other two departments show some variations in concentrations and time of the maximum inputs. The calibrated nitrate input chronicle is consistent with these fertilizer histories recorded in Brittany. The amount of fertilizer application at the Pleine-Fougères site might have been different than the mean of the Ille et Vilaine department. However, the calibrated nitrate inputs represent a well-defined nitrate input chronicle for the Pleine-Fougères site to further study nitrate transport and degradation processes (chapter 5).

Chapter 5: Structure of groundwater denitrification

5.1 Introduction

In this chapter, the fate of nitrate is investigated by using the methodology presented in chapter 2, the groundwater flow information derived in chapter 3 and nitrate inputs determined in chapter 4.

To investigate denitrification processes at the site, tracer data, like O_2, NO_3^-, and N_2 excess, is used to inform the model. In particular, the investigation of sources for the observed diverse denitrification rates at the study site, like elsewhere in the world, are central of this study. Generally, observed reaction times for oxygen reduction and denitrification are obtained from drilled wells. However, effective reactivity is highly variable, because reactivity does not seem to occur continuously over the full flow paths length, rather the location of the reactive zone that is characterized by anoxic conditions, electron donor availability and microbes, is the source of reaction rate diversity.

The interest is, therefore, to use the existing modeling framework to further investigate effective reactivity by incorporating different concepts that count for different locations of the reactive zone.

5.2 Article: “Structure of groundwater denitrification” (in preparation)

Structure of aquifer denitrification

Publication in preparation

Keywords: reaction times, autotrophic denitrification, residence time, constraining groundwater resilience to nitrate pollution with a parsimonious data-driven approach

---

Most of Earth's aquifers have been contaminated with anthropogenic nitrate (NO_3^-) from excess fertilizer, urbanization, and human and livestock waste. Denitrification, the main process in groundwater reducing nitrate potentially to N_2, depends strongly on anoxic conditions, and available electron donors as well as microbes that are capable for denitrification. Favorable conditions for denitrification are difficult to locate from pointwise measurements in monitored wells and therefore often assumed to occur homogeneous distributed in the aquifer to determine apparent nitrate reduction times. Extensive field studies show that these apparent reaction times over– or underestimate actual reactivity, because of a non-uniform distribution of denitrification activity. Here, we present an interpretation framework to extract complex denitrification structures from apparent reaction times. We demonstrate how apparent reaction times that are simple to obtain from well investigations provide new knowledge on the location of denitrification activity in the aquifer and how these structures reveal actual rates that strongly impact groundwater resilience.

Ecological and socioeconomic problems from NO_3^- pollution cost billions of dollars annually, but even if all anthropogenic NO_3^- inputs were stopped today, elevated NO_3^- in many groundwater aquifers would persist for decades. Quantifying the resilience of groundwater ecosystems to nutrient loading is essential to identify sustainable limits and predict recovery timeframes of freshwater ecosystems. The rate of recovery of groundwater quality following NO_3^- contamination depends on water residence time and the rate of denitrification, the microbial reduction of NO_3^- to dinitrogen gas (N_2). While there is an increasing diversity of tools to estimate water residence time with a variety of data inputs, predicting denitrification in aquifers remains elusive due to a lack of knowledge about the physical location of this process (vertical and lateral positions in the aquifer) and temporal variability of reaction rates.

Denitrification depends on the co-occurrence of substrate (NO_3^- as the electron acceptor and organic carbon or pyrite as electron donors), denitrifying bacteria or archaea, and hypoxic conditions (i.e. O_2 < 2 mg L^-). Since directly measuring these parameters is impractical in most aquifers, predicting denitrification rates depend on constraining assumptions about the vertical distribution of substrate, O_2, and microbial community. Current reactive transport models assume uniform or randomly distributed electron donors in aquifers and consequent denitrification rates. While this approach has proved adequate in some sedimentary aquifers, it could vastly over- or underestimate

actual denitrification rates in aquifers with non-random distributions of electron donors and reaction rates due to differences between apparent and actual denitrification rates. Microbial communities and electron donors are known to vary systematically with depth (Ben Maamar et al., 2015), with organic carbon sources and microbial abundance decreasing with depth, and reduced iron and pyrite increasing with depth.

Here, we use a conceptual framework of denitrification structures to develop a generally applicable method for estimating actual denitrification rates in groundwater. We coupled recent advances in hydrogeological and reactive transport modeling with widely available well data (i.e. NO_3^-, O_2, CFCs and N_2 excess) to determine the structure of the denitrifying bioreactor within aquifers. The comparison of conservative and reactive information containing complementary behaviors allows to reconstruct the dominant phases of transport and reactivity. It opens the capacity to interpret apparent reaction times in terms of actual denitrification activity and to locate reactivity. With the aid of transport modeling, mixing in the well and in the aquifer turns from a methodological inconvenience to an advantage for more representative process sampling. Contrary to predictions from homogeneous and hotspot models, we found that apparent rates of O_2 and NO_3^- reduction in fractured aquifers are often completely unrelated, indicating substantial vertical gradients in electron donor availability and actual denitrification rates. Based on these results and a meta-analysis of previously published NO_3^- and O_2 reduction rates, we present an integrated and quantitative method for assessing aquifer resilience to NO_3^-.

Vertical gradients in denitrification substrate

There are two types of denitrification, each with different expected vertical distributions in aquifers. During heterotrophic denitrification, organic carbon acts as electron donor and carbon source for denitrifiers reducing NO_3^-. For autotrophic denitrification, iron, pyrite, or various sulfur compounds provide electrons, and inorganic carbon (e.g. CO_2, HCO_3^-) is fixed during NO_3^- reduction. Assuming that microbial activity follows substrate availability, which is reasonable at multi-annual timescales, the vertical distribution of autotrophic and heterotrophic denitrification depends on the abundance of electron donors, determined by geologic substrate, bedrock age (degree of previous weathering), and surface inputs of NO_3^- as well as organic carbon. Because soil and near-surface groundwater systems have residence times on the order of years to decades, historical conditions are often more influential than current state (e.g. current NO_3^- or organic carbon input). Oxygen reduction, like denitrification, depends strongly on the distribution of electron donors, and similar actual reduction times could show up in different relations of apparent reaction times. There are four possible distributions of denitrification rates based on different geologic and land-use scenarios leading to different correlations of apparent oxygen and nitrate reduction times (*Fig. 1*).

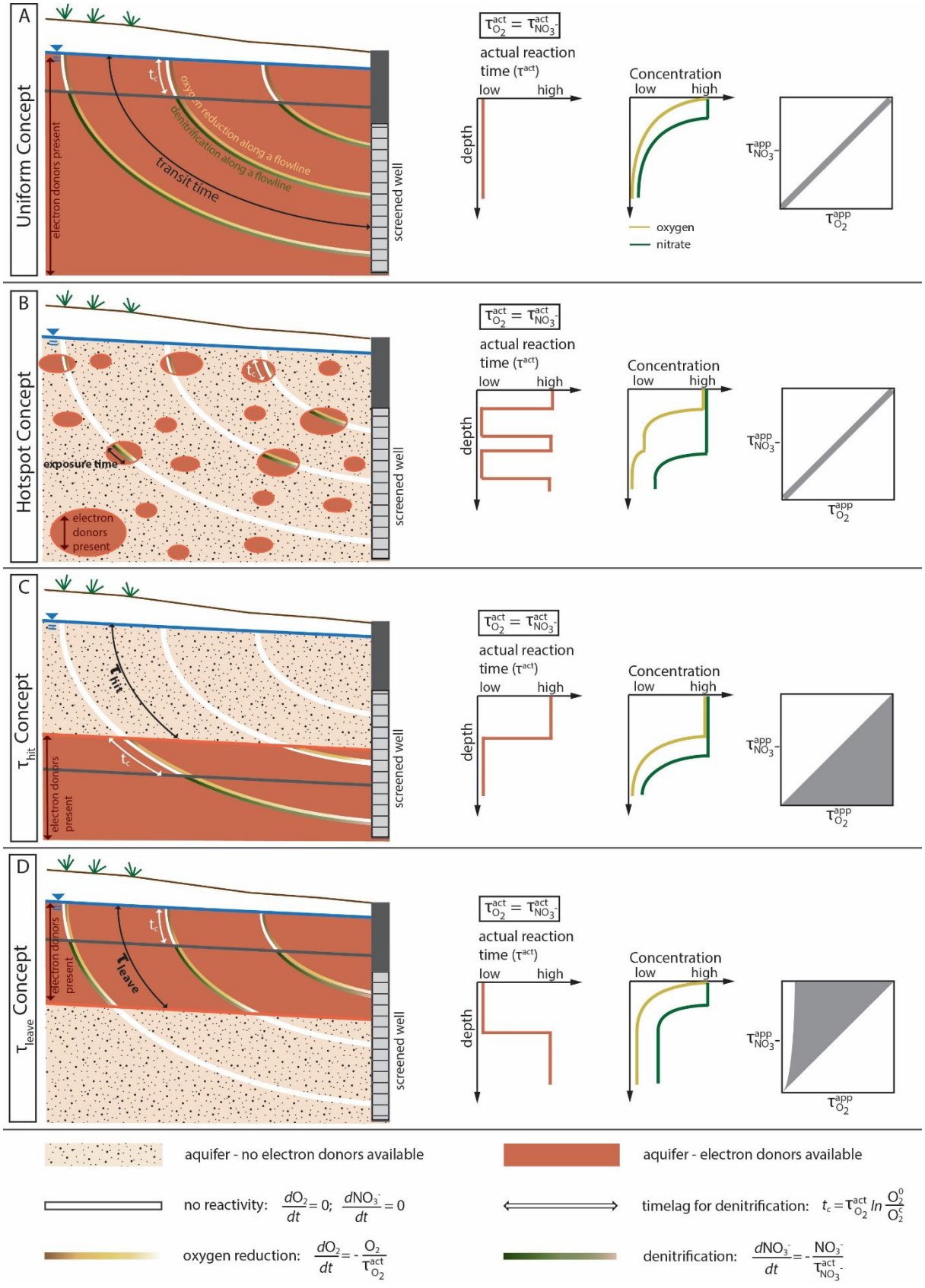

Fig. 1: Potential vertical denitrification distributions.

First, when electron donors are evenly distributed throughout the aquifer, such as in bedrock with abundant iron and pyrite, uniform denitrification rates could be temporarily sustained (*Fig. 1A*), until the top-down depletion of electron donors induced by weathering (or recharge) repetition creates a gradient. Second, if electron donors are distributed randomly or semi-randomly due to bedrock lithology or land-use history,

denitrification can occur in discrete zones or hotspots (*Fig. 1B*). Third, in the absence of organic carbon inputs, autotrophic denitrification could be limited to deeper layers where reduced elements, e.g. pyrite, have not been depleted from weathering (*Fig. 1C*). Fourth, abundant organic carbon in near-surface groundwater could create an active zone of heterotrophic denitrification in the top of the aquifer, underlain by an inactive zone where NO_3^- is transported conservatively (*Fig. 1D*). These four hypothetical structures create different patterns in apparent and actual O_2 and NO_3^- reduction times allowing determination of the vertical location of denitrification activity based on point measurements of chemistry and flow path modeling. To test this conceptual framework, we compared observed O_2 and NO_3^- reaction times in various aquifer types, i.e. an unconfined crystalline aquifer located in an intensive used agricultural area in the northeast of France (Kolbe et al., 2016), and furthermore, data published by Green et al. (2016) and Tesoriero and Puckett (2011) located in fine- and coarse-grained sediments, medium to fine sand, alluvial sand, silt and clay and glacial outwash (*Fig. 2*).

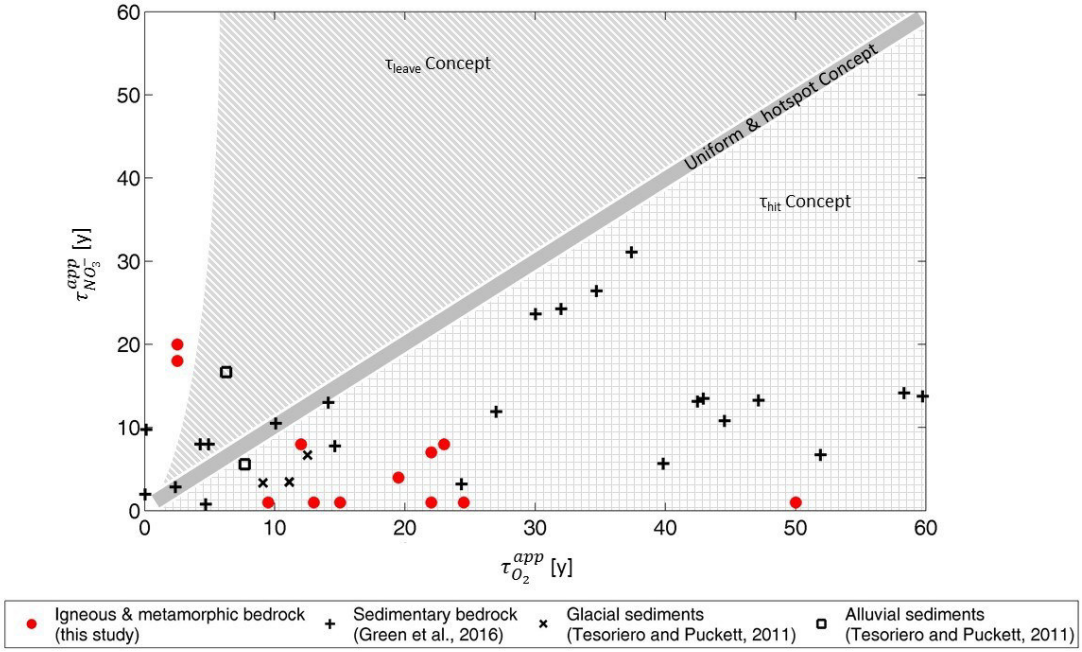

Fig. 2: Apparent oxygen versus apparent nitrate reduction times in different aquifer types. The correlation of apparent reaction times give information on the vertical distribution of oxygen and nitrate reduction.

Aquifers showed evidence of all four vertical distributions of denitrification rates, relatively independent of the aquifer type, suggesting heterogeneity of vertical substrate distributions. Only 5 % of the study sites followed the uniform prediction, demonstrating the need for a more powerful approach of estimating actual denitrification activity.

Assuming a uniform concept with similar actual reaction times for oxygen and nitrate reduction (x=y line, *Fig. 1A* and *Fig. 2*) would lead to similar apparent degradation times. In the case of localized electron donors (hotspot concept), apparent oxygen and nitrate reduction times would shift equally (x=y line, *Fig. 1B* and *Fig. 2*). They could be dealt with using well-established concepts of exposure times that extract the duration of contact between the flow path and the hotspot as effective reaction times. However, only a very few data points correspond to this situation that might be more relevant for soils

(unsaturated biologically active zone) than for aquifers (low C environment). In most cases degradation is apparently more efficient for nitrate than for oxygen, an observation that supports a geological control on reaction processes. Linked availability of accessible lithological electron donors in carbon sources or minerals strongly delays reactivity until transported oxygen and nitrate hit some reductive zones (τ_{hit} concept, *Fig. 1C* and *Fig. 2*). Delaying the start of actual oxygen reduction strongly increases its apparent reduction time but only marginally affects the assessment of nitrate reduction that starts when oxygen has been depleted enough. Field studies show that nitrate gets reduced quickly if hitting such a reactive zone in a deeper zone of the aquifer (Böhlke et al., 2002; McMahon et al., 2008), and that sulfide minerals are present in deeper fractured zones of crystalline aquifers (Pauwels et al., 2010) where a reactive zone is observed (Ayraud et al., 2006, 2008). Within the τ_{hit} concept reactions do not start immediately below the groundwater table, instead a time to hit this layer has to pass. The effective reaction time is then associated just with the time spent in the reactive zone. Lithological electron donors, e.g. pyrite, have been observed in several field studies for autotrophic denitrification and it has been shown that autotrophic denitrification is the dominant nitrate reduction process, even in the presence of organic carbon. Green et al. (2016) and Tesoriero and Puckett (2011), also hypothesize that lithological electron donors are the main energy sources for denitrification at their sites.

On the contrary, if surface derived organic carbon exists, reactivity just occurs in the upper part of the aquifer (τ_{leave} concept, *Fig. 1D* and *Fig. 2*). The groundwater table is then usually close to the surface, the reason why organic carbon can be transported to the aquifer as an energy source for heterotrophic denitrification. First oxygen and then nitrate is reduced in the reactive zone where electron donors are available. If oxygen and nitrate rich water leaves this zone (τ_{leave} concept) to an unreactive part of the aquifer, oxygen and nitrate are transported conservatively. Actual and apparent oxygen reduction times would be similar, whereas apparent denitrification times would be larger than actual nitrate reduction times. For short oxygen and large nitrate reduction times (blank area in *Fig. 1*) actual reaction times and the time to leave the reactive layer are determined with large uncertainties. Just a very few points fall in this concept, indicating that it plays a minor role for interpreting denitrification processes at those sites.

Importance of denitrification structures for groundwater management

The comparison of apparent reaction times for oxygen and nitrate reduction shows a wide variety of patterns disclosing multiple reactivity structures in aquifers. These structures affect aquifer functions and services as well as management strategies regarding water quality in different ways. Within the τ_{hit} concept, where denitrification is associated with autotrophic denitrification most likely in a deeper part of the aquifer, land use changes and changes in nitrate input concentrations are observed for short groundwater transit times. Short term nitrate fluxes are strongly impacted by changes in agricultural practices. Regarding longer groundwater travel times, nitrate gets transported most likely to the active denitrification zone where it gets degraded, affecting nitrate legacy positively. Within the τ_{leave} concept, where denitrification is observed close to the groundwater table and associated with heterotrophic denitrification, changes in nitrate input concentrations might not be observed for short groundwater transit

times, because nitrate is most likely reduced if conditions for denitrification are fulfilled. In the case of semi optimal conditions where nitrate inputs are not completely degraded, nitrate that leaves the reactive zone is further transported conservatively. This would impact nitrate legacy negatively and nitrate persists for several decades in the aquifer.

Knowing these denitrification structures in the aquifer from apparent reaction times, management as well as monitoring strategies, e.g. sampling depths in monitoring wells, should be adapted. Apparent reactions times can be widely compared and are cost- and computational effective to obtain.

Methods

Methods and any associated references are found attached to this document (page 9 - 10).

Additional Information

Field data is shown in Appendix A (page 10 - 11). Apparent and actual concentration distributions regarding the τ_{hit} and τ_{leave} concept are presented in Appendix B (page 12 - 16). Correlations of apparent reaction times within the τ_{hit} and τ_{leave} concept are further examined in Appendix C (page 17 - 21).

References

Ayraud, V., Aquilina, L., Labasque, T., Pauwels, H., Molenat, J., Pierson-Wickmann, A.C., Durand, V., Bour, O., Tarits, C., Le Corre, P., Fourre, E., Merot, P., Davy, P., 2008. Compartmentalization of physical and chemical properties in hard-rock aquifers deduced from chemical and groundwater age analyses. Appl. Geochemistry 23, 2686–2707. doi:10.1016/j.apgeochem.2008.06.001

Ayraud, V., Aquilina, L., Pauwels, H., Labasque, T., Pierson-Wickmann, A.C., Aquilina, A.M., Gallat, G., 2006. Physical, biogeochemical and isotopic processes related to heterogeneity of a shallow crystalline rock aquifer. Biogeochemistry 81, 331–347. doi:10.1007/s10533-006-9044-4

Ben Maamar, S., Aquilina, L., Quaiser, A., Pauwels, H., Michon-Coudouel, S., Vergnaud-Ayraud, V., Labasque, T., Roques, C., Abbott, B.W., Dufresne, A., 2015. Groundwater Isolation Governs Chemistry and Microbial Community Structure along Hydrologic Flowpaths. Front. Microbiol. 6, 1457. doi:10.3389/fmicb.2015.01457

Böhlke, J.K., Wanty, R., Tuttle, M., Delin, G., Landon, M., 2002. Denitrification in the recharge area and discharge area of a transient agricultural nitrate plume in a glacial outwash sand aquifer, Minnesota. Water Resour. Res. 38, 10–1–10–26. doi:10.1029/2001WR000663

Green, C.T., Jurgens, B.C., Zhang, Y., Jeffrey Starn, J., Singleton, M.J., Esser, B.K., 2016. Regional oxygen reduction and denitrification rates in groundwater from multi-model residence time distributions, San Joaquin Valley, USA. J. Hydrol. doi:10.1016/j.jhydrol.2016.05.018

Hosono, T., Tokunaga, T., Tsushima, A., Shimada, J., 2014. Combined use of δ13C, δ15N, and δ34S tracers to study anaerobic bacterial processes in groundwater flow systems. Water Res. 54, 284–296. doi:10.1016/j.watres.2014.02.005

Kolbe, T., Marçais, J., Thomas, Z., Abbott, B.W., de Dreuzy, J.-R., Rousseau-Gueutin, P., Aquilina, L., Labasque, T., Pinay, G., 2016. Coupling 3D groundwater modeling with CFC-based age dating to classify local groundwater circulation in an unconfined crystalline aquifer. J. Hydrol. 543.

doi:10.1016/j.jhydrol.2016.05.020

McMahon, P.B., Böhlke, J.K., Kauffman, L.J., Kipp, K.L., Landon, M.K., Crandall, C.A., Burow, K.R., Brown, C.J., 2008. Source and transport controls on the movement of nitrate to public supply wells in selected principal aquifers of the United States. Water Resour. Res. 44, 1–17. doi:10.1029/2007WR006252

Pauwels, H., Ayraud-Vergnaud, V., Aquilina, L., Molénat, J., 2010. The fate of nitrogen and sulfur in hard-rock aquifers as shown by sulfate-isotope tracing. Appl. Geochemistry 25, 105–115. doi:10.1016/j.apgeochem.2009.11.001

Tesoriero, A.J., Puckett, L.J., 2011. O 2 reduction and denitrification rates in shallow aquifers. Water Resour. Res. 47, 1–17. doi:10.1029/2011WR010471

Methodology

We use tracer information and modeling to derive apparent reaction times at each well location. Mixing of different waters arriving at the well provide the capacity to determine oxygen as well as nitrate reduction times. Based on apparent reaction times, actual reaction times and the time needed to hit (τ_{hit} concept) or to leave (τ_{leave} concept) the active denitrification zone can be determined.

Data. *Field data.* CFC-12, O_2, NO_3^-, and N_2 gas plus additional noble gases to determine N_2 excess, were measured in 16 wells at three sampling dates (Dec 2014, Mar 2015, and Oct 2015, Appendix A). N_2 excess reveals the amount of nitrate that has been degraded in the groundwater using the methodology presented in Aeschbach-Hertig et al. (1999) and Aeschbach-Hertig et al. (2001). The amount of degraded nitrate is necessary to determine reactivity and to calculate the total nitrate concentration (nitrate concentration measured in a well plus the amount of nitrate degraded) for reconstructing nitrate inputs to the aquifer.

Transit time distributions. Transit time distributions at each well location can be derived by groundwater flow and transport modeling or lumped parameter models. In this study, CFC dating proxies interpreted within a formerly developed groundwater flow and transport model were used to generate transit time distributions (Kolbe et al., 2016). While site transmissivity and porosity were well constrained by the overall flux and CFC-12 concentrations, local sampling conditions in agricultural wells were adapted thanks to the detailed conservative tracer information. This becomes current practice for wells, which are not drilled initially for scientific monitoring (Jurgens et al., 2016).

Modeling approach. A time-based modeling approach is used to reconstruct nitrate inputs to the aquifer and to calibrate apparent as well as actual reaction times and the time to hit or leave the denitrification zone, respectively.

The simulation of apparent and actual concentrations at a well $C(t)$ is based on the convolution integral presented by Maloszewski and Zuber (1982) (*Eq. 1*).

$$C(\mathrm{t}) = \int_0^\infty p(\tau)\, C^0(t-\tau)\, r(\tau)\; d\tau \qquad (1)$$

With $p(t)$ the transit time distribution, $C^0(t)$ the input concentrations, and $r(t)$ the reaction term. A comparison of apparent and actual concentration distributions is given in Appendix B.

Calibration of nitrate inputs to the aquifer. Land use information from 1991-2013 shows a wide uniformity of agricultural practices over the catchment area with no significant evolution of land use types, supporting the assumption of uniformly distributed nitrate inputs to the aquifer. Overall nitrate input concentrations have however strongly evolved with a production increase around the 1945-1980 period and a maximum reached around 2000 before inputs were reduced slowly (Aquilina et al., 2012). Because of some local adaptions of practices, we use the extensive dataset of NO_3^- concentrations, N_2 excess and transit time distributions to reconstruct a nitrate input chronicle $C^0_{NO_3^-}$ (*Eq. 1*). In this sense, the multi-proxy concentration data complemented with consistent transport modeling has been set up to increase the potential coverage of nitrate degradation capacity much beyond the existing monitoring network.

Calibration of apparent and actual reaction times. Apparent and actual reaction times for oxygen reduction and denitrification are calibrated to fit simulated with measured concentrations. The reaction term is defined depending on the vertical distribution of electron distributions (*Eq. 1* and *Fig. 1*). Oxygen and nitrate concentrations decrease

via a first-order reaction. The decay reaction is applied to each flowline without any exchange between them before concentrations get mixed in the well. Denitrification is assumed to occur after oxygen has been decreased to an oxygen concentration of 2 mg/l. Initial oxygen concentration of 7 mg/l are constant over time. The initial oxygen concentrations are equal to the concentrations measured in shallow piezometers at the site. The model has two degrees of freedom, either the apparent reaction times for oxygen and nitrate reduction or the actual reaction times that are similar for oxygen and nitrate and the time needed to hit or to leave the active denitrification zone.

References

Aeschbach-Hertig, W., Beyerle, U., Holocher, J., Peeters, F., Kipfer, R., 2001. Excess air in groundwater as a potential indicator of past environmental changes. Study Environ. Chang. Using Isot. Tech. 174–183.

Aeschbach-Hertig, W., Peeters, F., Beyerle, U., Kipfer, R., 1999. Interpretation of dissolved atmospheric noble gases in natural waters. Water Resour. Res. 35, 2779–2792. doi:10.1029/1999WR900130

Aquilina, L., Vergnaud-Ayraud, V., Labasque, T., Bour, O., Molénat, J., Ruiz, L., de Montety, V., De Ridder, J., Roques, C., Longuevergne, L., 2012. Nitrate dynamics in agricultural catchments deduced from groundwater dating and long-term nitrate monitoring in surface- and groundwaters. Sci. Total Environ. 435-436, 167–178. doi:10.1016/j.scitotenv.2012.06.028

Jurgens, B.C., Böhlke, J.K., Kauffman, L.J., Belitz, K., Esser, B.K., 2016. A partial exponential lumped parameter model to evaluate groundwater age distributions and nitrate trends in long-screened wells. J. Hydrol. 543, 109–126. doi:10.1016/j.jhydrol.2016.05.011

Kolbe, T., Marçais, J., Thomas, Z., Abbott, B.W., de Dreuzy, J.-R., Rousseau-Gueutin, P., Aquilina, L., Labasque, T., Pinay, G., 2016. Coupling 3D groundwater modeling with CFC-based age dating to classify local groundwater circulation in an unconfined crystalline aquifer. J. Hydrol. Accepté. doi:10.1016/j.jhydrol.2016.05.020

Maloszewski, P., Zuber, A., 1982. Determining the turnover time of groundwater systems with the aid of environmental tracers. 1. Models and their applicability. J. Hydrol. 57, 207–231. doi:10.1016/0022-1694(82)90147-0

Appendix A: Field data and location of wells

Tab. A.1: CFC-12, O_2, NO_3^- and NO_3^- degraded concentrations for each sampling campaign (Dec 2014, Mar 2015 and Oct 2015)

ID	CFC-12 [pptv]			O_2 [mg/l]			NO_3^- [mg/l]			NO_3^- degraded [mg/l]		
	Dec-14	Mar-15	Oct-15	Dec-14	Mar-15	Oct-15	Dec-14	Mar-15	Oct-15	Dec-14	Mar-15	Oct-15
1	397.94	251.65	337.34	0.16	0.07	0.54	23.56	26.06	26.57	41.44	32.76	32.73
2	377.06	263.35	313.38	0.44	0.39	0.16	0.00	0.00	0.09	10.44	9.96	8.82
3	521.38	329.29	460.82	5.05	6.18	6.36	51.84	48.98	50.32	12.34	12.63	2.87
4	192.67	107.23	141.06	2.18	1.45	0.71	0.33	0.12	0.00	23.87	35.57	37.88
5	-	227.51	242.92	2.39	2.60	1.63	26.34	33.53	22.78	29.12	22.97	40.43
6	188.08	73.24	108.97	1.54	1.15	1.70	37.76	37.77	37.70	27.58	30.34	27.69
7	-	98.51	99.91	-	0.32	0.29	-	0.00	0.00	-	52.97	46.64
8	437.05	261.75	410.69	6.24	5.59	5.32	63.63	63.57	68.19	19.42	17.13	16.52
9	36.08	36.49	33.63	0.10	0.41	0.20	0.00	0.00	0.00	19.25	17.81	17.54
10	464.76	91.75	33.14	4.16	3.94	0.88	0.00	0.00	0.00	14.17	2.06	7.13
11	11.08	36.36	29.83	0.15	0.85	0.04	0.00	0.00	0.00	10.55	10.20	15.83
12	82.14	126.68	103.18	0.24	1.30	1.60	0.00	0.00	0.04	36.72	44.55	37.18
13	134.58	125.20	95.75	1.56	1.18	0.78	37.96	38.78	24.04	19.52	19.04	19.71
14	435.60	254.18	480.63	6.76	6.78	7.20	42.60	52.37	39.08	2.03	4.11	0.00
15	933.77	-	746.32	2.87	3.88	2.39	32.04	61.81	32.70	11.82	11.45	12.48
16	-	-	220.00	-	-	7.66	-	-	75.02	-	-	0.00

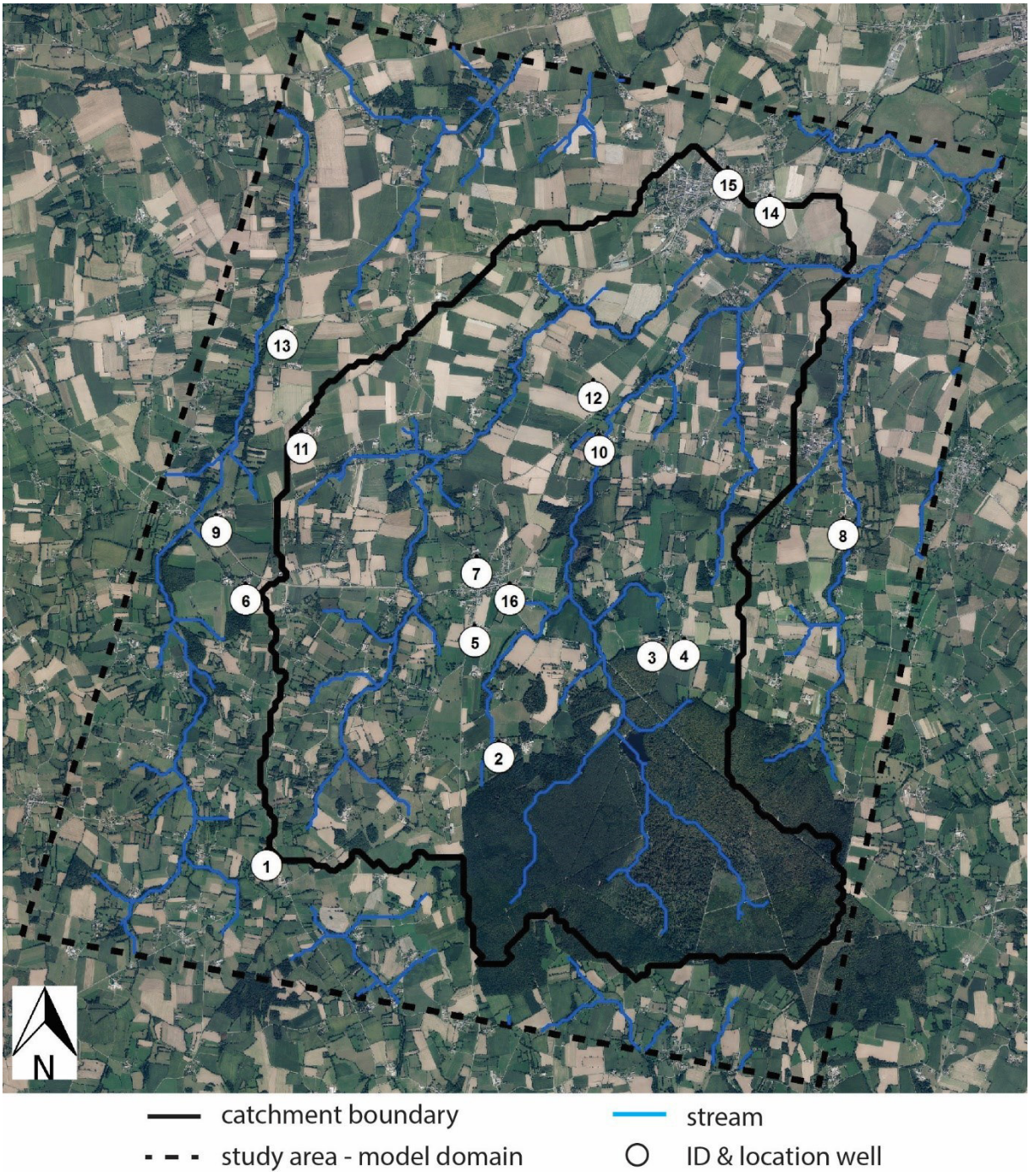

Fig. A.1: Location of wells in the study area.

Appendix B: Apparent and actual concentration distributions – τ_{hit} and τ_{leave} concept

Here, a uniform transit time distribution and constant input concentrations are used to present how oxygen and nitrate concentrations evolve with time within the τ_{hit} and τ_{leave} concept in comparison to the uniform concept. The uniform transit time distribution depends on the minimum time t_{min} and the maximum time t_{max} of water arrivals at a well (*Fig. B.1A*). The minimum time is set to 0 y, whereas the maximum time is 70 y. Oxygen and nitrate input concentrations are constant over time, e.g. C_{02} = 7 mg/l and C_{NO3^-} = 28 mg/l (*Fig. B.1B*).

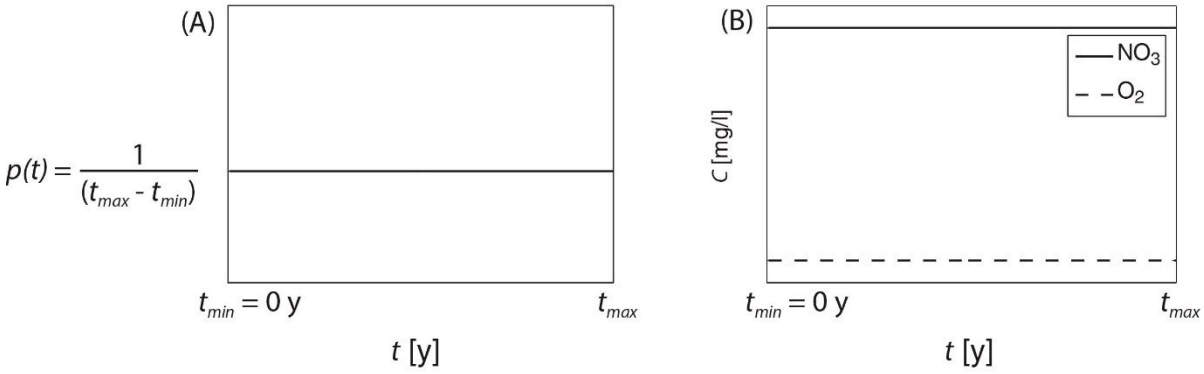

Fig. B.1: Uniform transit time distribution (A) and constant concentration inputs (B).

Apparent and actual reaction times are calibrated to match apparent and actual concentrations at a sampling location.

Apparent Concentrations

Apparent concentrations C^{app} in a well are calculated by convoluting the input concentrations C^0 with the transit time distribution *p(t)* and applying a first-order reaction term (*Eq. B.1A - B.2B*). Reactions are assumed to occur along the full flowline. Solutions are valid for t_c (time lag for denitrification) larger than t_{min} and smaller than t_{max}.

$$C_{O_2}^{app} = \int_{t_{min}}^{t_{max}} \frac{1}{t_{max} - t_{min}} C_{O_2}^0 e^{-\frac{t}{\tau_{O_2}^{app}}} dt \qquad \text{(B.1A)}$$

$$C_{O_2}^{app} = C_{O_2}^0 \frac{\tau_{O_2}^{app}\left(e^{-\frac{t_{min}}{\tau_{O_2}^{app}}} - e^{-\frac{t_{max}}{\tau_{O_2}^{app}}}\right)}{t_{max} - t_{min}} \quad \text{(B.1B)}$$

$$C_{NO_3^-}^{app} = \int_{t_{min}}^{t_{max}} \frac{1}{t_{max} - t_{min}} C_{NO_3^-}^0 \, e^{-\frac{t - t_c^{app}}{\tau_{NO_3^-}^{app}}} \, dt \quad \text{(B.2A)}$$

$$C_{NO_3^-}^{app} = C_{NO_3^-}^0 \frac{\tau_{NO_3^-}^{app}\left(1 - e^{-\frac{t_{max} - t_c^{app}}{\tau_{NO_3^-}^{app}}}\right) - t_{min} + t_c^{app}}{t_{max} - t_{min}} \quad \text{(B.2B)}$$

Actual concentrations - τ_{hit} Concept

Within the τ_{hit} concept, actual reaction times are calibrated to fit actual with apparent concentrations. Actual oxygen $C_{O_2}^{act}$ and nitrate $C_{NO_3^-}^{act}$ concentrations are calculated with *Eq. B.3A - B.4B*. The solutions are valid for $\tau_{hit} + t_c$ larger than t_{min} and smaller than t_{max}.

$$C_{O_2}^{act} = \int_{t_{min}}^{\tau_{hit}} \frac{1}{t_{max} - t_{min}} C_{O_2}^0 \, dt + \int_{\tau_{hit}}^{t_{max}} \frac{1}{t_{max} - t_{min}} C_{O_2}^0 \, e^{-\frac{t - \tau_{hit}}{\tau_{O_2}^{act}}} \, dt \quad \text{(B.3A)}$$

$$C_{O_2}^{act} = C_{O_2}^0 \frac{\tau_{O_2}^{act}\left(1 - e^{-\frac{t_{max} - \tau_{hit}}{\tau_{O_2}^{act}}}\right) + \tau_{hit} - t_{min}}{t_{max} - t_{min}} \quad \text{(B.3B)}$$

$$C_{NO_3^-}^{act} = \int_{t_{min}}^{\tau_{hit} + t_c^{act}} \frac{1}{t_{max} - t_{min}} C_{NO_3^-}^0 \, dt + \int_{\tau_{hit} + t_c^{act}}^{t_{max}} \frac{1}{t_{max} - t_{min}} C_{NO_3^-}^0 \, e^{-\frac{t - \tau_{hit} - t_c^{act}}{\tau_{NO_3^-}^{act}}} \, dt \quad \text{(B.4A)}$$

$$C_{NO_3^-}^{act} = C_{NO_3^-}^0 \frac{\tau_{NO_3^-}^{act}\left(1 - e^{-\frac{t_{max} - \tau_{hit} - t_c^{act}}{\tau_{NO_3^-}^{act}}}\right) + \tau_{hit} + t_c^{act} - t_{min}}{t_{max} - t_{min}} \quad \text{(B.4B)}$$

Fig. B2 shows how apparent and actual concentrations evolve within time. Apparent oxygen concentrations decrease slower than nitrate concentrations. The apparent oxygen reduction time of 15.2 y leads to a time lag for denitrification of 19 y. If the apparent oxygen concentration is lower than 2 mg/l, apparent nitrate gets reduced quickly with a reaction time of 2.3 y.

Apparent reaction times can be interpreted with an actual reaction time of 5 y for oxygen and nitrate reduction, and the time to hit the layer (τ_{hit} = 10 y). The faster actual than apparent oxygen reduction leads to a shorter actual time lag for denitrification of 6.3 y. Actual nitrate concentrations start to decrease after 16.3 y with an actual reduction time of 5 y.

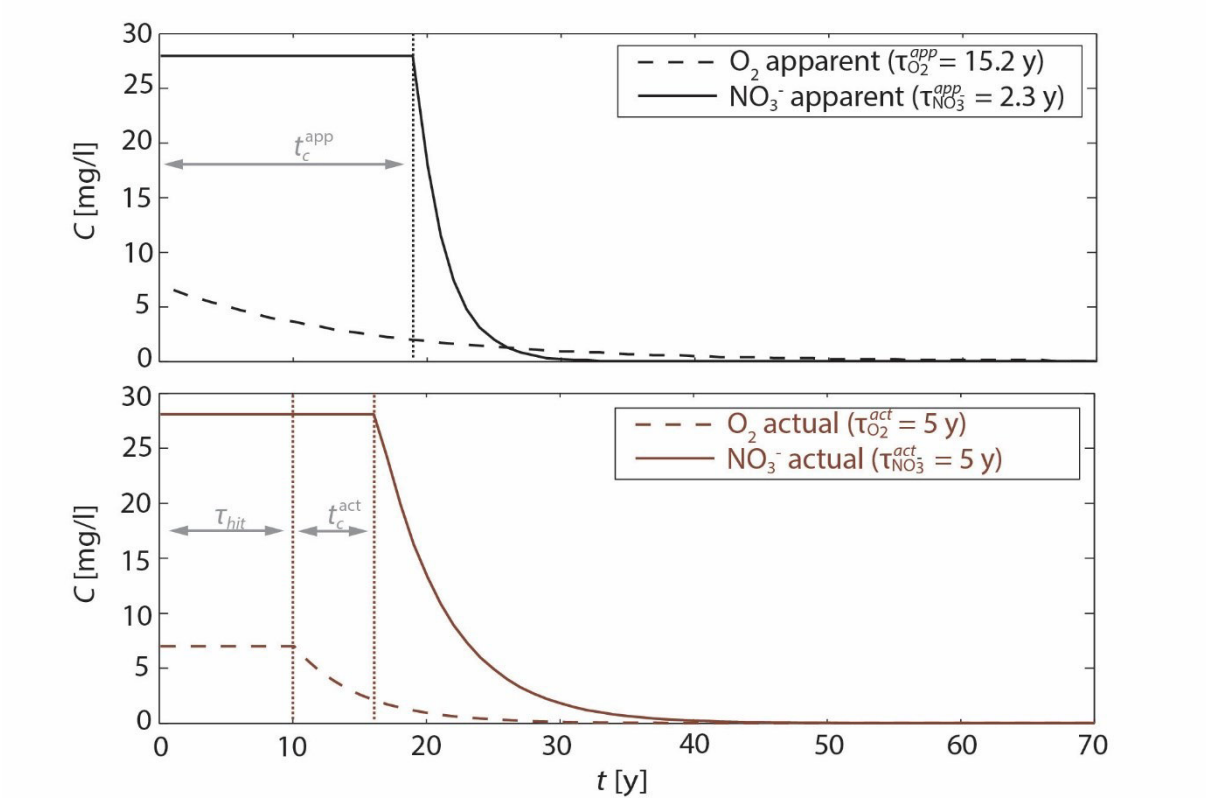

Fig. B.2: Actual oxygen and nitrate concentrations (τ_{hit} concept) with time in comparison to apparent concentrations.

Actual concentrations - τ_{leave} Concept

Within the τ_{leave} concept, actual reaction times are calibrated to fit actual concentrations with apparent concentrations. Actual oxygen $C_{O_2}^{act}$ and nitrate $C_{NO_3^-}^{act}$ concentrations are calculated with *Eq. B.5A - B.6B*. The solutions are valid for τ_{leave} + t_c larger than t_{min} and smaller than t_{max}.

$$C_{O_2}^{act} = \int_{t_{min}}^{\tau_{leave}} \frac{1}{t_{max} - t_{min}} C_{O_2}^0 \, e^{-\frac{t}{\tau_{O_2}^{act}}} \, dt + \int_{\tau_{leave}}^{t_{max}} \frac{1}{t_{max} - t_{min}} C_{O_2}^0 \, e^{-\frac{\tau_{leave}}{\tau_{O_2}^{act}}} \, dt \qquad \text{(B.5A)}$$

$$C_{O_2}^{act} = C_{O_2}^0 \frac{\tau_{O_2}^{act} \, e^{-\frac{t_{min}}{\tau_{O_2}^{act}}} + \left(t_{max} - \tau_{leave} - \tau_{O_2}^{act}\right) e^{-\frac{\tau_{leave}}{\tau_{O_2}^{act}}}}{t_{max} - t_{min}} \qquad \text{(B.5B)}$$

$$C_{NO_3^-}^{act} = \int_{t_{min}}^{\tau_{leave}} \frac{1}{t_{max} - t_{min}} C_{NO_3^-}^0 \, e^{-\frac{t - t_c^{act}}{\tau_{NO_3^-}^{act}}} \, dt + \int_{\tau_{leave}}^{t_{max}} \frac{1}{t_{max} - t_{min}} C_{NO_3^-}^0 \, e^{-\frac{\tau_{leave} - t_c^{act}}{\tau_{NO_3^-}^{act}}} \, dt \qquad \text{(B.6A)}$$

$$C_{NO_3^-}^{act} = C_{NO_3^-}^0 \frac{\tau_{NO_3^-}^{act} + \left(t_{max} - \tau_{leave} - \tau_{NO_3^-}^{act}\right) e^{-\frac{\tau_{leave} - t_c^{act}}{\tau_{NO_3^-}^{act}}} + t_c^{act} - t_{min}}{t_{max} - t_{min}} \qquad \text{(B.6B)}$$

Fig. B.3 shows how apparent and actual concentrations evolve within time. Apparent oxygen concentrations decrease faster than apparent nitrate concentrations. The apparent oxygen reduction time of 12.5 y leads to a time lag for denitrification of 15.6 y. If the apparent oxygen concentration is lower than 2 mg/l, apparent nitrate gets reduced with a reaction time of 24.2 y.

Apparent reaction times can be interpreted with an actual reaction time of 5 y for oxygen and nitrate reduction, and the time to leave the layer (τ_{leave} = 10 y). The faster actual oxygen reduction leads to a shorter actual time lag for denitrification of 6.3 y. Actual nitrate concentrations start to decrease after 6.3 y. When nitrate loaded water leaves the reactive zone after 10 y, nitrate is further transported conservatively.

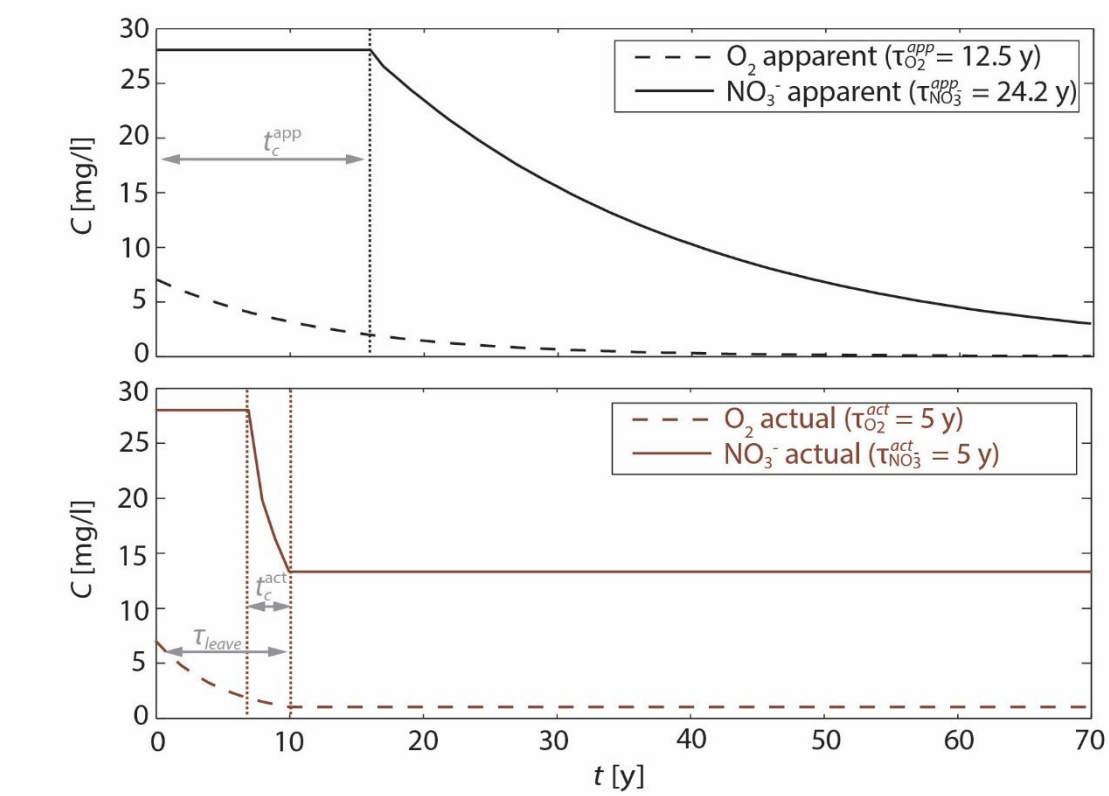

Fig. B.3: Actual oxygen and nitrate concentrations (τ_{leave} concept) within time in comparison with apparent concentrations.

Even if the inputs (transit time distribution and concentration distribution) are simplified, the results give some general understanding on how actual and apparent concentrations are related to each other.

Appendix C: Correlations of apparent reaction times within the τ_{hit} and τ_{leave} concept

Based on Appendix B, analytical solutions for apparent (uniform concept) and actual concentrations (τ_{hit} and τ_{leave} concept) by considering a uniform transit time distribution and constant concentration inputs are given. Here, possible correlations of apparent reaction times by applying the τ_{hit} and τ_{leave} concept are developed. By fitting apparent and actual concentrations in a sampling location, combinations of actual reaction times and times to leave (τ_{leave}) or to hit (τ_{hit}) the reactive layer are displayed in the plot of apparent reaction times.

Actual reaction times τ^{act} (similar for oxygen and nitrate reduction) and times to hit or leave the reactive layer vary between 1 y and 68 y. Oxygen and nitrate inputs are set to a constant value (C_{02} = 7 mg/l and C_{NO3^-} = 28 mg/l). The uniform transit time distribution is determined by the minimum and maximum time. The minimum time is set to 0, whereas the maximum time is either 70 y or 195 y (the mean of the maximum times arriving at the 16 wells of the Pleine-Fougères aquifer), resulting in $p(t)$ = 0.014 or $p(t)$ = 0.005 (*Fig. B.1*).

τ_{hit} Concept

Fig. C.1 demonstrates how actual reaction times and the times to hit the reactive layer evolve within the plot of apparent reaction times for two different uniform transit time distributions. *Fig. C.1A* and *C.1C* show correlations of apparent reaction times for different values of τ^{act} and varying values of τ_{hit}, whereas *Fig. C.1B* and *C.1D* show correlations of apparent reaction times for different τ_{hit} and varying τ^{act} values. Generally, larger apparent reaction times for oxygen reduction than for denitrification appear.

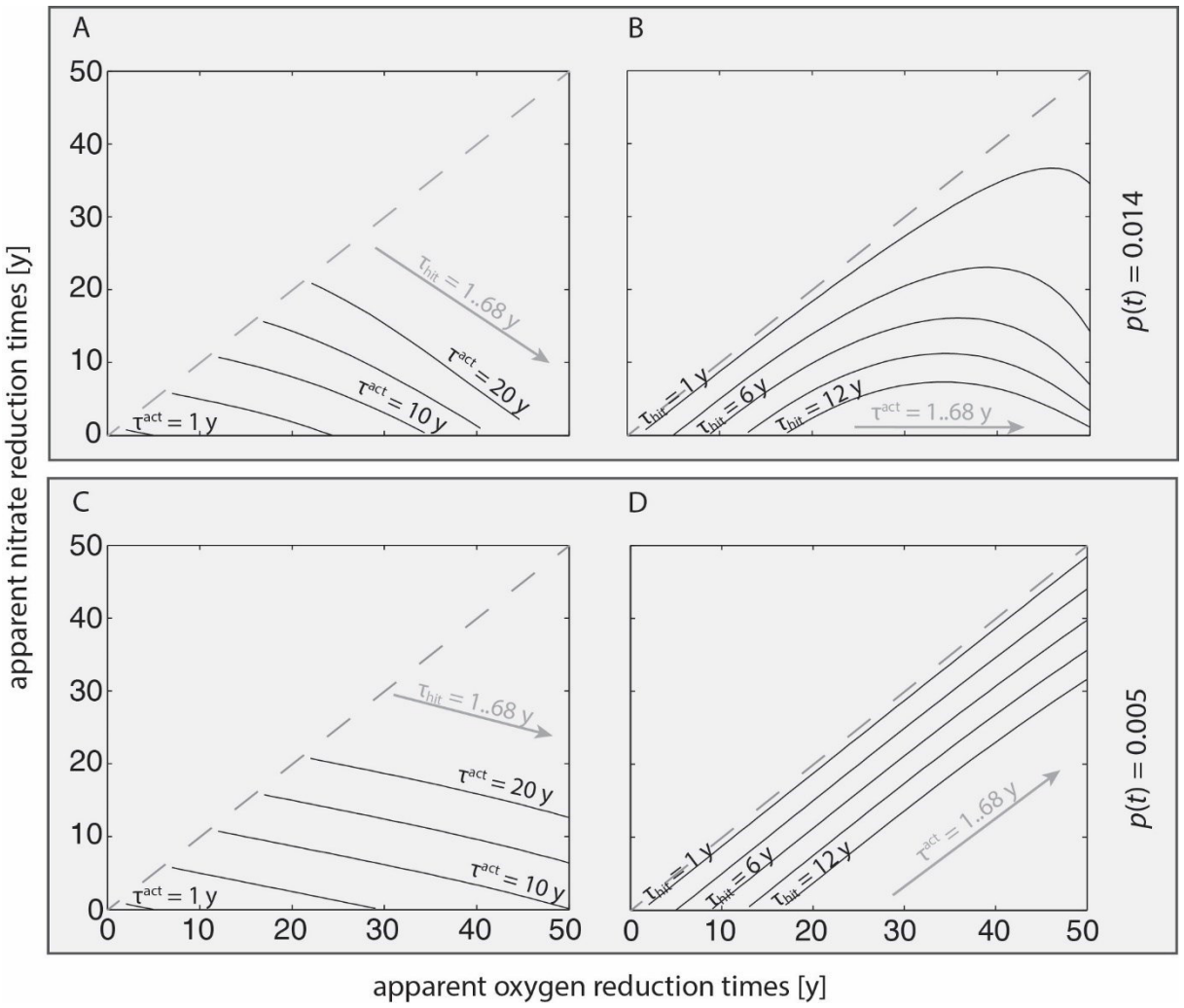

Fig. C.1: The evolution of τ^{act} and τ_{hit} is presented in the plot of apparent oxygen and nitrate reduction times.

Displaying all tested combinations of τ^{act} and τ_{hit} shows that correlations of apparent oxygen and nitrate reduction times below the 1:1 line can be reached with the τ_{hit} concept (*Fig. C.2*).

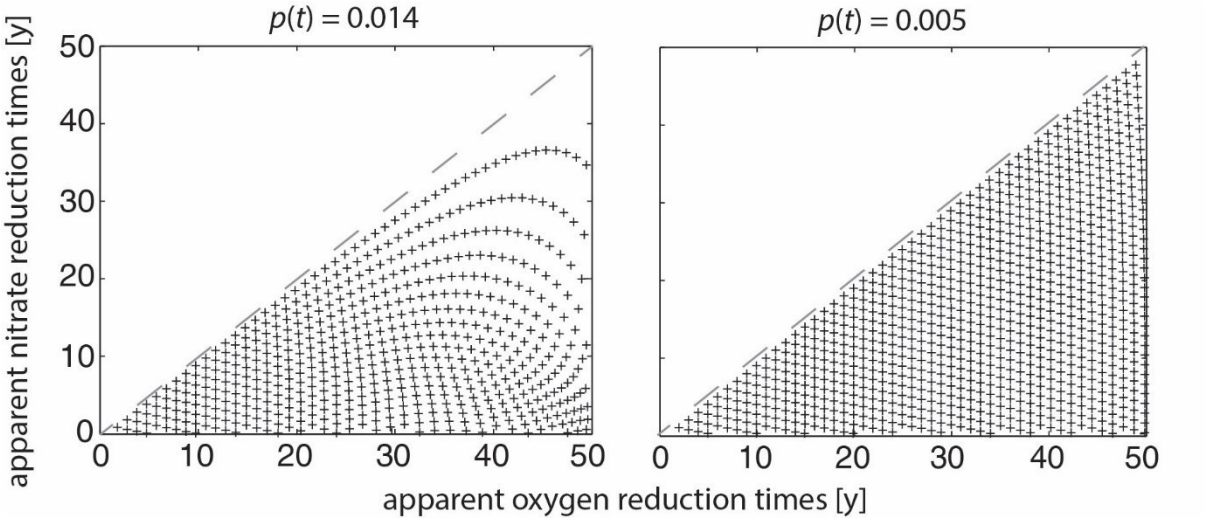

Fig. C.2: Apparent reaction time correlations within the τ_{hit} concept.

τ_{leave} Concept

Fig. C.3 shows how actual reaction times and times to leave the reactive layer evolve in the plot of apparent oxygen nitrate reduction times. *Fig. C.3A* and *C.3C* show correlations of apparent reaction times for different values of τ^{act} and varying values of τ_{hit}, whereas *Fig. C.3B* and *C.3D* show correlations of apparent reaction times for different τ_{hit} and varying τ^{act} values. Generally, *Fig*shorter apparent reaction times for oxygen reduction than for denitrification appear.

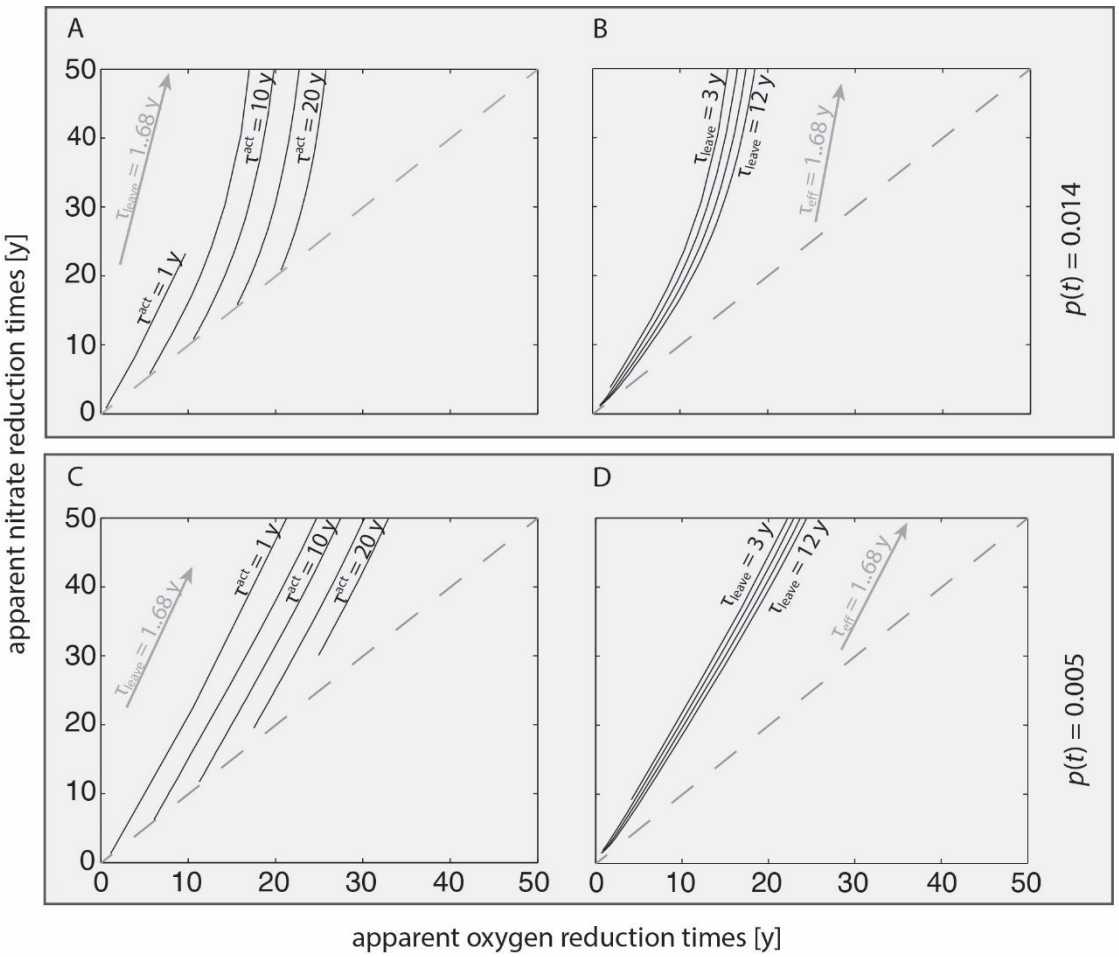

Fig.C.3: The evolution of τ^{act} *and* τ_{leave} *is presented in the plot of apparent oxygen versus nitrate reduction times.*

Displaying all tested combinations of τ^{act} and τ_{leave} shows that correlations of apparent reaction times above the 1:1 line occur (*Fig. C.4*), except correlations of relatively small oxygen reduction times compared to large nitrate reduction times. This exception is reasoned by the fact that a short apparent oxygen reduction time result from short actual oxygen reduction time, and the assumption that actual reduction times are similar for oxygen and nitrate reduction. Large apparent reduction times for denitrification cannot be reached, while apparent oxygen reduction times are short. Decreasing the time in the reactive zone (small τ_{leave} value) would increase apparent nitrate reduction times by keeping actual reduction times for nitrate, but in fact, the decrease of time in the reactive zone would entail a decrease of the actual oxygen reduction time, and for actual denitrification time, too. Therefore, a decrease of time in the

reactive zone induces a decrease of actual reduction times and large apparent nitrate reduction times and small oxygen reduction times cannot be reached.

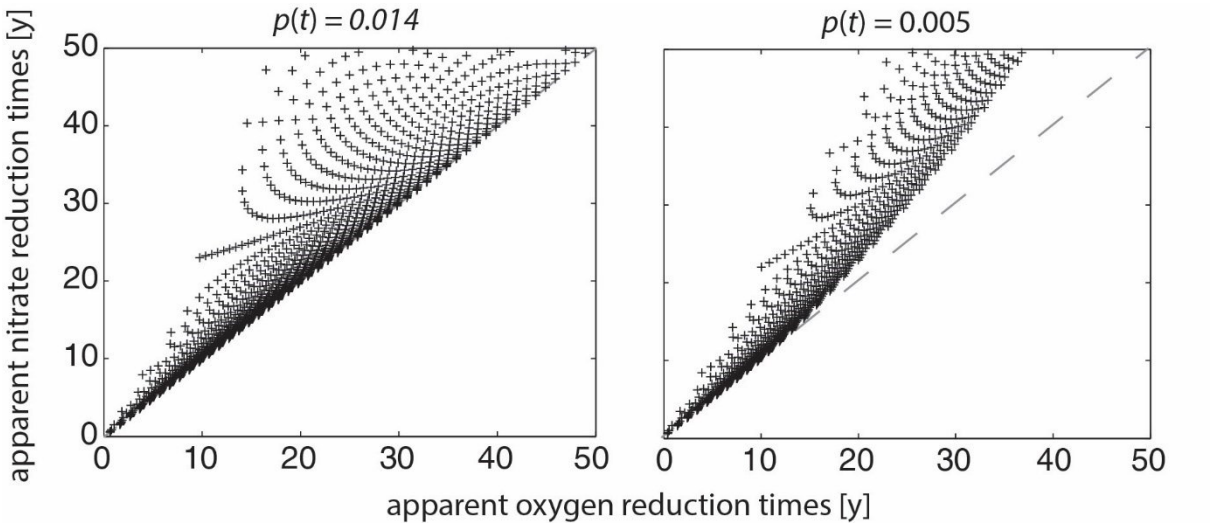

Fig. C.4: Apparent reaction time combinations are presented for different combinations of τ^{act} *and* τ_{leave}.

The development of analytical solutions regarding apparent and actual reduction times considering the τ_{leave} and τ_{hit} concept are performed with simplified transit time and concentration input distributions. More complex transit time and concentration distributions are expected to change the relation of apparent oxygen and nitrate reduction times without changing the characteristic relation, meaning that $\tau_{O_2}^{app} > \tau_{NO_3^-}^{app}$ within the τ_{hit} concept and $\tau_{O_2}^{app} < \tau_{NO_3^-}^{app}$ within τ_{leave} concept.

Even if the inputs (transit time distribution and concentration distribution) are simplified, the results give some general understanding on how actual and apparent reduction times are related to each other.

5.3 Conclusion

The previous article shows the importance for investigating the physical location of denitrification processes. Widely accessible well data, like CFC-12, O_2, NO_3^-, and dissolved N_2 concentrations, are coupled to a time based modeling approach to derive actual reaction times for oxygen reduction and denitrification. Results show that apparent reaction times could over- or underestimate actual denitrification times in aquifers with non-uniform distributed electron donors. The interpretation framework provides new analysis capacities for observed reaction times and estimates on actual denitrification in aquifers. The framework is also applicable to other aquifer types and should be tested in a wide range of hydrogeological settings to gain more insights in actual denitrification.

Chapter 6: Discussion & Suggestions for Future Research

6.1 Discussion

The methodology was set-up at a crystalline aquifer, but can be applied also to other shallow unconfined aquifers. Flow structures and nitrate degradation are quite different between wells, even if they are located very close to each other in the catchment. The general methodology can be applied to a well or another well-defined outlet as long as the input area (i.e. capture zone) is known and the tracer is transported through a closed system (i.e. aquifer)

Groundwater flow dynamics and biogeochemical reactions are key controls in determining the fate of nitrate. The approach presented in this dissertation uses multiple tracers and modeling tools to infer denitrification processes in groundwater. Tracers are combined to infer groundwater age and nitrate loss during the time nitrate loaded water spent in the aquifer. Kazemi et al. (2006) give an overview about groundwater dating tools that can be alternatively used. O_2, NO_3^- and dissolved N_2 are necessary to measure and to determine the amount of nitrate that has been degraded in the aquifer. Mixing in a well makes it impossible to differentiate changes in nitrate concentrations due to reactivity or dilution based on only tracer measurements. However, in combination with mechanistic or lumped parameter models, transit time distributions complement tracer information to account for mixing processes. In fact, in this case mixing has a big advantage to determine oxygen and nitrate degradation and to define full oxygen and nitrate concentration distributions. Contrary to investigations at a single flowline, an entire picture of the interaction between reactivity and flow dynamics can be obtained using this approach.

6.1.1 Groundwater flow

In this study, the crystalline aquifer was partitioned into two main layers based on conceptual models presented in Aquilina et al. (2012), Ayraud et al. (2008), Maréchal et al. (2003), and Tarits et al. (2006) to simulate groundwater flow with a mechanistic groundwater flow model. The upper weathered zone, more permeable than the underlying fractured zone, is the main water bearing layer. The fresh bedrock is, like in other studies, assumed to be impermeable. These general assumptions proposed for crystalline aquifers give a relevance of the here obtained flow structures to other crystalline study sites. Faults or deep significant fractures are not accounted for in the model. Alternatively to mechanistic groundwater modeling, lumped parameter models provide a computational and time effective way to estimate transit time distributions (Jurgens et al., 2012; Marçais et al., 2015). Lumped parameter models depend just on a few parameter and assumptions on the aquifer geometry.

6.1.2 $r_{GW\text{-}LOCAL}$ and its application to other sites

Results presented in chapter 3 show that groundwater flow is local, but has a mean groundwater age of around 40 y that is relevant for past nitrate inputs to the aquifer. This dissertation demonstrates how groundwater flow can be classified in relation to the relatively short surface flow distances (reference distance) and presents the index $r_{GW\text{-}LOCAL}$ (ratio of mean groundwater travel distances and mean reference distances). The upland and lowland area, separated by a steep slope, show quite different behaviors of $r_{GW\text{-}LOCAL}$ with different recharge rates (*Fig. 15*). The initial recharge rate *R* is 167 mm/y and varies between *R*/10 and 4*R*. It becomes clear that the scale for groundwater flow investigations in this shallow aquifer should depend on the main topographical gradients and not be based on the overall catchment boundary.

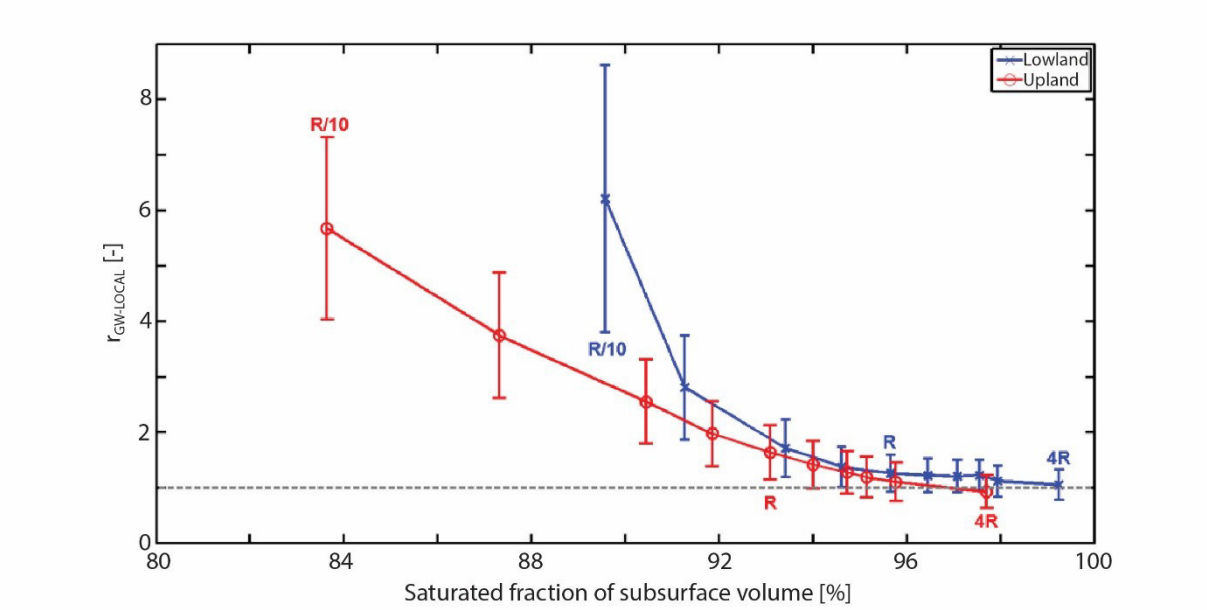

Fig. 15: $r_{GW-LOCAL}$ in relation to the saturated fraction of the subsurface volume presented for the upland (blue) and lowland (red) area of the Pleine-Fougères catchment.

Groundwater flow is localized at the Pleine-Fougères site and poses the question whether other topographies in Brittany create similar patterns. Two other catchments in Brittany were selected (Jet and Douffine, *Fig. 16*) to investigate groundwater circulation and to demonstrate how $r_{GW-LOCAL}$ evolves with different recharge rates. The area of Jet (122 km^2) and Douffine (182 km^2) are larger than the area of Pleine-Fougères (36 km^2). The global slope is smaller in Jet (1.2 %) and larger in Douffine (2.4 %) than in Pleine-Fougères (1.7 %). To compare the effects of different topographical structures, mechanistic groundwater flow models are set up with equal hydrogeological properties. The aquifer is defined as a homogeneous layer with equal hydraulic conductivities, porosities and thickness in all three cases. Calibrated parameter (hydraulic conductivity and porosity) of the Pleine-Fougères site are carried over to the other catchments. Virtual sampling all over the catchment areas provides

mean groundwater travel distances and mean reference distances to compute the index $r_{GW\text{-}LOCAL}$.

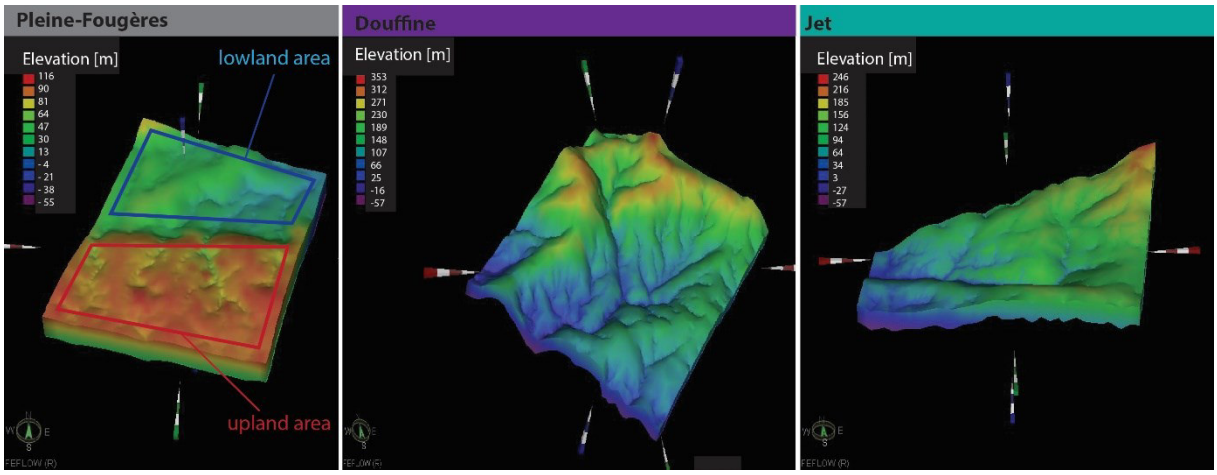

Fig. 16: Elevations of the Pleine-Fougères, Jet and Douffine catchment.

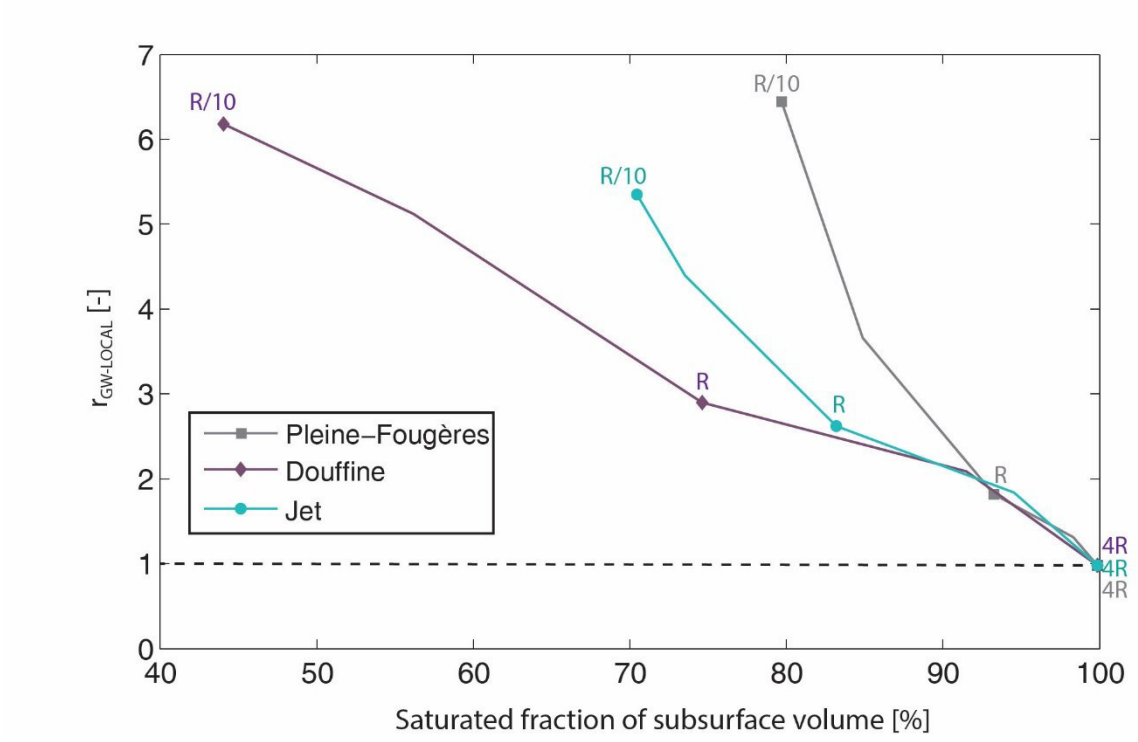

Fig. 17: $r_{GW\text{-}LOCAL}$ in relation to the saturated fraction of the subsurface volume presented for the Pleine-Fougères (grey, square), Douffine (purple, diamond) and Jet (cyan, circle) catchment.

Fig. 17 shows the comparison of $r_{GW\text{-}LOCAL}$ with different recharge rates for the three sites. With initial recharge rates, mean groundwater travel distances are twice to three

times higher than reference distances. For lower recharge rates groundwater travel distances increase stronger for Douffine and Jet than for Pleine-Fougères. The evolvement of $r_{GW\text{-}LOCAL}$ could be here assumed to develop in regard to the catchment size, but an extension of the Pleine-Fougères site up to 194 km^2 show that $r_{GW\text{-}LOCAL}$ evolve in a similar way (*Fig. 18*).

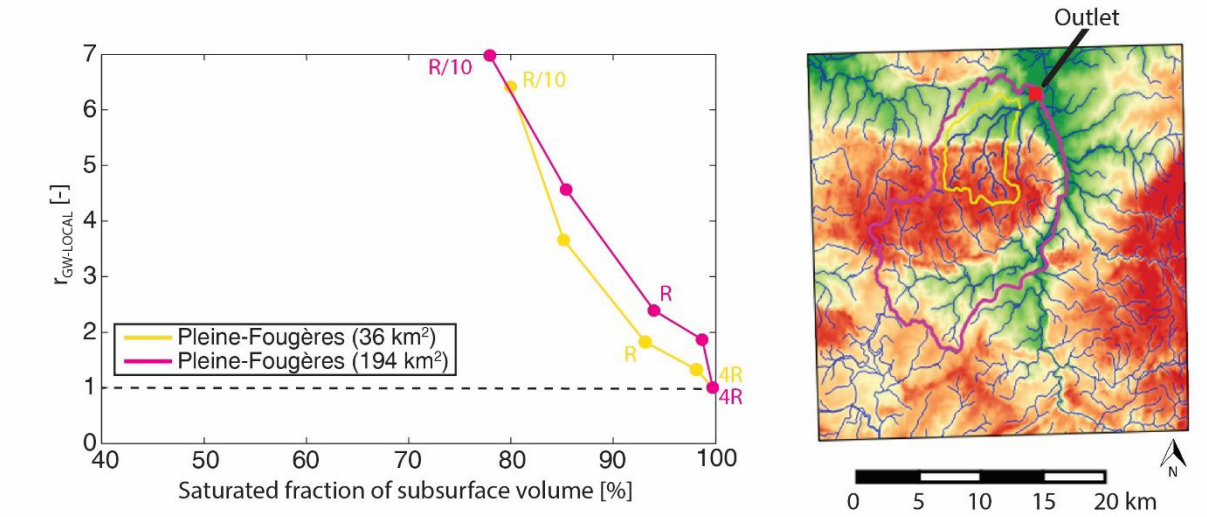

Fig. 18: Comparison of $r_{GW\text{-}LOCAL}$ obtained from the Pleine-Fougères (36 km^2) and the extended catchment (194 km^2)

It is hypothesized that the catchment size and the arrangement of topographical highs and lows in the catchment area control the evolvement of $r_{GW\text{-}LOCAL}$. As can been seen in Jet and Douffine, the dominant topographical high is at the catchment boundary, whereas in the extended Pleine-Fougères catchment the main topographical high is located in the center. Further investigations have to be performed to confirm this hypothesis.

The comparison of Pleine-Fougères with Jet and Douffine was based on a whole catchment analysis (*Fig. 17*). As presented in *Fig. 15*, groundwater circulation in Pleine-Fougères depends on topographical structures and develop differently in subareas of the catchment. To what extent the Jet and Douffine catchment can be

subdivided in their hydrogeological behavior in regard to topographical characteristics presents another interesting research question.

6.1.3 Denitrification processes

Data (i.e. CFC-12, O_2, NO_3^-, and dissolved N_2) measured at 16 wells in the Pleine-Fougères catchment are used to gain information on nitrate removal in the aquifer. With the data alone it is difficult to determine denitrification activity, because mixing in the well and aquifer makes it difficult to distinguish between degradation and dilution. But the data allow to assess some indications on denitrification activity in the aquifer. *Fig. 19* shows mean values calculated from the measurements obtained in Dec-2014, Mar-2015, and Oct-2015.

Higher CFC-12 concentrations represent older groundwater ages than lower concentrations. Oxygen and nitrate concentrations appear to have a positive correlation with CFC-12 data, whereas degraded nitrate concentrations have a negative correlation (*Fig. 19A - C*). This means that older groundwater has lower oxygen and nitrate concentrations. This fits with the observed correlation of degraded nitrate and CFCs. In older water more nitrate has been degraded. Interesting regarding the measured nitrate concentration is that either almost no nitrate or concentrations above 20 mg/l were measured. Concentrations between in this range have not been measured at the site. The CFC-12 values obtained for well 15 are not reliable because they exceed the maximum atmospheric CFC-12 concentration reported.

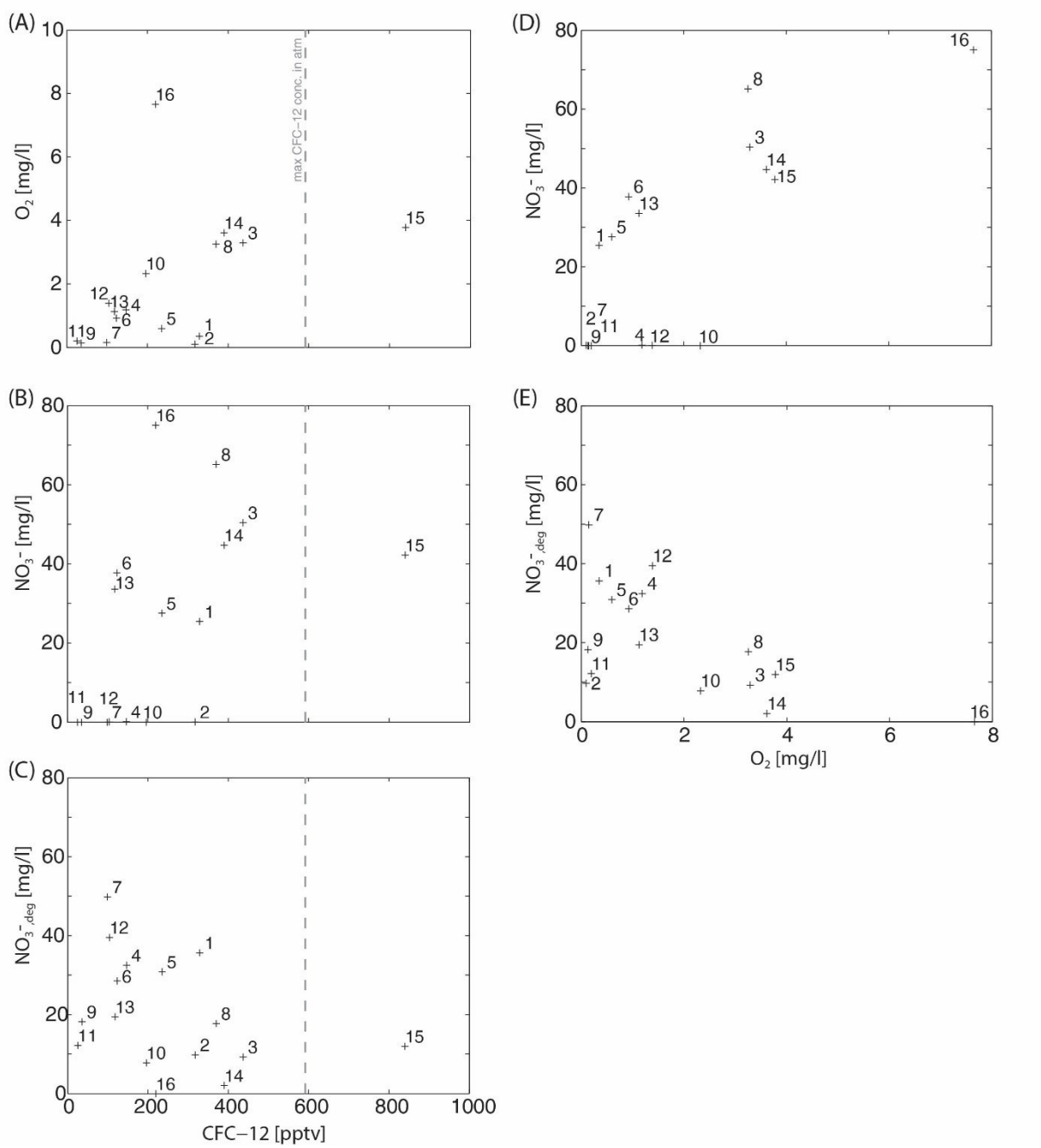

Fig. 19: Mean concentrations of oxygen and nitrate as well as the amount that has been degraded is presented in correlation to CFC-12 concentrations (A - C). Also the correlation of nitrate and degraded nitrate in correlation with oxygen is displayed (D and *E).*

Fig. 19D and E show the relation of nitrate and oxygen concentrations. They appear to be positively correlated, whereas degraded nitrate and oxygen seem to be

negatively correlated. These patterns are expected in an aquifer where denitrification occurs, because nitrate just degrades if oxygen concentrations are low.

Nitrate and sulfate stable isotopes were measured to give an additional indication on the dominant denitrification process, whether nitrate is degraded heterotrophic or autotrophic. *Fig. 20* shows the relation of nitrate and sulfate stable isotopes. A clear statement on heterotrophic or autotrophic denitrification cannot be given based on the data. Denitrification processes are too complex to follow the simplified conceptual evolution of nitrate and sulfate stable isotopes (*Fig. 20*).

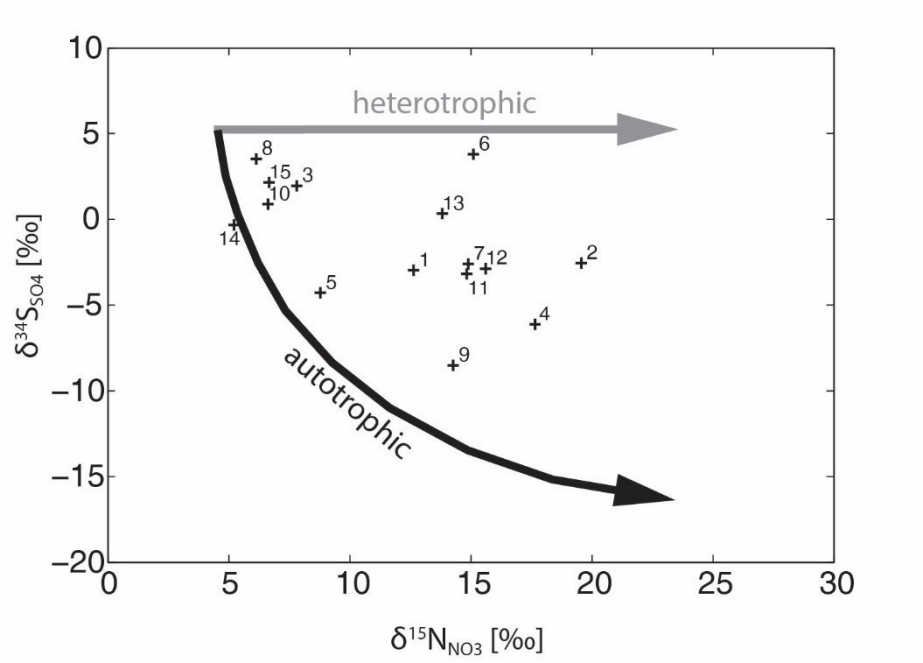

Fig. 20: Measured stable isotopes of nitrate and sulfate are presented in the conceptual evolution of nitrate and sulfate isotopes for heterotrophic and autotrophic denitrification given by (Hosono et al., 2014).

Stable isotope measurements became increasingly popular in investigating denitrification in aquifers, but in this study N_2 excess (derived by noble gas measurements of Ar, Ne, and N_2) that determine the amount of nitrate that has been degraded in the aquifer is a better indicator on denitrification activity.

6.1.4 Vertical distribution of denitrification

Groundwater flow and transport modeling is used to account for mixing processes and to determine denitrification activity. Time is the determining parameter in this approach. The developed conceptual framework to interpret apparent reaction times is based on the location of electron donors. Locations are transferred to times, i.e. time to hit (τ_{hit} concept) or to leave the reactive zone (τ_{leave} concept). It is demonstrated that the high spatial variability of apparent denitrification obtained from well data can be interpreted with the proposed framework. Apparent denitrification times might over- or underestimate actual denitrification times and the additional layering of reactive and non-reactive zones (i.e. τ_{hit} concept and τ_{leave} concept) might lead to errors in calculating nitrate budgets.

Autotrophic denitrification has been identified as the dominant nitrate removal process in aquifers even if the conditions for heterotrophic denitrification are fulfilled. At the Pleine-Fougères site, as well as in comparison to the other study sites, most of the presented sites in chapter 5 fall in the τ_{hit} concept that is representative for autotrophic denitrification. To validate these findings on other sites, complementary proxies like $\delta^{15}N$ and $\delta^{34}S$ could be used. Nitrate and sulfate stable isotopes might give additional information at other sites even if they showed not a clear pattern at the Pleine-Fougères site.

It might exist the case where a combination of heterotrophic and autotrophic denitrification determine nitrate removal in the aquifer, meaning that a combined τ_{hit} and τ_{leave} concept would be necessary to interpret apparent reaction times, but based on findings in the literature that demonstrate the dominance on autotrophic denitrification, a combination of concepts might be of minor importance.

A geological characteristic of the Pleine-Fougères site that is not explicitly described in the developed concepts is the distribution of vertical magmatic dikes over the catchment area (*Fig. 21*). The vertical magmatic dikes are north-south oriented (Aïfa et al., 1999) with a mineralogy richer in sulfide minerals than the surrounding geological substrates. Mapped magmatic dikes are close to some of the monitored wells, but their extension in length as well as their occurrence in other catchment locations is highly uncertain. Further investigations on their location and impact on autotrophic denitrification should be considered.

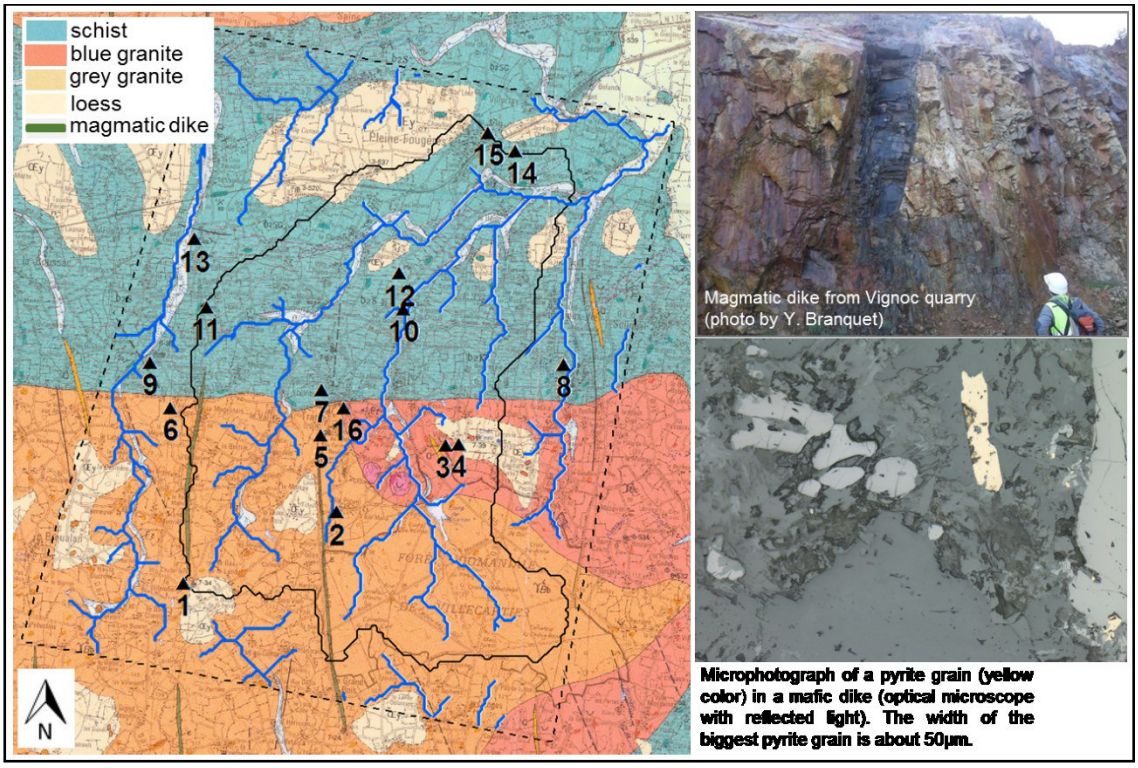

Fig. 21: Geological map of the study area (left). Example of vertical magmatic dike and microphotograph of a pyrite grain (right).

6.2 Suggestions for Future Research

Temporal and spatial constraints for investigating the nitrate removal capacity in aquifers are defining the scale for research activities. Temporal constraints are given by past nitrate inputs to the aquifer. Around 70 years ago, fertilization started to

increase sharply as well as the amount of nitrate that leached to the aquifer. Groundwater circulation in this time range (0 - 70 y) are relatively local, meaning that most of the recharged water potentially loaded with nitrate tend to outcrop at the closest river (Tóth, 1963; Tóth, 2009). Groundwater flow depends strongly on topographical gradients. The most appropriate spatial scale for groundwater flow dynamics that control nitrate transport to active denitrification zones and consider the temporal evolution of nitrate inputs is therefore the hillslope scale. Larger scales (i.e. catchment scale) integrate local flow structures and the different behaviors of subareas cannot be analyzed, whereas smaller scales (i.e. reach scale) might not incorporate the full groundwater flow behavior.

The hillslope scale is identified as the characteristic scale for denitrification investigations due to groundwater flow and reactivity structures. This dissertation proposes a partitioning of the catchment in hillslopes and to determine dominant hillslope types to upscale denitrification (*Fig. 22*). Based on dominant hillslope types nitrate transport should be studied and the proposed interpretation framework to estimate actual denitrification be tested and further investigated.

In regard to the Pleine-Fougères site, a characterization of hillslopes and identification of main hillslope types is proposed. Questionable is whether the 16 sampling locations are representative for the catchment area or not. The well information presented here should be grouped with regards to the hillslope type in which the wells are located. Do these sampling locations provide enough information to define denitrification at the characteristic hillslope types? If not, it might be appropriate to set-up new experiments to investigate characteristic hillslope types regarding their denitrification activity. A characterization of hillslope types and the assignment of well information to hillslope

types would allow to upscale denitrification and to give further indication on the overall nitrate budget in the aquifer.

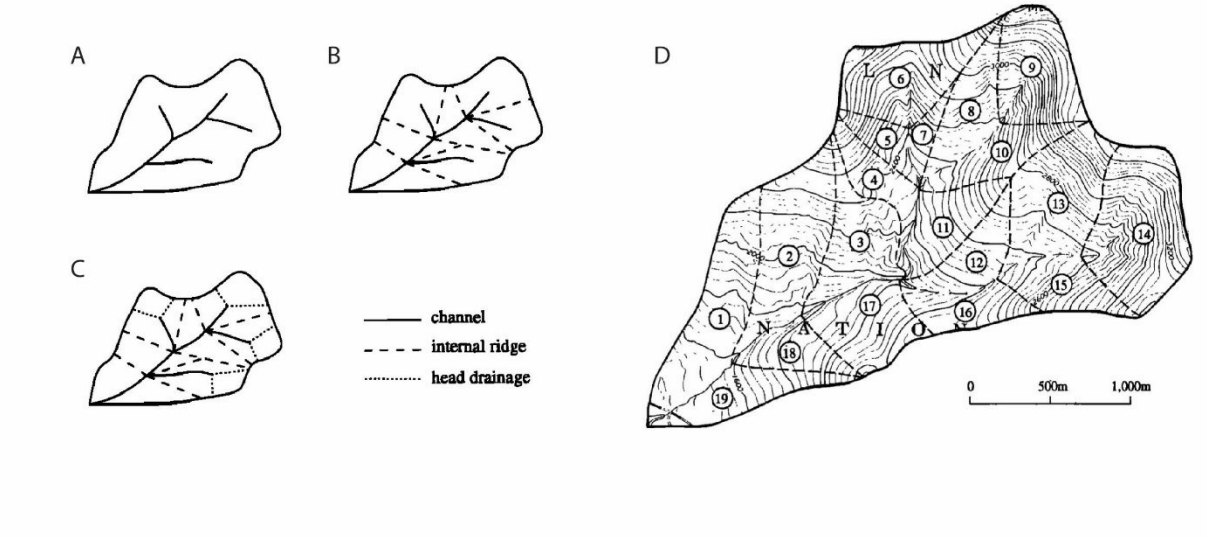

Fig. 22: Illustrative example to partition a catchment into hillslopes: A: catchment boundary and network, B: with internal ridge lines overlaid, and C: with channel head drainage areas delineated. D shows the partitioned catchment (Fan and Bras, 1998).

This general upscaling strategy could be transferred to other sites, where partitioning of the catchment in hillslopes and the identification of characteristic hillslopes is a first step followed by denitrification investigations at characteristic hillslopes and upscaling of these findings to a larger scale.

Short-term research activities could include the investigation of apparent oxygen and nitrate reduction times at dominant hillslopes types with different hydrogeological properties by applying the proposed interpretation framework (i.e. τ_{hit} and τ_{leave} concept). First, synthetic hillslope studies could be conducted and the impact of different transit time distributions derived by lumped parameter modeling on apparent and actual denitrification be determined. The nitrate input chronicle could be assumed to be uniform or with a simplified shape. These investigations could deliver a general understanding of the interaction between flow structures and reactivity at the hillslope

scale. Afterwards, the complexity regarding the shape of the hillslope, groundwater flow structures and the history of nitrate inputs to the aquifer could be increased step by step to gain more realistic denitrification estimates.

Mid-term to long-term research activities could include the testing of the proposed interpretation framework at different aquifer types. Collaborations with other research groups could be initiated to exchange data and modeling results. An extensive data analysis of existing data obtained from different sites would bring complementary information on denitrification structures. Additional to the existing data, new field experiments could be designed to determine oxygen and nitrate degradation in distinct hydrogeological settings. The investigation of nitrate inputs to the aquifer represents an additional research question. To reconstruct the full nitrate history for the research site enough data points with different groundwater ages have to be available. Land use information and fertilizer application should be analyzed and appended to the study to set-up an appropriate scale for the estimation of nitrate inputs and to verify determined nitrate inputs to the aquifer.

Regarding field experiments, the study could be extended with other proxies for autotrophic and heterotrophic denitrification (nitrate, oxygen, sulfate, and carbon stable isotopes). Strong signals on one or the other denitrification process (autotrophic or heterotrophic) could verify the τ_{leave} and τ_{hit} concept.

In addition to field experiments, laboratory experiments could be performed to gain further knowledge on heterotrophic as well as autotrophic denitrification and to inform the modeling approach. Controlled conditions, e.g. information of the geological substrate (pyrite content, initial $\delta^{34}S$ value), initial $\delta^{15}N$ value, and flow velocities, would give constraints on the use of stable isotopes as tracers for denitrification processes.

Long-term research activities could then be focused on the upscaling of characteristic hillslope denitrification to a regional scale, e.g. Europe. This would include the partitioning of a regional area in hillslopes and defining characteristic hillslopes in this area. An additional validation strategy has to be developed to use the right number of characteristic hillslopes and their denitrification estimates.

General Conclusion

Nitrate is the main groundwater pollutant in agricultural areas, affecting human as well as ecosystem wellbeing. Denitrification is a natural removal process that reduces nitrate to N_2O and N_2, if conditions for denitrification are given, e.g. absence of oxygen, microbes capable for denitrification and the availability of electron donors. Denitrification at the catchment scale poses a specific challenge, because of its high spatial variability. Complex groundwater flow structures as well as biogeochemical activity are controlling nitrate degradation. Both factors are difficult to measure sufficient at the catchment scale to evaluate N-applications due to extensive fertilization on groundwater quality.

The herein developed data- and modeling-driven approach uses easily accessible well data (O_2, NO_3^-, N_2, and CFC-12) and a time-based modeling approach to gain a general process understanding on denitrification in aquifers. The model was informed by collected data from 16 wells located in an agricultural study area of 76 km^2 at three sampling dates (Appendix B).

The general methodology presented in chapter 2 is based on a time-based modeling approach. Tracer concentrations in a well are derived by convoluting the uniformly distributed input concentration over the capture zone of the well with the corresponding transit time distribution. Transit time distributions inherently contain information about flow structures, storage and water origin and can be derived by explicit solutions of groundwater flow and transport or simplified models (lumped parameter models). Primarily, the approach is used to derive characteristic reaction times for oxygen and nitrate reduction to develop a new conceptual framework to interpret denitrification activity in aquifers.

Chapter 3 presents groundwater flow structures in the crystalline unconfined aquifer. A three-dimensional groundwater flow model was set-up with FEFLOW and the implemented particle tracking method used to derive transit time distributions for each of the wells. The model was calibrated against the baseflow at the catchment outlet and measured CFC-12 data. Results show that groundwater stays highly local with quite large groundwater ages (mean groundwater age of around 40 y). Furthermore, it has been shown that groundwater travel distances are correlated with surface water distances depending on the location of the groundwater table. The ratio of groundwater and surface water travel distances described by the index $r_{GW\text{-}LOCAL}$ seems to be a promising tool to derive information on groundwater circulation just from topographical gradients in unconfined aquifers. The index $r_{GW\text{-}LOCAL}$ should be evaluated on other study sites, where groundwater flow models already exist.

In chapter 4, historical nitrate inputs to the aquifer are estimated by using the methodology presented in chapter 2 and the derived information on groundwater flow structures in chapter 3. For the investigation of nitrate degradation processes it is necessary to know nitrate inputs to the system and to evaluate historical variations on nitrate contamination in groundwater. Tracer information, like CFC-12, NO_3^- and dissolved N_2, were used to inform the model and to reconstruct the nitrate input chronicle specific for the study area. A comparison to an existing nitrate input chronicle determined for the scale of Brittany shows a similar shape, but in general lower concentrations than derived for the Pleine-Fougères aquifer. This part of the work seems an interesting starting point for further investigations of nitrate inputs at the study site and also other scales.

Chapter 5 is dedicated to denitrification processes occurring in the crystalline unconfined aquifer. Observed characteristic denitrification times are derived by the modeling approach presented in chapter 2 and tracer measurements of CFC-12, O_2, NO_3^-, and N_2. Denitrification is highly spatially variable, like in several other study sites. Actual reaction times strongly depend on the availability of electron donors that can be either surface-derived or of lithological origin which leads to the development of a new conceptual framework to interpret observed reaction times in terms of actual reaction time and the time to hit or to leave the reactive zone. Results reveal that estimates on groundwater resilience strongly depend on the chosen concept, and that applying the classic concept based on continuous reactions along the flow line can lead to over- or underestimations of actual denitrification. The developed conceptual model is applicable to shallow aquifers and can be used to investigate actual denitrification in other hydrogeological settings. It's a computational and cost-effective method to gain an extensive knowledge on actual nitrate reduction in the aquifer of interest.

The here presented work uses point-wise derived data with a time based modeling approach to gain a general understanding on denitrification processes in unconfined aquifers. Data of a crystalline aquifer is used to set-up the methodology and derive to a comprehensive knowledge on groundwater flow and reactivity that define together the degradation capacity of the aquifer. The used tools and developed interpretation framework are applicable to other locations and should be verified in other hydrogeological settings to get better information on actual denitrification rates in the aquifer. With the proposed general interpretation framework regional groundwater denitrification and nitrate legacy can be assessed.

Appendix

Appendix A: Correlations between land use, O_2, NO_3^-, N_2 excess, and $\delta^{15}N$

Tab. A.1: Correlations between land use, O2, NO3-, N2 excess and δ15N [a]

	Pasture	Row crops	Forest	O_2	NO_3^-	N_2 excess
Pasture						
Row crops	0.14					
Forest	0.14	0.05				
O_2	-0.28	0.18	-0.04			
NO_3^-	-0.04	0.02	-0.03	0.79***		
N_2 excess	0.38	0.07	0.04	-0.65**	-0.42	
$\delta^{15}N$	0.12	-0.19	0.21	-0.69**	-0.53*	0.57*

[a] Strength of relationship was determined by Pearson product-moment correlation

* $p < 0.05$.

** $p < 0.01$.

*** $p < 0.001$.

Note: Land use types were sampled in the capture zone of each well. Sampling was performed on a yearly basis (from 1993 to 2013) with a regular grid. The extracted land use types for each well are shown in Appendix B. The percentages of pasture, row crops, and forest area in regard of the capture zone were correlated with O_2, NO_3^-, N_2 excess and $\delta^{15}N$.

Appendix B: Presentation of wells

All well characteristics are summarized for each of the 16 wells. The location is shown by a google maps image. Geological information are taken from Bogdanoff et al. (1997). Topographical information are given by a digital elevation model with a resolution of 2 m. Land use information from 1993 - 2013 are obtained from the LTER Zone Atelier, UMR Costel, Université Rennes 2. Land use types are regularly sampled in the capture zone of the well and the percentages of each group over the overall sample displayed. Groundwater samples were taken at three different dates (December 2014, March 2015, and October 2015) and CFC-12, O_2, NO_3^-, SO_4 concentrations as well as stable isotopes $\delta^{18}O$, $\delta^{15}N$, $\delta^{34}S$ measured and N_2 excess determined. The CFC-12 age reported is derived from CFC-12 measurements using a piston flow hypothesis. Groundwater table elevations are displayed based on the reference model presented in chapter 3. A well log shows the depth of the well and the calibrated screened part, which represents the depth of water arrivals. Virtual flow lines arriving at the full well length are presented (independent on the calibrated screened interval). Based on the sampled flow lines, transit time distributions are derived. Virtual sampling (from -5 m depth to -60 m depth) allowed to show the relation of transit times with depth. Oxygen and nitrate concentration distributions are displayed.

ID 1 (Coubertiere, F39) - Field Data

Location: lat: 48.470666, long: -1.617276

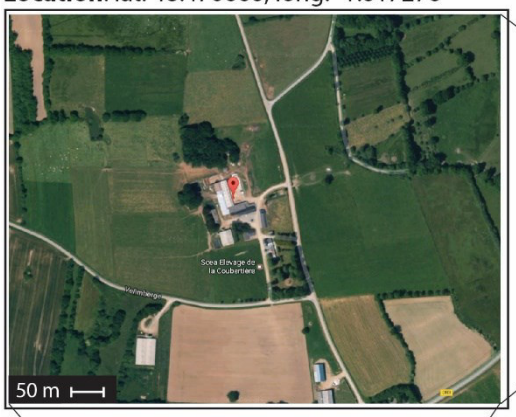

Topography

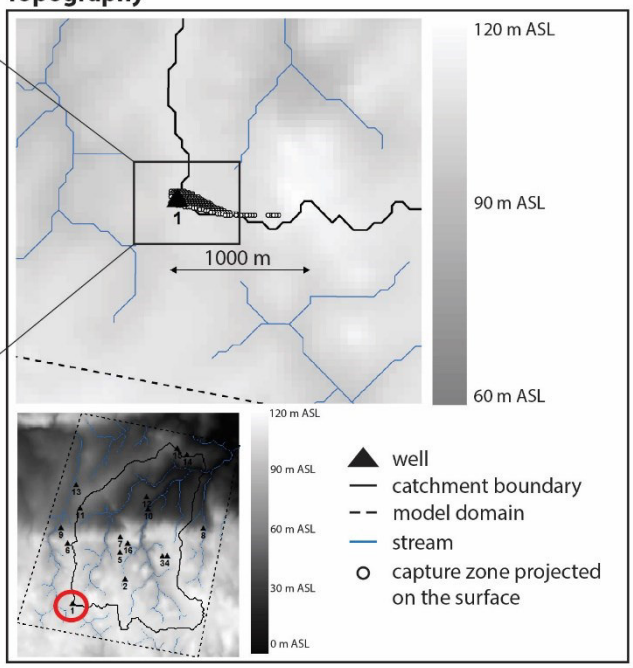

Geology

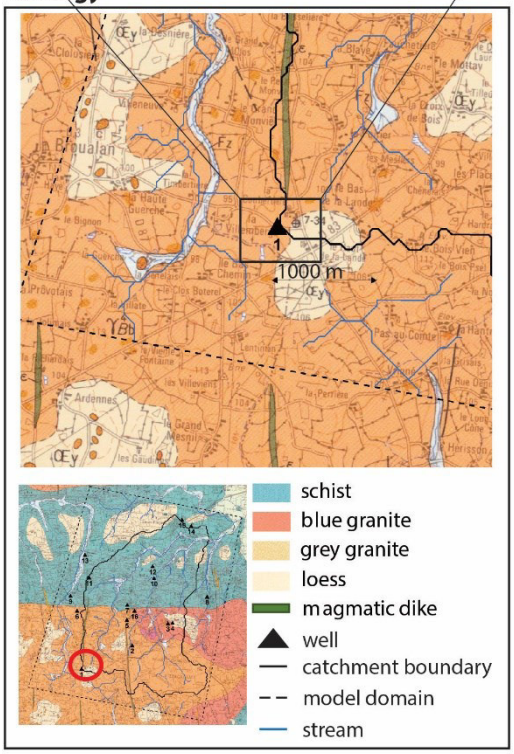

Land use

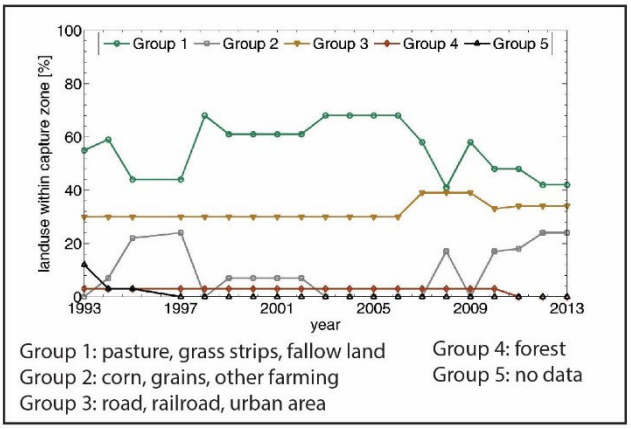

Group 1: pasture, grass strips, fallow land
Group 2: corn, grains, other farming
Group 3: road, railroad, urban area
Group 4: forest
Group 5: no data

Field data

	Dec-2014	Mar-2015	Oct-2015	Model
CFC-12 [pptv]	398	252	337	256
CFC-12 age [y]	29	39	33	38
O_2 [mg/l]	0.3	0.7	0.1	0.3
NO_3 [mg/l]	23.6	26.1	26.6	21.6
$NO_{3,deg}$ [mg/l]	41.4	32.8	32.7	29.0
$NO_{3,total}$ [mg/l]	65.0	58.8	59.3	50.6
SO_4 [mg/l]	51.0	53.2	53.4	-
$\delta^{18}O$ [‰]	9.3	9.0	9.0	-
$\delta^{15}N$ [‰]	12.6	12.7	12.6	-
$\delta^{34}S$ [‰]	-2.8	-3.1	-3.0	-

ID 1 (Coubertiere, F39) - Synthesis

Groundwater table elevation

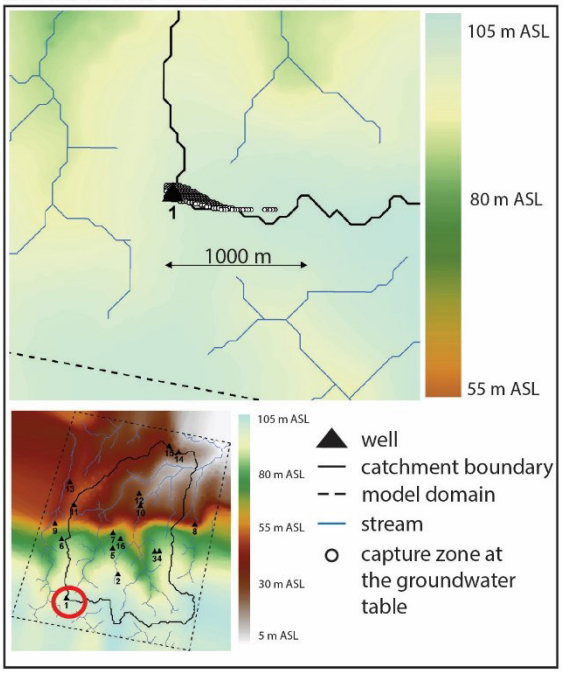

Concentration distributions

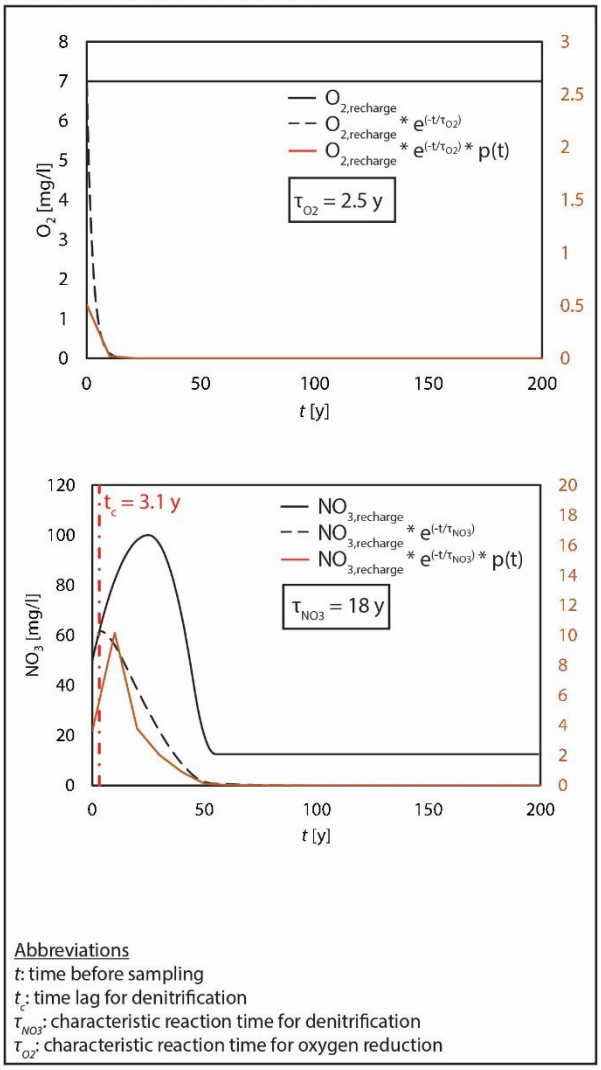

Abbreviations
t: time before sampling
t_c: time lag for denitrification
τ_{NO3}: characteristic reaction time for denitrification
τ_{O2}: characteristic reaction time for oxygen reduction

Transit time distribution

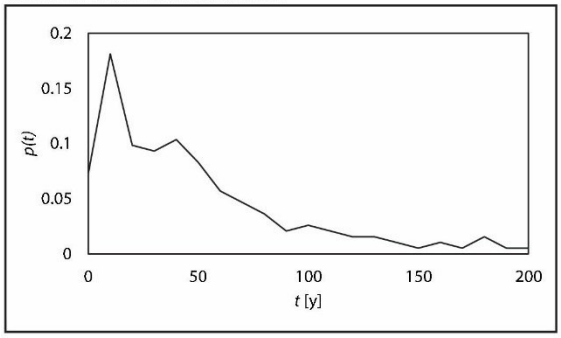

Well log

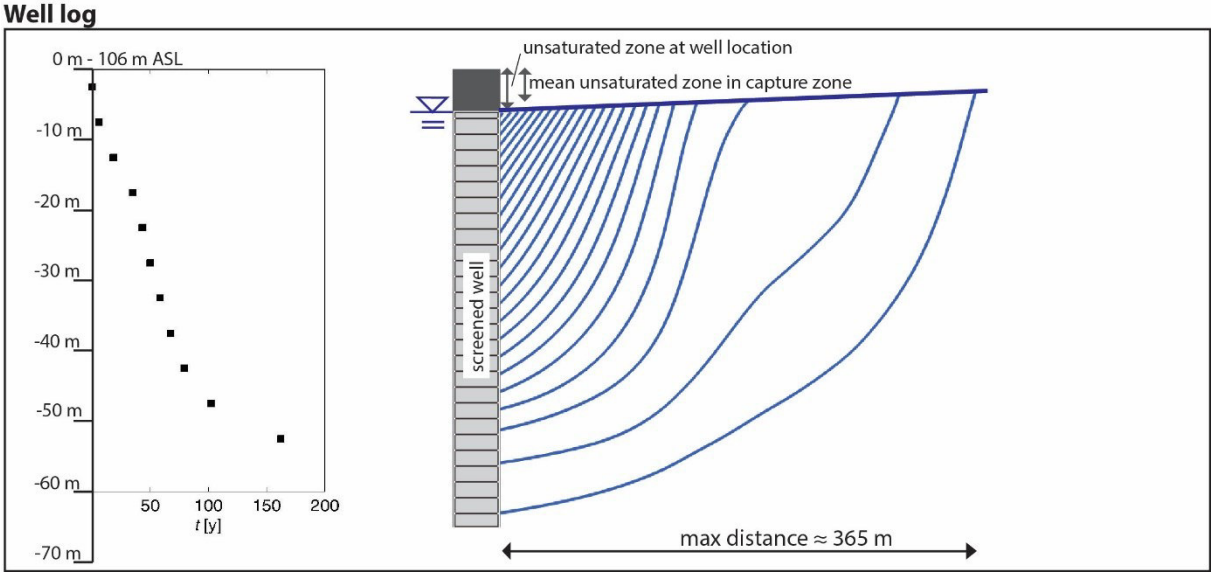

ID 2 (Ville Pican, F35) - Field Data

Location: lat: 48.48189, long: -1.58592

Topography

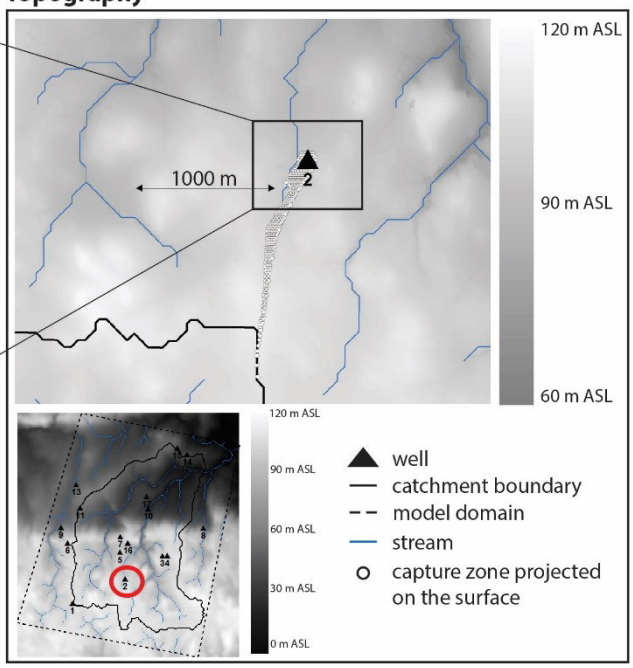

Geology

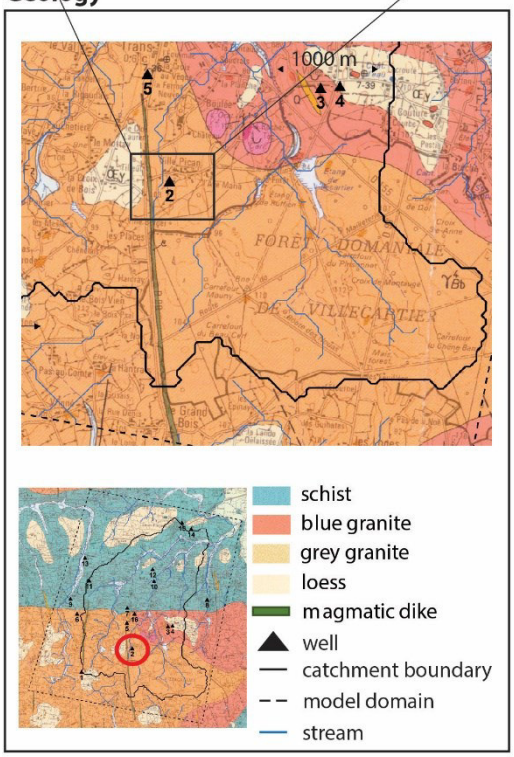

Land use

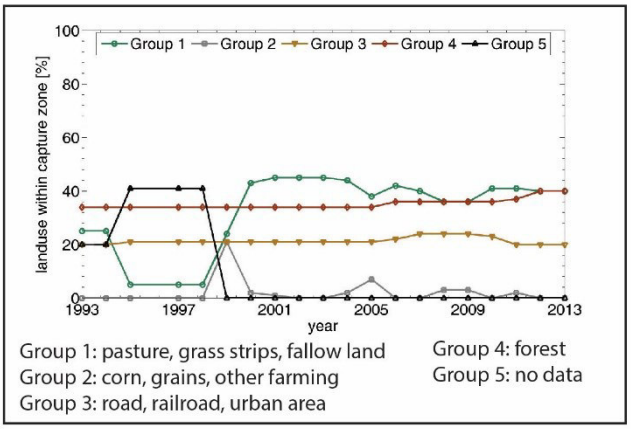

Group 1: pasture, grass strips, fallow land
Group 2: corn, grains, other farming
Group 3: road, railroad, urban area
Group 4: forest
Group 5: no data

Field data

	Dec-2014	Mar-2015	Oct-2015	Model
CFC-12 [pptv]	377	263	313	203
CFC-12 age [y]	31	38	35	41
O_2 [mg/l]	0	0	0.3	0.3
NO_3 [mg/l]	0	0	0.1	19.1
$NO_{3,deg}$ [mg/l]	10.4	10.0	8.8	21.7
$NO_{3,total}$ [mg/l]	10.4	10.0	8.9	40.8
SO_4 [mg/l]	11.5	12.4	10.7	-
$\delta^{18}O$ [‰]	17.0	13.7	14.7	-
$\delta^{15}N$ [‰]	13.8	17.8	27.2	-
$\delta^{34}S$ [‰]	-2.5	-	-	-

ID 2 (Ville Pican, F35) - Synthesis

Groundwater table elevation

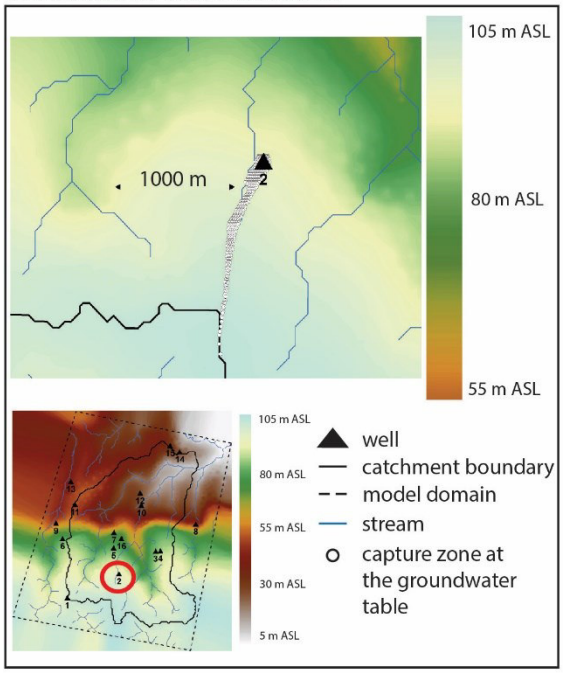

Concentration distributions

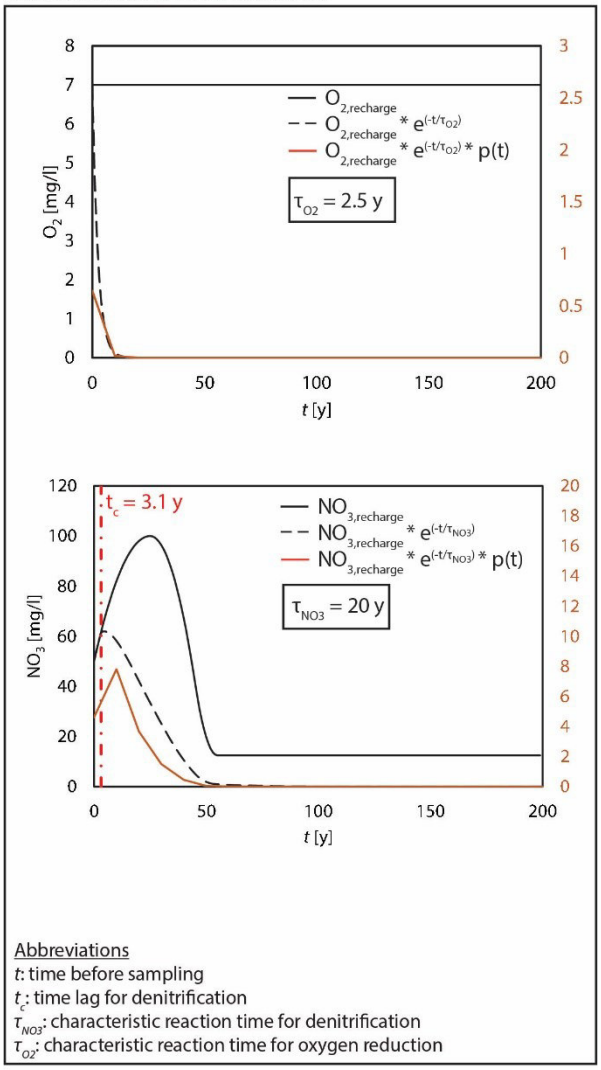

Abbreviations
t: time before sampling
t_c: time lag for denitrification
τ_{NO3}: characteristic reaction time for denitrification
τ_{O2}: characteristic reaction time for oxygen reduction

Transit time distribution

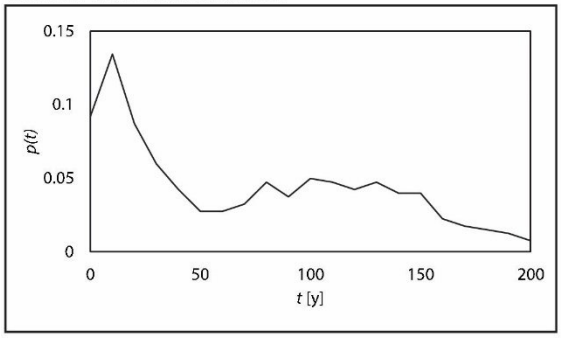

Well log

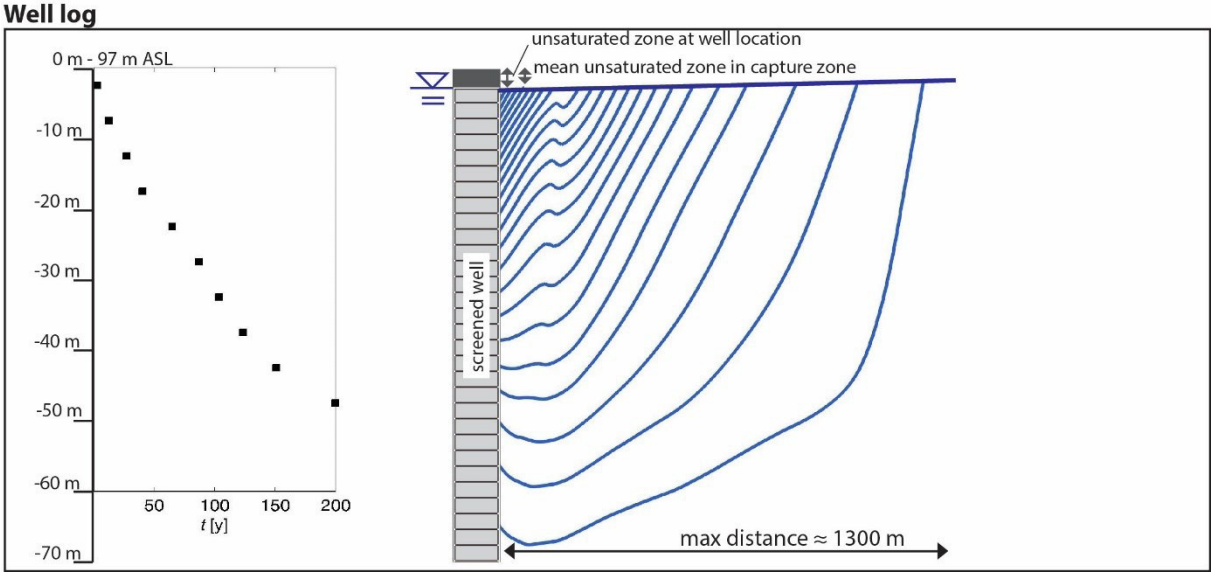

ID 3 (Villee, F99) - Field Data

Location: lat: 48.49212, long: -1.563926

Topography

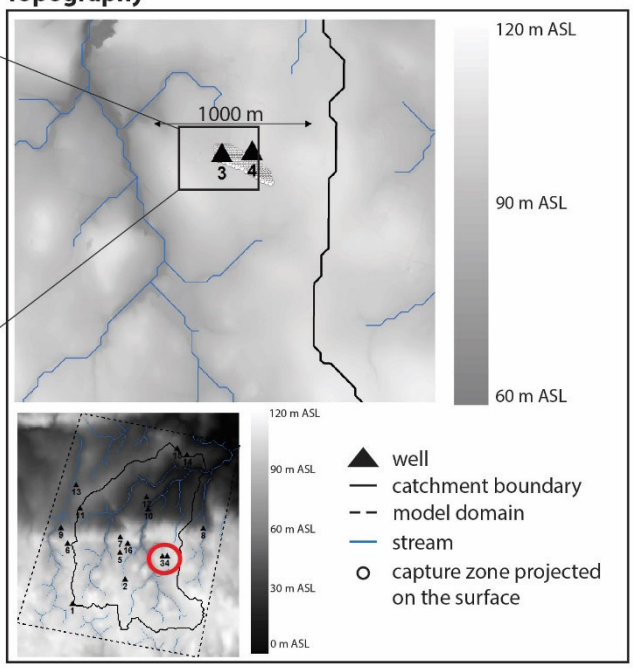

Geology

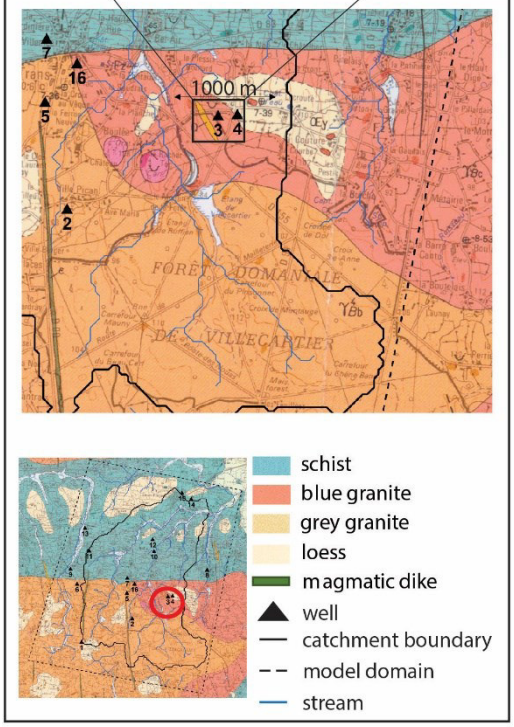

Land use

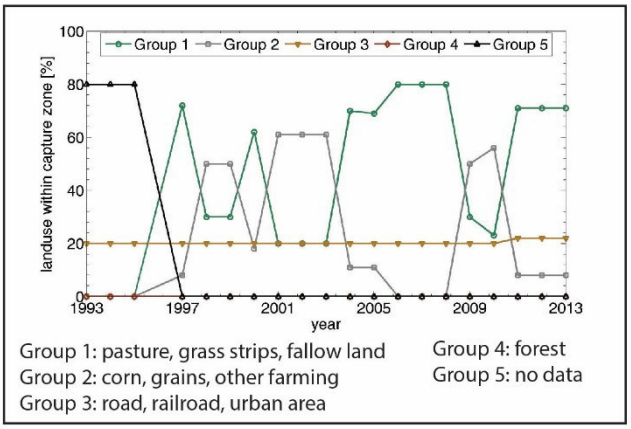

Group 1: pasture, grass strips, fallow land
Group 2: corn, grains, other farming
Group 3: road, railroad, urban area
Group 4: forest
Group 5: no data

Field data

	Dec-2014	Mar-2015	Oct-2015	Model
CFC-12 [pptv]	521	329	461	344
CFC-12 age [y]	1 or 22	33	26	33
O_2 [mg/l]	2.85	1.02	6	4.9
NO_3 [mg/l]	51.84	49.0	50.3	57.6
$NO_{3,deg}$ [mg/l]	12.3	12.6	2.9	2.1
$NO_{3,total}$ [mg/l]	64.2	61.6	53.2	59.7
SO_4 [mg/l]	35.0	35.7	34.0	-
$\delta^{18}O$ [‰]	3.4	3.1	3.4	-
$\delta^{15}N$ [‰]	7.9	7.8	7.7	-
$\delta^{34}S$ [‰]	2.6	1.3	1.9	-

ID 3 (Villee, F99) - Synthesis

Groundwater table elevation

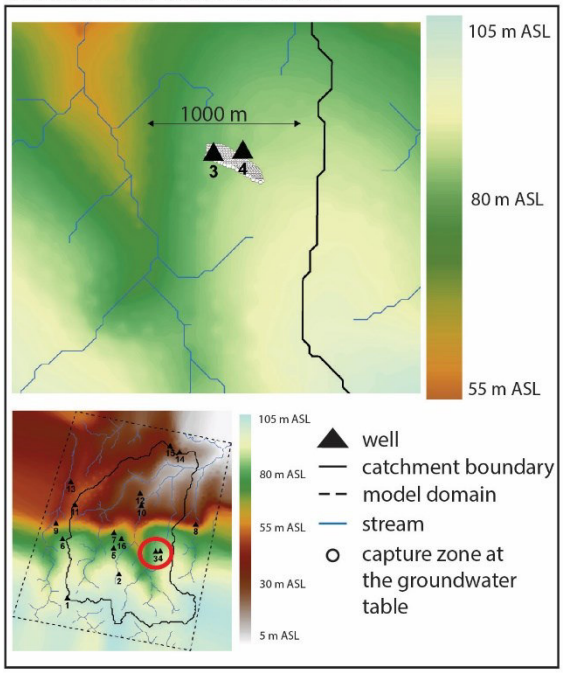

Concentration distributions

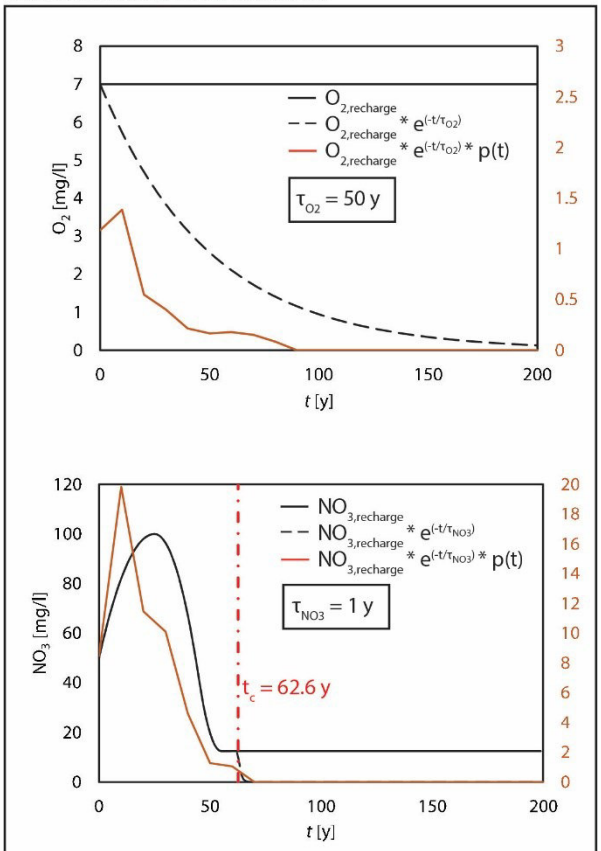

Abbreviations
t: time before sampling
t_c: time lag for denitrification
τ_{NO3}: characteristic reaction time for denitrification
τ_{O2}: characteristic reaction time for oxygen reduction

Transit time distribution

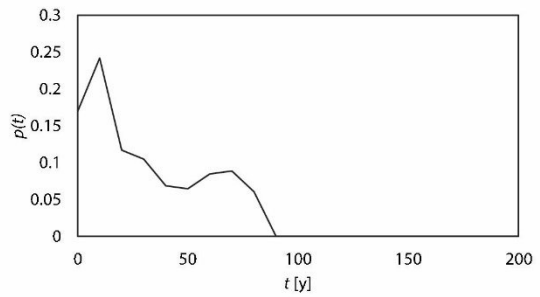

Well log

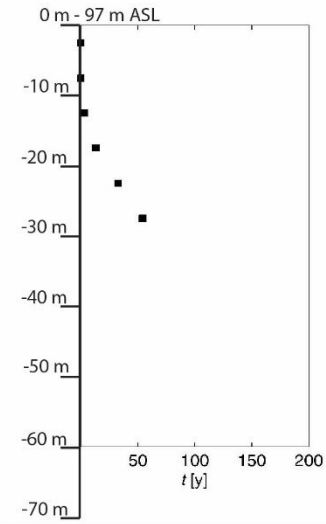

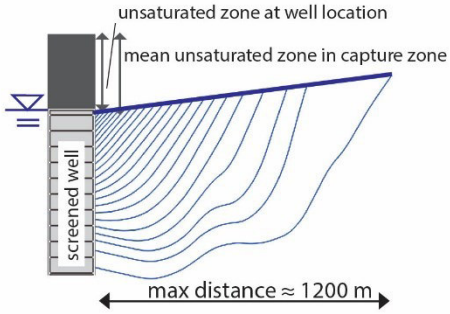

ID 4 (Chalerie, F23) - Field Data

Location: lat: 48.492388, long: -1.561016

Topography

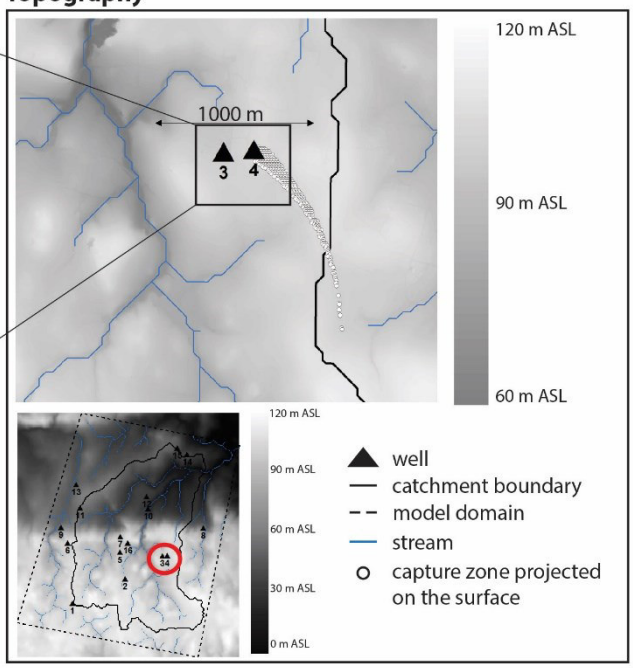

Geology

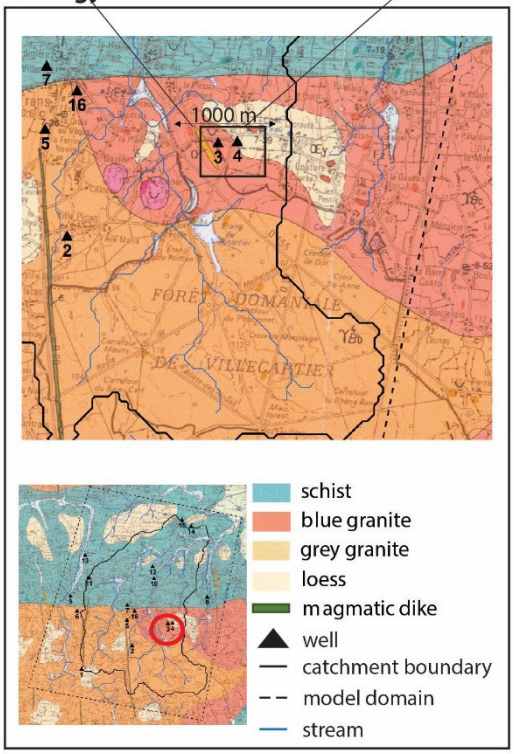

Land use

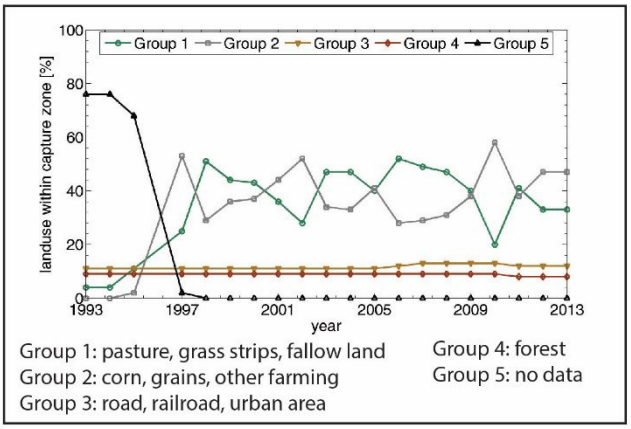

Group 1: pasture, grass strips, fallow land
Group 2: corn, grains, other farming
Group 3: road, railroad, urban area
Group 4: forest
Group 5: no data

Field data

	Dec-2014	Mar-2015	Oct-2015	Model
CFC-12 [pptv]	193	107	141	168
CFC-12 age [y]	41	47	44	43
O_2 [mg/l]	3.3	0	0.3	0.4
NO_3 [mg/l]	0.3	0.1	0	8.5
$NO_{3,deg}$ [mg/l]	23.9	35.6	37.9	30.7
$NO_{3,total}$ [mg/l]	24.2	35.7	37.9	39.2
SO_4 [mg/l]	58.1	54.2	61.9	-
$\delta^{18}O$ [‰]	25.8	10.8	19.0	-
$\delta^{15}N$ [‰]	12.4	22.3	18.2	-
$\delta^{34}S$ [‰]	-5.7	-6.3	-6.4	-

ID 4 (Chalerie, F23) - Synthesis

Groundwater table elevation

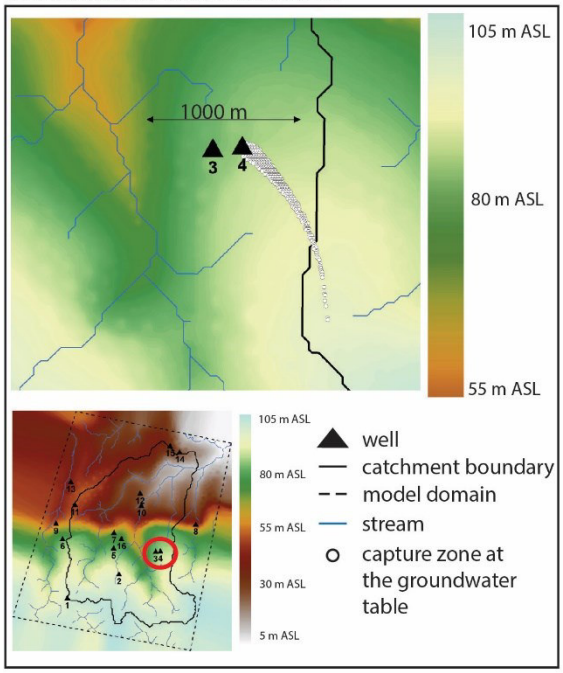

Concentration distributions

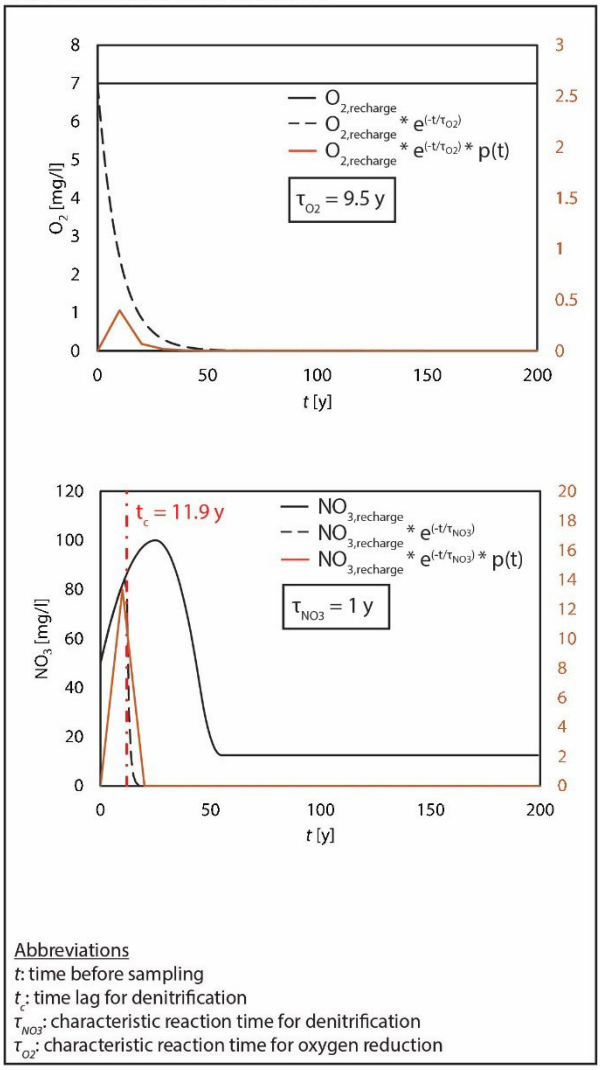

Abbreviations
t: time before sampling
t_c: time lag for denitrification
τ_{NO3}: characteristic reaction time for denitrification
τ_{O2}: characteristic reaction time for oxygen reduction

Transit time distribution

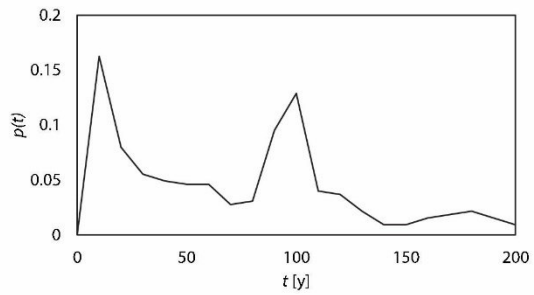

Well log

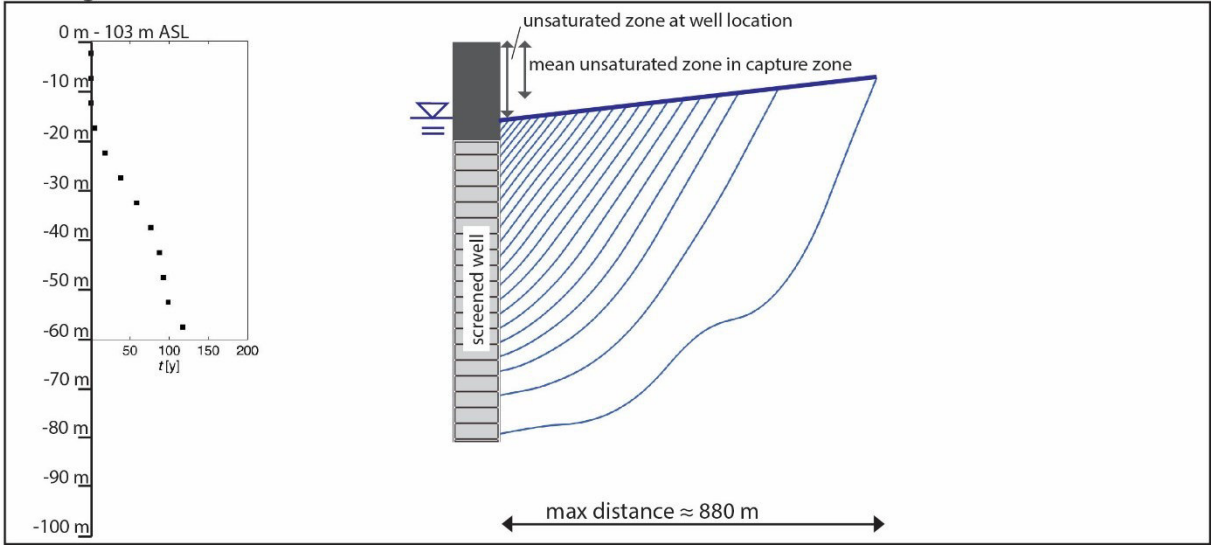

ID 5 (Croix au Veque, F49) - Field Data

Location: lat: 48.492497, long: -1.590177

Topography

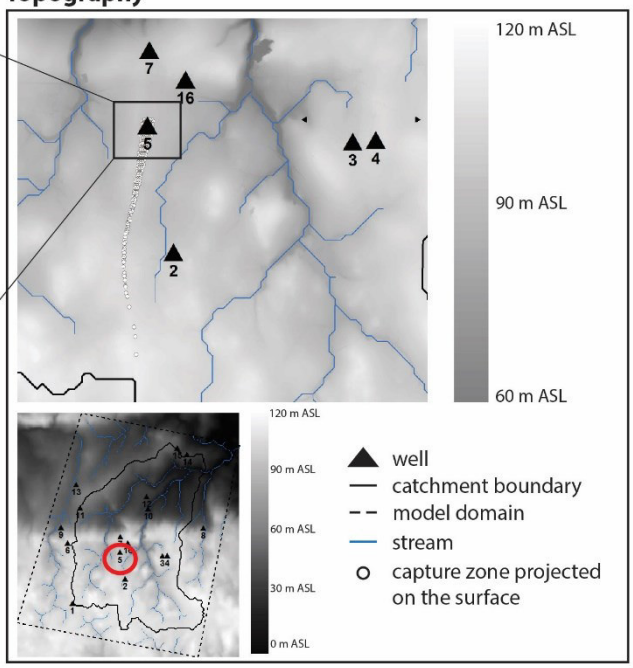

Geology

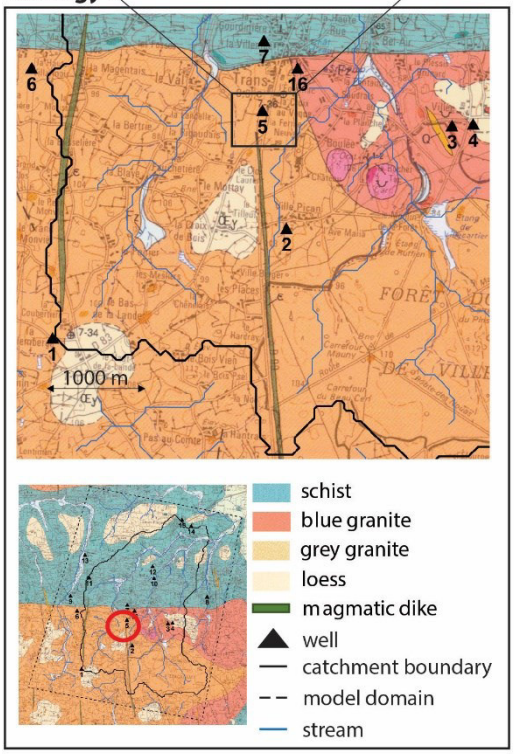

Land use

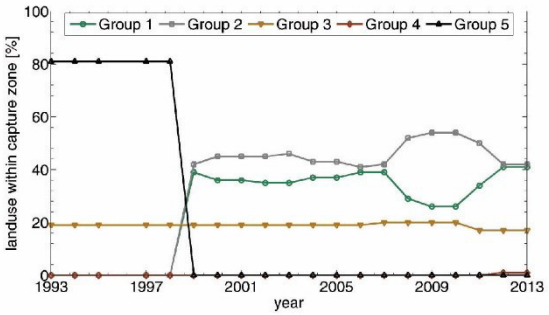

Group 1: pasture, grass strips, fallow land
Group 2: corn, grains, other farming
Group 3: road, railroad, urban area
Group 4: forest
Group 5: no data

Field data

	Dec-2014	Mar-2015	Oct-2015	Model
CFC-12 [pptv]	-	228	243	251
CFC-12 age [y]	-	40	39	39
O_2 [mg/l]	0.17	0.12	1.5	1.8
NO_3 [mg/l]	26.3	33.5	22.8	26.2
$NO_{3,deg}$ [mg/l]	29.1	23.0	40.4	19.7
$NO_{3,total}$ [mg/l]	55.4	56.5	63.2	45.9
SO_4 [mg/l]	77.3	76.6	79.6	-
$\delta^{18}O$ [‰]	4.2	4.4	4.1	-
$\delta^{15}N$ [‰]	8.6	8.8	8.9	-
$\delta^{34}S$ [‰]	-4.5	-3.8	-4.5	-

ID 5 (Croix au Veque, F49) - Synthesis

Groundwater table elevation

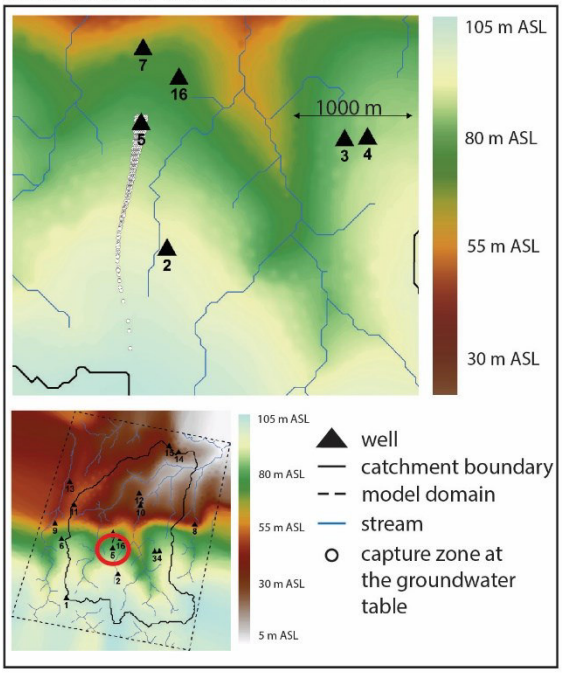

Concentration distributions

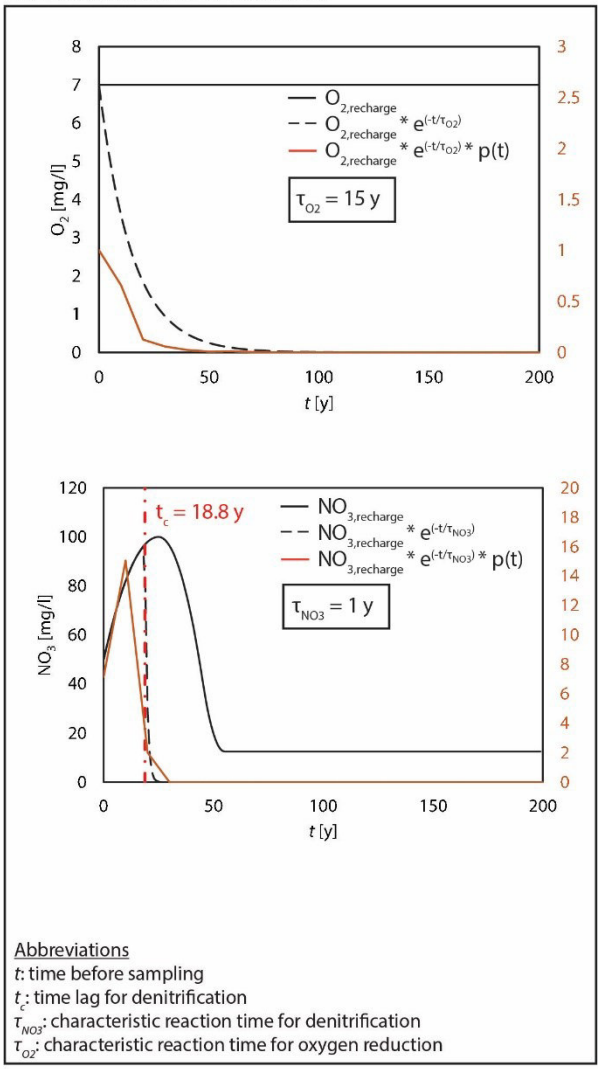

Abbreviations
t: time before sampling
t_c: time lag for denitrification
τ_{NO3}: characteristic reaction time for denitrification
τ_{O2}: characteristic reaction time for oxygen reduction

Transit time distribution

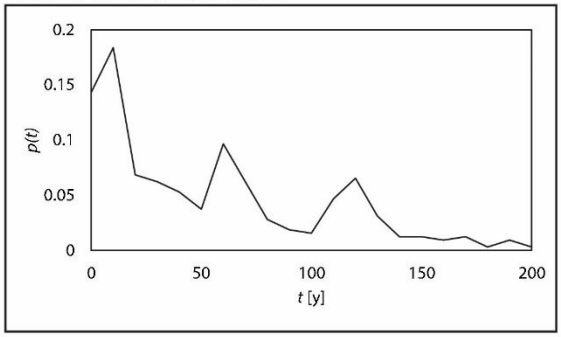

Well log

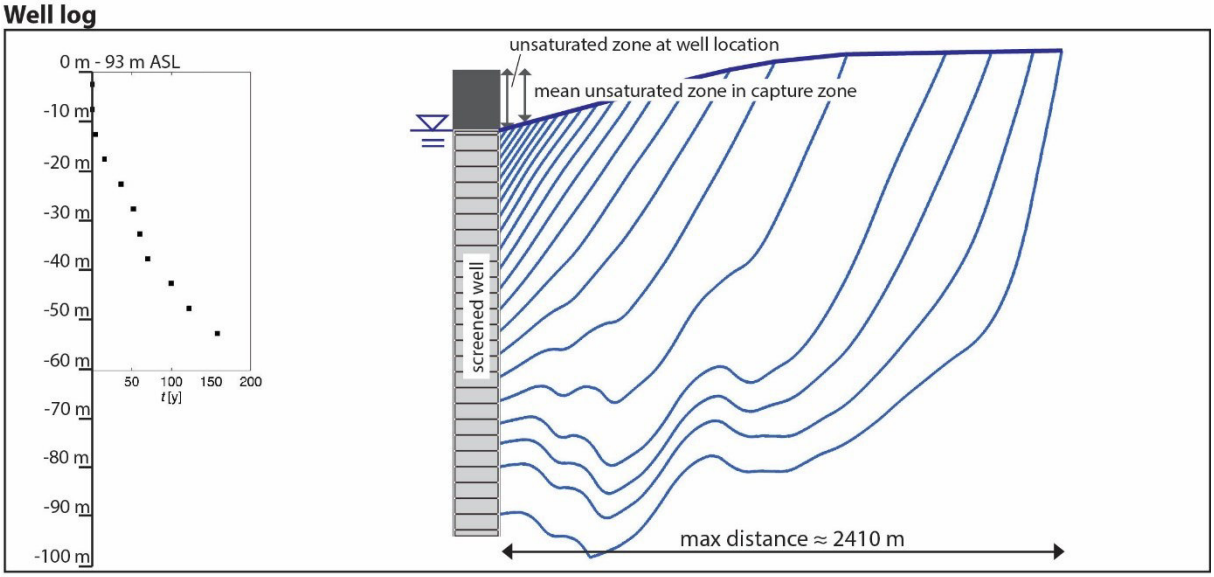

ID 6 (Haute Villarmois, F100) - Field Data

Location: lat: 48.495144, long: -1.622302

Topography

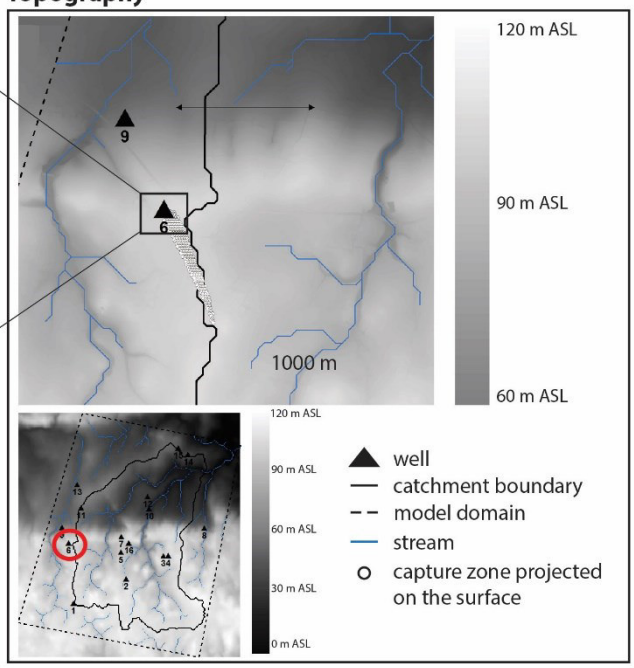

Geology

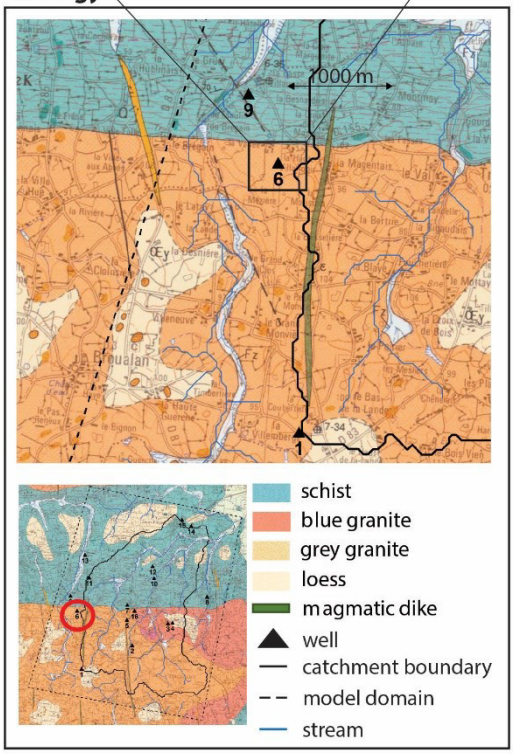

Land use

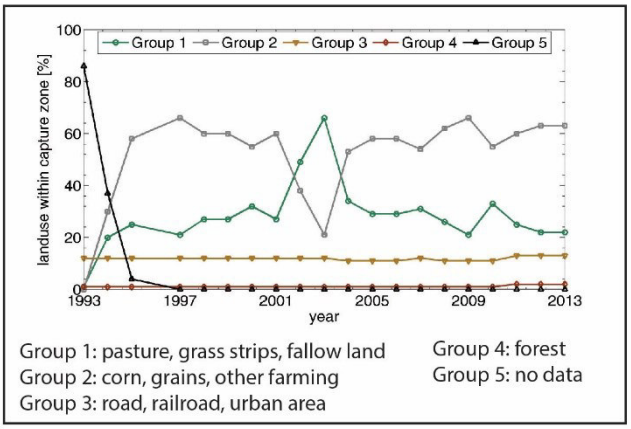

Group 1: pasture, grass strips, fallow land
Group 2: corn, grains, other farming
Group 3: road, railroad, urban area
Group 4: forest
Group 5: no data

Field data

	Dec-2014	Mar-2015	Oct-2015	Model
CFC-12 [pptv]	188	73.2	109	182
CFC-12 age [y]	42	49	46	42
O_2 [mg/l]	0	0.5	2.3	1.2
NO_3 [mg/l]	37.8	37.8	37.7	25.8
$NO_{3,deg}$ [mg/l]	27.6	30.3	27.7	16.9
$NO_{3,total}$ [mg/l]	65.3	68.1	65.4	42.7
SO_4 [mg/l]	56.5	61.1	60.0	-
$\delta^{18}O$ [‰]	9.5	9.4	9.9	-
$\delta^{15}N$ [‰]	14.2	15.2	15.9	-
$\delta^{34}S$ [‰]	4.1	3.8	3.5	-

ID 6 (Haute Villarmois, F100) - Synthesis

Groundwater table elevation

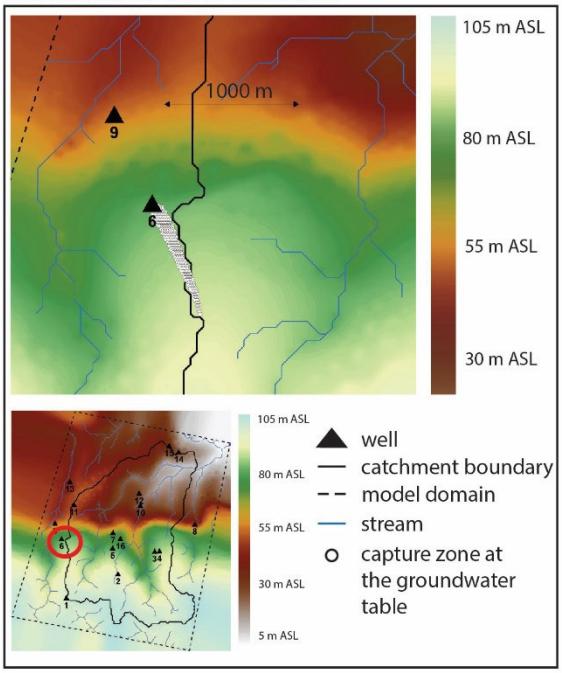

Concentration distributions

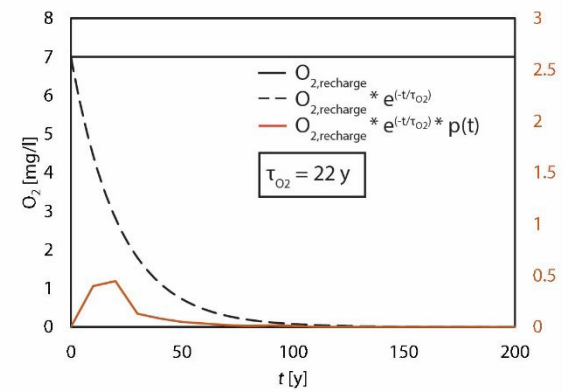

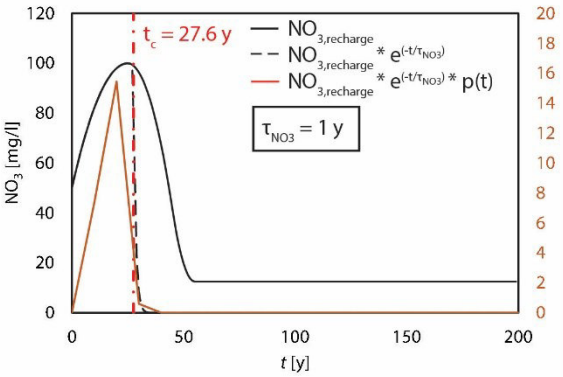

Abbreviations
t: time before sampling
t_c: time lag for denitrification
τ_{NO3}: characteristic reaction time for denitrification
τ_{O2}: characteristic reaction time for oxygen reduction

Transit time distribution

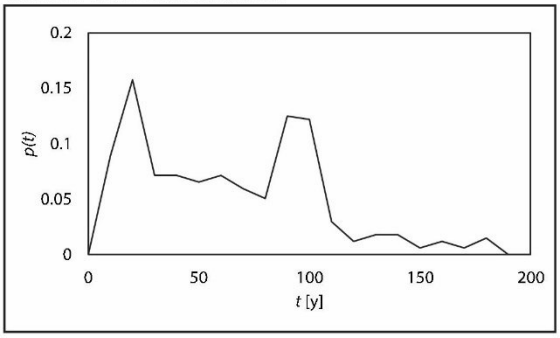

Well log

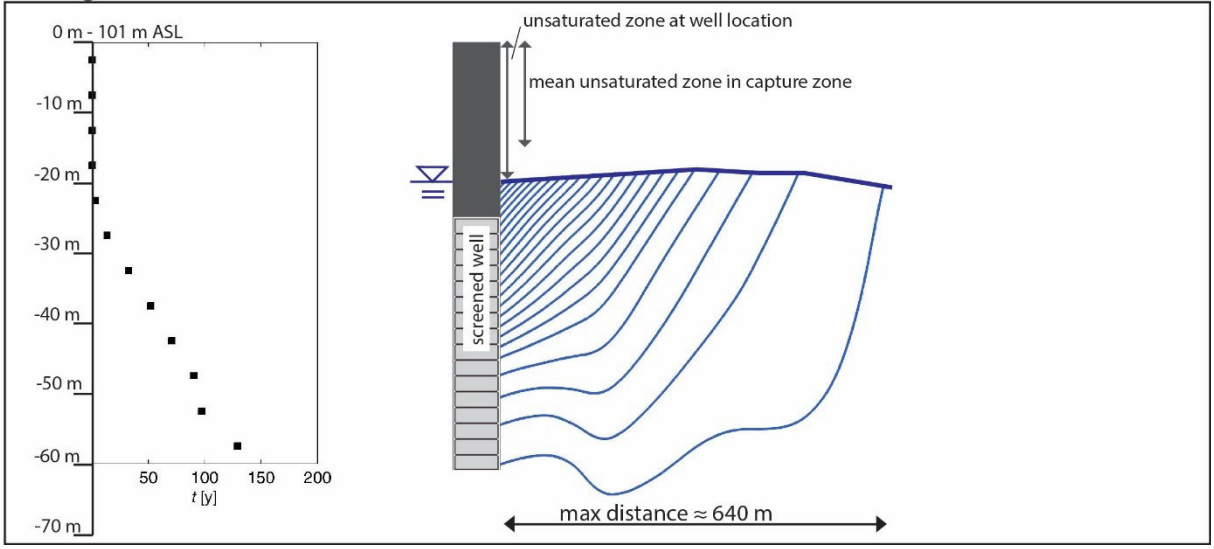

ID 7 (Gourdiniere, F103) - Field Data

Location: lat: 48.49928, long: -1.591116

Topography

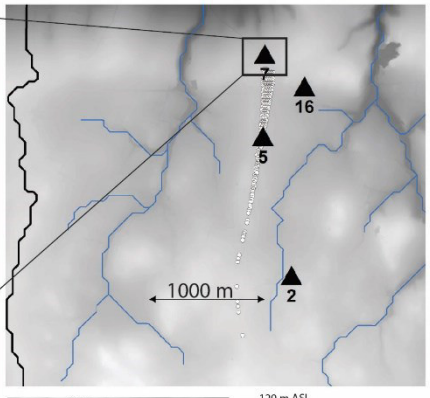

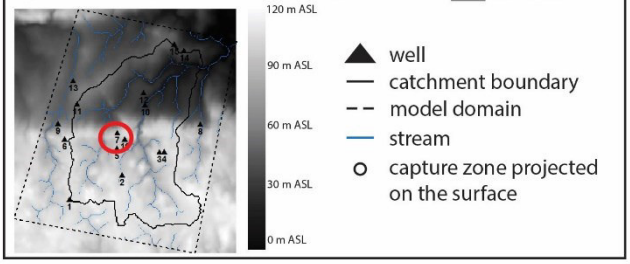

Geology

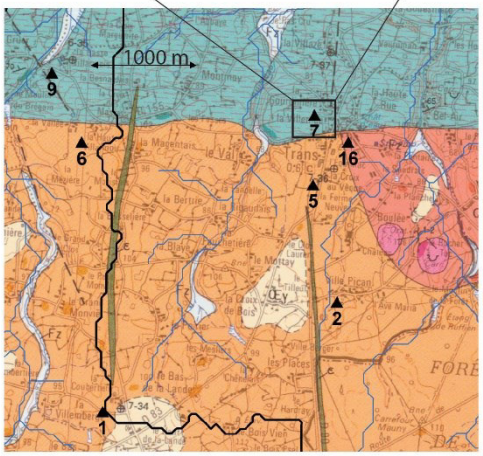

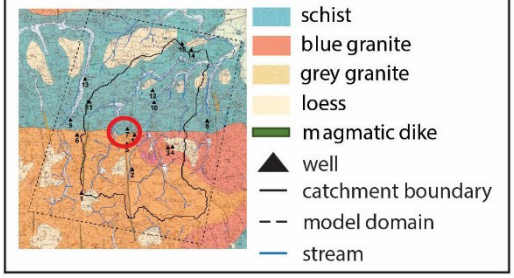

Land use

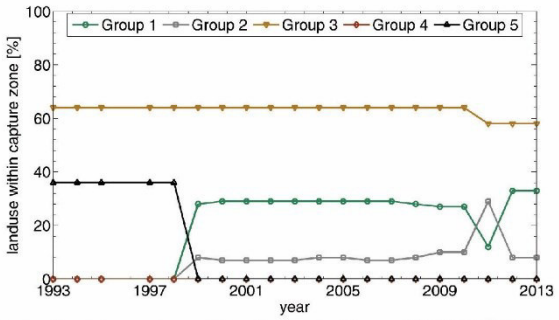

Group 1: pasture, grass strips, fallow land
Group 2: corn, grains, other farming
Group 3: road, railroad, urban area
Group 4: forest
Group 5: no data

Field data

	Dec-2014	Mar-2015	Oct-2015	Model
CFC-12 [pptv]	-	99	100	141
CFC-12 age [y]	-	47	47	44
O_2 [mg/l]	-	0	0.3	0.3
NO_3 [mg/l]	-	0	0	0.1
$NO_{3,deg}$ [mg/l]	-	53.0	46.6	40.9
$NO_{3,total}$ [mg/l]	-	53.0	46.6	41.0
SO_4 [mg/l]	-	54.9	50.5	-
$\delta^{18}O$ [‰]	-	16.7	14.4	-
$\delta^{15}N$ [‰]	-	22.4	7.3	-
$\delta^{34}S$ [‰]	-	-2.6	-2.6	-

ID 7 (Gourdiniere, F103) - Synthesis

Groundwater table elevation

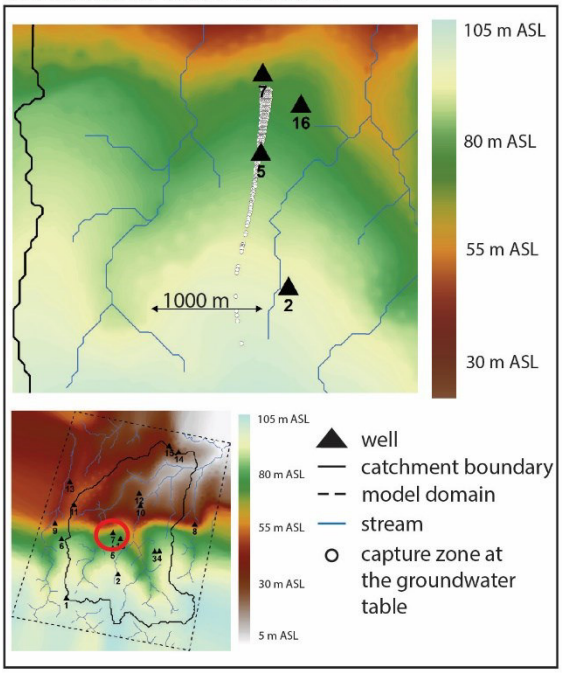

Concentration distributions

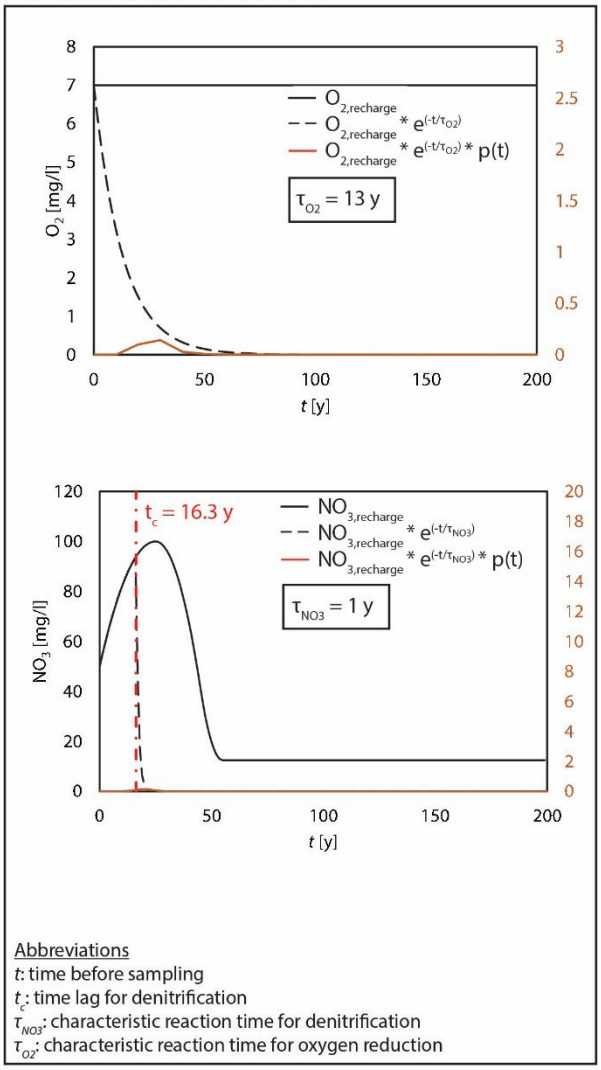

Abbreviations
t: time before sampling
t_c: time lag for denitrification
τ_{NO3}: characteristic reaction time for denitrification
τ_{O2}: characteristic reaction time for oxygen reduction

Transit time distribution

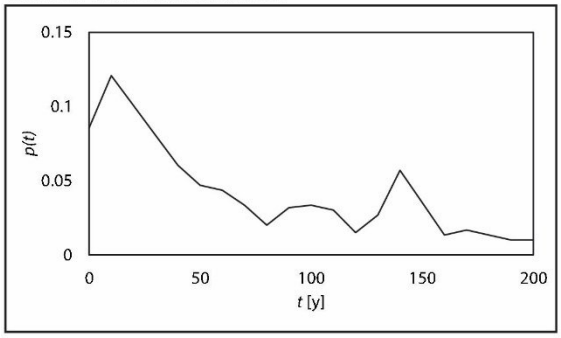

Well log

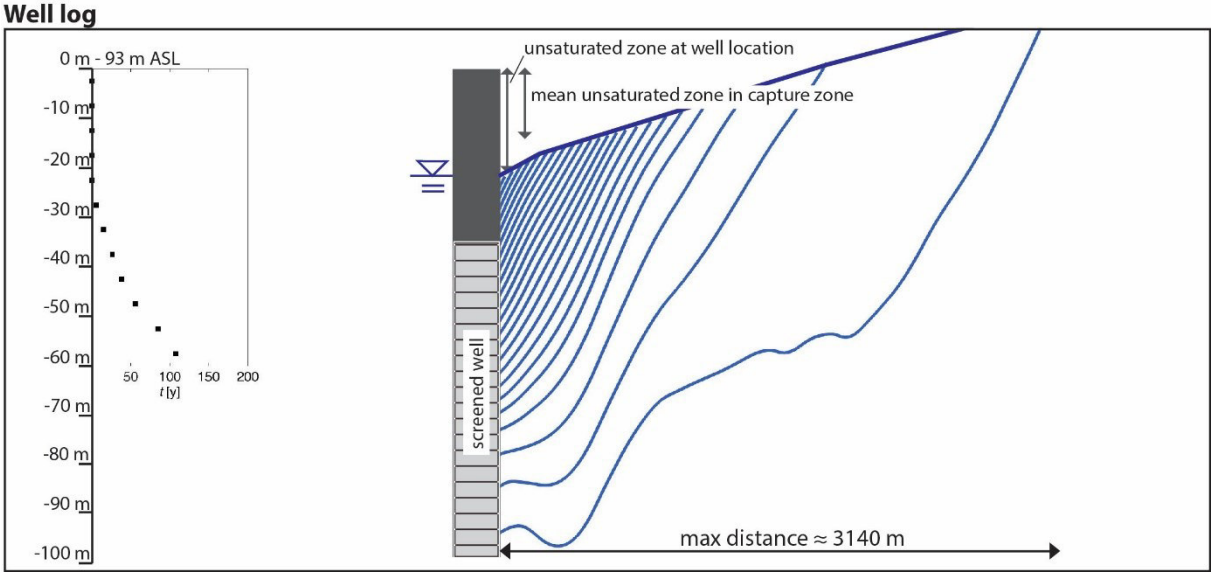

ID 8 (Maison Neuve VV, F22) - Field Data

Location: lat: 48.504358, long: -1.539936

Topography

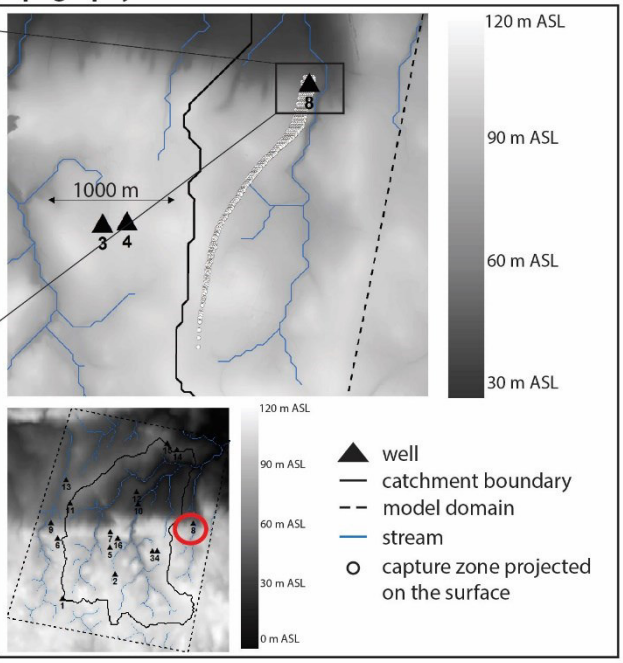

Geology

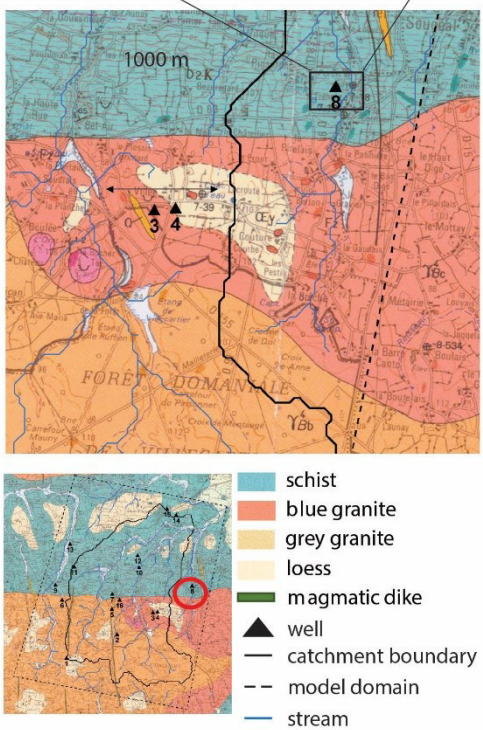

Land use

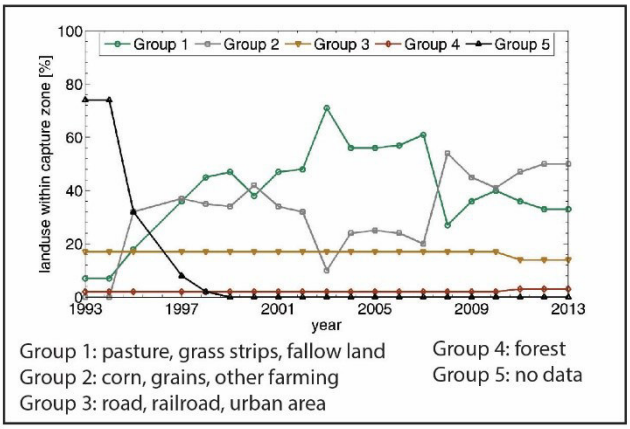

Field data

	Dec-2014	Mar-2015	Oct-2015	Model
CFC-12 [pptv]	437	262	411	212
CFC-12 age [y]	27	38	29	41
O_2 [mg/l]	2.0	1.8	6	2.7
NO_3 [mg/l]	63.6	63.6	68.2	37.8
$NO_{3,deg}$ [mg/l]	19.4	17.1	16.5	5.8
$NO_{3,total}$ [mg/l]	83.0	80.7	84.7	43.6
SO_4 [mg/l]	21.5	22.3	20.4	-
$\delta^{18}O$ [‰]	3.5	2.5	3.6	-
$\delta^{15}N$ [‰]	6.1	6.0	6.4	-
$\delta^{34}S$ [‰]	3.3	3.7	-	-

ID 8 (Maison Neuve VV, F22) - Synthesis

Groundwater table elevation

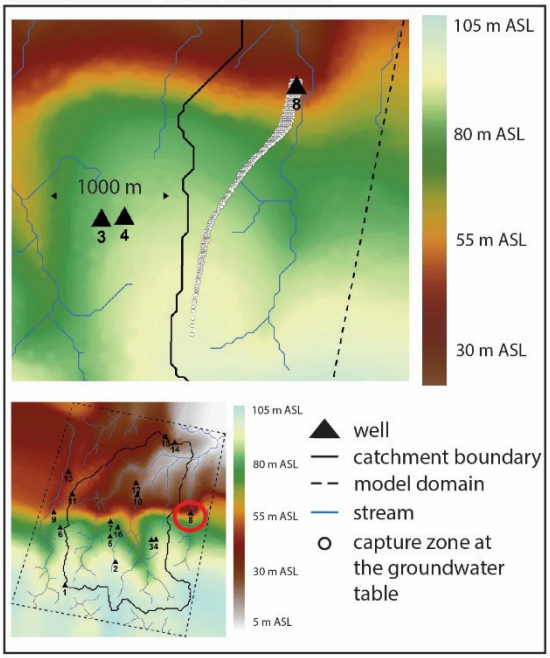

Concentration distributions

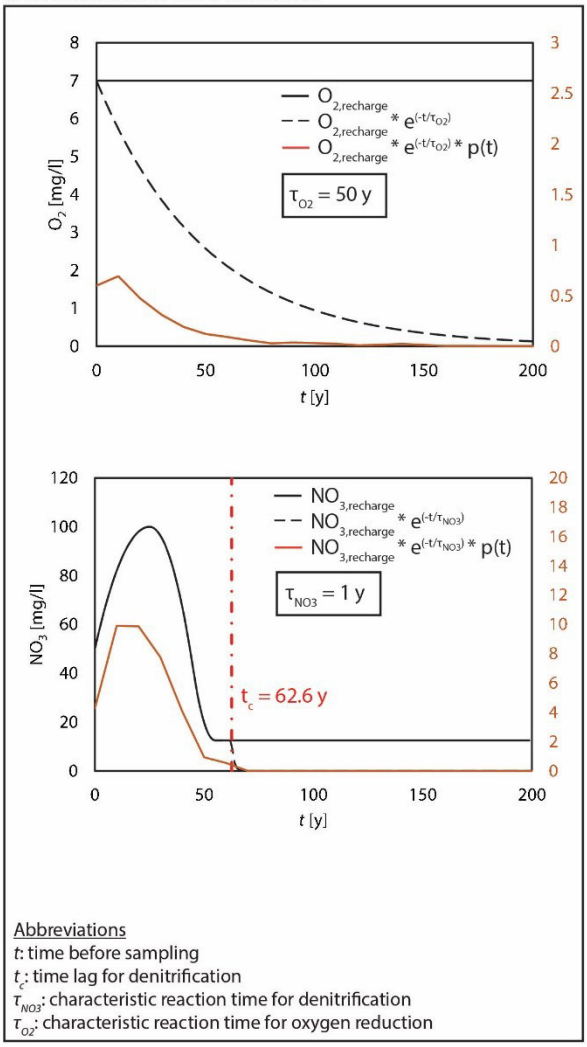

Abbreviations
t: time before sampling
t_c: time lag for denitrification
τ_{NO3}: characteristic reaction time for denitrification
τ_{O2}: characteristic reaction time for oxygen reduction

Transit time distribution

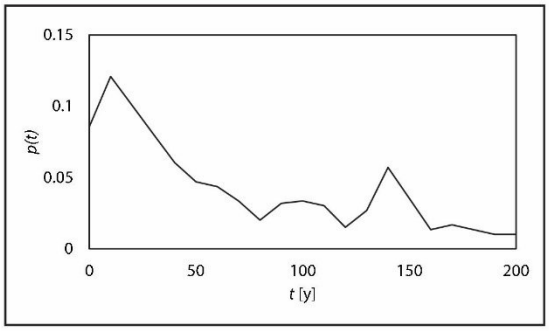

Well log

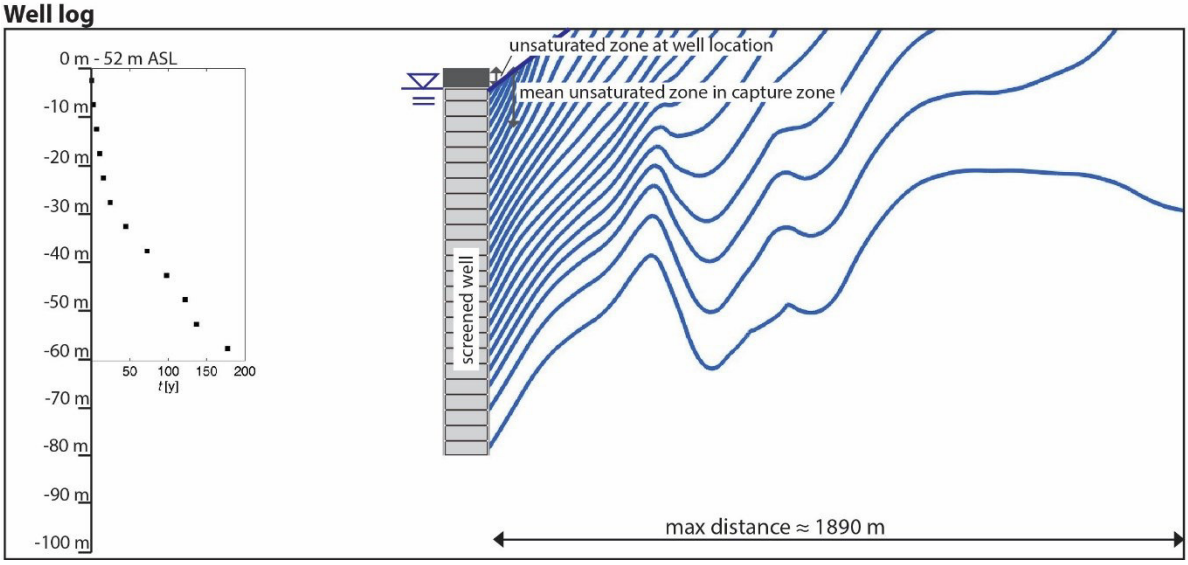

ID 9 (Basse Villarmois, F50) - Field Data

Location: lat: 48.50131, long: -1.626945

Topography

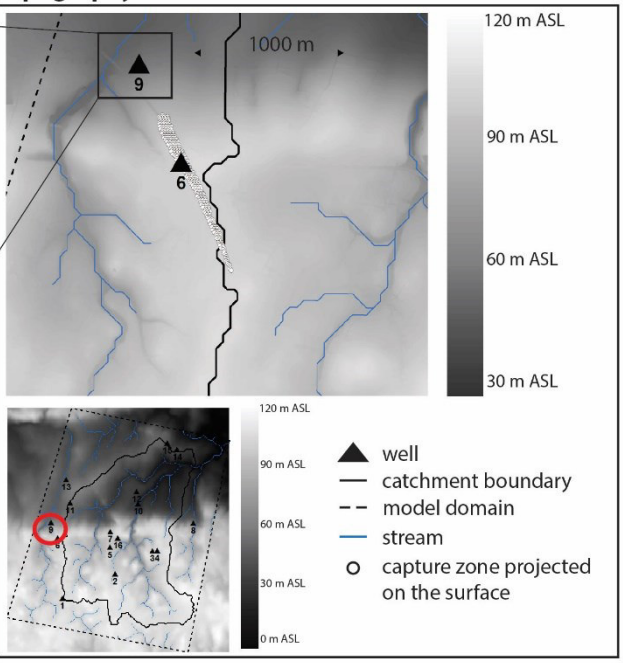

Geology

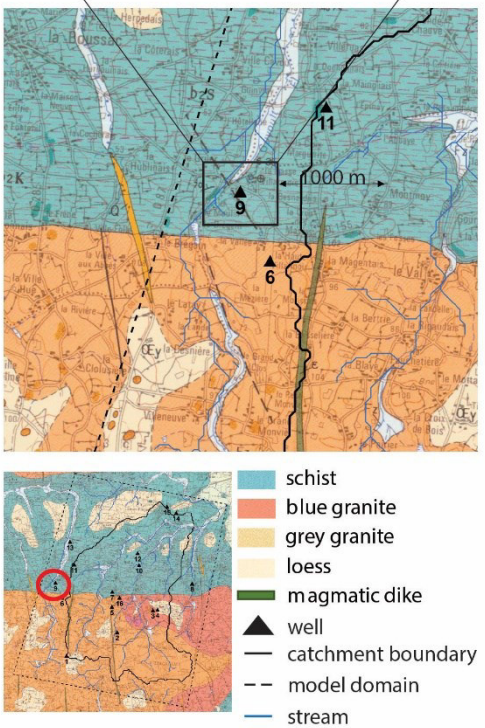

Land use

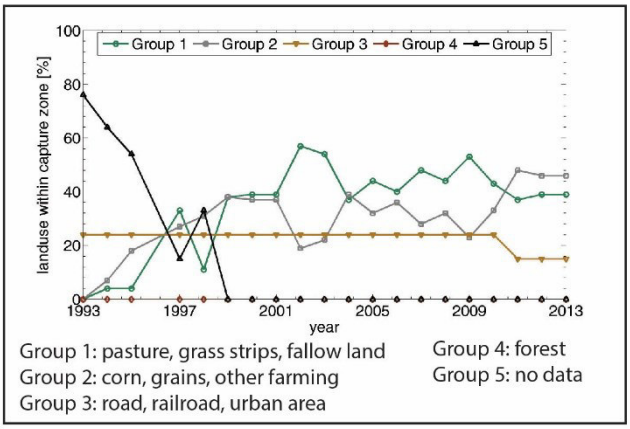

Group 1: pasture, grass strips, fallow land
Group 2: corn, grains, other farming
Group 3: road, railroad, urban area
Group 4: forest
Group 5: no data

Field data

	Dec-2014	Mar-2015	Oct-2015	Model
CFC-12 [pptv]	36	36	34	31
CFC-12 age [y]	55	55	55	56
O_2 [mg/l]	0	0	0.4	0.24
NO_3 [mg/l]	0	0	0	0.2
$NO_{3,deg}$ [mg/l]	19.2	17.8	17.5	18.3
$NO_{3,total}$ [mg/l]	19.2	17.8	17.5	18.5
SO_4 [mg/l]	35.4	36.8	35.6	-
$\delta^{18}O$ [‰]	20.9	11.5	21.2	-
$\delta^{15}N$ [‰]	17.0	6.2	19.7	-
$\delta^{34}S$ [‰]	-8.5	-8.4	-8.7	-

ID 9 (Basse Villarmois, F50) - Synthesis

Groundwater table elevation

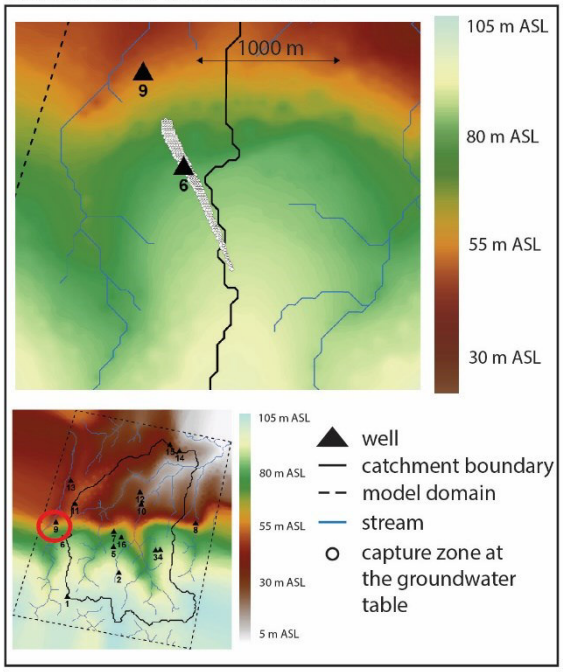

Concentration distributions

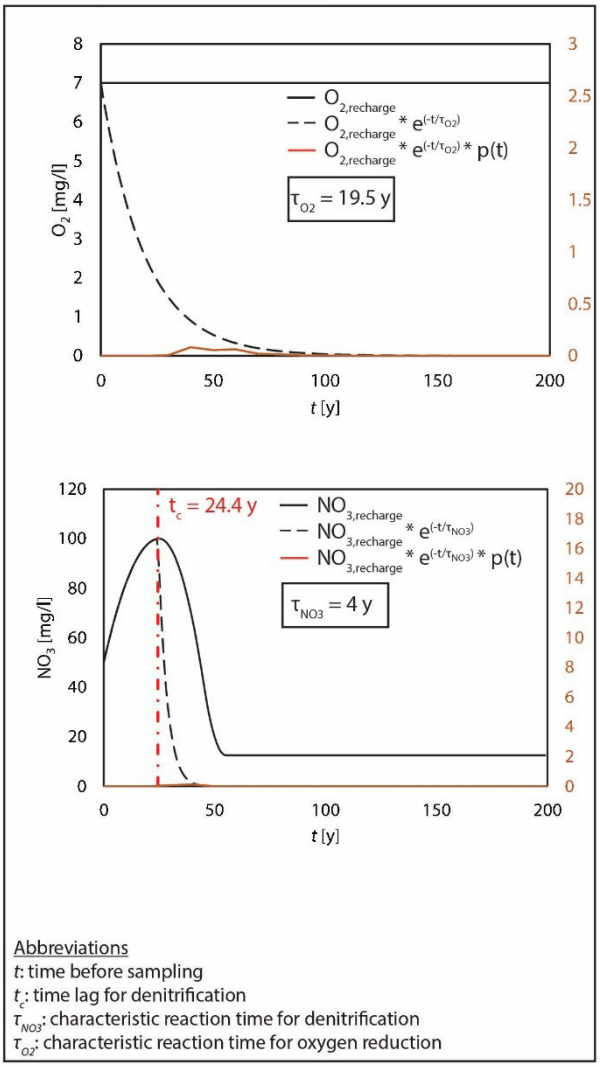

Transit time distribution

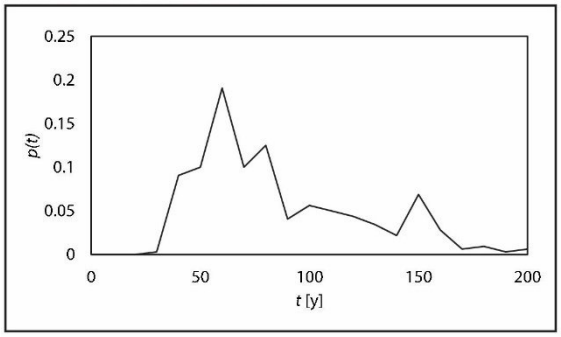

Well log

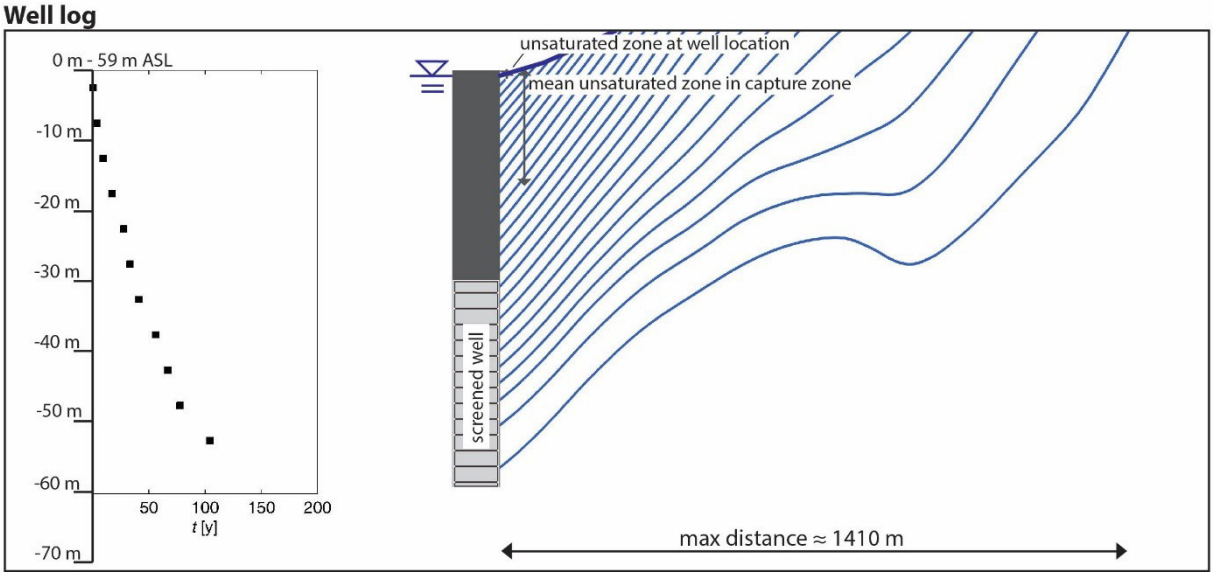

ID 10 (Launay, F54) - Field Data

Location: lat: 48.51081948, long: -1.574435

Topography

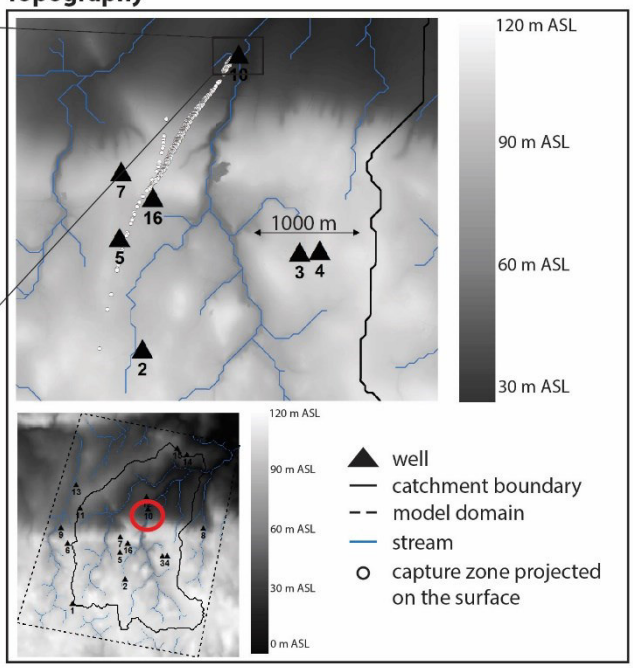

Geology

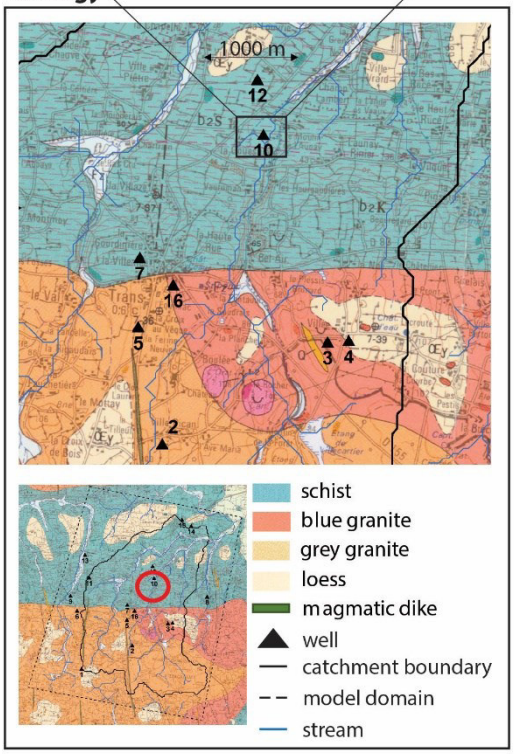

Land use

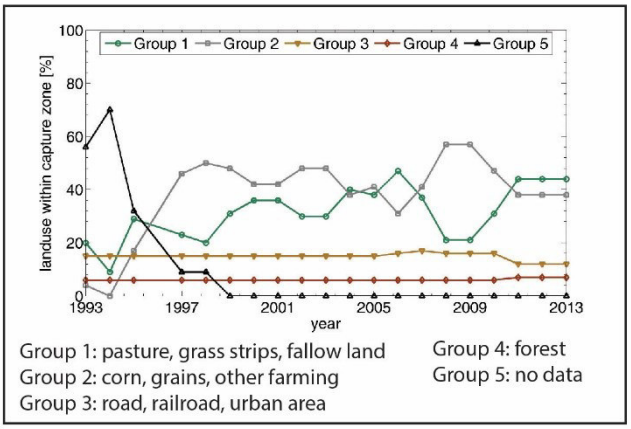

Group 1: pasture, grass strips, fallow land
Group 2: corn, grains, other farming
Group 3: road, railroad, urban area
Group 4: forest
Group 5: no data

Field data

	Dec-2014	Mar-2015	Oct-2015	Model
CFC-12 [pptv]	465	92	33	82
CFC-12 age [y]	26	48	55	49
O_2 [mg/l]	2.5	4.3	0.1	1.6
NO_3 [mg/l]	0	0	0	12.6
$NO_{3,deg}$ [mg/l]	14.2	2.1	7.1	10.3
$NO_{3,total}$ [mg/l]	14.2	2.1	7.1	22.9
SO_4 [mg/l]	13.8	14.5	14.0	-
$\delta^{18}O$ [‰]	0.5	3.8	7.2	-
$\delta^{15}N$ [‰]	4.4	4.6	10.9	-
$\delta^{34}S$ [‰]	0.9	-	0.9	-

ID 10 (Launay, F54) - Synthesis

Groundwater table elevation

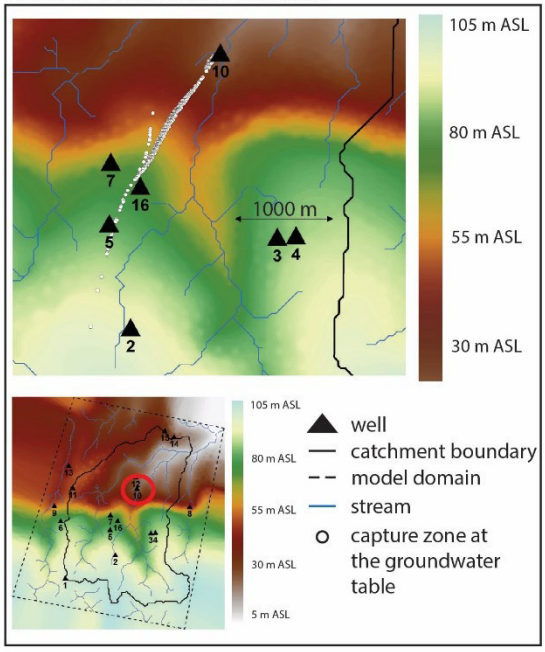

Concentration distributions

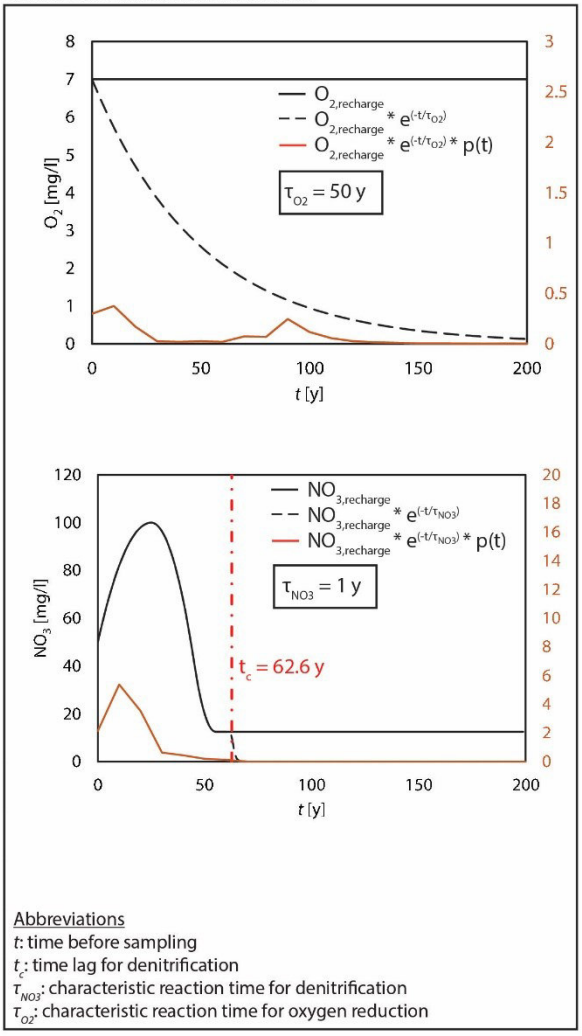

Abbreviations
t: time before sampling
t_c: time lag for denitrification
τ_{NO3}: characteristic reaction time for denitrification
τ_{O2}: characteristic reaction time for oxygen reduction

Transit time distribution

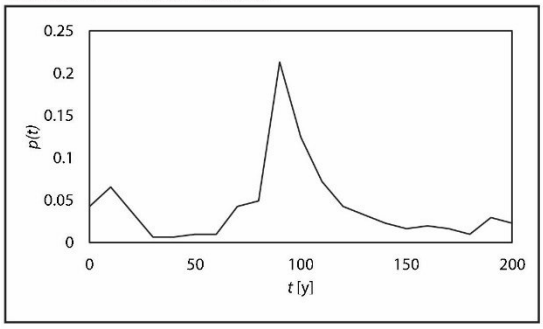

Well log

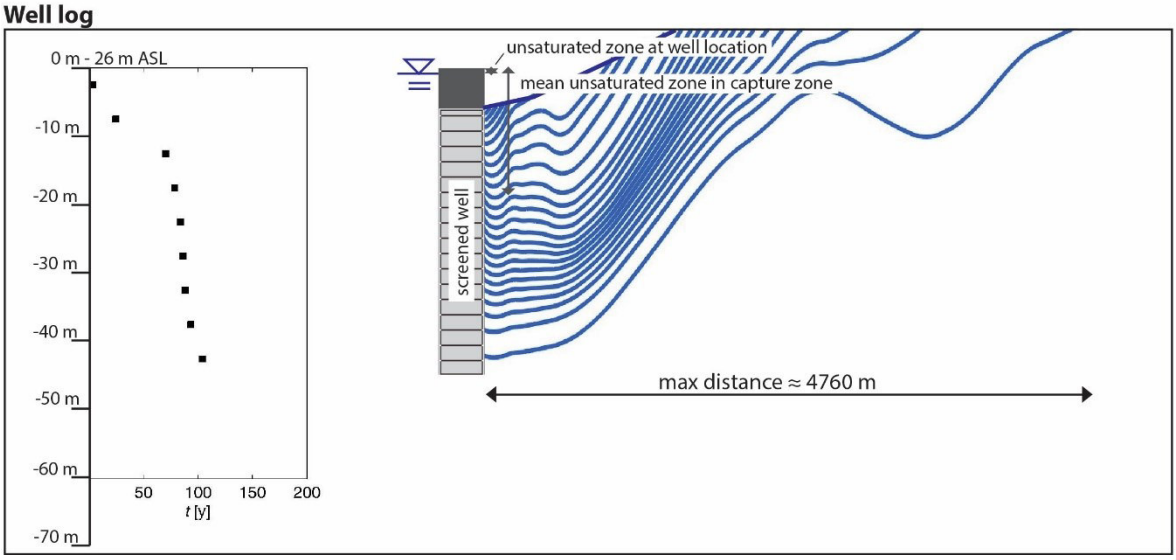

ID 11 (Mangais, F55) - Field Data

Location: lat: 48.509519, long: -1.615818

Topography

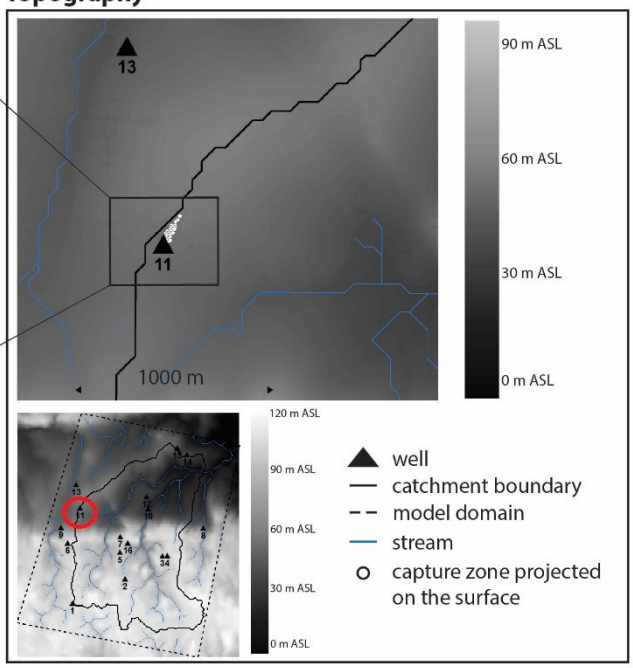

Geology

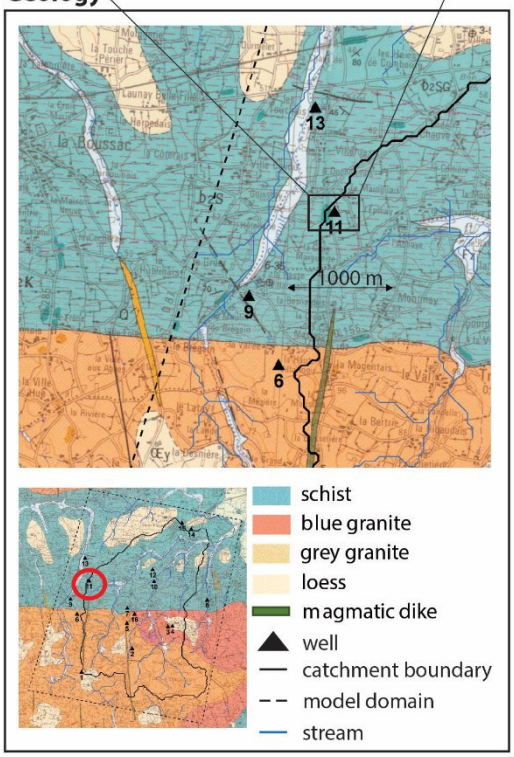

Land use

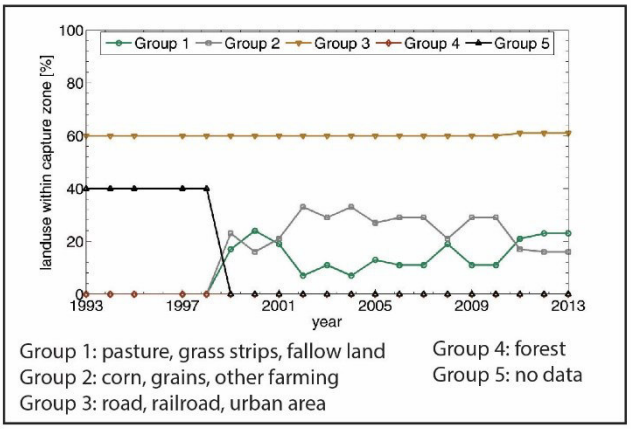

Group 1: pasture, grass strips, fallow land
Group 2: corn, grains, other farming
Group 3: road, railroad, urban area
Group 4: forest
Group 5: no data

Field data

	Dec-2014	Mar-2015	Oct-2015	Model
CFC-12 [pptv]	11	36	30	13
CFC-12 age [y]	63	55	56	62
O_2 [mg/l]	0	0	0.6	0.35
NO_3 [mg/l]	0	0	0	0.2
$NO_{3,deg}$ [mg/l]	10.6	10.2	15.8	12.4
$NO_{3,total}$ [mg/l]	10.6	10.2	15.8	12.6
SO_4 [mg/l]	17.0	37.7	17.2	-
$\delta^{18}O$ [‰]	19.5	16.5	16.8	-
$\delta^{15}N$ [‰]	16.0	16.2	12.3	-
$\delta^{34}S$ [‰]	-3.2	-	-3.1	-

ID 11 (Maingais, F55) - Synthesis

Groundwater table elevation

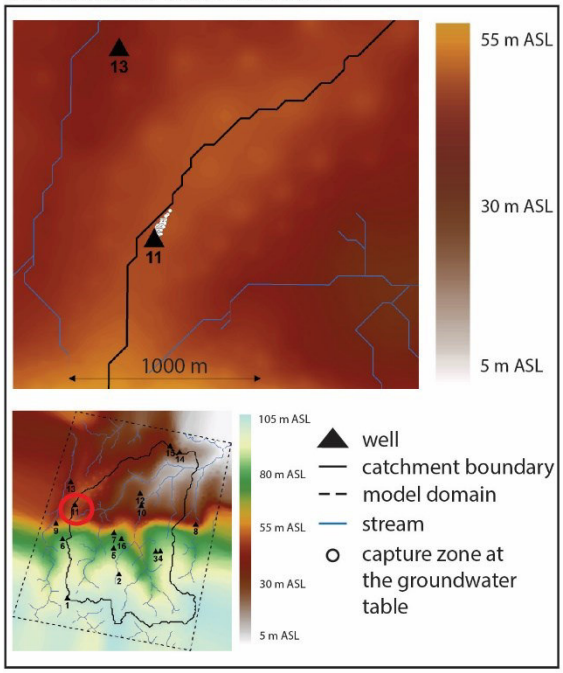

Concentration distributions

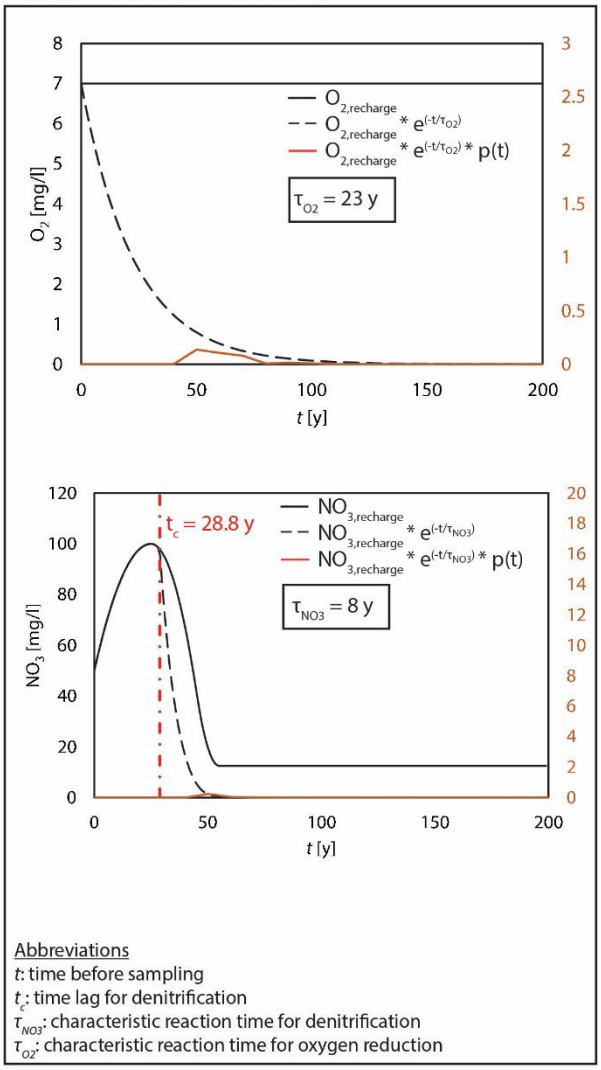

Abbreviations
t: time before sampling
t_c: time lag for denitrification
τ_{NO3}: characteristic reaction time for denitrification
τ_{O2}: characteristic reaction time for oxygen reduction

Transit time distribution

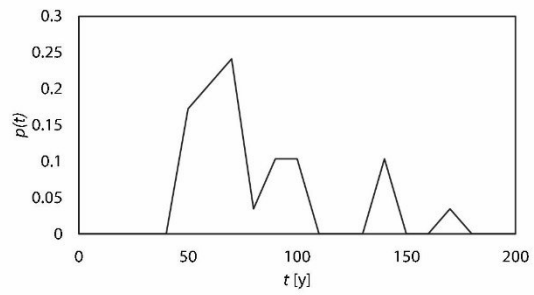

Well log

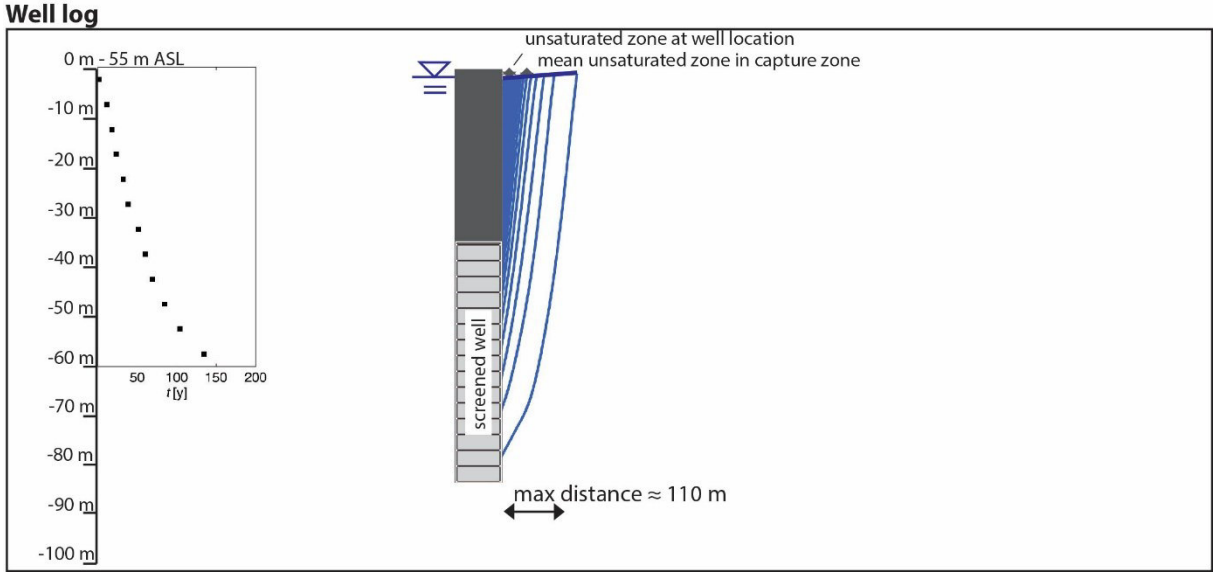

ID 12 (Maison Neuve PF, F56) - Field Data

Location: lat: 48.515817, long: -1.575705

Topography

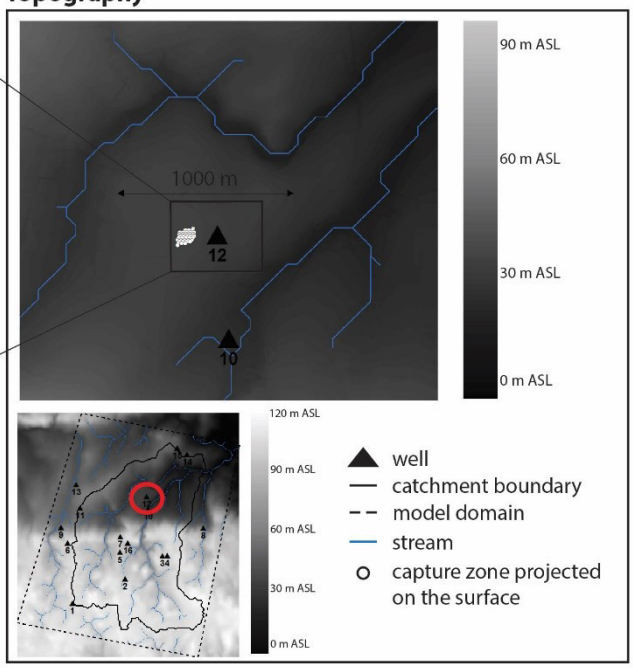

Geology

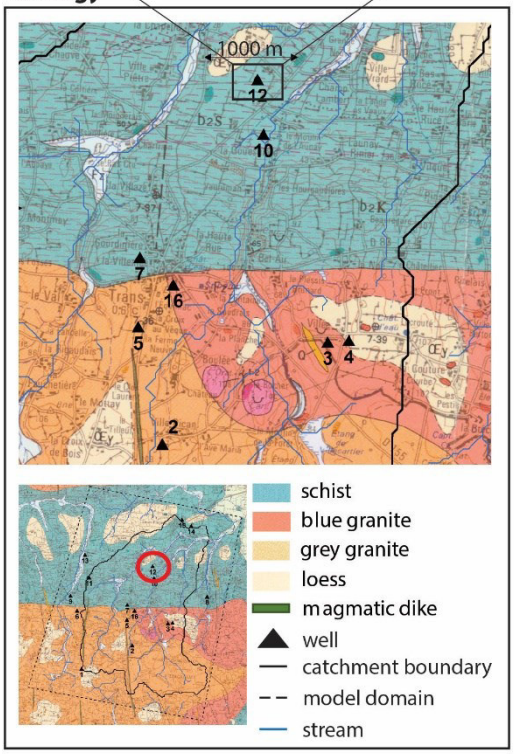

Land use

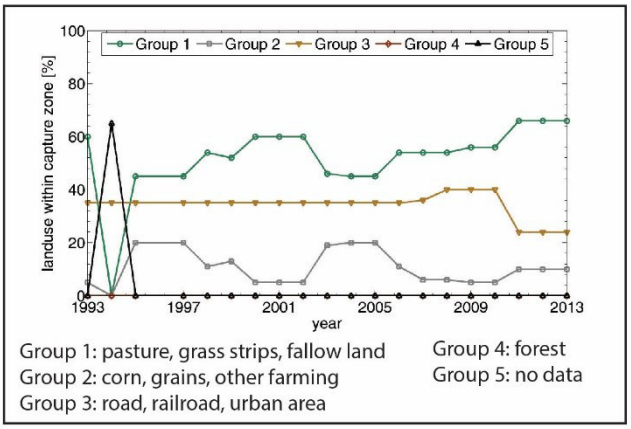

Group 1: pasture, grass strips, fallow land
Group 2: corn, grains, other farming
Group 3: road, railroad, urban area
Group 4: forest
Group 5: no data

Field data

	Dec-2014	Mar-2015	Oct-2015	Model
CFC-12 [pptv]	82	127	103	113
CFC-12 age [y]	49	45	47	46
O_2 [mg/l]	3.5	0.1	0.6	1.1
NO_3 [mg/l]	0	0	0	0
$NO_{3,deg}$ [mg/l]	36.7	44.6	37.2	35.8
$NO_{3,total}$ [mg/l]	36.7	44.6	37.2	35.8
SO_4 [mg/l]	55.5	67.9	54.7	-
$\delta^{18}O$ [‰]	21.5	15.3	17.3	-
$\delta^{15}N$ [‰]	15.0	17.2	14.6	-
$\delta^{34}S$ [‰]	-2.8	-	-2.7	-

ID 12 (Maison Neuve PF, F56) - Synthesis

Groundwater table elevation

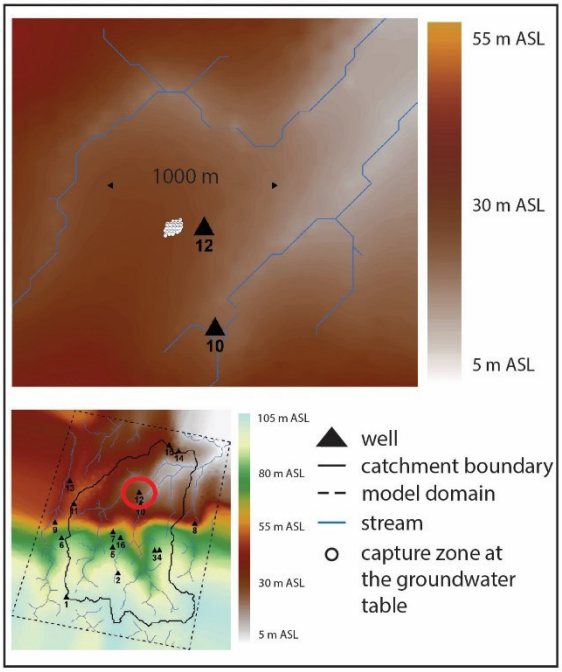

Concentration distributions

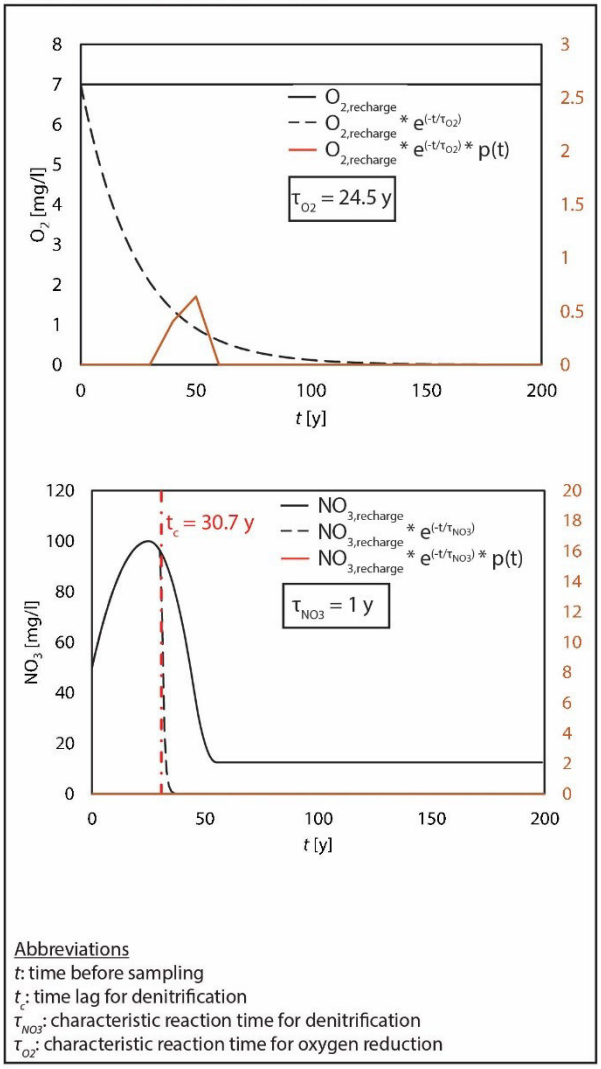

Abbreviations
t: time before sampling
t_c: time lag for denitrification
τ_{NO3}: characteristic reaction time for denitrification
τ_{O2}: characteristic reaction time for oxygen reduction

Transit time distribution

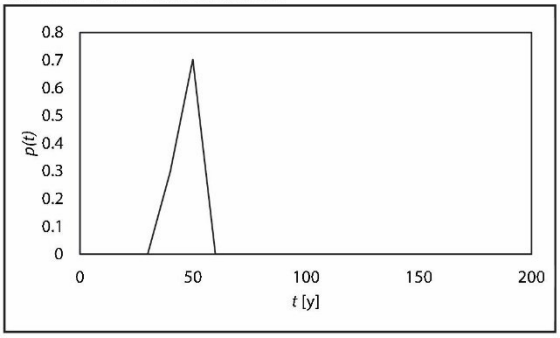

Well log

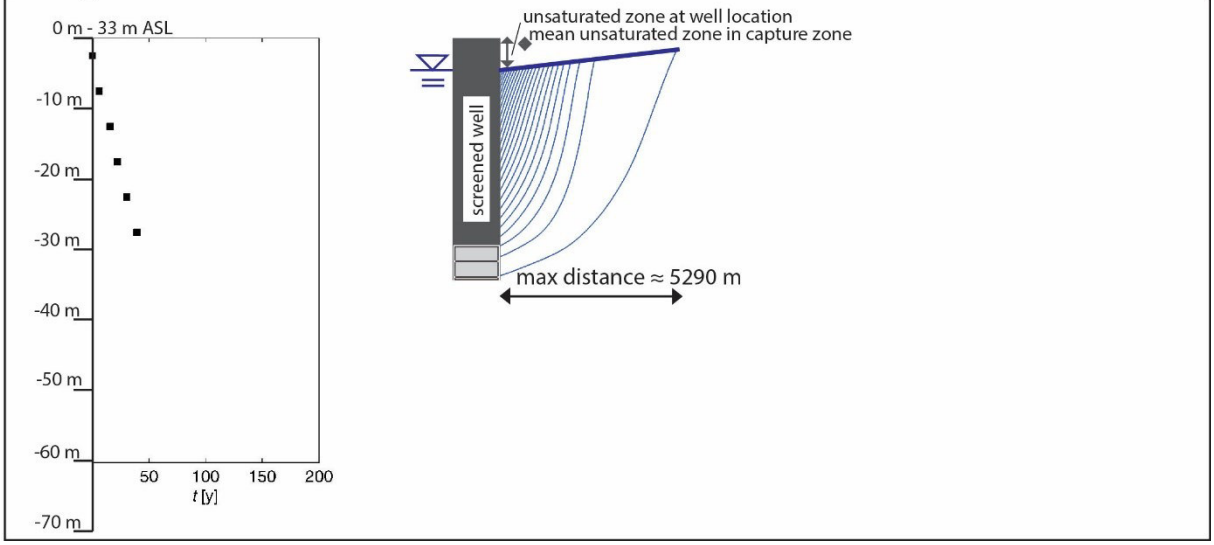

ID 13 (Le Chatel, F102) - Field Data

Location: lat: 48.518956, long: -1.619307

Topography

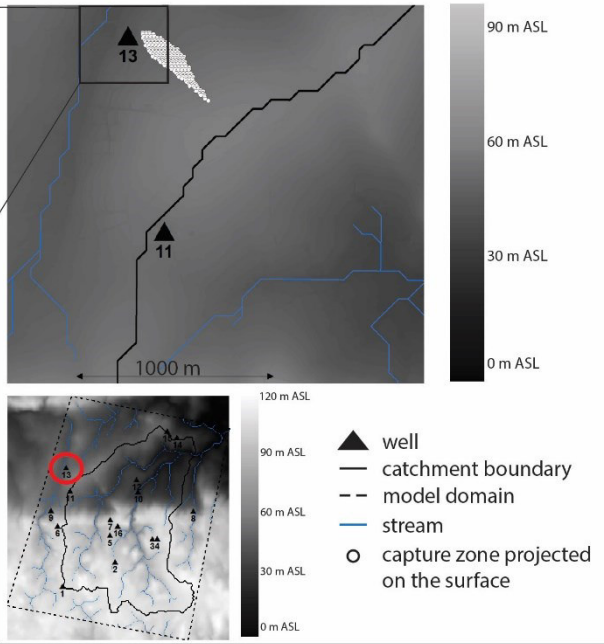

Geology

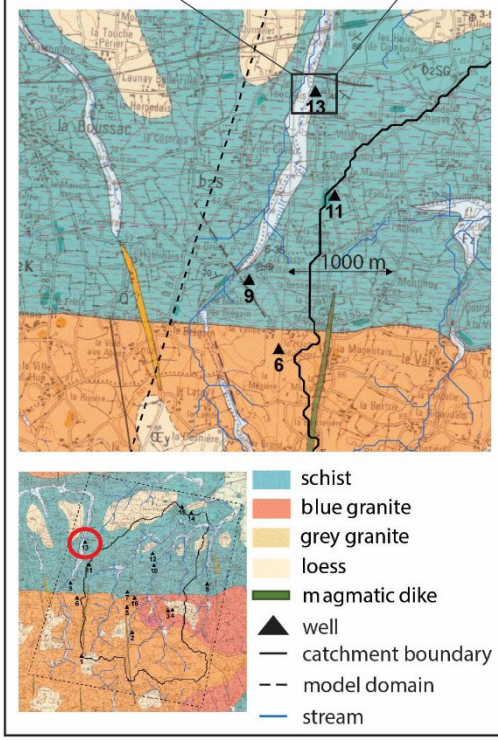

Land use

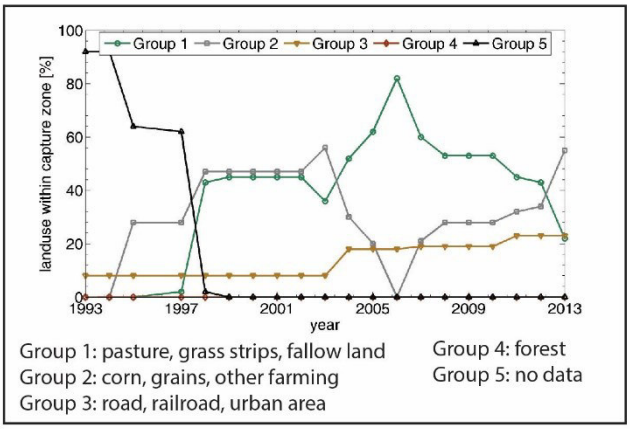

Group 1: pasture, grass strips, fallow land
Group 2: corn, grains, other farming
Group 3: road, railroad, urban area
Group 4: forest
Group 5: no data

Field data

	Dec-2014	Mar-2015	Oct-2015	Model
CFC-12 [pptv]	135	125	96	191
CFC-12 age [y]	45	45	47	42
O_2 [mg/l]	1.6	1.1	0.7	1.2
NO_3 [mg/l]	38.0	38.8	24.0	29.6
$NO_{3,deg}$ [mg/l]	19.5	19.0	19.7	16.6
$NO_{3,total}$ [mg/l]	57.5	57.8	43.7	46.2
SO_4 [mg/l]	50.9	61.6	46.8	-
$\delta^{18}O$ [‰]	9.3	8.0	10.8	-
$\delta^{15}N$ [‰]	13.6	13.4	14.5	-
$\delta^{34}S$ [‰]	0.8	0.8	-0.6	-

ID 13 (Le Chatel, F102) - Synthesis

Groundwater table elevation

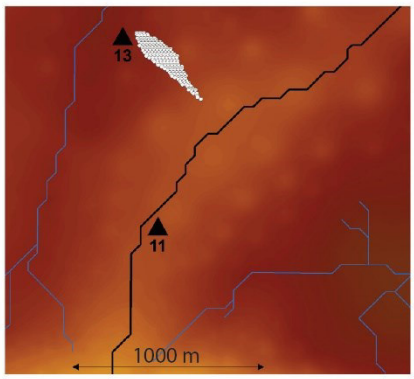

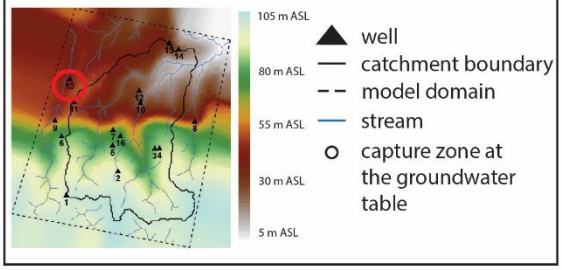

Concentration distributions

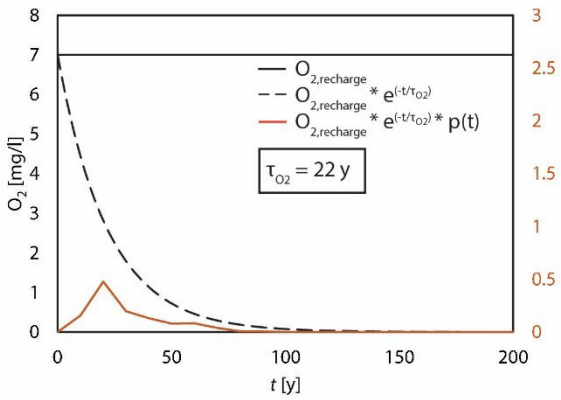

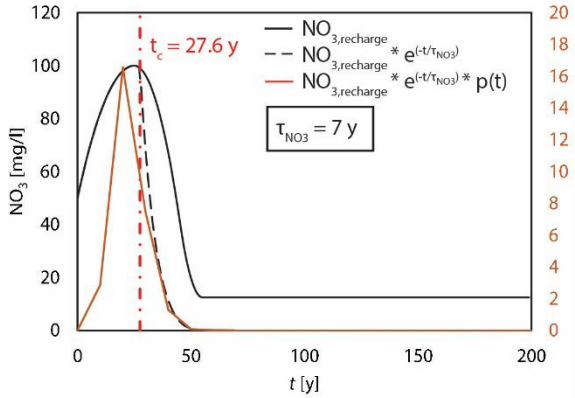

Abbreviations
t: time before sampling
t_c: time lag for denitrification
τ_{NO3}: characteristic reaction time for denitrification
τ_{O2}: characteristic reaction time for oxygen reduction

Transit time distribution

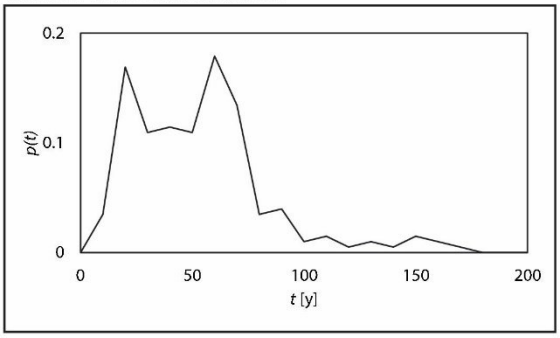

Well log

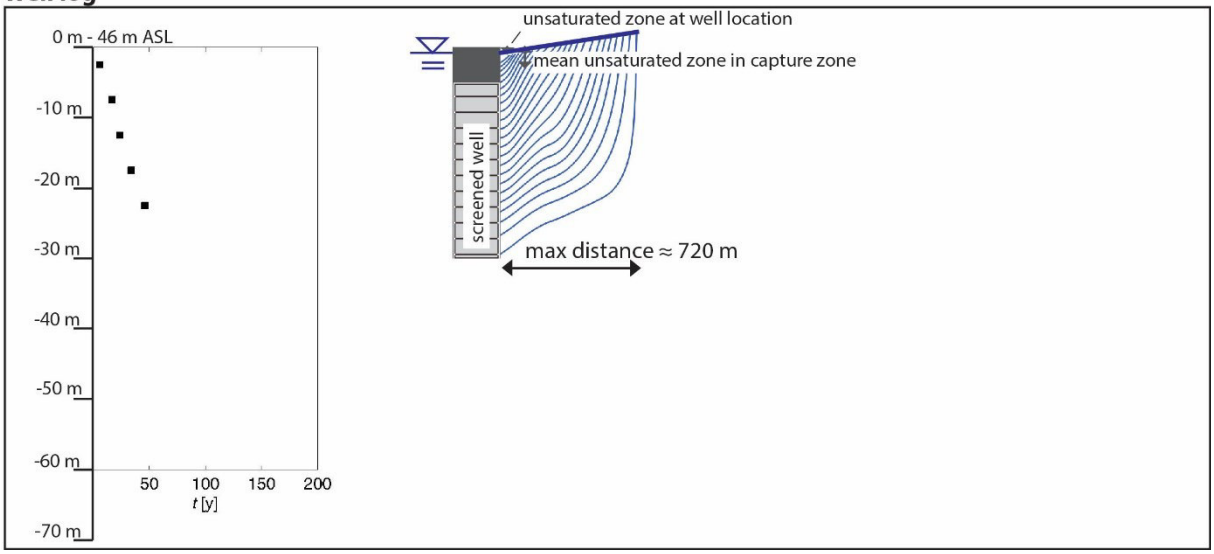

ID 14 (ZA de Budan, F86) - Field Data

Location: lat: 48.53386027, long: -1.5526493

Topography

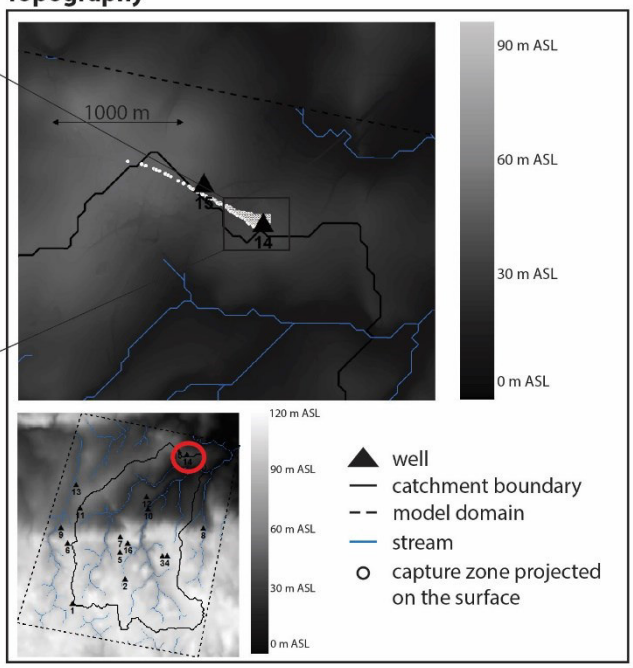

Geology

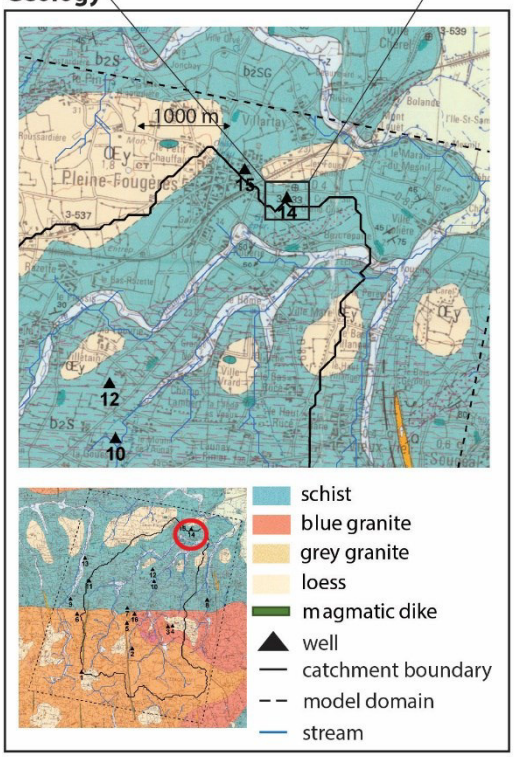

Land use

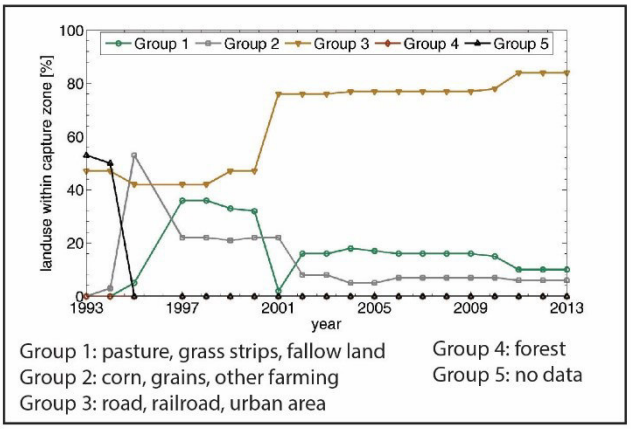

Group 1: pasture, grass strips, fallow land
Group 2: corn, grains, other farming
Group 3: road, railroad, urban area
Group 4: forest
Group 5: no data

Field data

	Dec-2014	Mar-2015	Oct-2015	Model
CFC-12 [pptv]	436	254	481	324
CFC-12 age [y]	27	38	25	34
O_2 [mg/l]	2.57	0.4	7.9	4.1
NO_3 [mg/l]	42.6	52.4	39.1	48.9
$NO_{3,deg}$ [mg/l]	2.0	4.1	0	3.9
$NO_{3,total}$ [mg/l]	44.6	56.5	39.1	52.8
SO_4 [mg/l]	37.1	34.4	42.0	-
$\delta^{18}O$ [‰]	2.4	2.2	2.5	-
$\delta^{15}N$ [‰]	5.0	5.2	5.4	-
$\delta^{34}S$ [‰]	-0.3	0.1	-0.8	-

ID 14 (ZA de Budan, F86) - Synthesis

Groundwater table elevation

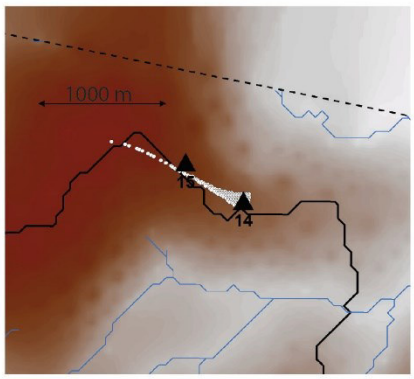

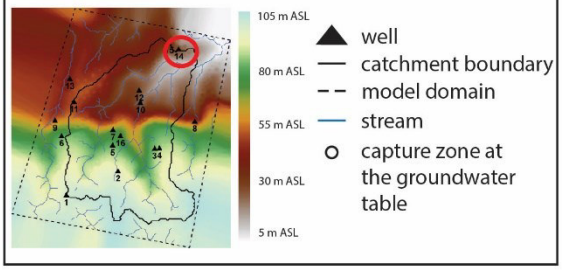

Concentration distributions

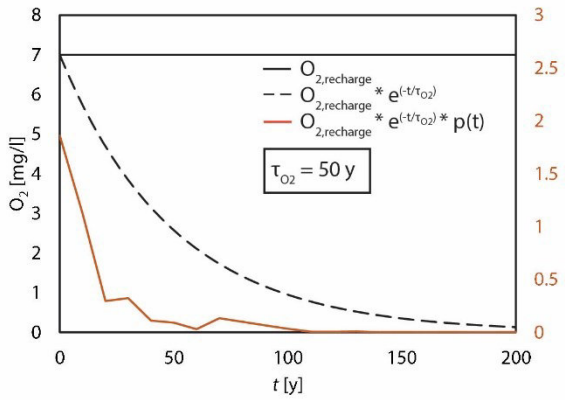

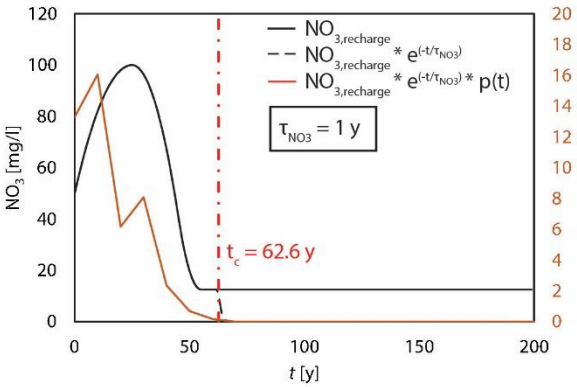

Abbreviations
t: time before sampling
t_c: time lag for denitrification
τ_{NO3}: characteristic reaction time for denitrification
τ_{O2}: characteristic reaction time for oxygen reduction

Transit time distribution

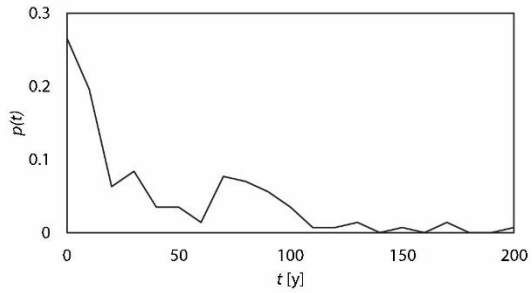

Well log

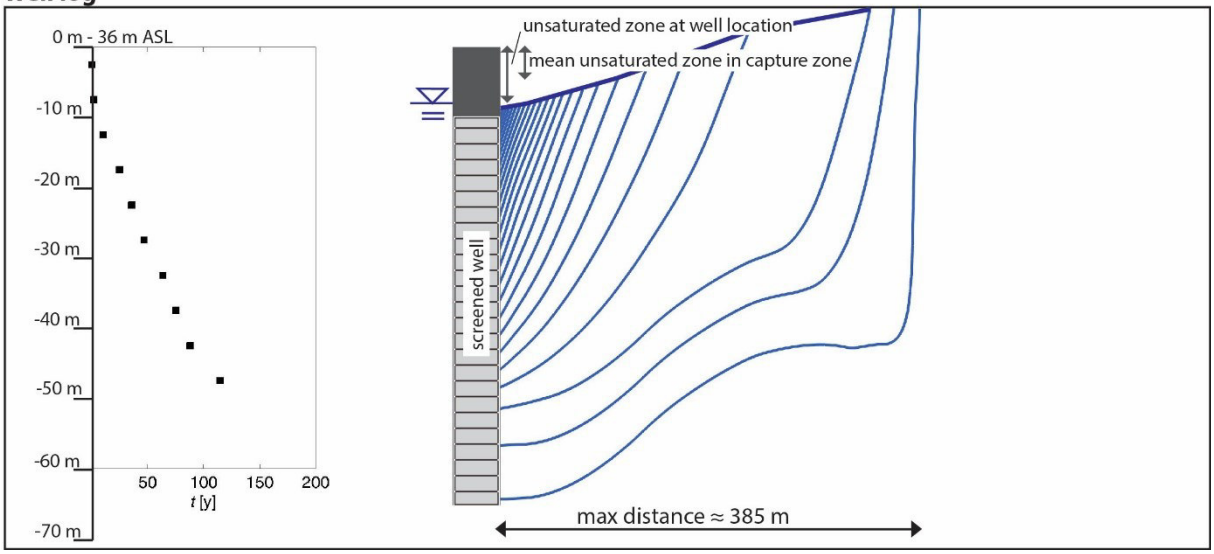

ID 15 (Mesanges, F101) - Field Data

Location: lat: 48.536201, long: -1.558703

Topography

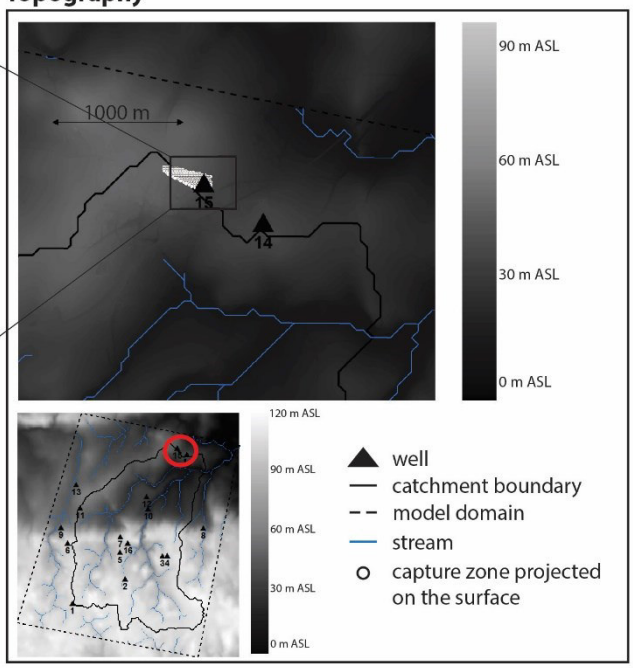

Geology

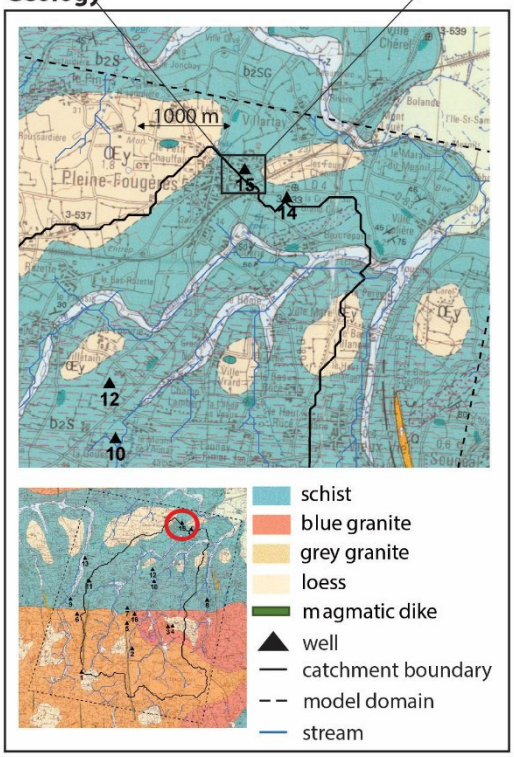

Land use

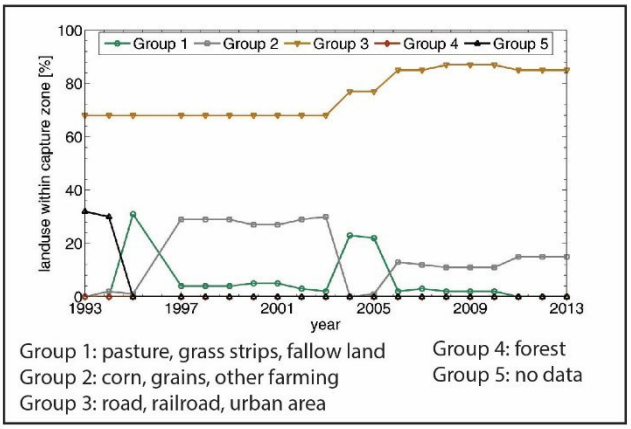

Group 1: pasture, grass strips, fallow land
Group 2: corn, grains, other farming
Group 3: road, railroad, urban area
Group 4: forest
Group 5: no data

Field data

	Dec-2014	Mar-2015	Oct-2015	Model
CFC-12 [pptv]	934	-	746	452
CFC-12 age [y]	-	-	-	27
O_2 [mg/l]	3.7	5	2.6	3.1
NO_3 [mg/l]	32.0	61.8	32.7	47.1
$NO_{3,deg}$ [mg/l]	11.8	11.4	12.5	24.9
$NO_{3,total}$ [mg/l]	43.9	73.3	45.2	72.0
SO_4 [mg/l]	45.2	57.5	44.2	-
$\delta^{18}O$ [‰]	2.5	2.6	2.5	-
$\delta^{15}N$ [‰]	6.2	7.5	6.3	-
$\delta^{34}S$ [‰]	1.2	3.9	1.4	-

ID 15 (Mesanges, F101) - Synthesis

Groundwater table elevation

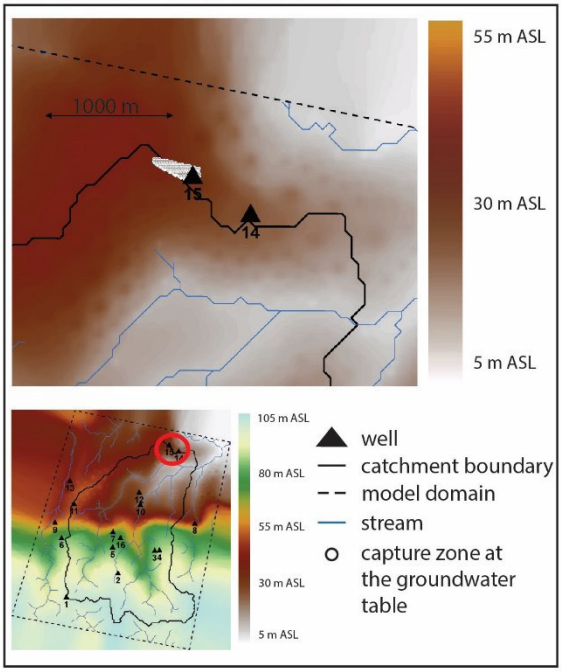

Concentration distributions

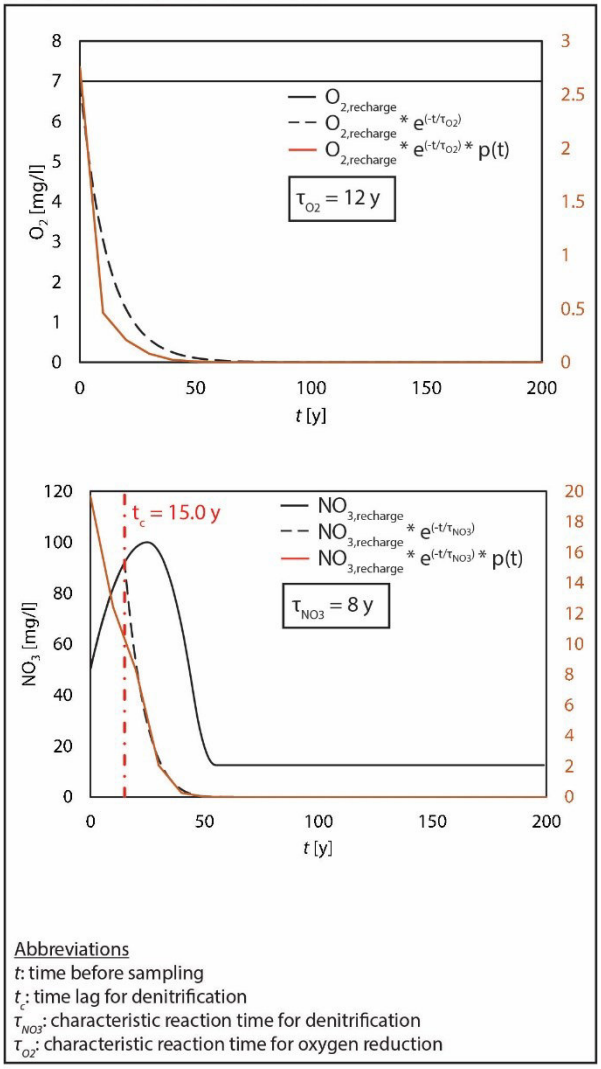

Abbreviations
t: time before sampling
t_c: time lag for denitrification
τ_{NO3}: characteristic reaction time for denitrification
τ_{O2}: characteristic reaction time for oxygen reduction

Transit time distribution

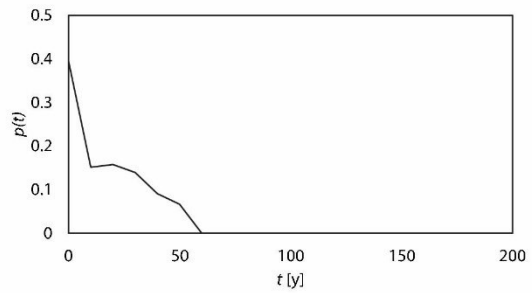

Well log

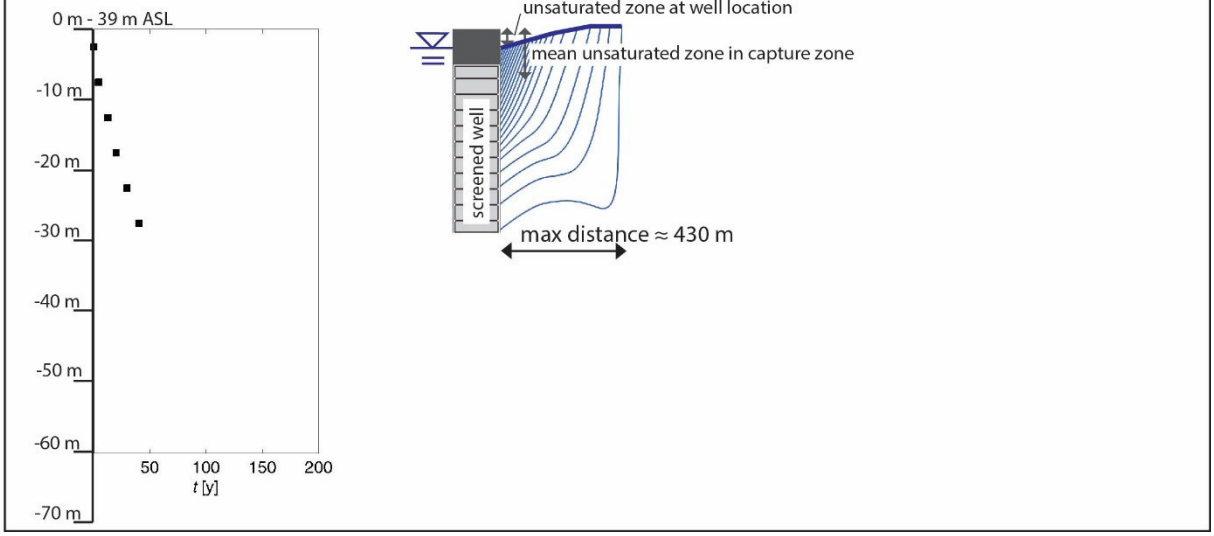

ID 16 (Ville Cartier, F105) - Field Data

Location: lat: 48.496557, long: -1.585674

Topography

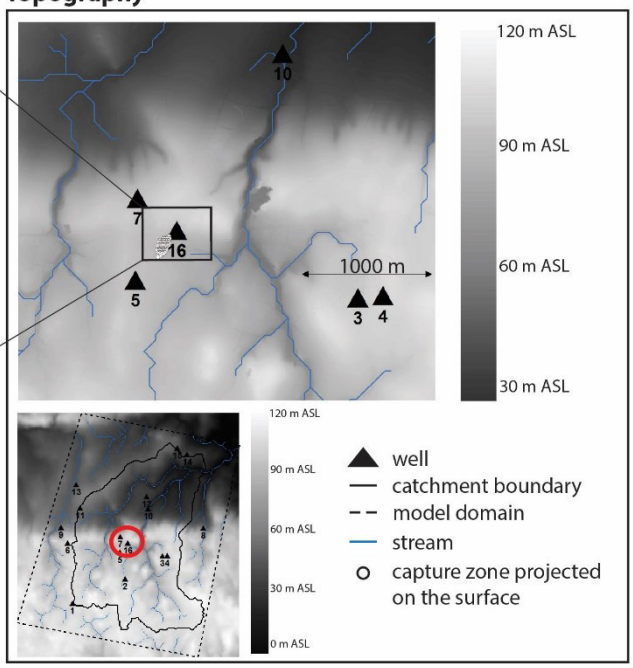

Geology

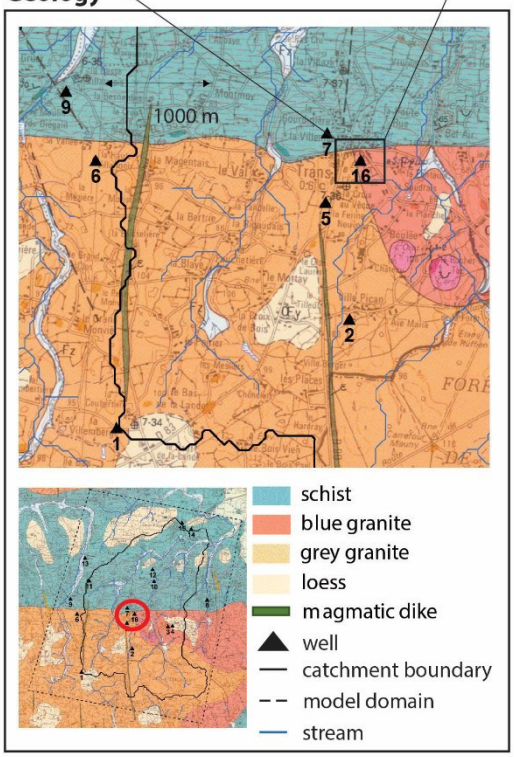

Land use

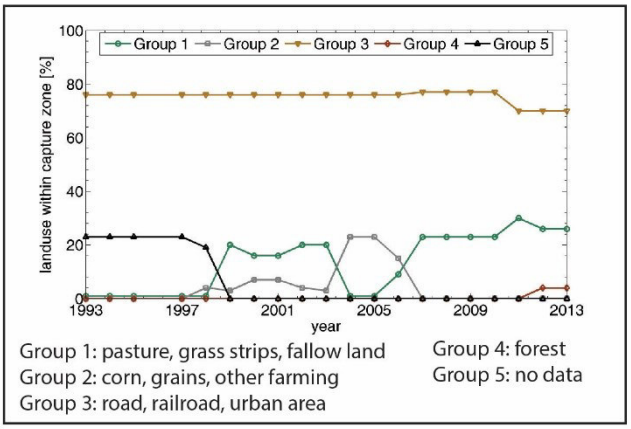

Group 1: pasture, grass strips, fallow land
Group 2: corn, grains, other farming
Group 3: road, railroad, urban area
Group 4: forest
Group 5: no data

Field data

	Dec-2014	Mar-2015	Oct-2015	Model
CFC-12 [pptv]	-	-	220	340
CFC-12 age [y]	-	-	40	33
O_2 [mg/l]	-	-	7.7	3.7
NO_3 [mg/l]	-	-	75.0	82.8
$NO_{3,deg}$ [mg/l]	-	-	0	0
$NO_{3,total}$ [mg/l]	-	-	75.0	82.8
SO_4 [mg/l]	-	-	37.4	-
$\delta^{18}O$ [‰]	-	-	3.9	-
$\delta^{15}N$ [‰]	-	-	8.1	-
$\delta^{34}S$ [‰]	-	-	-	-

ID 16 (Ville Cartier, F105) - Synthesis

Groundwater table elevation

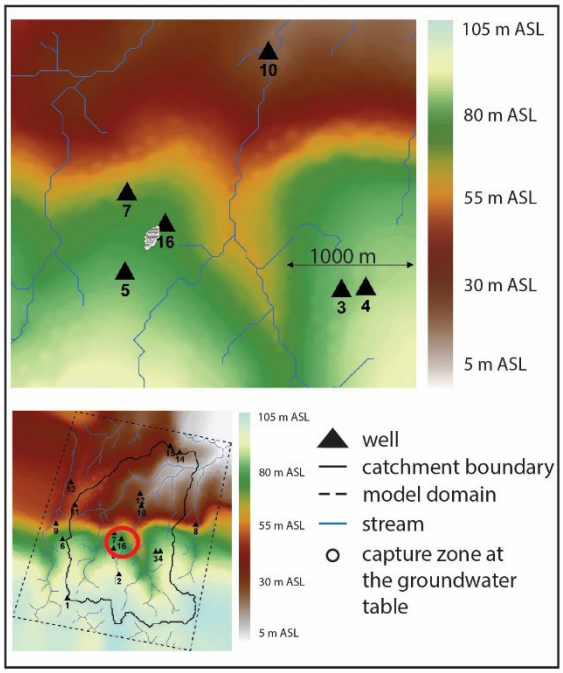

Concentration distributions

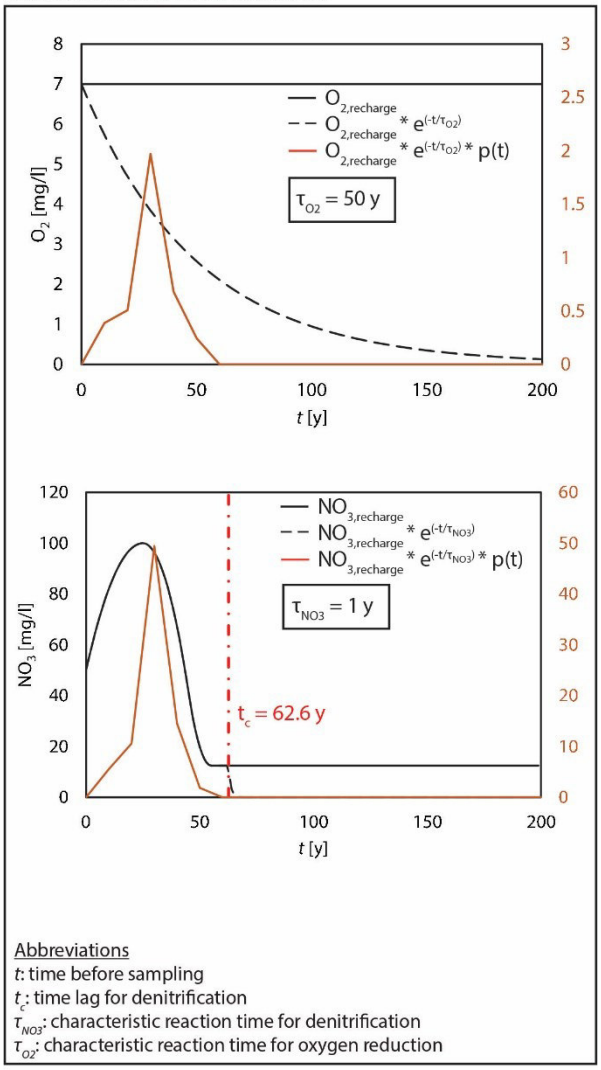

Abbreviations
t: time before sampling
t_c: time lag for denitrification
τ_{NO3}: characteristic reaction time for denitrification
τ_{O2}: characteristic reaction time for oxygen reduction

Transit time distribution

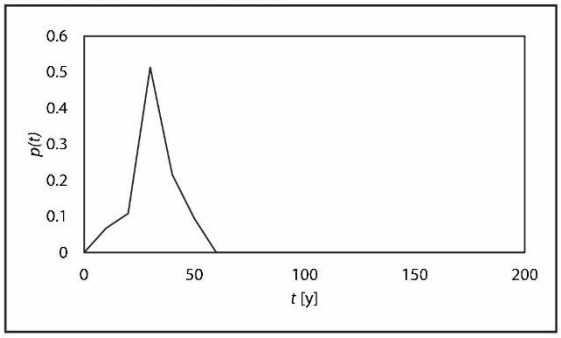

Well log

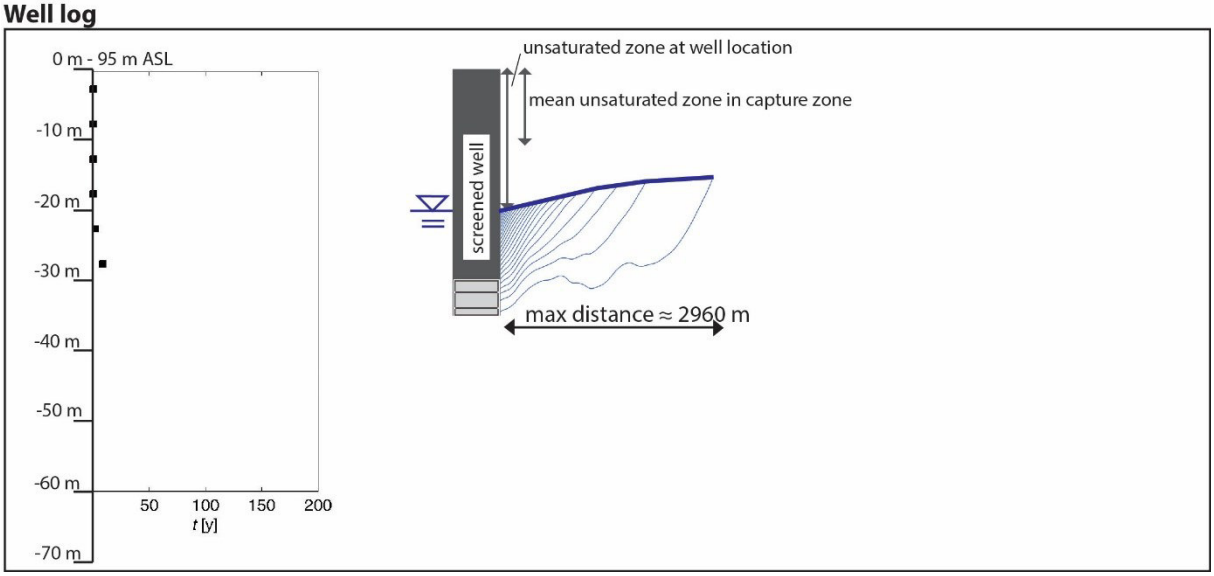

References

Abbott, B.W., Baranov, V., Mendoza-Lera, C., Nikolakopoulou, M., Harjung, A., Kolbe, T., Balasubramanian, M.N., Vaessen, T.N., Ciocca, F., Campeau, A., Wallin, M.B., Romeijn, P., Antonelli, M., Gonçalves, J., Datry, T., Laverman, A.M., de Dreuzy, J.-R., Hannah, D.M., Krause, S., Oldham, C., Pinay, G., 2016. Using multi-tracer inference to move beyond single-catchment ecohydrology. Earth-Science Rev. 160. doi:10.1016/j.earscirev.2016.06.014

Aelion, C., Höhener, P., Hunkeler, D., Aravena, R., 2009. Environmental isotopes in biodegradation and bioremediation.

Aeschbach-Hertig, W., Beyerle, U., Holocher, J., Peeters, F., Kipfer, R., 2001. Excess air in groundwater as a potential indicator of past environmental changes. Study Environ. Chang. Using Isot. Tech. 174–183.

Aeschbach-Hertig, W., Peeters, F., Beyerle, U., Kipfer, R., 1999. Interpretation of dissolved atmospheric noble gases in natural waters. Water Resour. Res. 35, 2779–2792. doi:10.1029/1999WR900130

Aïfa, T., Lefort, J.P., Guennoc, P., 1999. Anisotropy of magnetic susceptibility investigations of the St Malo dyke swarm (Brittany, France): Emplacement mechanism of doleritic intrusions. Geophys. J. Int. 139, 573–582. doi:10.1046/j.1365-246X.1999.00975.x

Almasri, M.N., Kaluarachchi, J.J., 2007. Modeling nitrate contamination of groundwater in agricultural watersheds. J. Hydrol. 343, 211–229. doi:10.1016/j.jhydrol.2007.06.016

Aquilina, L., Vergnaud-Ayraud, V., Labasque, T., Bour, O., Molénat, J., Ruiz, L., de Montety, V., De Ridder, J., Roques, C., Longuevergne, L., 2012. Nitrate dynamics in agricultural catchments deduced from groundwater dating and long-term nitrate monitoring in surface- and groundwaters. Sci. Total Environ. 435-436, 167–178. doi:10.1016/j.scitotenv.2012.06.028

Aravena, R., Robertson, W.D., 1998. Use of Multiple Isotope Tracers to Evaluate Denitrification in Ground Water: Study of Nitrate from a Large-Flux Septic System Plume. Ground Water 36, 975–982. doi:10.1111/j.1745-6584.1998.tb02104.x

Ayraud, V., Aquilina, L., Labasque, T., Pauwels, H., Molenat, J., Pierson-Wickmann, A.C., Durand, V., Bour, O., Tarits, C., Le Corre, P., Fourre, E., Merot, P., Davy, P., 2008. Compartmentalization of physical and chemical properties in hard-rock aquifers deduced from chemical and groundwater age analyses. Appl. Geochemistry 23, 2686–2707. doi:10.1016/j.apgeochem.2008.06.001

Balderacchi, M., Filippini, M., Gemitzi, A., Klöve, B., Petitta, M., Trevisan, M., Wachniew, P., Witczak, S., Gargini, A., 2014. Does Groundwater Protection in Europe Require New Eu-Wide Environmental Quality Standards? Front. Chemestry 2, 1–6. doi:10.3389/fchem.2014.00032

Beauchamp, E., Trevors, J., Paul, J., 1989. Carbon sources for bacterial denitrification. Adv. soil Sci. doi:10.1007/978-1-4613-8847-0_3

Bogdanoff, S., Jourdan, C., Lafond, R.L., 1997. Carte géol. France (1/50 000), feuille Dol-de-Bretagne (246). Orléans: BRGM. Notice explicative par S. Bogdanoff, M. Julien, avec la collaboration de R.L. Lafond, A. Carn, M. Vaginay (1996), 47 p.

Böhlke, J.-K., 2002. Groundwater recharge and agricultural contamination. Hydrogeol. J. 10, 153–179. doi:10.1007/s10040-001-0183-3

Böhlke, J.K., Wanty, R., Tuttle, M., Delin, G., Landon, M., 2002. Denitrification in the recharge area and discharge area of a transient agricultural nitrate plume in a glacial outwash sand aquifer, Minnesota. Water Resour. Res. 38, 10–1–10–26. doi:10.1029/2001WR000663

Botter, G., Bertuzzo, E., Bellin, A., Rinaldo, A., 2005. On the Lagrangian formulations of reactive solute transport in the hydrologic response. Water Resour. Res. 41. doi:10.1029/2004WR003544

Botter, G., Bertuzzo, E., Rinaldo, A., 2010. Transport in the hydrologic response: Travel time distributions, soil moisture dynamics, and the old water paradox. Water Resour. Res. 46, 1–18. doi:10.1029/2009WR008371

Botter, G., Milan, E., Bertuzzo, E., Zanardo, S., Marani, M., Rinaldo, A., 2009.

Inferences from catchment-scale tracer circulation experiments. J. Hydrol. 369, 368–380. doi:10.1016/j.jhydrol.2009.02.012

Boyer, E.W., Alexander, R.B., Parton, W.J., Li, C., Butterbach-Bahl, K., Donner, S.D., Skaggs, R.W., Grosso, S.J. Del, 2006. Modeling Denitrification in Terrestrial and Aquatic Ecosytems at Regional Scales. Ecol. Appl. 16, 2123–2142. doi:10.1890/1051-0761(2006)016[2123:MDITAA]2.0.CO;2

Busenberg, E., Plummer, L.N., 1992. Use of chlorofluorocarbons (CCl 3 F and CCl 2 F 2) as hydrologic tracers and age-dating tools: The alluvium and terrace system of central Oklahoma. Water Resour. Res. 28, 2257–2283. doi:10.1029/92WR01263

Craig, J.R., 1993. The Metamorphism of Pyrite and Pyritic Ores: An Overview. Mineral. Mag. 57, 3–18. doi:10.1180/minmag.1993.057.386.02

Eberts, S.M., Böhlke, J.K., Kauffman, L.J., Jurgens, B.C., 2012. Comparison of particle-tracking and lumped-parameter age-distribution models for evaluating vulnerability of production wells to contamination. Hydrogeol. J. 20, 263–282. doi:10.1007/s10040-011-0810-6

Fan, Y., Bras, R.L., 1998. Analytical solutions to hillslope subsurface storm flow and saturation overland flow. Water Resour. Res. 34, 921–927. doi:10.1029/97WR03516

Fischer, A., Theuerkorn, K., Stelzer, N., Gehre, M., Thullner, M., Richnow, H.H., 2007. Applicability of stable isotope fractionation analysis for the characterization of benzene biodegradation in a BTEX-contaminated aquifer. Environ. Sci. Technol. 41, 3689–3696. doi:10.1021/es061514m

Flavelle, P., 1992. A quantitative measure of model validation and its potential use for regulatory purposes. Adv. Water Resour. 15, 5–13. doi:10.1016/0309-1708(92)90028-Z

Galloway, J.N., Aber, J.D., Erisman, J.W., Seitzinger, S.P., Howarth, R.W., Cowling, E.B., Cosby, B.J., 2003. The Nitrogen Cascade. Am. Inst. Biol. Sci. 53, 341. doi:10.1641/0006-3568(2003)053[0341:TNC]2.0.CO;2

Green, C.T., Böhlke, J.K., Bekins, B.A., Phillips, S.P., 2010. Mixing effects on apparent

reaction rates and isotope fractionation during denitrification in a heterogeneous aquifer. Water Resour. Res. 46, 1–19. doi:10.1029/2009WR008903

Green, C.T., Jurgens, B.C., Zhang, Y., Jeffrey Starn, J., Singleton, M.J., Esser, B.K., 2016. Regional oxygen reduction and denitrification rates in groundwater from multi-model residence time distributions, San Joaquin Valley, USA. J. Hydrol. doi:10.1016/j.jhydrol.2016.05.018

Haitjema, H.M., 1995. On the residence time distribution in idealized groundwatersheds. J. Hydrol. 172, 127–146. doi:10.1016/0022-1694(95)02732-5

Höhener, P., Werner, D., Balsiger, C., Pasteris, G., 2003. Worldwide Occurrence and Fate of Chlorofluorocarbons in Groundwater. Crit. Rev. Environ. Sci. Technol. 33, 1–29. doi:10.1080/10643380390814433

Horneman, A., Stute, M., Schlosser, P., Smethie, W., Santella, N., Ho, D.T., Mailloux, B., Gorman, E., Zheng, Y., van Geen, A., 2008. Degradation rates of CFC-11, CFC-12 and CFC-113 in anoxic shallow aquifers of Araihazar, Bangladesh. J. Contam. Hydrol. 97, 27–41. doi:10.1016/j.jconhyd.2007.12.001

Hosono, T., Tokunaga, T., Tsushima, A., Shimada, J., 2014. Combined use of δ13C, δ15N, and δ34S tracers to study anaerobic bacterial processes in groundwater flow systems. Water Res. 54, 284–296. doi:10.1016/j.watres.2014.02.005

Höyng, D., Prommer, H., Blum, P., Grathwohl, P., Mazo D'Affonseca, F., 2015. Evolution of carbon isotope signatures during reactive transport of hydrocarbons in heterogeneous aquifers. J. Contam. Hydrol. 174, 10–27. doi:10.1016/j.jconhyd.2014.12.005

Jaunat, J., Huneau, F., Dupuy, a., Celle-Jeanton, H., Vergnaud-Ayraud, V., Aquilina, L., Labasque, T., Le Coustumer, P., 2012. Hydrochemical data and groundwater dating to infer differential flowpaths through weathered profiles of a fractured aquifer. Appl. Geochemistry 27, 2053–2067. doi:10.1016/j.apgeochem.2012.06.009

Jurgens, B.C., Böhlke, J.K., Eberts, S.M., 2012. TracerLPM (Version 1): An Excel workbook for interpreting groundwater age distributions from environmental tracer data: U.S. Geological Survey Techniques and Methods Report.

Jurgens, B.C., Böhlke, J.K., Kauffman, L.J., Belitz, K., Esser, B.K., 2016. A partial exponential lumped parameter model to evaluate groundwater age distributions and nitrate trends in long-screened wells. J. Hydrol. 543, 109–126. doi:10.1016/j.jhydrol.2016.05.011

Kazemi, G.A., Lehr, J.H., Perrochet, P., John Wiley & Sons., 2006. Groundwater age. Wiley-Interscience.

Kendall, C., Doctor, D.H., Young, M.B., 2013. Environmental Isotope Applications in Hydrologic Studies. Treatise Geochemistry Second Ed. 7, 273–327. doi:10.1016/B978-0-08-095975-7.00510-6

Kendall, C., McDonnell, J.J., 1998. Isotope Tracers in Catchment Hydrology, Isotope Tracers in Catchment Hydrology. Elsevier. doi:10.1016/B978-0-444-81546-0.50009-4

Korom, S.F., 1992. Natural denitrification in the saturated zone A review 28, 1657–1668. doi:10.1029/92WR00252

Kovács, G., 2011. Seepage Hydraulics. Elsevier.

Leray, S., de Dreuzy, J.-R., Bour, O., Labasque, T., Aquilina, L., 2012. Contribution of age data to the characterization of complex aquifers. J. Hydrol. 464-465, 54–68. doi:10.1016/j.jhydrol.2012.06.052

Leray, S., Engdahl, N.B., Massoudieh, A., Bresciani, E., McCallum, J., 2016. Residence time distributions for hydrologic systems: Mechanistic foundations and steady-state analytical solutions. J. Hydrol. doi:10.1016/j.jhydrol.2016.01.068

Maloszewski, P., Zuber, A., 1982. Determining the turnover time of groundwater systems with the aid of environmental tracers. 1. Models and their applicability. J. Hydrol. 57, 207–231. doi:10.1016/0022-1694(82)90147-0

Marçais, J., de Dreuzy, J.R., Ginn, T.R., Rousseau-Gueutin, P., Leray, S., 2015. Inferring transit time distributions from atmospheric tracer data: Assessment of the predictive capacities of Lumped Parameter Models on a 3D crystalline aquifer model. J. Hydrol. 525, 619–631. doi:http://dx.doi.org/10.1016/j.jhydrol.2015.03.055

Maréchal, J.C., Wyns, R., Lachassagne, P., Subrahmanyam, K., 2003. Vertical anisotropy of hydraulic conductivity in the fissured layer of hard-rock aquifers due to the geological patterns of weathering profiles. J. Geol. Soc. India 63.

Marler, R., Arora, J., 2004. Survey of multi-objective optimization methods for engineering. Struct. Multidiscip. Optim. doi:10.1007/s00158-003-0368-6

McClain, M.E., Boyer, E.W., Dent, C.L., Gergel, S.E., Grimm, N.B., Groffman, P.M., Hart, S.C., Harvey, J.W., Johnston, C. a., Mayorga, E., McDowell, W.H., Pinay, G., 2003. Biogeochemical Hot Spots and Hot Moments at the Interface of Terrestrial and Aquatic Ecosystems. Ecosystems 6, 301–312. doi:10.1007/s10021-003-0161-9

McMahon, P.B., Böhlke, J.K., Kauffman, L.J., Kipp, K.L., Landon, M.K., Crandall, C.A., Burow, K.R., Brown, C.J., 2008. Source and transport controls on the movement of nitrate to public supply wells in selected principal aquifers of the United States. Water Resour. Res. 44, 1–17. doi:10.1029/2007WR006252

McMahon, P.B., Chapelle, F.H., 2008. Redox processes and water quality of selected principal aquifer systems. Ground Water 46, 259–271. doi:10.1111/j.1745-6584.2007.00385.x

McMahon, P.B., Chapelle, F.H., Bradley, P.M., 2011. Evolution of Redox Processes in Groundwater. pp. 581–597. doi:10.1021/bk-2011-1071.ch026

Molénat, J., Gascuel-Odoux, C., Aquilina, L., Ruiz, L., 2013. Use of gaseous tracers (CFCs and SF6) and transit-time distribution spectrum to validate a shallow groundwater transport model. J. Hydrol. 480, 1–9. doi:10.1016/j.jhydrol.2012.11.043

Nielsen, M., Fisk, M., Istok, J., Pedersen, K., 2006. Microbial nitrate respiration of lactate at in situ conditions in ground water from a granitic aquifer situated 450 m underground. Geobiology. doi:10.1111/j.1472-4669.2006.00068.x

Osenbrück, K., Fiedler, S., Knöller, K., Weise, S.M., Sültenfuß, J., Oster, H., Strauch, G., 2006. Timescales and development of groundwater pollution by nitrate in drinking water wells of the Jahna-Aue, Saxonia, Germany. Water Resour. Res. 42, 1–20. doi:10.1029/2006WR004977

Pärn, J., Pinay, G., Mander, Ü., 2012. Indicators of nutrients transport from agricultural catchments under temperate climate: A review. Ecol. Indic. 22, 4–15. doi:10.1016/j.ecolind.2011.10.002

Pauwels, H., Ayraud-Vergnaud, V., Aquilina, L., Molénat, J., 2010. The fate of nitrogen and sulfur in hard-rock aquifers as shown by sulfate-isotope tracing. Appl. Geochemistry 25, 105–115. doi:10.1016/j.apgeochem.2009.11.001

Pauwels, H., Kloppmann, W., Foucher, J.C., 2000. Denitrification and mixing in a shist aquifer : influence on water chemiistry and isotopes. Chem. Geol. 2000, p. 307-324. doi:10.1016/S0009-2541(00)00201-1

Poisvert, C., Curie, F., Moatar, F., 2016. Annual agricultural N surplus in France over a 70-year period. Nutr. Cycl. Agroecosystems. doi:10.1007/s10705-016-9814-x

Postma, D., Boesen, C., Kristiansen, H., Larsen, F., 1991. Nitrate reduction in an unconfined sandy aquifer: water chemistry, reduction proceses, and geochemical modeling. Water Resour. Res. doi:10.1029/91WR00989

Refsgaard, J.C., Thorsen, M., Jensen, J.B., Kleeschulte, S., Hansen, S., 1999. Large scale modelling of groundwater contamination from nitrate leaching. J. Hydrol. 221, 117–140. doi:10.1016/S0022-1694(99)00081-5

Rempe, D.M., Dietrich, W.E., 2014. A bottom-up control on fresh-bedrock topography under landscapes. Proc. Natl. Acad. Sci. U. S. A. 111, 6576–6581. doi:10.1073/pnas.1404763111

Rinaldo, A., Botter, G., Bertuzzo, E., Uccelli, A., Settin, T., Marani, M., 2006a. Transport at basin scales: 1. Theoretical framework. Hydrol. Earth Syst. Sci. 10, 19–29.

Rinaldo, A., Botter, G., Bertuzzo, E., Uccelli, A., Settin, T., Marani, M., 2006b. Transport at basin scales: 2. Applications. Hydrol. Earth Syst. Sci. Discuss. 10, 31–48.

Rivett, M.O., Buss, S.R., Morgan, P., Smith, J.W.N., Bemment, C.D., 2008. Nitrate attenuation in groundwater: A review of biogeochemical controlling processes. Water Res. 42, 4215–4232. doi:10.1016/j.watres.2008.07.020

Schwientek, M., Einsiedl, F., Stichler, W., Stögbauer, A., Strauss, H., Maloszewski, P., 2008. Evidence for denitrification regulated by pyrite oxidation in a heterogeneous porous groundwater system. Chem. Geol. 255, 60–67. doi:10.1016/j.chemgeo.2008.06.005

Seitzinger, S., Harrison, J., Bohlke, J., Bouwman, A., Lowrance, R., Peterson, B., Tobias, C., Van Drecht, G., 2006. Denitrification across landscaes and waterscapes: a synthesis. Ecol. Appl. 16, 2064–2090. doi:10.1890/1051-0761(2006)016[2064:DALAWA]2.0.CO;2

Shapiro, S.D., Schlosser, P., Smethie, W.M., Stute, M., 1997. The use of 3H and tritiogenic 3He to determine CFC degradation and vertical mixing rates in Framvaren Fjord, Norway. Mar. Chem. 59, 141–157. doi:10.1016/S0304-4203(97)00007-8

Starr, R., Gillham, R., 1993. Denitrification and organic carbon availability in two aquifers. Ground Water. doi:10.1111/j.1745-6584.1993.tb00867.x

Starr, R., Gillham, R., 1989. Controls on denitrification in shallow unconfined aquifers. Contam. Transp. Groundwater.

Strebel, O., Böttcher, J., Fritz, P., 1990. Use of isotope fractionation of sulfate-sulfur and sulfate-oxygen to assess bacterial desulfurication in a sandy aquifer. J. Hydrol. 121, 155–172. doi:10.1016/0022-1694(90)90230-U

Strebel, O., Duynisveld, W.H.M., Böttcher, J., 1989. Nitrate pollution of groundwater in western Europe. Agric. Ecosyst. Environ. 26, 189–214. doi:10.1016/0167-8809(89)90013-3

Tarits, C., Aquilina, L., Ayraud, V., Pauwels, H., Davy, P., Touchard, F., Bour, O., 2006. Oxido-reduction sequence related to flux variations of groundwater from a fractured basement aquifer (Ploemeur area, France). Appl. Geochemistry 21, 29–47. doi:10.1016/j.apgeochem.2005.09.004

Taylor, R., Howard, K., 2000. A tectono-geomorphic model of the hydrogeology of deeply weathered crystalline rock: evidence from Uganda. Hydrogeol. J. 8, 279–294. doi:10.1007/s100400050015

Tesoriero, A.J., Liebscher, H., Cox, S.E., 2000. Mechanism and rate of denirification

in an agricultural watershed: Electron and mass balance along groundwater flow paths. Water Resour. Res. 36, 1545–1559. doi:10.1029/2000WR900035

Tesoriero, A.J., Puckett, L.J., 2011. O 2 reduction and denitrification rates in shallow aquifers. Water Resour. Res. 47, 1–17. doi:10.1029/2011WR010471

Tesoriero, A.J., Saad, D.A., Burow, K.R., Frick, E.A., Puckett, L.J., Barbash, J.E., 2007. Linking ground-water age and chemistry data along flow paths: Implications for trends and transformations of nitrate and pesticides. J. Contam. Hydrol. 94, 139–155. doi:10.1016/j.jconhyd.2007.05.007

Thullner, M., Centler, F., Richnow, H.H., Fischer, A., 2012. Quantification of organic pollutant degradation in contaminated aquifers using compound specific stable isotope analysis - Review of recent developments. Org. Geochem. 42, 1440–1460. doi:10.1016/j.orggeochem.2011.10.011

Toran, L., Harris, R.F., 1989. Interpretation of sulfur and oxygen isotopes in biological and abiological sulfide oxidation. Geochim. Cosmochim. Acta 53, 2341–2348. doi:10.1016/0016-7037(89)90356-6

Tóth, J., 2009. Gravitational Systems of Groundwater Flow: Theory, Evaluation, Utilization. Cambridge University Press.

Tóth, J., 1963. A theoretical analysis of groundwater flow in small drainage basins. J. Geophys. Res. 68, 4795–4812. doi:10.1029/JZ068i016p04795

Van Breukelen, B.M., Prommer, H., 2008. Beyond the rayleigh equation: Reactive transport modeling of isotope fractionation effects to improve quantification of biodegradation. Environ. Sci. Technol. 42, 2457–2463. doi:10.1021/es071981j

Van Stempvoort, D.R., Hendry, M.J., Schoenau, J.J., Krouse, H.R., 1994. Sources and dynamics of sulfur in weathered till, Western Glaciated Plains of North America. Chem. Geol. 111, 35–56. doi:10.1016/0009-2541(94)90081-7

Wright, E.P., Burgess, W.G., 1992. The hydrogeology of crystalline basement aquifers in Africa. Geol. Soc. Spec. Publ. 1–27.

Wyns, R., Baltassat, J.M., Lachassagne, P., Legchenko, A., Vairon, J., Mathieu, F., 2004. Application of proton magnetic resonance soundings to groundwater

reserve mapping in weathered basement rocks (Brittany, France). Bull. La Soc. Geol. Fr. 175, 21–34. doi:10.2113/175.1.21

Zhang, Y.C., Prommer, H., Broers, H.P., Slomp, C.P., Greskowiak, J., Van Der Grift, B., Van Cappellen, P., 2013. Model-based integration and analysis of biogeochemical and isotopic dynamics in a nitrate-polluted pyritic aquifer. Environ. Sci. Technol. 47, 10415–10422. doi:10.1021/es4023909

Zhang, Y.C., Slomp, C.P., Broers, H.P., Bostick, B., Passier, H.F., Böttcher, M.E., Omoregie, E.O., Lloyd, J.R., Polya, D.A., Van Cappellen, P., 2012. Isotopic and microbiological signatures of pyrite-driven denitrification in a sandy aquifer. Chem. Geol. 300-301, 123–132. doi:10.1016/j.chemgeo.2012.01.024